

University of Southampton Research Repository ePrints Soton

Copyright © and Moral Rights for this thesis are retained by the author and/or other copyright owners. A copy can be downloaded for personal non-commercial research or study, without prior permission or charge. This thesis cannot be reproduced or quoted extensively from without first obtaining permission in writing from the copyright holder/s. The content must not be changed in any way or sold commercially in any format or medium without the formal permission of the copyright holders.

When referring to this work, full bibliographic details including the author, title, awarding institution and date of the thesis must be given e.g.

AUTHOR (year of submission) "Full thesis title", University of Southampton, name of the University School or Department, PhD Thesis, pagination

UNIVERSITY OF SOUTHAMPTON

FACULTY OF PHYSICAL SCIENCES AND ENGINEERING

Electronics and Computer Science

Degradation by Partial Discharge in Cavities under AC Electric Field

by

Cheng Chang

Thesis for the degree of Master of Philosophy

October_2015

UNIVERSITY OF SOUTHAMPTON

ABSTRACT

FACULTY OF PHYSICAL SCIENCES AND ENGINEERING

ELECTRONICS AND COMPUTER SCIENCE

Master of Philosophy

Thesis for the degree of Master of Philosophy

DEGRADATION BY PARTIAL DISCHARGE IN CAVITIES UNDER AC ELECTRIC FIELD

Cheng Chang

Partial discharge (PD) is a localized electrical breakdown event inside solid or fluid insulating materials. PD does not link the two conductors directly. However, it can cause damage to the insulating material, and eventually build up a damaged channel leading to final breakdown.

In general, PD events can be classified based on their discharge mechanisms, such as surface discharge, corona discharge, and free space cavity discharge which is the main focus of this work. Cavity discharge studied in this work is generated by an air-filled spherical cavity inside the insulating material, which is epoxy resin. Such small cavities exist in many high voltage equipment where polymeric insulating materials are involved. Detection of cavity PD is generally believed to be very concerned by industrial operators, and sometimes an immediate replacement of the plant is required.

However, with the growing understanding of material degradation induced by cavity PD, it is possible to assess the degradation level by PD behaviour. By understanding the link between PD behaviour and degradation level, equipment's' service life may be extended to their maximum.

Cavity PD in epoxy resin was found to develop itself through five stages in this work, defined by clear variations in terms of their phase resolved partial discharge (PRPD) patterns. Optical and scanning electron microscopic observations at degradation surfaces also confirmed the physics behind PD stage transition. Previous researchers usually focus on PRPD patterns against cavity air consumption for short life materials such as polyethylene, or singular pulse characters against degradation surface with long life materials such as epoxy resin. In this work, the feedforward

(usually termed as feedback by other researchers, however, considering the fact that after each discharge event the cavity suffers deterioration and become a slightly different system, feedforward is a more accurate term from system control theory) or memory effect between adjacent pulses, short term surges, and long term behaviours were the main focus of discussion. The cavity losing its feedforward capability or memory capacity, as well as PD events getting localized onto specific damaged points, are experimentally shown to be the driving force from one degradation stages to another showed by PRPD pattern transitions.

Results achieved in this work successfully established the link between various aspects of information which were usually studied in a less interactive manner. The results suggest that accumulative PD behaviour transition along degradation time is governed heavily by the cavity surface condition, the two of which form a closed loop. Pulse train analysis studies the capability of feedforward capability of degraded cavity surfaces. Both PRPD analysis and pulse train analysis take step changes in a synchronized manner with the discovery of new-born surface condition features. Some of the surface condition features can induce later stage discharge patterns such as swarming and treeing ("wing-like") patterns, feedforward capability study of such patterns can directly be utilized to determine degradation level at such surface locations.

Such information could be used to qualitatively, and quantitatively determine the level of degradation induced by cavity PD. At this stage, PRPD patterns can be used to predict degradation surface conditions, and a number of factors related to the PD feedforward capability of such degraded cavities are found. The feedforward capability was never investigated to such depth, and was never used as a condition monitoring tool in the past. This thesis contributes towards a new way of thinking for cavity PD degradation assessment, and if materialized, a longer and more reliable service life of polymeric insulating materials if cavities are involved.

Table of Contents

Table (of Content	tsii	i		
DECLA	RATION O	F AUTHORSHIPvi	i		
Ackno	Acknowledgementsix				
Definit	tions and A	Abbreviationsx	i		
Chapt	er 1:	Introduction	L		
1.1	General	introduction and nature of cavity partial discharge1	L		
	1.1.1	Nature of cavity partial discharge	L		
	1.1.2	Partial discharge mechanism2	<u>)</u>		
	1.1.3	Partial discharge simulation	<u>.</u>		
1.2	Content	s of this thesis)		
1.3	Objectiv	ve and contribution of this work10)		
1.4	Summa	ry11	L		
Chapt	er 2:	Degradation Mechanism by Cavity Partial Discharge and Simulation	13		
2.1	Degrada	ation of Electrical Insulation Systems13	}		
2.2	Phenom	nenological Models14	ļ		
2.3	Physical	Models14	ļ		
	2.3.1	Field Limited Space Charge Model15	5		
	2.3.2	Dissado-Montanari-Mazzanti Model16	5		
	2.3.3	Electro-dynamic Stress Models	7		
	2.3.4	Cavities and Free Volumes	3		
2.4	Degrada	ation induced by cavity partial discharge20)		
	2.4.1	Cavity PD degradation mechanism21	L		
	2.4.2	Interaction between PD behaviours, cavity air, and surface degradation	n		
		22	<u> </u>		
2.5	Summa	ry30)		
Chapt	er 3:	Test Samples and Experimental Methods31	L		
2 1	Tost san	mnlos 21			

	3.1.1	Epoxy Resin Samples	. 31
3.2	Experim	ental Methods	. 37
	3.2.1	Test sample setup	. 38
	3.2.2	Experiment setup	. 39
	3.2.3	System calibration	. 39
	3.2.4	Initial Validation Tests	40
	3.2.5	Epoxy resin validation tests	41
3.3	Summai	ry	43
Chapt	ter 4:	Epoxy Resin Degradation Experiments	. 45
4.1	Validatio	on tests and initial degradation experiments	45
4.2	16 epox	y resin samples degradation experiments	. 50
	4.2.1	Experimental method and PD data acquisition	50
	4.2.2	PRPD behaviour with degradation and analysis	. 52
	4.2.3	Pulse sequence in time domain and statistical analysis – evaluation	of
		PD feedforward	62
	4.2.4	Possible indication of future degradation stages – below the hard	
		threshold	. 73
4.3	Microsc	opic observation of deteriorated surfaces	76
4.4	Summai	ry	. 80
Chapt	ter 5:	Cavity Surface Analysis	. 82
5.1	RAMAN	spectroscopy	82
	5.1.1	Experimental method	. 82
	5.1.2	Initial tests and cavity surface focusing methods	83
	5.1.3	Degradation test for epoxy resin samples – Group B	89
	5.1.4	Summary	90
5.2	Scannin	g Electron Microscopy (SEM) and Energy Dispersive Spectroscopy (E	DS)
			90
	5.2.1	SEM samples preparation	91
	5.2.2	SEM imaging	92
	5.2.3	Energy Dispersive Spectroscopy (EDS)	. 98

	5.2.4	Summary			
5.3	UV degr	adation – surface conductivity enhancement on cavity surfaces withou	t		
	geomet	rical modification102			
	5.3.1	Experimental method			
	5.3.2	Experimental results and discussions			
	5.3.3	Summary			
5.4	Conclus	ion105			
Chapt	ter 6:	Simulation of PRPD Patterns106			
6.1	Niemey	er's model106			
	6.1.1	Electric field calculation			
	6.1.2	Streamer discharge inception107			
	6.1.3	Statistical time-delay simulation			
	6.1.4	Discharge magnitude			
	6.1.5	Surface charge decay109			
	6.1.6	Matlab simulation110			
6.2	Variable	es related to PD degradation process111			
6.3	Simulati	on of PD degradation process113			
6.4	Future s	imulation directions116			
	6.4.1	Simulation of pitting discharge116			
	6.4.2	Possible life model construction117			
6.5	Summai	γ119			
Chapt	ter 7:	Conclusion and Future Work121			
Appen	dices				
Apper	ndix A	PRPD results of epoxy resin degradation test, sample group B 124 $$			
Apper	ndix B	PRPD results of epoxy resin degradation test, sample group C 141			
Apper	ndix C	Microscopic images of sample group C185			
Apper	Appendix D Simulation code based on Niemeyer's algorithm204				
Refere	ences	211			

DECLARATION OF AUTHORSHIP

I, Cheng Chang, declare that this thesis and the work presented in it are my own and has been generated by me as the result of my own original research.

Degradation by Partial Discharge in Cavities under AC electric Field

I confirm that:

- This work was done wholly or mainly while in candidature for a research degree at this University;
- 2. Where any part of this thesis has previously been submitted for a degree or any other qualification at this University or any other institution, this has been clearly stated;
- 3. Where I have consulted the published work of others, this is always clearly attributed;
- 4. Where I have quoted from the work of others, the source is always given. With the exception of such quotations, this thesis is entirely my own work;
- 5. I have acknowledged all main sources of help;
- 6. Where the thesis is based on work done by myself jointly with others, I have made clear exactly what was done by others and what I have contributed myself;
- 7. Parts of this work have been published as: [please list references below]:
 - C. Chang, T. Bai, P.L. Lewin, P.H.F. Morshuis, J.A. Pilgrim, A. Cavallini, A.S. Vaughan, G.C. Montanari, and S. Serra. "Developing an experimental method for a cavity PD based life model", Solid Dielectrics (ICSD), 2013 IEEE International Conference, 30 Jun 4 July 2013, Bologna, Italy, pp. 780-783.

Signed:	 	
· ·		
Date:		

Acknowledgements

First of all, I would like to give Prof. Paul Lewin my most sincere gratitude for his guidance, patience, and support throughout this project as my main supervisor. Also I would like to acknowledge Prof. Alun Vaughan and Dr. James Pilgrim for their supervision and support.

Also, I would like to thank TechImp in Bologna Italy and TDHVL in University of Southampton for the financial support they provide to this work. Many students and stuff in both TDHVL Southampton and high voltage lab in University of Bologna have been very helpful during my research work, to name a few: Andrea Cavallini, Stefano Serra, and Peter Morshuis from the Bologna side; Celia Yeung, Demetres Evagorou, Jack Hunter, Matthew Praeger, Michael Smith, Neil Palmer, and Nik Hakimi from TDHVL.

My family and my friends, thank you for the mental support during the difficult times of mine.

Definitions and Abbreviations

AFM Atomic force microscope **EDS** Energy dispersive spectroscopy **EEDF** Electron energy distribution function EIS Electrical insulation systems **ESCA** Electron spectroscopy for chemical analysis **FLSC** Field Limited Space Charge GUI Graphical user interface PC Personal computer PDPartial discharge **PRPD** Phase resolved partial discharge **PSA** Pulse sequence analysis SEM Scanning electron microscope WB Wide band XPS X-ray photoelectron spectroscopy Radius of cavity along field direction (mm) а В Cavity gas ionization factor \mathcal{C} Capacitance of the cavity (C) C_{rad} Radiation and gas interaction factor E_i Electric field inside the cavity (kV/mm) E_0 Applied field in the insulation bulk (kV/mm) E_{inc} Inception field (kV/mm) E_{res} Residual field (kV/mm) E_q Field induced by surface charge (kV/mm) ΔE Field collapse during PD (kV/mm) e Elementary charge (C)

 f_c

K	Field enhancement factor
	A dimensionless factor depending on cavity
	shape, depending on the ratio of axial diameter
	of the cavity a/h
	, , , _b
$K_{\mathcal{S}}$	Surface conductivity (S/m)
k	Boltzmann constant
N_{dt}	Number of detrappable electrons
\dot{N}_e	Surface emission rate
\dot{N}_{v}	Volume generation rate
p	Gas pressure in the cavity (Pa)
q	True PD charge (C)
q'	Apparent charge (C)
q_s	Surface charge magnitude (C)
T	Absolute temperature (K)
t	Time interval since previous discharge (s)
Δt_{inc}	Statistical inception time delay (s)
V_{eff}	Effective gas volume inside the cavity (m ³)
v	Over voltage ratio
v_0	Fundamental phonon frequency
\mathcal{E}_{r}	Relative permittivity of the material (F/m)
β	Exponent in approximation for effective
	ionization coefficient
η_i	Ionization mechanism factor
\emptyset_{rad}	Quantum flux density of radiation
$(\frac{\rho}{p})_0$	Pressure reduced density of the gas
$(\overline{p})_0$	Effective work function
ϕ	
τ	Effective decay time constant (s)
ξ	dimensionless factor for detrappable electrons
	at polarity reversal

Chapter 1: Introduction

In this chapter, a general introduction to this work is included. Cavity partial discharge (PD) mechanisms and state of the art PD simulation models are reviewed. PD simulation models are developed to enhance the understanding of PD mechanism, by reproducing experimental and field PD behaviours, thus to verify all physical parameters involved. Well known PD simulation models include the three capacitance model, Pederson's model, and Niemeyer's model. All above mentioned models are critically reviewed in this chapter, and a finite element analysis model developed at the University of Southampton. The content and structure of this thesis is also introduced at the end of this chapter.

1.1 General introduction and nature of cavity partial discharge

Partial discharge as a type of discharge activities usually takes place in the relatively weaker part of electrical insulation systems (EIS). PD does not link the two electrodes directly, not until final breakdown. Although being minor in scale, it is considered one of the most alarming effects that can happen to EIS. Charge bombardment generated by PD against insulating materials can have accumulated damage, propagating through the material, and eventually causing final breakdown.

The objective of this work is to study partial discharge in cavities based on polymeric insulating materials. Such cavities are millimetre level or even smaller in scale, and are commonly seen in polymeric insulation systems. At the end of this study, a link between PD behaviour and material degradation shall be established through long term degradation experiments and simulation of PD behaviour. The outcome of this work shows that degradation level can be understood more than the transition of degradation stages, quantification of such process is possible.

1.1.1 Nature of cavity partial discharge

Defects, including cracks, contaminants, and cavities are believed to be unavoidable during the manufacturing process of polymeric insulation systems [1, 2]. Partial discharge in a cavity is a local breakdown event, which only bridges the free space between cavity walls instead of the whole insulation bulk.

A gas-filled cavity has lower permittivity than the surrounding polymeric materials, as the gas inside being air which is formed by approximately 20% oxygen and 80% nitrogen. Lower permittivity will lead to electric field enhancement inside the cavity, for instance the permittivity difference between XLPE and air will cause approximately between 1 and 2.3 times field

enhancement in the air depending on the shape of cavities. The breakdown strength in air is also lower than the breakdown strength in polymeric materials, thus local breakdown is more likely to take place in these cavities.

1.1.2 Partial discharge mechanism

Inception of PD in a void requires that the electric field in the cavity exceeds its breakdown strength, hence leading to the definition of "inception voltage". Inception voltage for a specific sample depends on the nature of insulation and the cavity gas, shape and size of the void [3, 4, 5, 6, 7, 8]. This conclusion is based on electron avalanche process for a PD, where impact ionization is essential, which means one electron has enough energy by the electric field before impacting onto a gas molecule to release another electron and a positive ion, thus forming a chain effect. The energy involved is mostly kinetic energy that requires the electron to have a high enough acceleration and a long enough mean free path before impact, thus the permittivity of the gas and solid insulation, gas density, cavity shape and size are decisive during this process [4, 9]. Some publications state that ambient temperature is also an important factor to determine the inception voltage, as they can either raise the internal energy level of gas molecules, or help the electrons to overcome the energy barrier considering first electron generation [3, 5, 6, 7, 8]. Recent work reported by Hazlee Illias [10] established a simulation model based on experimental observation on PD behaviour change under different local temperatures.

Electrons will be able to gain sufficient energy to form a self-sustaining avalanche when the inception voltage is achieved; however, a seed electron is still needed as a start of the process. This electron is usually assumed to originate from surface emission or volume ionization.

Surface emission assumes that electrons gain sufficient energy to be injected from the cavity surface overcoming the energy barrier, where the applied electric field is the major source of energy, and other sources include material temperature. First electrons can be detrapped from shallow traps, or injected from the electrode. During the injection process, the voltage applied, material and gas properties, size and shape of the cavity, and also location of the cavity can all have an effect [11].

Volume ionization is when a neutral gas molecule releases an electron under radiation impact from photons or other particles with sufficient energy within free space. This electron generation process is more likely the case of first electron generation for a virgin cavity, because the energy required for this mechanism is usually higher than others for a cavity that has had PD in the past [12].

Due to the need for first electrons, inception of PD is usually delayed from the time that inception voltage is exceeded, this is due to the stochastic nature of first electron injection.

A single electron avalanche has a time scale of nanoseconds. Between two consecutive avalanches, at least one first electron may need to be produced either by positive ion impact on returning to the cathode, but this is very unlikely as ions have fairly low energy as they travel on very low velocities although with quite high mass, hence usually are not sufficient to release electrons overcoming the cathode energy barrier; or by photons emitted from excited molecules or ions impacting the cathode; or metastable atoms exited by electron collision may defuse back to the cathode with excessive energy; and also electrons can be deployed at the cavity surface by the previous discharge that has not been defused away.

Electrons and ions drift through the free space, and hit opposite cavity surfaces during the PD process. These charge carriers accumulate on cavity surfaces, build up an opposing electric field against the applied field, and will eventually force the overall electric field in the cavity to drop below the sufficient value, so that electrons are insufficient in terms of energy to carry on the avalanche process. Theoretically this extinction field should be the same as the inception field. However, PD extinction field is usually lower than inception field due to space charge accumulation, which will cause an abundant supply of initial electrons. Also, cavity modification during the time of PD can lead to lower inception voltage, such as geometrical modification and chemical accumulation can cause local field concentration, which will again lead to lower measured value of extinction voltage comparing to the inception value.

A classical equivalent circuit to describe PD behaviour is shown in Figure 1-1,

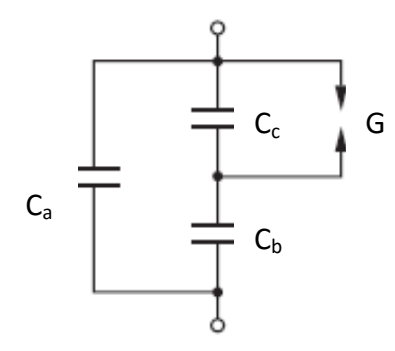


Figure 1-1: Equivalent circuit of partial discharge in a cavity [13].

where capacitor C_c and spark gap G describes the void, and the other two capacitors describe the other parts of the insulation bulk. If an AC voltage is applied to the circuit, a typical discharge waveform can be as shown in Figure 1-2.

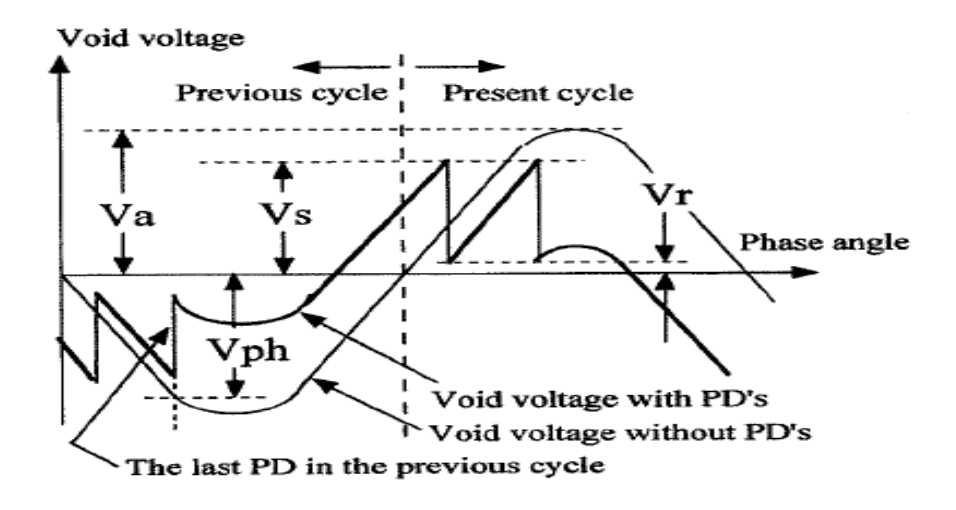


Figure 1-2: Typical cavity partial discharge signal waveform [13].

From the equivalent circuit and the discharge waveform, the discharge magnitude in Coulombs can be derived with reference to Figure 1-2 as:

$$Q = (V_s - V_r)C_a \dots (1 - 1)$$

This expression is based on the simple assumption that the discharge event acts exactly like discharging a capacitor. It begins when the breakdown strength of the capacitor is exceeded, and the magnitude can be calculated by the product of the voltage drop during the discharge and the capacitance. However, this is only a simple approximation, a cavity discharge process is far more complicated, and both inception and extinction of a PD events are stochastic in nature, hence the discharge magnitude will be stochastic as well.

According to Townsend, the avalanche process can be governed by three coefficients, two major ones of which are defined as Townsend first and second coefficients, and the third one defines the attachment process. The first coefficient governs the ionization process, stating an exponential increase in the total electron number against the distance travelled by them. The second coefficient controls the probability of secondary electron production, which means the possibility of a first electron to be generated after the current avalanche, in other words, the chance for this avalanche process to be self-sustaining. A self-sustaining PD event is governed by the two coefficients, and for which discharge magnitude being proportional to voltage drop is termed as a Townsend discharge. This kind of discharge usually is not significant in size, thus will not cause severe damage to the insulation bulk. However, a Townsend discharge can transform to a more severe type: streamer discharge if the following criterion is met: electron avalanches can get to a very energetic level that feedforward can happen in the air gap, instead of at the interfaces only [11]. A cavity based streamer discharge can usually be observed under sufficiently high electric fields if the void is not too small. The discharge current will be initially like a

Townsend discharge, but increases by at least an order of magnitude after changing to a streamer type. This change is due to space charge accumulation leading to severe field distortion, and higher energy electrons from an enhanced avalanche will provide more first electrons from gas molecule ionization in addition to the ones generated from the cathode. Streamer type PD is believed to cause more severe damage to the insulation compared to Townsend type discharge, thus most PD models focus on streamer type only in terms of real life applications such as remnant life time estimations.

1.1.3 Partial discharge simulation

1.1.3.1 Three capacitance model

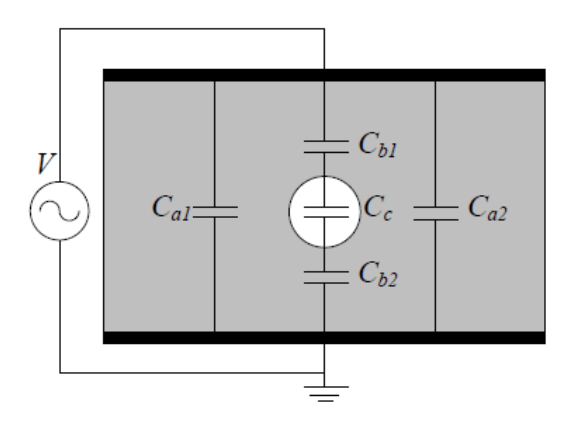
The most basic and commonly used early stage model, the three capacitance model, also called the ABC model is based on an equivalent circuit describing a cavity contained in the insulation bulk, as shown in Figure 1-3.

From Figure 1-3 (a), the cavity is represented by capacitor C_c , whilst the insulation system surrounding it is represented by C_a and C_b . This circuit can be simplified to Figure 1-3 (b), by combining the side capacitors C_a and other capacitors C_b along the field direction.

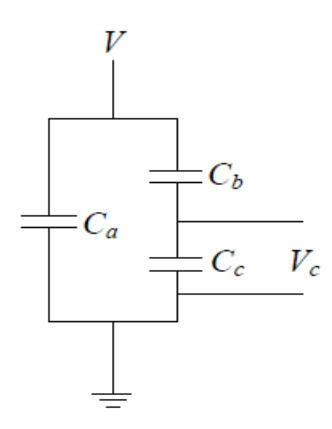
PD in this model can be simulated via discharging C_c , by replacing the capacitance with a spark gap or short circuit. Discharge will start and cease when the inception voltage and the extinction voltage is approached during simulation. During the discharge process, the voltage across C_c will drop, and the discharge magnitude is estimated using the voltage drop.

The three capacitance model provides a very good simulation for the transient during PD events, due to the similarity between a capacitor and a cavity when under electric stress. However, partial discharge in a cavity surrounded by insulating materials is indeed a complicated process, which is very hard to reproduce using simple equivalent circuits. Firstly, inception of a PD event is a stochastic process due to the need of first electrons, and this character is difficult to include in the equivalent circuit model. Factors such as "PD delay time [13, 14]" were first introduced by Laue to account for stochastic time delay. Laue stated that the probability for PD not happening when seeing a voltage higher than inception voltage decreases exponentially from unity with elapsed time. Experiments were performed by the N. Hozumi [14] to confirm this statement, by triggering PD using periodical square pulses, and recording the statistical distribution of the time lag. This theory was also simulated under AC voltage, successfully producing the well-known rabbit ear like PD pattern. Niemeyer [13] also succeeded in reproducing PD repetition rate against AC phase angle utilizing Laue's probability theory. These early results included some assumptions that have

been improved upon in later models. For example, PD time lag difference between first and following generation of PD events is now represented using electron generation rate, the voltage scaling factor to suit the space charge effect on the electric field can now be calculated considering space charge distribution, and exponential decay of space charge via cavity wall conductivity are now modelled using surface property changes and electron trapping and detrapping mechanisms [15]. These initial results did show the capability of a three capacitance model, but also its limitations. The physical and chemical properties of a cavity and the PD event itself are hard to be represented using simple circuit analysis.



(a) Complete model



(b) Simplified model

Figure 1-3: Three capacitance model equivalent circuit [16].

1.1.3.2 Pedersen's Model

The three capacitance model is based on Laplacian field between the capacitor electrodes, which means the cavity is regarded as space charge free. Pederson introduced the induced charge concept to include space charge effects, so that the overall field in the cavity can be calculated as

the sum of Laplacian field (the background applied field) and Poissonian field (electric field induced by space charge) [17, 18, 19]. Surface charge accumulation at the cavity walls will decrease the overall field across the cavity, and cease the discharge event. Dipole orientation caused by space charge can be used to calculate induced charge. The definition of induced charge is "The difference between the charge on an electrode following discharge activity and the charge on the electrode prior to this activity" [17], it can be described through dipole orientation

$$q = -\vec{\mu} \cdot \vec{\nabla} \lambda = -\left(\int_{S} \vec{r} \, \sigma dS\right) \cdot \vec{\nabla} \lambda \dots \dots (1 - 2)$$

in which $\vec{\mu}$ is the induced dipole moment, S accounts for surface charge deposition, \vec{r} is the radius vector along the surface S, σ is the charge density on cavity surface, and λ is a dimensionless scalar, determined by Laplace's equation regarding to dS [20, 21].

Equation (1-3) is a simplified version of equation (1-2), which can be applied to spherical or ellipsoidal cavities:

$$q = -K\Omega\varepsilon(E_{inc} - E_{ext})\vec{\nabla}\lambda_0 \dots \dots (1-3)$$

in above equation factor K is determined by cavity's shape, size, and orientation, but only to be applied to spherical and ellipsoidal voids, Ω is the cavity volume, ε being the permittivity of the bulk insulation, λ_0 is the solution of Laplace's equation at the location of the cavity, with the boundary conditions as $\lambda_0=1$ for the measuring electrode and $\lambda_0=0$ for the other electrode, please note that the Laplace's equation should be solved under the condition that the insulation is cavity free, where E_{inc} and E_{ext} represent the inception and extinction field respectively [22].

The induced charge on the electrode can also be calculated using the voltage drop ΔV and charge increment ΔQ on the electrode from external system:

$$q = C\Delta V + \Delta Q \approx C\Delta V \dots (1-4)$$

In the cases when discharge circuit impedance is dominantly large, ΔQ can be neglected.

1.1.3.3 Niemeyer's Model

Niemeyer's model simulates streamer type discharge. The model is able to mathematically describe streamer inception, streamer discharge process, discharge magnitude, electric field distortion, and space charge decay under AC applied voltage in spherical or ellipsoidal cavities.

The inception field level of a streamer discharge in Niemeyer's model is the threshold for ionization inside the void to release first generation electrons [23]. This process is mathematically

described accounting some measurable physical constants such as cavity size (length and width) and pressure, and some other constants regarding the ionization process which are not directly measurable, but can be derived from PD experiments, and proved to be unchanged for a defined gas type. Laplacian field enhancement inside the cavity is simply determined by permittivity difference between the gas and the insulation bulk.

Inception delay in this case is controlled by natural radiation, void volume, pressure, and over voltage ratio. Natural radiation constants are defined in [24] to be held constant for air. For the following generation of avalanches, accounting the fact that first electrons can also be deployed from the cavity surface, this model utilized thermal field emission scaling to quantify the surface electron emitting rate [12]. Phonon impact and temperature are assumed to be the major source of energy to overcome the emitting energy barrier.

Niemeyer's model estimates discharge amount through voltage collapse after a PD event, which is similar to the three capacitance model. On top of that, Niemeyer's model also adopted Pederson's idea of "induced charge": finding cavity surface charge distribution by solving Poisson's equation, which distribution is governed by cavity size, shape, orientation, gas pressure and applied field [18, 22].

Simulation results have been compared to experimental data, close match was declared between the two. However, additional experiments have not been reported in the literature that justify measured and derived constants are suitable under different field strength, frequency, or other working environments. The author of this thesis felt the need of the justification work due to the model does not directly simulate the physical processes such as first electron injection, but utilizes adjustable coefficients which can affect them, and these assumptions may need to be altered from case to case.

1.1.3.4 Finite Element Analysis Model

A field-based partial discharge model was developed by Illias based on earlier work [25]. The model utilizes COMSOL to achieve finite element analysis for electric field calculation, interfaced with MATLAB which adopts Niemeyer's model as the core part of PD simulation. Spherical cavities were studied, and PD events were simulated by changing the cavity conductivity to the electron conductivity in the plasma, as streamer discharge can modify the free space inside cavities to a plasma state; discharge magnitude was calculated by integrating the current through the ground electrode; space charge decay was simulated by changing the cavity surface conductivity [26, 27, 28]. PD behaviour under various applied voltage amplitude and frequency was also studied [29, 30]. Finite element analysis has significant advantage performing above simulations. Besides,

effects brought by local temperature and pressure changes were also studied using respective modules by COMSOL [10, 31, 32]. Simulated results were found to have good match with experimental data, and conclusion was drawn that local temperature change brought by PD should not be significant enough to affect the PD event itself.

This field-based finite element analysis model significantly improved the simulation accuracy as a great amount of computing power was available, however, detailed physics regarding the PD avalanche itself and the effect of PD on degradation were still not included so that the PD event was still simulated using the same assumptions as previous models. If one wants to study ageing and degradation caused by PD, a model with complete and accurate physics is required ideally.

1.2 Contents of this thesis

This thesis starts with an introduction and a review of state of the art cavity PD simulation and degradation life models in chapter 1 and 2. Chapter 3 includes sample preparation methods developed, basic PD experimental method, and data acquisition systems. Validation tests for epoxy resin samples prepared and experimental systems are also included in chapter 3.

Chapter 4 includes PD degradation experiments Initial validation experiments with sample group A and B are discussed in brief, including a 2000 hours degradation experiment with 4 group B samples. Phase resolved partial discharge (PRPD) pattern features and pulse train sequence pattern features are both analyzed, and an initial definition of degradation stages are discussed. A full 1970 hours of degradation test with 16 group C samples is also included in chapter 4, with upgraded experimental methods to focus on the study of PD feedforward capability and its quantification. Microscopic images taken with time intervals during degradation process are also reported in this chapter.

Chapter 5 reports detailed study on degradation surfaces. RAMAN spectroscopy (RAMAN), Scanning Electron Microscopy (SEM), and Energy Dispersive Spectroscopy (EDS) were utilized for the purpose. The relationship between surface deterioration and PD behaviour is discussed in this chapter.

Simulation of featured PRPD patterns is reported in chapter 6. A simulation model with Niemeyer's algorithms presented with its simulation results. Possible methods for the simulation of late degradation stage PD behaviour are discussed, including possible methods to quantify degradation level based on PD behaviour.

A conclusion with discussion of possible future directions is included in chapter 7.

1.3 Objective and contribution of this work

The initial objective of this work was to study the link between partial discharge in cavities and resulted degradation, leading to the construction of a degradation/life model. The initial proposed method was to utilize Sanche and Montanari's work, which was to simulate degradation through electron impact and deterioration to the surface, and to approximately calculate the overall damage.

However, through the progress of this study, the author found that the initially proposed method was unpractical, due to the random nature of cavity partial discharge. Thus, it was proposed by the author and agreed by the main supervisor Prof. Lewin to alter the general objective of this work as to experimentally study cavity partial discharge and resulted degradation to the material. Detailed aims are as such:

- A detailed and thorough study on the state of the art of cavity PD and degradation models.
- 2. A long term degradation experiment that involves a decent amount of samples.
- 3. Detailed research on PD data to establish distinctive degradation stages.
- 4. Acquire optical microscopic images throughout degradation experiments, to support degradation stage observation from PRPD results.
- 5. Perform chemical examination and Scanning Electron Microscope observations on deteriorated surfaces.
- 6. Put all findings in 2, 3, and 4 into a closed and interlinked circle, so that cavity PD behaviour and sample degradation can be interpreted physically by each other.
- To establish a method that can be used to quantify the degradation process, and if possible, a life model.

As far as contribution is concerned, the length of degradation experiments and the depth of related study have already made this work a fine extension of the previous research in the area. Furthermore, the discovery of pitting as possible electric tree initiation in spherical cavities, and also the method of using PD feedforward capability to quantify degradation level make this work unique.

Speaking with more details: this work analyzes all aspects of PD behaviour during degradation including PRPD pattern transition, pulse train sequence features, geometric analysis of degradation surfaces, and chemical study of degradation surfaces of epoxy resin for a degradation duration of 2000 hours. Such long term degradation experiments were rarely reported on this subject. The few reported work only focus on a few aspects of the ones listed above, thus their

conclusions were sometimes different due to the different focusing points of the works. This thesis provides a relatively full picture of the subject.

In terms of degradation life models, phenomenological models are based on experience from accelerated life tests, the application of which can be very limited due to the variation of conditions. Physical models are in general based on inclusive relationships between applied voltage and service life. Degradation mechanisms such as mechanical stress, thermal stress, electro-dynamic stress, and space charge are all reported by published research works, however missing the detailed physical links between the exact degradation site and damage accumulation, instead the EIS were treated as a whole in such models. This also happens to cavity PD degradation models. The most detailed PD degradation model up to date in terms of local physics and damage accumulation is introduced by Sanche and Montanari, which will be discussed in chapter 2. However, their method of calculating damage accumulation from PD magnitude has some tricky issues to be solved, one of which is how to distribute the damage across the entire cavity surface, and another one is that the overall damage trend calculated by discharge magnitude by time may change due to cavity and ambient conditions.

Based on above issues of state of the art models, this thesis presents another way of thinking when it comes to evaluating degradation level under cavity PD: by evaluating PD feedforward capability level which is dominated by cavity surface conditions, degradation level can be in turn estimated based on discharging physics. The advantage of this method is that it avoids the damage calculation part which can be tricky as PD changes its impacting location from time to time. Instead, converging trends for many parameters related to PD feedforward capability are found to be reliable throughout the degradation process, thus they can be used estimating the degradation level. Another advantage of this method is that it focuses only on the exact discharge location, as it is only estimating the damage level on the exact location by analysing PD activities from the location only. Thus it can be applied globally as long as the insulating material and cavity type are justified.

1.4 Summary

This chapter includes a general introduction of the work. Firstly the subject of cavity PD and state of the art simulation models are reviewed. The reviewed models have concluded the up to date understanding about PD considerably well. A PD event as a physical process and most aspects which may affect the PD event have been studied and included in the models. Most PD events from experiments can be reproduced by simulation models by adjusting physical factors and boundary conditions. The most influential PD models include three capacitance model, Pedersen's

model, and Niemeyer's model. A latest finite element model developed in TDHVL is also introduced. Although earlier models like Niemeyer's and Pedersen's can only produce conclusive information about PD events such as discharge magnitude and energy level, key parameters governing PD features are relatively well considered. With polymeric insulating materials, some of these influential parameters can be altered by PD degradation process, such parameters will be studied in detail with both experiments and mathematical simulation work in this project.

A brief introduction of the content in this thesis is also included. The chapter is finished with a discussion of contribution by this thesis.

Chapter 2: Degradation Mechanism by Cavity Partial

Discharge and Simulation

Ageing and degradation models are reviewed in this chapter, of which models can be concluded into 2 major categories. Earlier models developed are mainly based on engineering experience and data bases, they rely on simple energy/damage relationships, thus are named as phenomenological models. With the development of experimental technology, later models are designed to focus on detailed physical/chemical processes of degradation, thus are called physical models.

2.1 Degradation of Electrical Insulation Systems

Degradation can be defined as a change of state and property under all kinds of stresses applied, that usually leads to a degree of malfunction [11]. In the case of electrical insulation systems (EIS), and according to IEC and IEEE standards, it is termed as "occurrence of irreversible, deleterious change in insulating materials or systems which affect their serviceability, i.e. their ability to satisfy requested performances" [33]. Applied stresses such as electrical, thermal, mechanical, and other environmental effects can all be accounted as factors that cause or accelerate the degradation process. Degradation of EIS can lead to reduction of performance such as designed capacity and lifetime; hence it must be well understood throughout the industrial line of these systems, from design, quality control, maintenance, online inspection and diagnostics, to offline or destructive assessments.

EIS are required to work under various conditions, sometimes rather complicated, suffering from combinations of different stresses, models of which are difficult to produce due to the applied stresses that can interact with each other, affecting the degradation process. Hence one major stress applied and its related degradation process is usually selected and studied, depending on the working conditions applied.

When electrical insulation material is considered, manufacturing defects are currently unavoidable, for instance micro cavities, and they are generally assumed to be a major source of high level degradation. Initially, insufficient tools prevented researchers from understanding the physics behind materials and their degradation processes, phenomenological models were designed and used. These models are mostly products of experience, developed by curve fitting techniques; nevertheless they serve a purpose to a certain degree as the creation of experience data bases and accelerated test results are abundant. Today, much more detailed physical-

chemical reactions are being studied and included in models, including electrical space charge effects and partial discharge effects, providing useful understanding of ageing/degradation processes associated with electrical insulation materials.

2.2 Phenomenological Models

Phenomenological models are generated from equipment service life databases or accelerated life tests. Electrical, thermal, and mechanical stresses are the major factors considered in these models. Phenomenological models usually take an inverse power or negative exponential form, which states the service lifetime decreases with the increase of certain applied stresses. Although without such clear understanding of the local chemistry and physics, phenomenological models can only provide a fair estimation of service lifetime under specified applied stresses.

Phenomenological models were and are still widely used, as they have been proved to be dependable. Most famous ones are the Dakin model, the inverse power model, and the exponential model which are based on electrical ageing, the Arrhenius model based on thermal ageing, and the Eyring model accounts for electrical stress which can cause electromechanical effects [34, 35, 36, 37, 11, 38, 39]:

Dakin Model:
$$L = C_E E^{-n} (2 - 1)$$

Exponential Model:
$$L=L_0 \exp[-n(E-E_{cr})] \dots \dots (2-2)$$

Arrhenius Model:
$$L = L_0 \exp\left[\frac{\Delta\emptyset}{k}\right] \left(\frac{1}{T} - \frac{1}{T_0}\right) \dots \dots (2-3)$$

Eyring:
$$L = C_E \frac{h}{kT} \exp\left(\frac{\Delta G}{kT}\right) \dots \dots (2-4)$$

In the above models L in common represents the predicted lifetime of the electrical insulation system, E is the electric field, E_{cr} is the critical electric field where above which ageing and degradation take place, T is the absolute temperature, $\Delta \emptyset$ is the activation energy of degradation, ΔG is the Gibbs free energy of electro-thermal degradation, h is the Plank constant, and k is the Boltzmann constant. C_E and n are model coefficients that depend on material properties, electric field, and ambient temperature.

2.3 Physical Models

Physical models of ageing are established to simulate insulation system ageing based on physical-chemical processes. Compared to phenomenological models, physical models contain better understanding of physical-chemical processes during ageing, especially the knowledge regarding

to micro defects. Defects, such as contaminants, micro cavities, conductive particles, and metallic protrusions, can provide zones with electric field distortion and enhancement, but lower breakdown strength, or act as significant space charge injection sources, leading to final breakdown of insulation bulk.

2.3.1 Field Limited Space Charge Model

The Field Limited Space Charge (FLSC) model emphasizes on space charge injection from electrodes, it is based on Field Limited Space Charge Current theory [40, 41, 42] which states a critical electric field value as a threshold. The theory considers that below the threshold, injected charge carriers have very low mobility, however, if the threshold field is exceeded, charge mobility shows a non-linear increase against local field strength, so that by space charge penetrating into the insulation bulk, a space charge current can be induced, and as a result reducing the electric field at insulation-electrode interfaces rapidly [43, 44]. Electric field enhancement can be achieved by space charge accumulation, or local defects such as metallic particles presenting in the insulation bulk [42, 43].

The energy brought by the space charge current into the insulating material may lead to local damage initiation or propagation. Moreover, Boggs et al. [45, 46] state that space charge accumulation to a certain degree can produce enough electric field enhancement to initiate partial discharge events if a free space is available locally. The presence of high electric field can enhance local conductivity considering the relationship between activation energy and electric field, this fact can lead to filamentary conductive paths, which will then lead to final breakdown if a critical length of the conductive path has been reached [47].

To conclude, a final life model was proposed under DC conditions:

$$L \propto \frac{1}{r^2 E_l (\frac{E}{E_c} - 1)^2} \dots \dots (2 - 5)$$

in the equation L represents the predicted lifetime, which is predicted to be decreasing against the charge injecting tip radius r, Laplacian electric field E_l , and local Poisson field E. E_c is the onset threshold of FLSC. Note, the equation only holds when local Poisson field is greater than the threshold field, to let the term $\frac{E}{E_c}$ stay greater than 1.

This model was also developed to describe AC conditions, by accounting in angular frequency and dielectric permittivity. The major consideration of this AC model is that recombination process releases energy, which will then reduce the threshold field value of space charge injection.

The FLSC model only considers very high field conditions (e.g. >100 kV/mm), which will only happen in circumstances such as embedded metallic particles, or long time space charge accumulation under DC conditions. Under above conditions, other local breakdown methods such as PD can also be easily triggered, which may be the major reason for final breakdown instead of FLSC as a source to induce and grow damage sites.

2.3.2 Dissado-Montanari-Mazzanti Model

The Dissado-Montanari-Mazzanti (DMM) Model assumes the ageing and degradation process is mainly induced and accelerated by electrical and thermal stress. Chemical moieties, which are considered to be the elements forming an insulating system, are micro structures as individual units that can be damaged under a simple assumption: a moiety can transfer between two thermal equilibrium states, an initial state which is not damaged, and a final state which is damaged. This transferring reaction is assumed to be able to go both ways, governed by a free energy barrier ΔG , which is shown in Figure 2-1:

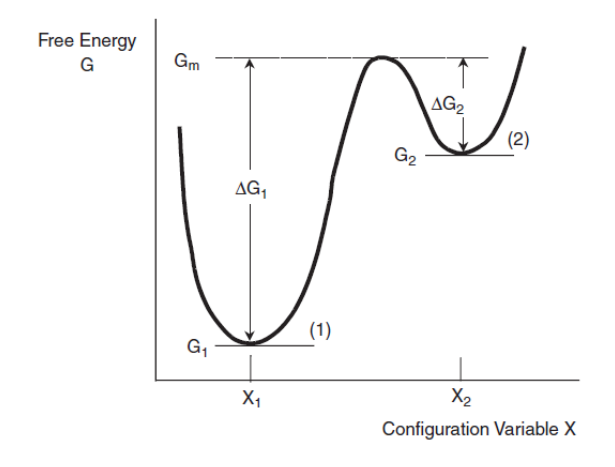


Figure 2-1: Free energy barrier theory [11].

The energy barrier can be overcome by electric field enhancement induced by space charge accumulation, which will increase local free energy hence will reduce the energy barrier. This will normally take place around defect zones in the insulation bulk. Thermal energy is also a vital source for overcoming the energy barrier in this model, which will include ambient temperature and the thermal energy released by space charge trapping and detrapping process.

The major hypothesis of this model is that there is a critical damaged fraction A^* , exceeding it in a zone will disrupt this zone, hence enlarging the micro defect beside which this process takes place, hence creating suitable conditions for higher level degradation processes such as partial discharge. Also, electrostatic and electromechanical stress will accelerate the ageing process, especially

electromechanical stress can accelerate reactions converting a group of atoms to a plastically deformed state, thus it may lead to the formation of micro cracks, and possibly treeing.

The failure criterion of the DMM model is hence the formation of a large enough cavity to initiate partial discharge, by turning a fraction of moieties larger than A^* locally in that region. The model in DC conditions can be expressed as:

$$\begin{cases}
L(E,T) = \frac{h}{2kT} \exp\left(\frac{\Delta H}{k} - \frac{C'E^{4b}}{2} - \frac{\Delta S}{k}\right) \ln\left[\frac{A_{eq}(E)}{A_{eq}(E) - A^*}\right] \left[\cosh(\frac{\Delta}{k} - C'E^{4b})\right]^{-1} \\
M_{eq}(E) = \left[1 + \exp(\frac{\Delta}{k} - C'E^{4b})\right]^{-1}
\end{cases} \dots \dots (2 - 6)$$

where $A_{eq}(E)$ represents the equilibrium state, which is the value of A^* between forward and backward reactions, T is the absolute temperature, E the Laplacian field, Δ is the free energy gap between pure deformed (product) state and pure undeformed state (reactant), ΔH and ΔS are activation enthalpy and entropy per moiety, C' is a constant derived from material properties, including both electrical properties and mechanical ones, and B governs the stored charge per charge centre and applied field, as space charge is assumed to be uniformly distributed in a sphere each charge centre for the purpose to simplify the model [48].

This model was later adapted to work under AC conditions, by accounting in the effects of electrical fatigue induced by alternating electric field. Mazzanti, Montanari, and Dissado [49, 50] validated the model with experiments under different applied electric field levels, ambient temperatures, and frequencies, the results showed good match between the two. Moreover, later work with local elemental strain was studied and utilized to modify the model [51].

2.3.3 Electro-dynamic Stress Models

Some researchers believe thermodynamic stresses caused by electric fields can be the source of insulation ageing and degradation. The major assumption for these models is that the insulation goes from an unaged state to an aged state, overcoming a free energy barrier with the help from electrical and other applied stresses.

A model proposed by Lewis considers the electro-mechanical stress which can bring destructive effects to the insulation countering cohesive forces [52, 53]. According to the Helmholtz expression, electromechanical stress can be divided into three sub-terms: a contribution from Columbic forces due to interaction between the field and charges; a stress from non-uniform distribution of permittivity within the insulation, so that regions with higher permittivity are being

pulled into the ones with lower permittivity; and a volumetric electrostrictive stress due to the change in permittivity against density. Apart from the above, the author also considered mechanical stress contributing to overcome the free energy barrier, under which consideration the applied mechanical stress is defined to have a linear effect on free energy gained by the insulation material.

The model ends when cracks are initiated, and enlarged to be sufficient in size for higher level degradation mechanisms, for instance partial discharge. However, a very intensive electric field (>100 kV/mm) would be required for such deformation, thus it is supposed to only happen in defective regions, and to grow the defects until global breakdown. The model equation under DC conditions is,

$$L = \left(\frac{h}{2kT}\right) \exp\left(\frac{\Delta G}{kT}\right) \operatorname{csch}\left(\frac{\varepsilon \cdot \Delta V \cdot E^2}{2kT}\right) \dots \dots (2-7)$$

where L is the predicted lifetime, ΔG is the activation energy barrier, ΔV is the activation volume, ε is the permittivity, h and k being the Plank and Boltzmann constant respectively, and T is the absolute temperature. The model has an AC version, simply by replacing the first bracket by $(\frac{1}{2f})$. Crine also proposed a thermal energy driven model, determining the rate of zonal disruption by overcoming the free energy barrier. In above works, efforts were made to understand multifactor stressing on ageing. However, due to the complexity of the process, proposed life models are usually with limited dominating factors instead of considering everything, which is a reasonable assumption [52].

Despite the maturity of this theory, there has not been many systematic experimental validations for it due to the free energy theory containing coefficients or constants which are hardly measurable by experiment, especially considering ΔG as a material property constant that can affect the predicted life in an exponential way, any inaccuracy in it will induce significant inaccuracy in predicted lifetime.

2.3.4 Cavities and Free Volumes

Many models described above regard the enlargement of cavities and free volumes, for instance cavities or cracks to be the initiation sign of higher level degradation activities such as PD, which will lead the insulation system to final breakdown with much higher rates. There should be no doubt against the theory on how PD can be formed, however, whether partial discharge avalanches in cavities can enlarge the cavity or form electrical trees is yet to be proved. Even before there is enough free space for the avalanche to take place, the theory supported by

previous models that nanometre scale defects can be grown into micrometer scale ones is also not proved yet in practice, as it requires the presence of electric fields in excess of the designed field, unless in some extreme cases such as the presence of extreme space charge accumulation or introduction of metallic contaminants.

So, it may be more appropriate to take a cavity with sufficient size as a starting point, and look into how PD damage can be introduced and enlarged instead of growth of the whole cavity, as there has been practical proof already for pitting induced by PD activities from a cavity [54, 55]. More work is required to classify the degradation and breakdown mechanism from cavity PD to a global breakdown, as it seems many breakdown mechanisms overlap each other, thus subtle differences in the degradation process may trigger totally different breakdown mechanisms. This fact means that the experiments to grow electrical trees from cavities are very difficult, as thermal runaway may take over at any moment during the accelerated process leading to rapid failure.

Work reported in [56] provides an excellent foundation for researchers trying to find out detailed mechanisms involved between void partial discharge and final breakdown. By firing electrons into thin polyethylene films, detailed scattering and energy transfer mechanisms were studied and classified, defining the affects brought by electron with an energy range between 0 - 20eV impinging into insulating surface, such as bound reorientation and lattice dissociation. The dissociation threshold for pure polyethylene was defined to be around 8eV. The conclusion from above experiments by Sanche was a three stage process for electronic ageing: space charge trapping and detrapping to rearrange polymeric bonds, hence creating micro cavities; hot electrons produced to cause bond breaking effects, hence enlarging micro cavities; PD avalanches increasing until final breakdown.

There are some arguable points in the above conclusions. The first one is the creation and enlargement of micro cavities, from previous discussion it can hardly happen under designed field levels, unless there is severe field distortion such as metallic elements in the material. Ultra clean insulating materials produced nowadays can eliminate cavities larger then 100µm, and any impurity which can distort local field at that level. However, this does not mean we will be free from partial discharge, due to the fact that designers always want to produce the most cost effective system, in other words, to operate close to the limits, which means micro cavities may be enlarged, electrons may be accelerated to the sufficient energy level with a much shorter mean free path to trigger PD in much smaller cavities. The second one is the enlargement of cavities, as discussed in earlier sections, pitting is more likely the case. Also, the most important one may be the ultrahigh vacuum condition in which the experiments were done. This was

undertaken because the author only aimed to find out what pure electron impinging can do, however, chemical production and accumulation, especially oxides, are very important factors in terms of energy transfer process and local conductivity and field change. Thus more work is needed here, but understanding what pure hot electrons can do is nevertheless an important foundation to studying partial discharge induced damage.

One typical work based on electron scattering theory was introduced by the Montanari et al. [57, 58]. The produced PD model was based on Niemeyer's theories; however, PD electron avalanches are physically described in this model. Via simulating electron avalanches, the proportion of hot electrons can be derived, so as the damage caused. Electron avalanches are simulated with the idea of electron energy distribution function (EEDF), which can be calculated with reasonable speed when assuming the electrons are stationary, and spatially the electric field within the thin slab being looked at holds constant. EEDF makes it possible to the find out electron velocity distribution assuming all energy is kinetic energy, thus spatial distribution of this thin slab of electrons can be predicted at the next time step. Using an electron multiplication factor to derive overall electron number, iterative calculations can then be used to simulate electron avalanches through differentiated axial space and time steps, eventually giving the energy distribution of electrons colliding into the opposite insulation wall of a cavity. The stop point of this model is a critical damaged size along the applied field direction, which is enough to trigger electrical treeing. Damage growth is estimated with an idea of disruption rate, that a slab of certain thickness is damaged when enough energy carried by hot electrons collides into it, a calculated value termed as time to disruption can provide an estimation of insulation life.

The above model has been validated with experimental results in terms of PD amplitude and repetition rate, a fine fit was found regarding PD behaviour, whilst the degradation mechanism was hard to validate. The fact is, most up to date void discharge ageing models define tree triggering as the stop point, however, bush and branch type treeing from a discharging cavity has not yet been seen experimentally. Referring to Sanche's experimental findings, hot electrons can indeed dissolve cavity walls, but are there enough hot electrons from cavity PD under most experimental conditions is one question to be answered, while the other one is with existence of air, hence the possibility of chemical reactions, there is a chance that other degradation mechanisms or even breakdown mechanisms dominate instead of a long term treeing mechanism.

2.4 Degradation induced by cavity partial discharge

It is widely reported and believed that although partial discharge in air filled cavities cannot bridge the two electrodes directly, its accumulative damage to the surrounding polymeric dielectric materials can gradually lead to the final breakdown of the system [11]. As discussed in earlier sections, the most widely accepted theory that leads the system from cavity PD to final breakdown depends on electrical trees to be developed by the PD [59, 57]. However, this hypothesis is not yet proven by experiment. Nevertheless, the initiation of internal PD is still recognized as the signal for the very last stage of insulation lifetime.

Most life models discussed in this section have not studied this far to quantify the life time after the occurrence of internal PD, because of it is relatively short in terms of time if compared with the full lifetime of the system, and also because of the stochastic behaviour of internal PD itself. Although there is not yet a well-rounded internal PD life model, research work in the past has provided a good foundation to work towards it.

2.4.1 Cavity PD degradation mechanism

PD activity can modify the air/polymer interface in two ways: electron/ion bombardment [60], and/or chemical reactions [61]. The accumulative effect from electron and ion bombardment is reported being able to develop micro pits as discussed in [54, 56, 55]. Simultaneous chemical reactions within the cavity air assist the damaging process on the cavity surface, induced by high energy PD activities, these reactions can produce atomic oxygen, ozone and nitrogen oxide, these are highly reactive molecules which can then react with the cavity surface to induce further damage [61]. The micro pits are hypothesized to initiate electrical trees by Montanari and Dissado [58, 11], and they can be the weak points to initiate cracking as the pressure with temperature under PD activities.

There are three main categories of PD degradation by-products identified from a cavity: gaseous, liquid droplets, and solids [62, 63]. Gaseous degradation by-products are mainly hydrogen, carbon monoxide and dioxide, and methane [64]. Carbonyl products are believed to be from oxidation of material fragments, it has been verified by experiments that energized charge carriers can break - CH₂ groups from polymer chains, as an approximate equivalence has been found between charge carriers from discharge activities and -CH₂ groups affected [65].

Liquid droplets are also widely discovered with many insulating materials, such as polyethylene, polypropylene, and epoxy resin [66]. It is also noticed that H, C, and O were essential for the production of liquid droplets, as there will be no droplet found when either one of the three is absent from the environment [67]. The formation of liquid droplets is due to the polymeric chain scission and oxidation, short chain fragments produced by which reactions are then dissolved in water to form droplets. Water in this case is induced by the oxidation process under PD activities,

experiments have shown that water can be formed when there is oxygen in the atmosphere inside the cavity, even with very dry air.

Liquid droplets are then precipitated to become solid crystals. These crystals can enhance the local electric field to a very high level, and bring PD activities to a much localized area around it. Pits or craters are discovered in the vicinity of crystals [65]. A strong injection of electrons at the pits has been discovered by using micro charge probes, this may be the indication of the treeing process as hypothesized by many other researchers [68].

However, the process from the formation of pitting to the final breakdown is short in terms of time. Earlier researchers discovered a quiet period without observable PD above measurement noise level before breakdown [69, 70]. Swarming discharge, also termed glow discharge or pitting discharge by some researchers was discovered by optical observation. Thus instead of no discharge at all, there are small discharge events under the noise level that keep occurring after the formation of craters, and only around the craters, until the final breakdown takes place [68, 54].

2.4.2 Interaction between PD behaviours, cavity air, and surface degradation

PD behaviours can include many aspects, such as individual pulse behaviours, pulse sequence behaviours, and accumulated PD behaviours. Early research mainly focused on individual pulse behaviours, while later on accumulated PD behaviours were also studied. Change in PD behaviours was interpreted in two major aspects: change of gas composition and cavity surface modification. Works from the major groups in this area are discussed in this section.

Sekii et al. observed a dropping trend in terms of pulse amplitude with 0.1mm flat cavities with both LDPE and epoxy resin, he also reported a difference in amplitude dropping rate depending on the concentration of oxygen. The reason for that amplitude drop is attributed to consumption of oxygen, which is an electronegative gas that can limit the number of electrons in the space as potential initial electrons for future avalanches. The consumption of oxygen leads to a richer reservoir of initial electrons, hence bring the discharge amplitude down [71]. Sekii also used an atomic force microscope (AFM) to observe the irregularity caused by PD activities on the material surface. In air, around 800nm – 900nm of irregularities were observed for both LDPE and epoxy resin in the first 200 hours of voltage application. In 99% nitrogen, only around 600nm of irregularities were induced under the same voltage application conditions [71]. In addition, different irregularity heights were reported with different concentration of oxygen in the environment, from 820nm in normal air, to 420nm when oxygen concentration was controlled at 5% [72]. Sekii and his colleges then went on to distinguish the difference between degradation

processes in different gaseous environment: the existence of oxygen was proved to be a key factor for surface deterioration under PD activities [73, 72]. Hence, the oxidation process is determined to have a key effect on the erosion of material surfaces. FTIR analysis with aged LDPE from the experiment reveals the production of carbonyl groups at 1715cm⁻¹ as oxidized polymers. In Sekii's later experiments antioxidants were used, results of which confirmed the suppression of oxidation processes when both irregularity height and the carbonyl group at 1715cm⁻¹ were both compressed [74]. Sekii and his colleges employed a chromatograph-mass spectrometer and a gas sampling system to confirm the relationship between oxidation process and the production of CO₂ [75], and also established a scheme of oxidative degradation of polymeric material and the possible use of antioxidants (Figure 2-2):

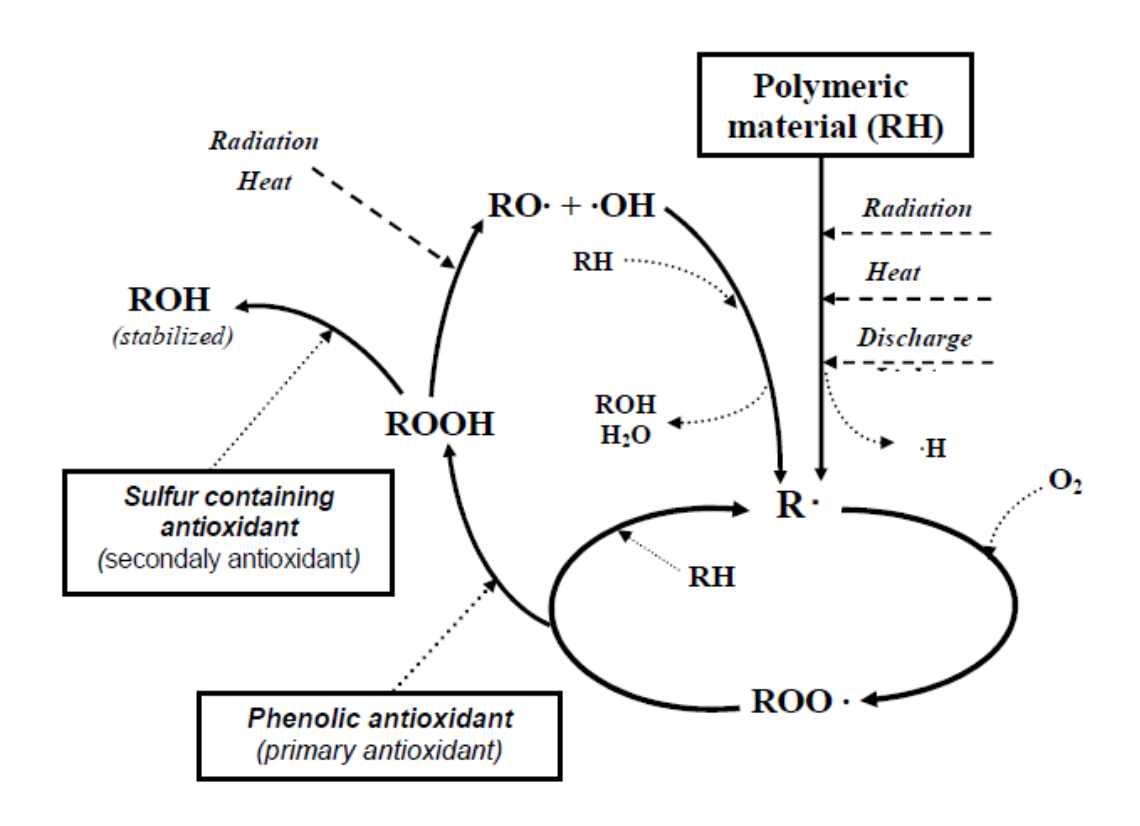


Figure 2-2: Chemical reaction during degradation by PD [23].

Mizutani et al. observed the change of PRPD patterns and individual pulse shape throughout the lifetime of LDPE sandwich samples containing a flat cavity. A general trend of PRPD pattern is shown in Figure 2-3.

Initially the "rabbit-like" pattern with short ears in Figure 2-3 (a) only lasted for a few minutes, this transition between (a) and (b) was explained by the consumption of oxygen due to LDPE oxidation under PD activities. Such consumption of electron negative gas would bring the PD level down, and eventually below the detectable level. Then observable PD occurred again after several hours as a "rabbit-like" form with long ears in stage (c), which was attributed to the production of

electronegative gases such as CO and CO₂, which could also explain why the first discharges after polarity reversal showed a longer delay and higher overvoltage ratio. Then it was suspected that due to the formation of pits, swarming PD events took place under noise level in stage (d). Stage (d) lasted for several hours, and then just before breakdown, electronegative gas content increased again to bring PD up to an observable level in stage (e).

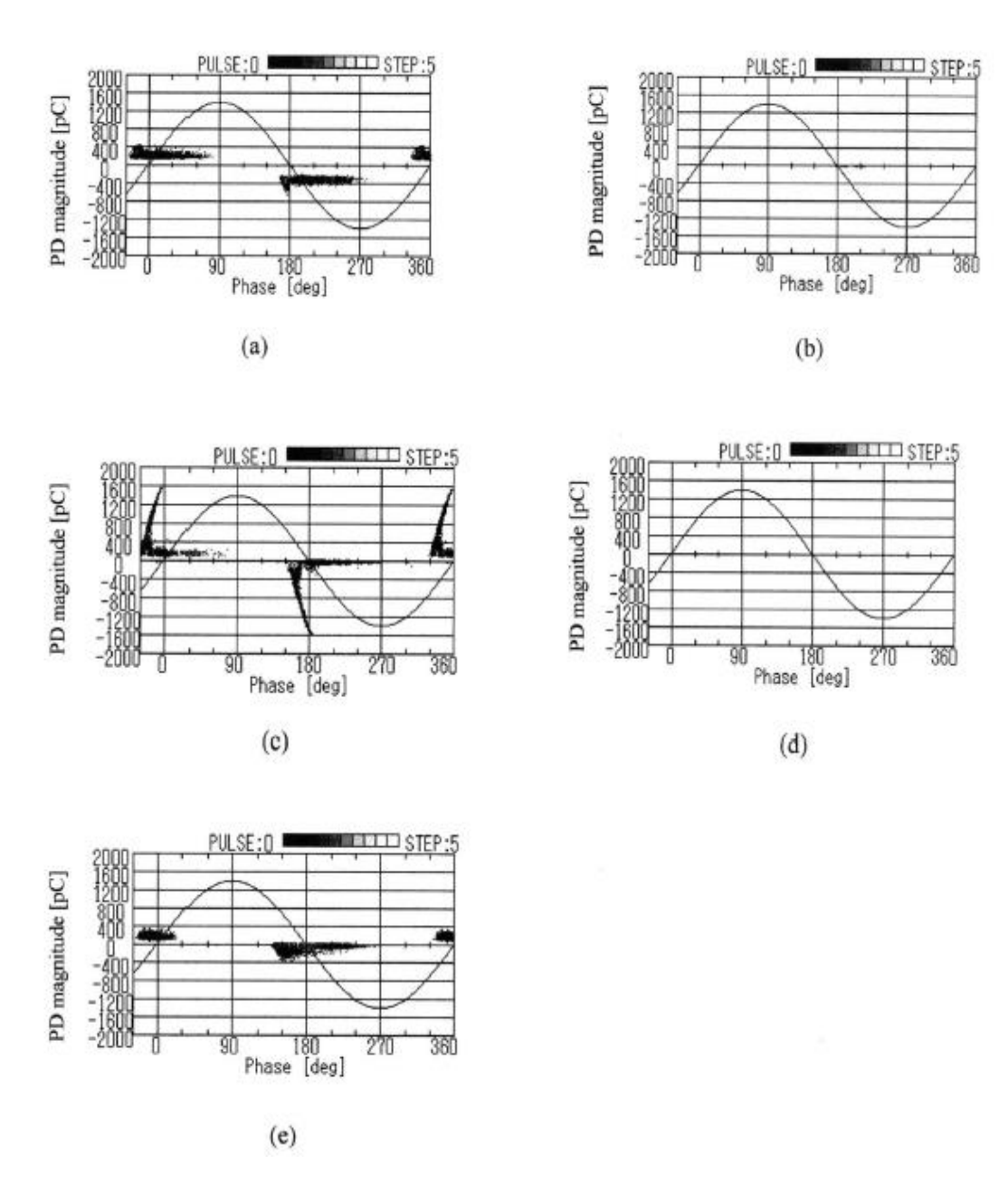


Figure 2-3: Degradation stages with LDPE by Mizutani [24].

Gas production was determined experimentally using a movable piston to measure gas volume inside the cavity, which reported a drop to 80% from stage (a) to (b), a rise to 95% to stage (c), then a slow decrease was reported until the final rise before breakdown [76]. Gas volume and density of electronegative gases are shown in Figure 2-4 and Figure 2-5.

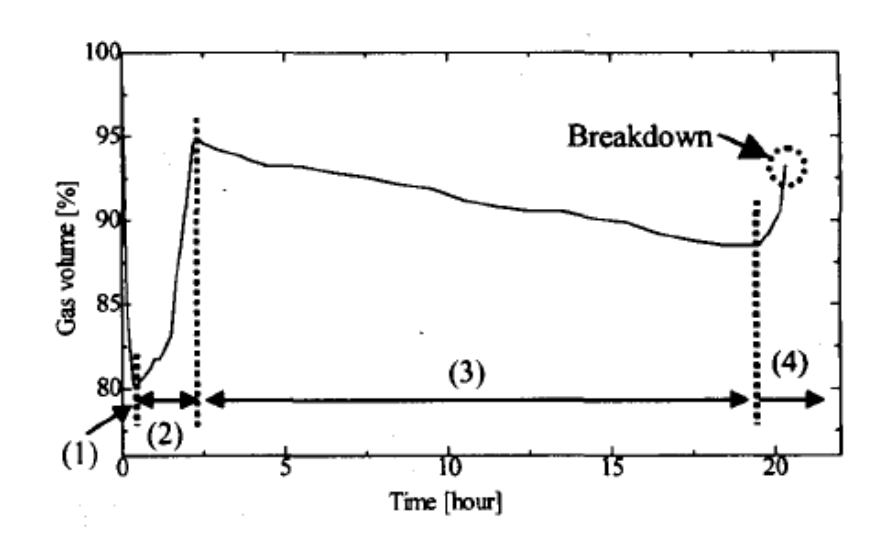


Figure 2-4: Gas volume throughout degradation time by PD [24].

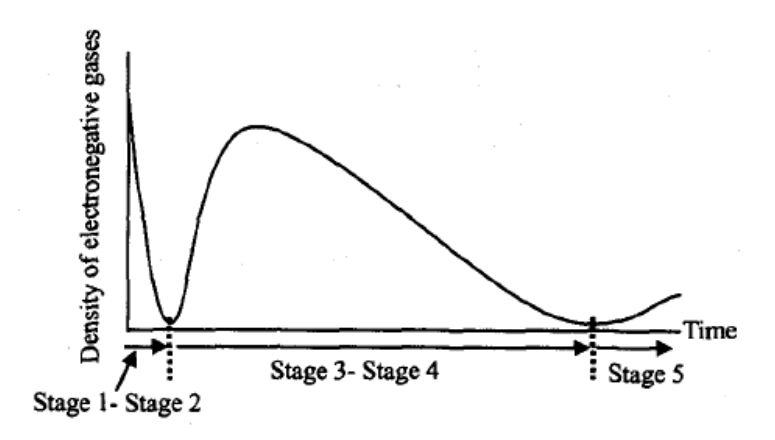


Figure 2-5: Electronegative gas density throughout degradation time by PD [24].

Ito et al. arrived at the same conclusion supporting this theory [77]. These works used optical microscopes to examine the cavity surface after degradation, and a change in individual pulse shapes was clearly observed in terms of pulse shape, rise time, decay time, and other characteristics such as kurtosis between degradation phases. Following up works done by Mizutani's group has repeated work done with LDPE [78, 79]

Air composition change in the cavity as discussed above has shown accurate correspondence with PRPD pattern transitioning, also it has been reported that with a cavity that can be reopened, introducing fresh air back in at any point during the degradation stages, PRPD pattern of the very first stage can be restored [80]. It can be expected that the concentration of electronegative gas and cavity surface conditions both can have an effect on PRPD pattern shapes, but between the two surface conditions are irreversible once modified by PD. Thus it may be difficult to draw any conclusion from LDPE experiments due to its surface degradation rate being too fast, thus its

entire lifetime can be significantly controlled by both air composition and surface conditions, and the relationship between the two cannot be distinguished easily.

Instead of air composition inside the cavities, some researchers focused on cavity surface deterioration instead. Morshuis reported a general PD individual pulse behaviour transition from streamer discharge to Townsend discharge after 5 minutes to 5 hours, and eventually to pitting discharge after 10 hours to 100 hours with polyethylene sandwich samples [81]. The transition from streamer type to Townsend type is attributed to the formation of a conductive layer on cavity surfaces, which could lower the electron detrapping work function, thus discharges shall happen with shorter delay [82]. This layer was observed to be acid droplets, and a rise of conductivity was measured by two electrodes painted with conductive paints. In the Townsend discharge stage, acid liquid droplets turn into solid crystals due to hydration, and grow into large crystal clusters. The formation of these large conductive clusters can result in pitting discharge as termed by Morshuis [83]. Pitting discharge events are much localized due to the electric field distortion, and also the abundant charge supply from conductive pits. Optical observation of PD events by a CCD camera was performed in parallel with high frequency electrical detection system, finding significant differences in PD behaviours for all three stages as displayed in Figure 2-6.

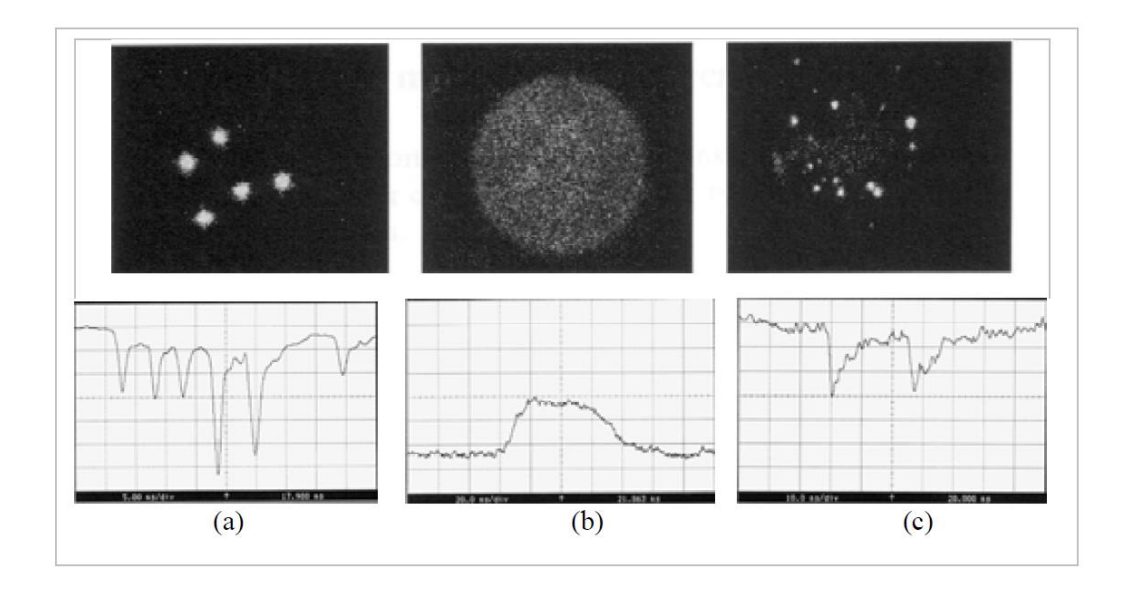


Figure 2-6: PD pulse shape vs. discharge area [84].

Initially the pulse shape was divided into different groups by simple characteristics: streamer discharges have high magnitude but small width, in accompany with small area but intensive light registered by the camera; Townsend discharges have lower magnitude but large width, discharge light for which is dispersed and not so intensive; Pitting discharges have very low magnitude and small width, happening only at specific points where pitting is happening as registered by the camera.

Hudon studied discharge between two epoxy resin coated electrodes in an unvented test cell, and concluded similar results as Morshuis [85], with the transition timings being 180-320 hours from streamer to Townsend type, and 800 hours for pitting discharge to initiate. During the degradation process liquid droplets and solid crystals were also observed. Furthermore, a saturation of surface conductivity was reported at around 200 hours. Conductivity of the surface rises from 10^{-16} (Ω -cm) $^{-1}$ to a saturated value of 10^{-10} (Ω -cm) $^{-1}$. Similar results were reported in [86]. It is interesting to see that the saturation time was very close to the transition time from streamer to Townsend type of discharge, which is also the time when liquid droplets over the entire surface start to turn into crystal clusters. This indicates that since the initiation of Townsend discharge and solid crystals, degradation on the surface by PD has turned into localized scale.

Hudon also used pure O_2 and pure N_2 to determine that oxygen is the main source of chemical degradation processes. X-ray photoelectron spectroscopy (XPS) was used to find 58% of O_2 and 42% of carbon in degradation by-products. Also, an experiment in open air showed that the discharge pattern transition took place regardless to air composition and pressure [87]. This as discussed with Sekii's and Mizutani's work where LDPE was used, air composition played an important role in PD behaviour transitioning, due to the lifetime of LDPE was too short to show separate affects of surface deterioration from air composition change.

From Figure 2-7, degradation by-products under XPS analysis was determined to be mainly carboxylic (COOH) and ester (COOR) groups, concentration of which raised from 10% (virgin sample) to 18% (transition to Townsend discharge) to 29% (transition to pitting discharge). Formation of these by-products was attributed to polymer radicals generated by PD activities including electron and ion bombardment, UV radiation, thermal energy transfer, etc. These radicals react with oxygen via peroxide reaction to generate organic hydroperoxide ROOH, which in turn attacks the cavity surface to produce carbonyl groups [88]. Furthermore, the oxygen/carbon ratio in the by-products was rising throughout the experimental period under electron spectroscopy for chemical analysis (ESCA), suggesting continuous oxidation activities although the test was taken place in unvented test cells [89].

Exp.	C-H	C-O-R	C=O	COOH	0	C
time	C-C	C-OH	0-C-0	COOR		
h	C_1	C_2	C_4	Сз	ļ	
0	61.0	28.0	< 1.0	10.0	27	73
240	45.0	34.0	3.0	18.0	44	56
1000	32.0	34.0	5.0	29.0	52	48

Figure 2-7: XPS scan on epoxy resin aged by PD [54].

Also, a degradation process was reported to have created a carbonized layer below the cavity surface. The dark layer had its depth saturated at 300µm with a degradation time of 1745 hours, after which time only the colour went darker with further PD stressed applied [89].

Hepburn utilized FTIR to achieve similar results when analyzing degradation by-products in epoxy resin cavities [90, 91, 92], who determined O, C, H, N are the main reactive radicals in air atmosphere. With oxygen present, peroxy, carbonyl, oxalic and formic acid groups are major products of PD degradation.

Cavity air composition and surface deterioration under PD for polymeric materials are well studied as discussed above, yet there has been very limited number of attempts to summarize the findings into a degradation model. A number of difficulties in simulating cavity PD degradation up to this stage can be defined if summarizing above discussions.

Firstly, most research works focuses on identifying degradation stages by individual pulse behaviour, especially with the case of epoxy resin, there has not been any mature attempt to establish the relationship between accumulated PD behaviour and degradation level under PD stress. For polyethylene, most works were carried out with LDPE if accumulated PD behaviour was concerned, in which case air composition was the main factor to control PRPD pattern transition, and the material indeed needed longer lifetime if any surface deterioration effect could be studied with it. Thus, degradation as an accumulated effect over the material cannot be simulated without the knowledge of accumulated PD behaviour throughout the lifetime.

Secondly, the degradation effect by PD is hard to quantify. Sanche's work [56] quantified degradation by individual electrons to a certain degree, but only with LDPE. Also, a linear injection of electron beam is very different from real cavity PD events, to utilize Sanche's findings, the accumulated PD behaviour is essential, not to mention the accumulated behaviour can vary with all sorts of geometrical and insulating material change of the cavities.

Thirdly, PD degradation has its induced effects, such as pressure and thermal effects, which for instance can crack epoxy resin and burn silicone rubber or PE on top of charge bombardment and chemical reactions induced. Thus understanding these induced effects is also essential for an accurate degradation model.

Thus, to have a physical degradation model for cavity PD, three separate physical effects need to be considered. 1: Pure charge bombardment and chemical reactions related to the specific type of material and for all possible charge carrier energy levels; 2: induced mechanical and thermal effects to the material by PD activities; 3: accumulated PD behaviour. Montanari [93] was one of the very firsts trying to establish a physical cavity PD degradation model. Sanche's work is utilized

to fulfil requirement 1 as discussed in previous subsection; requirement 2 at the moment has not been considered; and for requirement 3, the PD behaviour is summarized by multiplying number of charges from individual discharge events to the repetition rate [94].

This model defined the degradation stages also by PD repetition rate N_w and average discharge magnitude Q_{alfa} [94] as shown in Figure 2-8.

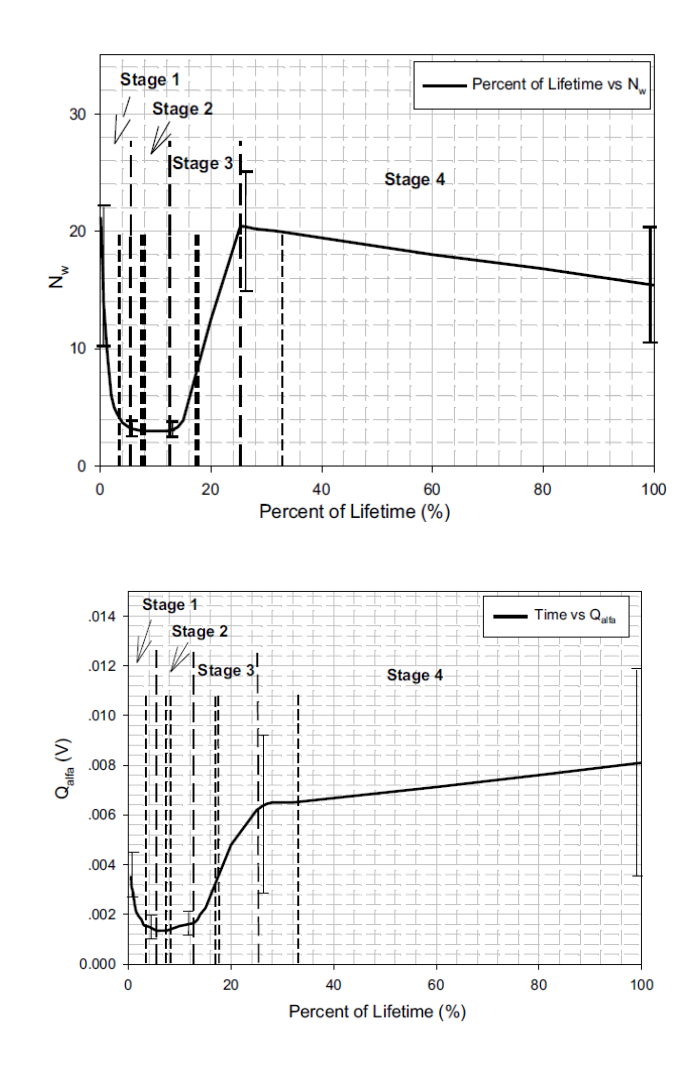


Figure 2-8: Degradation stages defined by impact charge magnitude [95].

Despite the clear stage transition in terms of N_w and Q_{alfa} , PRPD patterns of the PE sandwich samples used were not showing much change, instead the patterns were "rabbit-like" ones throughout the degradation life. Also, experiments were carried out under constant gas pressure and constant gas volume inside the cavity [96, 97], results of which was not much different from the ones shown above.

A simulation model based on N_w * Q_{alfa} , which is the total charge landed on insulation surface was then produced [93, 58, 57], in combination of Sanche's theory and an avalanche model to simulate electron avalanches and their final electron energy distribution [58].

2.5 Summary

Degradation models including phenomenological and physical models have been discussed in this chapter. Earlier phenomenological models consider the degradation process of polymeric materials under electric stress as simple energy/damage relationships. Most physical models also consider degradation as thermal/mechanical processes, and take the enlargement of free space in the material as the end point if the free space is large enough to trigger PD. As far as PD degradation is concerned, the most up to date model is that of Montanari which is designed by looking into electron avalanches down to the level of single electron motion, and simulating the avalanches using the energy and the speed carried by electrons. However, this seems to be the end point of our current knowledge about PD, a conclusion can be drawn that PD events from virgin cavities are very well understood, and beyond a virgin cavity is the area we do not have complete understanding. Montanari's model has provided a very good foundation to look into the unknown area, as we are now working with single electrons instead of electron avalanches carrying a certain amount of energy. So, how PD will damage the insulation, and how the damage sites can come back to affect future PD behaviour, and how this loop can go on until insulation failure are what is lacking in the knowledge database. What exactly happens from cavity partial discharge to final breakdown is the question that this project aims to answer.

Chapter 3: Test Samples and Experimental Methods

This Chapter details the preparation of test samples, experimental setup, initial tests for prepared samples, validation tests for experimental methods and test rigs. Test samples used for this study are made from epoxy resin. Samples take a disk shape with a single air filled cavity injected in the middle during epoxy resin curing process. Initial experiments were conducted alongside with a cavity PD project with silicone rubber in TDHVL as a reference and calibration method for the test system. Ideally multiple samples need to be stressed and observed simultaneously for better efficiency of experiments, as epoxy resin is a very resilient insulating material. Thus multiple channel experiment was designed and tested. Solutions to issues occurred such as cross-talk between channels is documented in this chapter.

3.1 Test samples

Three types of samples have been considered: epoxy resin with injected cavity, LDPE with cavities created using a foaming agent, and a LDPE sandwich containing a cylindrical cavity. In this report, epoxy resin samples are developed, various methods used to control sample quality are reported. Preparation method for LDPE/XLPE sandwich sample is mature and has been used extensively for research at the University of Bologna, but it only produces cylindrical cavities. The use of foaming agent was not considered due to its possible physical and chemical effect during the degradation process. Epoxy resin was finally chosen due to its excellent mechanical and thermal properties, as this would help to isolate degradation purely by PD instead of studying a mixture of damage by PD, mechanical stress, and thermal breakdown at the same time.

3.1.1 Epoxy Resin Samples

Epoxy resin is a highly cross-linked addition polymer. As a thermosetting polymer, it cures when mixed with a hardener under various temperatures depending on the properties of the epoxy resin and the hardener [98]. Epoxy resin generally has high viscosity from the cross linking, but still lower than PE, hence bubble injection with a syringe becomes possible during the curing process. Curing time can be handled by adjusting curing temperature [99].

Apart from being a very good electrical insulator, epoxy resin possesses excellent mechanical strength, thermal stability, and chemical resistance. Its properties can be further enhanced by a post curing process, usually at high temperature levels. Epoxy resin is frequently used as a solid insulating material in a wide range of equipment, for instance generators, motors, transformers, bushings, and switchgear.

Epoxy resin samples in this study are required to contain an air filled spherical cavity, ideally located exactly in the middle along the applied field direction, allowing enough space for any potential degradation to grow into before final breakdown. Samples are also required to be transparent to allow non-destructive optical inspection.

3.1.1.1 Epoxy resin curing method

The chosen epoxy resin was D.E.R. 332 from Sigma Aldrich, and hardener was Jeffamine D-230 from Huntsman. Other epoxy resin and hardener pairs were also tested, such as Araldite Rapid from Huntsman, for which bubble injection was much easier to handle as it cures at room temperature. Jeffamine D230 as a hardener could produce very clear transparent samples, which could allow non-destructive optical observation of the cavity. On the other hand, other epoxy resin/hardener combinations tested could not provide transparency. Hence D.E.R. 332 and Jeffamine D230 were selected.

Before preparing the sample, the epoxy resin jar should be put into a water bath at 50°C with the lid open, because the resin used solidifies itself at room temperature. After all the epoxy resin has turned into liquid, resin and hardener are mixed with an exact resin/hardener ratio of 1000/344 by weight. When mixing, it is important to ensure that the hardener is poured into the epoxy resin, this is due to the high viscosity of epoxy resin than the hardener used. The mixture should be stirred at 50°C for at least 15 minutes, and an electrical stirrer was used for this purpose. 50°C was found to be the optimum temperature when working with this epoxy resin and hardener mixture, as at this temperature the mixture was highly fluid and could stay in that condition for a reasonable period of time (e.g. several hours). Temperature overshot can result in resin mixture curing easily.

After mixing the epoxy resin and the hardener, the mixture was poured into moulds. Moulds used in this project were silicone rubber tins, which were found to be the best practice working with epoxy resin, as cured samples could be easily removed from silicone rubber containers with no removing agent needed. Syringe injectors and an electronic balance were used when distributing the mixture into the moulds. A vacuum oven should be preheated to 50°C, and used to degas the samples. Degassing takes at least 20 minutes, if visible bubbles still exist after degassing, a longer time should be applied.

Samples removed from the vacuum oven need to be immediately placed into a preheated 100°C fan oven for the curing process, or kept at 50°C. With the selected epoxy resin/hardener combination, a curing temperature of 100°C and a curing time of 24 hours are being applied.

3.1.1.2 Cavity injection

During the curing process, a cavity filled with air could be injected vertically from the top by a precise needle injector (Hamilton precise syringe 600 series, 2.5 µL, supplied by Sigma-Aldrich), with a precise timing when the epoxy resin/hardener mixture had a certain viscosity during precuring. It was noticed that the mixture taken out from the curing oven could still turn solid rapidly with the remaining heat carried, thus the bubble injection must be quick and precise.

Samples produced were 2.8mm thick disks with 4.5g of resin/hardener mixture. A single cavities filled with air is injected by pushing 0.524 μ L of air (room temperature and pressure at the time of manufacturing) to produce a spherical cavity with diameter of 1mm. The accuracy of air volume injected was only manually controlled handling the precise syringe, however, the size of the bubble injected would go through another selection process as illustrated in Figure 3-7.

Samples made with above method were clean, transparent, cylindrical disks with a 1mm \pm 100 μ m diameter spherical cavity in the middle. No trace of the injecting needle was observed post cure. Figure 3-1 shows a completed sample, which is a circular disk with 50mm diameter, 2.8mm thickness, and 1mm diameter cavity injected in the middle.

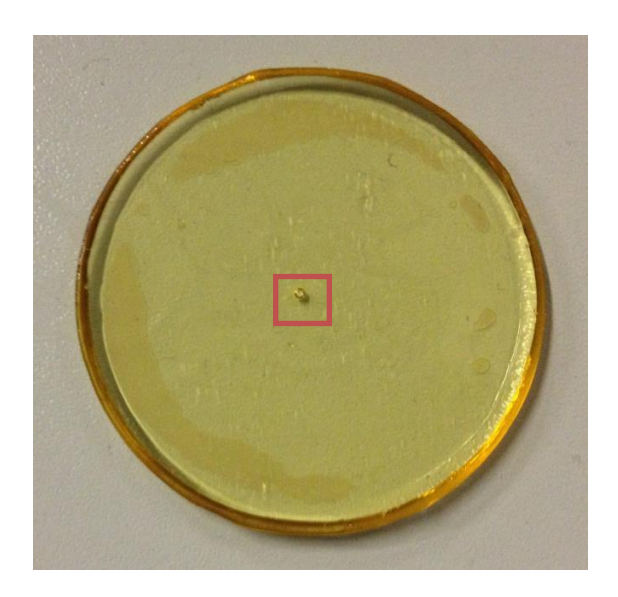


Figure 3-1: Completed sample, cavities are circled in red.

Samples were produced by combining two layers, due to the buoyancy force would not allow the cavity to remain in the middle as expected. The bottom layer carries the cavity on its top, the top layer then covers the bottom one with calculated thickness. There were two assumptions with this approach: Firstly, epoxy resin layers could combine without compromising mechanical properties, which means one sample of epoxy resin could be cured into or adjacent to another previously cured sample without any gap in between. Although the interface might still be detectable under electrical stress, it should only cause minimum effects to the experiment as it

was perpendicular to applied field direction. Figure 3-2 shows an interface of two combined pieces of epoxy resin, this confirms a good combination of two separate blocks of epoxy resin, as no trace of the combination interface can be observed in the picture.



Figure 3-2: Interface of two combined pieces of epoxy resin

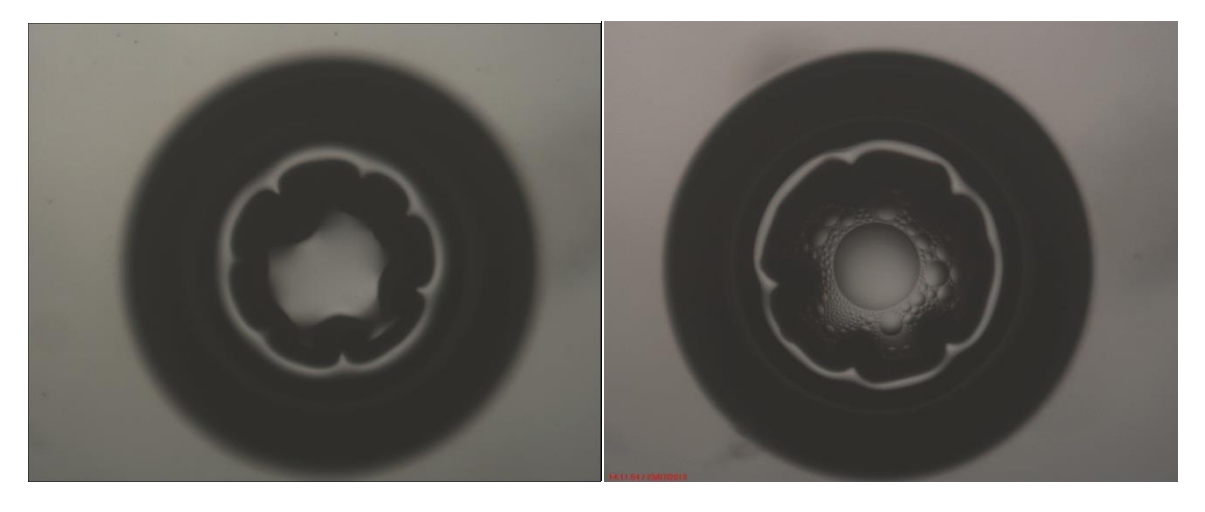
Secondly, the cavity injection timing must be as early as possible during the curing process. This ensured that the resin would flow to remove any needle trace, and the bubble under buoyancy force would move to the top of the sample so that its vertical positioning is guaranteed. Then placing another epoxy resin layer with calculated thickness on top would ensure that the cavity is in the middle of the combined block. A potential issue for early injection was when the bubble moves, its shape might change, Figure 3-3 shows a cavity created by early injection and flew up to the top, and still is spherically shaped.



Figure 3-3: bubble injected early flows up due to buoyancy force

Prepared samples were 2.8 mm thick disks, a cavity with diameter of 1mm \pm 100 μ m was placed vertically in the middle, leaving 0.9 mm both to the top and to the bottom of the sample. The shape of prepared samples was a thin disk with curved edge for better electric field distribution. Two flat surfaces on top and bottom were of 50 mm diameter and 45 mm diameter respectively. The colour of samples was bright brown, with good visual transparency in the top-bottom direction, but difficult to see through the edge.

However, some samples produced with this method were found to contain defects under microscopic inspection. Failed samples had cavities with rather symmetrical salient patterns on the surface shown in Figure 3-4.



(macro shape defect between two layers)

(macro shape + micro droplets between layers)

Figure 3-4: Defects induced by the introduction of the second layer.

The bottom layer of these failed samples had good spherical cavities before combining with the top layers. Figure 3-5 shows a typical cavity without the top layer.

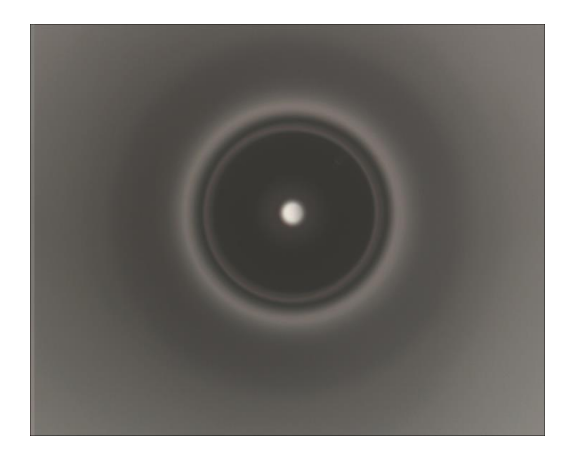


Figure 3-5: First layer image that all failed samples started with.

From Figure 3-5 and Figure 3-4, it can be seen that the cavity itself was unchanged as a spherical void with smooth surface, but the covering of second layer on top produced the patterns in Figure 3-4. It was found that a combination of effects from fan oven vibration and fast second layer curing at 100°C was causing this matter. This was because the cavity top exceed the upper surface of the bottom layer due to buoyancy force, thus a quick change of top layer viscosity did not allow a perfect covering on top of the cavity, especially when the top layer itself was curing very quickly, allowing the covering to take place within very limited time and in a vibrating environment produced by the fan oven. A lower temperature (75°C) was found capable to cure the top layer in

a fan-free oven to produce a good combination, and then the curing temperature could be gradually increased to 100°C after the top layer turned solid.

Microscopic images of successfully prepared samples are shown in Figure 3-6, and cavity size measurements can be seen in Figure 3-7.

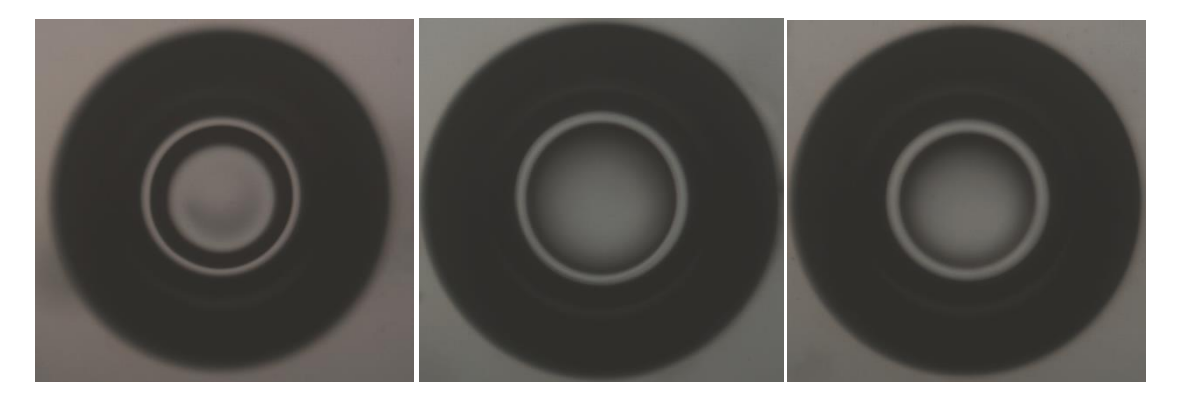


Figure 3-6: Microscopic images of well-made epoxy resin samples.



Figure 3-7: Microscopic size measuring of cavities.

The double layer method was proved successful, and the detailed production procedure is finalized as follows:

- Blend epoxy resin (SIGMA D.E.R.[™] 332) and hardener (Jeffamine D-230 from HUNTSMAN)
 with the ratio of 1000:334 by weight.
- Stir the mixture at 50° C for at least 15 minutes.
- Put 3.5g mixture into the mould, this will produce a 1.9 mm thick bottom layer including the cavity to be injected later.
- Degas for at least 30 minutes at 50° C. The degassing procedure can last longer if necessary, however, it will affect the injection timing if the samples stays in the vacuum oven over 60 minutes at 50° C.
- Transfer the specimen quickly into a 100° C oven, for 10 minutes 40 seconds.
- Injection, 0.524 μ L of air was injected by the precise syringe to create a spherical cavity with diameter of 1mm \pm 100 μ m.
- Put the specimen back into the 100° C oven immediately after injection, cure for 24

hours. This will cause some difference regarding the cross-linking or thermal ageing level of the two layers, but the bottom layer must be cured to a certain level, so that the thin film covering the cavity can sustain the pressure during the degassing and post curing of the top layer, otherwise the cavity wall will break and allow liquid epoxy resin from the top layer to flow into it.

- Blend an overall 1.5g of epoxy resin and hardener mixture, again with the ratio of 1000:344 by weight. This will produce a 0.9 mm top layer.
- Stir the mixture at 50° C for at least 15 minutes.
- Put the mixture on top of the bottom layer in the mould. Do not take the bottom layer
 out of the mould before the entire sample is cured, otherwise the thickness ratio between
 the two layers and cavity position cannot be guaranteed.
- Degas at 50° C for at least 30 minutes. Extend this procedure as long as needed until all unwanted air is removed.
- Cure at 75° C for at least 4 hours. Check using a microscope for cavity surface combination before the final curing process.
- Final curing at 100° C, for at least 24 hours.

3.2 Experimental Methods

The objective of the experimental part of this research is to observe the unknown link between cavity partial discharge and degradation until final breakdown of polymeric insulation materials. Due to differences in terms of material properties, ageing and degradation mechanisms can vary from material to material, even with the same material under similar stressing and discharging conditions.

Previous work at the Tony Davies High Voltage Laboratory has investigated degradation of silicone rubber samples with single injected cavities. The major hypothesis of this experiment was that if multiple identical samples can be stressed under identical conditions until one fails, then the others might carry different levels of degradation sites which could be observed. Along with the ageing and degradation process, PD signals were also recorded using Phase-Resolved Partial Discharge Analysis (PRPDA). Recorded PD signals were studied to improve understanding of ageing and degradation, and vice versa.

Work described in this section started with the experiments with silicone rubber, it was regarded as the initial validation tests to examine the experimental design, and as a calibration between different experimental setup and PD measurement systems.

3.2.1 Test sample setup

Figure 3-8 shows the high voltage electrode and ground electrode with the test rig. The upper high voltage electrode on the right hand side had a diameter of 130mm. The ground electrode was combined with 5 smaller electrodes of 15mm diameter, placed onto the larger electrode which was the same size as the HV one. All electrodes were made of stainless steel.

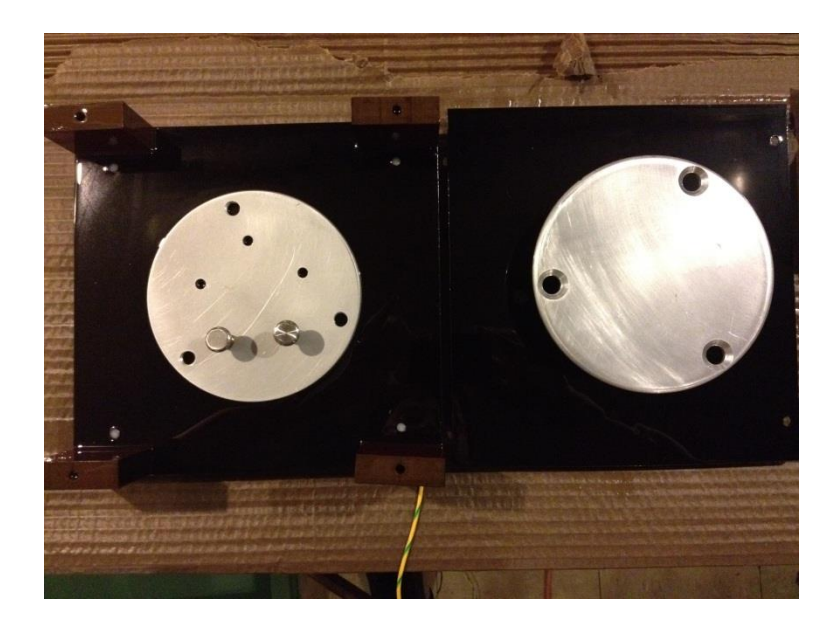


Figure 3-8: HV and ground electrodes with test rig.

The test samples were held by a test rig as shown in Figure 3-9. The test rig was made from Paxolin, with plastic screw connections, 220mm×220mm in size. A 22mm diameter copper pipe was used for high voltage connection, and a copper wire was used for ground connection.



Figure 3-9: Test rig setup.

The test rig was immersed in silicone oil bath to prevent potential surface discharge. The silicone oil had a breakdown field of 15kV/mm. A silicone oil bath was utilized due to its higher dielectric strength than air.

3.2.2 Experiment setup

The PD measurement unit used for the experiment was PDBaseII, manufactured by TechImp Spa, Italy. Alongside with PDBaseII, an Mtronix MOD 600 from OMICRON was also used as a synchronization check during the validation experiments. PDBaseII is a fully digital system, specifically designed for laboratory PD measurements. This system provides advantages over the Mtronix system by allowing simultaneous multiple channel acquisition (4 channels) and greater manual control and adjustment especially considering functions such as noise filtering and cluster mapping.

A full setup of the experiment is shown in Figure 3-10. It was constructed using a high voltage supply consisting of a control unit and step up transformer, a high voltage filter, a coupling capacitor, the test specimen, and PD measurement units with a coupling device. High voltage connections were constructed with copper tubes, and ground connections were established using copper wires. Both PD measurement units were connected to a personal computer (PC) via fibre optic cables in order to store captured data and undertake further analysis.

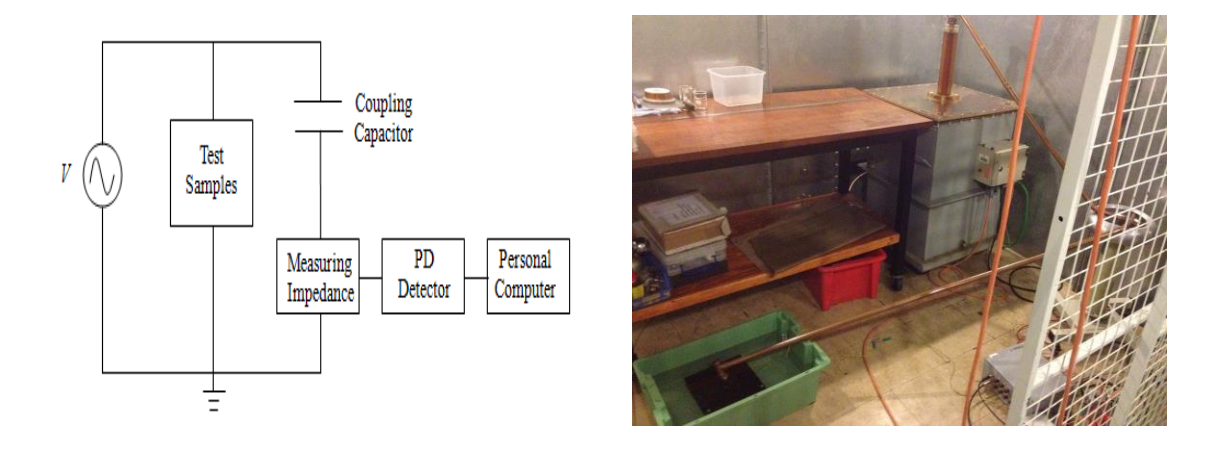


Figure 3-10: Full setup of multiple samples stressing experiment.

The voltage source combined with a 1V/2000V amplifier had a range from 0kV to 20kV peak to peak, with an input impedance of $25k\Omega$ nominal. The coupling capacitor was 1nF. The graphical user interface (GUI) was PDBaseII Standard version 5td1.01.12, with PD Framework version 01.02.52, and PD Support version 01.01.42.

3.2.3 System calibration

Every restart of the system required a calibration procedure for the entire system. Both PDBaseII and Mtronix allow digital calibration. A digital calibrator was used to input a target discharge magnitude, allowing the measurement units to pick up and adjust the readings to the target value.

Under IEC Standard 60627 mode with PDBaseII, it could be done automatically once the target value has been set with the GUI. When using the Wide Band (WB) mode of PDBaseII, a calibrated ratio between the input PD magnitude in pC and measurement readings in Volts must be recorded for future conversion between the two.

The calibrator used in this work was the Mtronix CAL 542 manufactured by OMICRON. The calibration signal used had a range of 1pC to 100pC.

3.2.4 Initial Validation Tests

PDBaseII had multiple bandwidth choices when measuring PD signals. As a starting point, it was set to IEC Standard 60270, which corresponds to the Mtronix settings, to confirm that there was a fine synchronization between the two measurement units. Calibration tests and simple PD tests were carried out, and the results confirmed that the two measurement units were reporting the same readings.

3.2.4.1 Multiple silicone rubber sample tests

Full load tests with five silicone rubber samples were performed after validating the functionality of the entire system. There were foreseeable similarities between this experiment with silicone rubber and the future ones with other materials.

Through the degradation process, recorded PRPD signals generally had four characteristic forms, normally: "turtle-like" pattern, rabbit ear pattern, minor discharge pattern, and no discharge. The aim of the silicone rubber project was to investigate the chemical and physical degradation of silicone rubber, and to see if it was possible to produce any bush-branch type of electrical trees from cavity PD, hence a five sample simultaneous stressing experiment was developed to meet these objectives. However, knowledge gained from this type of experiment was mostly from degraded samples and improvements of the experimental technique to ensure repeatable degradation. However, the partial discharge behaviour recorded offers limited knowledge of the degradation process. This is due to the difficulties in allocating individual samples to a particular PD behaviour accordingly, as signals from individual samples could not be separated from superpositioned PRPD patterns captured.

Successfully acquired degraded samples were samples with observable pitting sites. Failed samples offered no knowledge on how pitting led to failure due to a complete thermal destruction along the field direction covered all evidence. Information was very limited because failed samples and degraded samples were not the same ones, so there was no guarantee that

they had been through the same degradation process for which the only difference was degradation level.

Nevertheless, treeing PD patterns have been observed with silicone rubber samples containing a high voltage needle electrode, conducting channel discharge patterns have been reported in published literature for a range of different materials. Published works [98, 99] observe this type of PD patterns using needle electrodes, which can act as infinite hot electron sources to achieve polymeric bond breaking in order to facilitate bush-branch type treeing. Although the discharging sources are different, published works confirm treeing PD patterns accompany the growth of electrical trees by the fact that these patterns are only observed when an electrical tree is growing. High speed cameras were used to help observe tree growth. Thus, treeing PD patterns are generally regarded as the discharge pattern from conducting treeing channels instead of PD from the cavity itself.

Treeing was not observed in silicone rubber experiments due to the switching off timing to reserve degraded samples with possible electrical trees instead of failed ones, among which the failed ones would have all evidence of degradation destroyed during the thermal process of failing. To date no experimental evidence of tree growth from a cavity without the presence of a sharp and conducting electrode has been reported.

3.2.5 Epoxy resin validation tests

Epoxy resin as an insulating material is different from silicone rubber in terms of many properties, especially thermal and mechanical properties. Life cycle experiments with epoxy resin will occupy much longer time period than the ones with silicone rubber, in which case detailed behaviour of individual samples during a multiple sample stressing test cannot be neglected. Thus, stressing experiment with both single and multiple epoxy resin samples were conducted to examine the possibility observing the PD behaviour of each individual sample during a multiple sample test.

3.2.5.1 System PD tests

The system was put through a PD test without the test rig being connected, to make sure there were no other discharge sources within the system circuit. The circuit was PD free under 20kV of applied voltage for 10 minutes, which was the maximum stress it would experience due to the flashover threshold for samples of suitable size. The experiment was repeated with the test rig connected, using a cavity free epoxy resin disk as the test sample. The whole system remained PD free under an applied voltage of 20kV for 10 minutes, which justified that the test rig was capable

for the experiments, and that the sample dimensions were large enough to ensure no surface discharging.

3.2.5.2 Single sample PD inception and extinction voltage tests

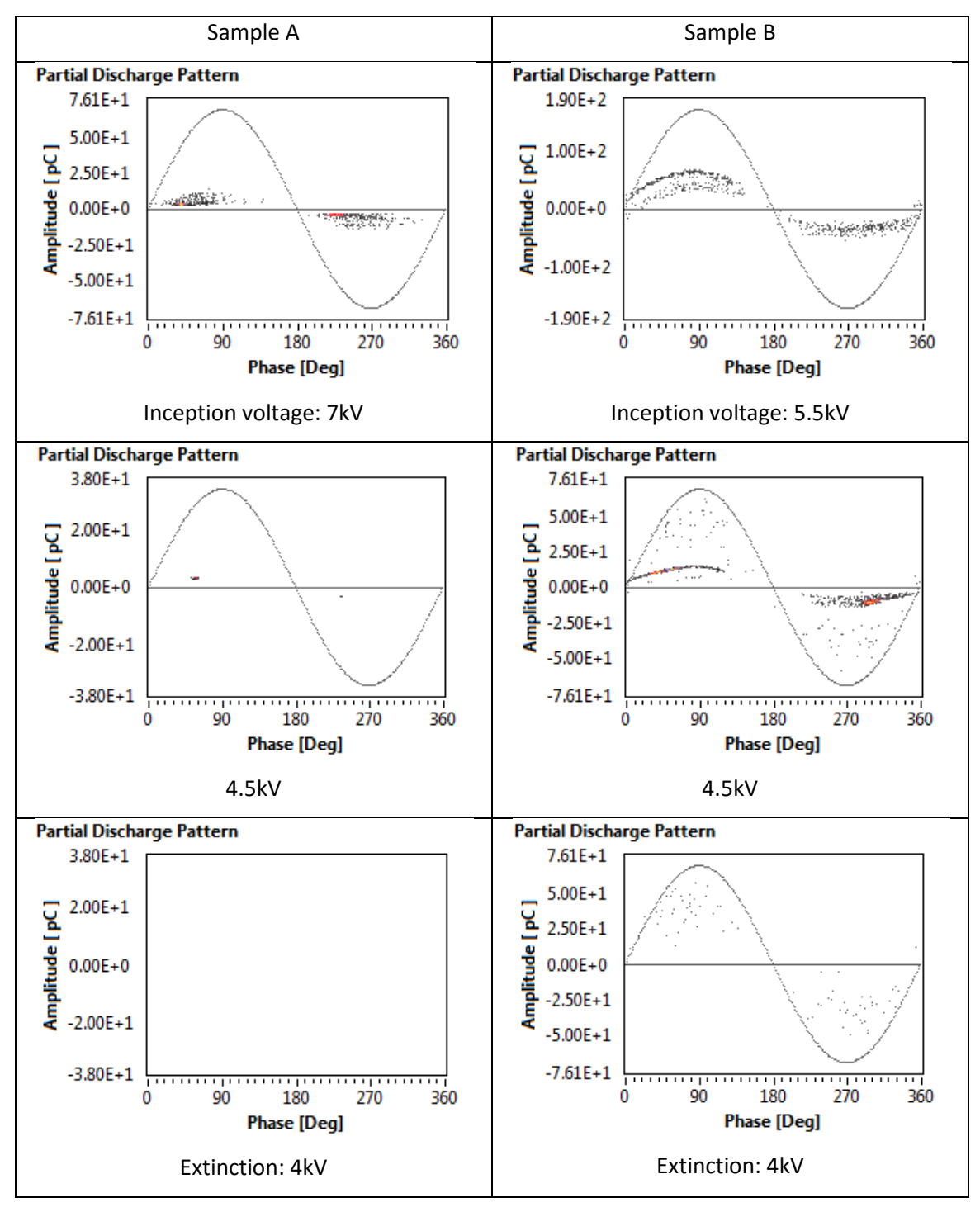


Figure 3-11: Epoxy resin sample inception and extinction voltage test.

PD inception voltage or extinction voltage were recorded by increasing or decreasing applied voltage with 1kV steps, for each step 1500 cycles (30 seconds) were given for PD to occur or cease before proceeding to the next voltage level.

Two samples were put through tests. Sample A had its inception on 7kV, and a complete extinction on 4kV; sample B had PD inception on 5.5kV, and extinction on 4kV.

With reference to Figure 3-11, the 4kV PRPD pattern for sample B was cleared as soon as the voltage got lower than 4kV, thus 4kV was determined to be the extinction voltage.

3.3 Summary

In this chapter the epoxy sample preparation method is reported, including air filled cavity injection technique and precise cavity locating method. Prepared samples were 2.8mm thick disks with a 1mm diameter cavity located in the middle, 0.9mm away from both top and bottom surface of the sample. A multiple sample simultaneous PD experiment was designed. It was found that cross-talk was the major issue with the experiment designed. Mechanisms to conduct cross-talk were investigated, and solutions based on data post processing were provided. A maximum number of 3 samples could be observed simultaneously, this number limit was determined by experimental space available to eliminate cross-talk. It was decided that for epoxy resin PD experiments the data acquisition was going to be off-line, which means to turn the stress off and test all samples one by one. This was because epoxy resin life cycle was determined to usually last for longer than 1000 hours, thus real time observation was not practical. However, off-line PD measurements do have limitations, as although PD behaviours are mostly dominant by cavity surface conditions, it is still dependent on other conditions such as cavity gas randomness of first electron production. Thus the samples must be given a certain period of time under stress to restore their PD behaviours under constant stress.

Chapter 4: Epoxy Resin Degradation Experiments

This chapter reports degradation experimental results for epoxy resin samples introduced in the previous chapter. Full length degradation experiments were conducted over 2000 hours. PD data was acquired for each sample individually at regular time intervals. Features from PRPD data were analyzed and reported in this chapter, followed by PD pulse sequence behaviour analysis in time domain, and also microscopic imaging results at degradation surfaces for each specimen.

A number of validation experiments were initially conducted. Sample group A was used for simultaneous PD data acquisition test only. Sample group B was used for a 2000 hours degradation test with four specimens, in order to have an overall understanding of the possible time span of the test, degradation behaviours, and key features of data acquired. Then a full 2000 hour degradation experiment was carried out including 16 samples labelled as sample group C, with a slight modification made due to initial experimental findings.

Results from group C in general repeated the findings with group B in terms of degradation stages marked by typical PRPD patterns. In addition, a detailed pulse sequence study was carried out for sample group C as PD data were acquired with longer acquisition time to fit the purpose of such studies. Pulse sequence behaviour in time domain was discovered as the major source of information as far as the estimation of degradation level was concerned.

4.1 Validation tests and initial degradation experiments

Group A samples were used for experimental method tests. The initial idea was to utilize the full four channels on PDBase II, so that all four samples could be monitored online with each sample assigned to its respective channel. However this idea was proved unsuccessful due to airborne and common ground feedforward interference.

Group B samples were then assigned to a long term degradation experiment under 17kV, which lasted 2100 hours without final breakdown in any of the four samples used. PD triggering threshold was set constant at 3pC throughout the experiment. Samples were stressed for every 48 hours in between two consecutive PD data acquisition. Every PD acquisition generated a PRPD data file with 30s or a maximum of 20,000 data points as the limit. Whilst data acquisition electric stress on all samples was stopped as degradation stressing and PD tests shared the same Faraday cage. This set of experiments indicated three degradation stages which can be distinguished by their typical PRPD patterns. Figure 4-1 includes the typical degradation stages and PRPD patterns respectively.

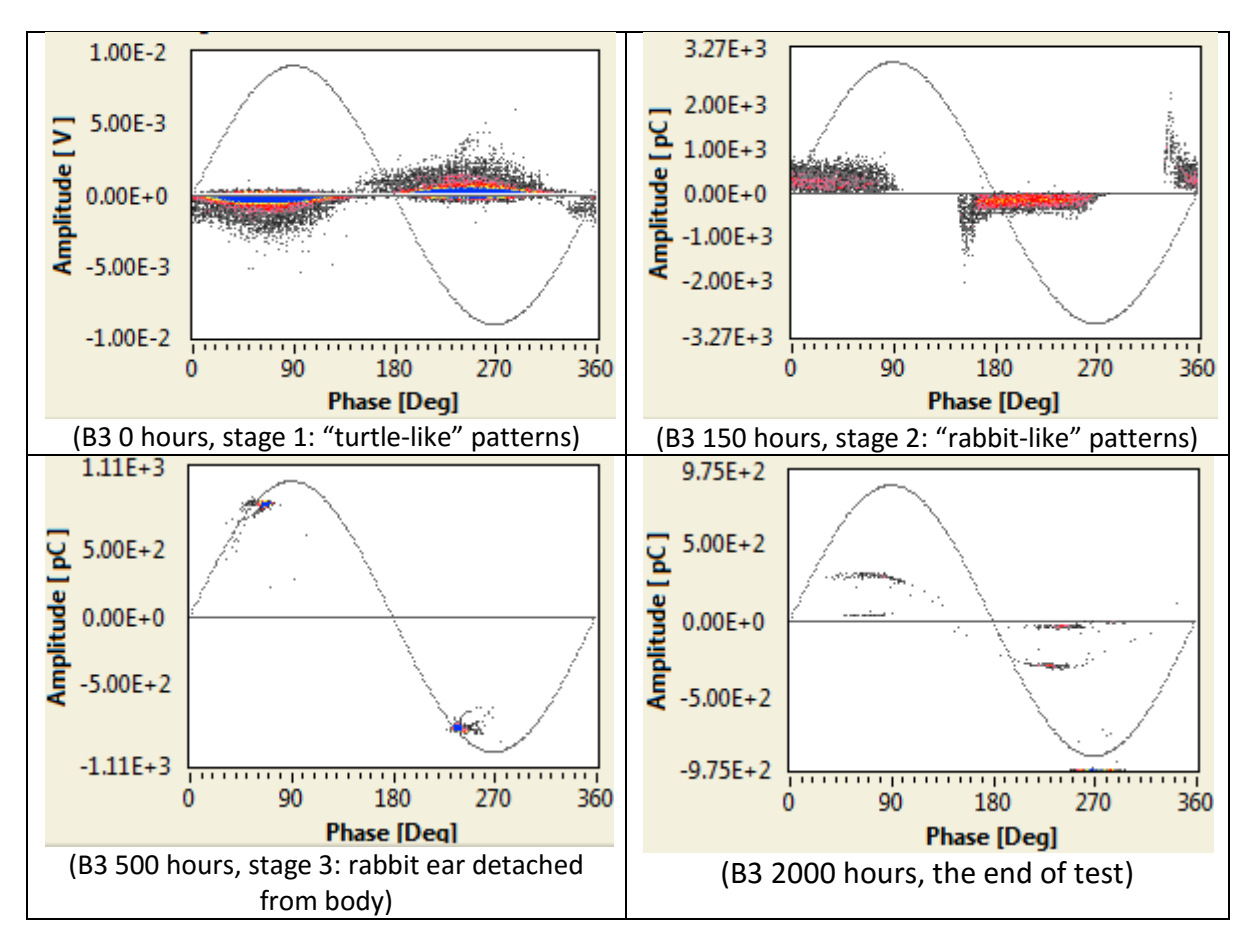


Figure 4-1: Typical PRPD pattern transition throughout 2000 hour degradation test.

Similar degradation stage transition in Figure 4-1 was found by many researchers in the area, their work comparing to this one was heavily discussed in this section and section 5. The reason for such transition to take place is due to surface deterioration brought by repetitive PD impact, the surface loses its ability to hold charges which are stored by previous PD events mainly due to increased surface conductivity and the creation of deeper charge traps by degradation by-products [65]. Hence the chance of using residual charges as first electrons for the triggering of future PD events decreases with degradation time [100, 79]. Thus after polarity reversal, the first discharge event gets increasingly delayed, turning "turtle-like" PRPD patterns into "rabbit-like", and then into "detached rabbit ear" patterns. Eventually, a certain localized area gets contaminated with highly conductive carbonized by-products and with sharply edged geometry, which then act as first electron generators to cause the continuous low magnitude swarming discharge. This mechanism will be further discussed in details with group C results as they are very consistent with group B and contain a much larger sample data base. Figure 4-2 to Figure 4-4 clearly show the pulse sequence behaviour change in time domain as described above, by showing typical pulse train behaviours over a small number of applied voltage cycles.

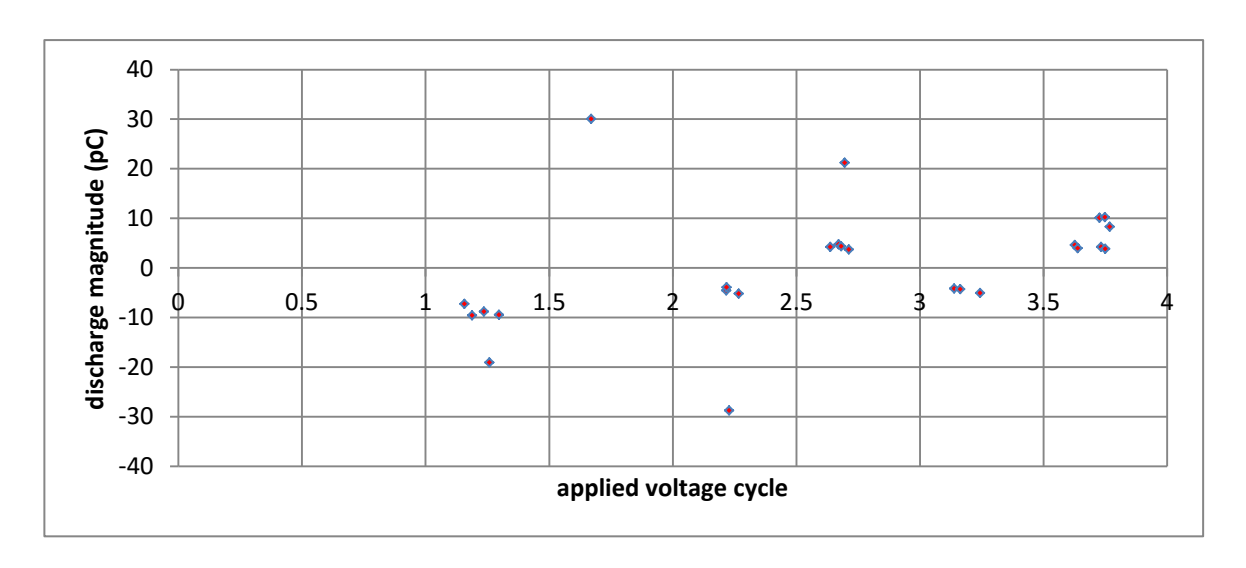


Figure 4-2: typical pulse sequence for degradation stage 1 – "turtle-like" discharge.

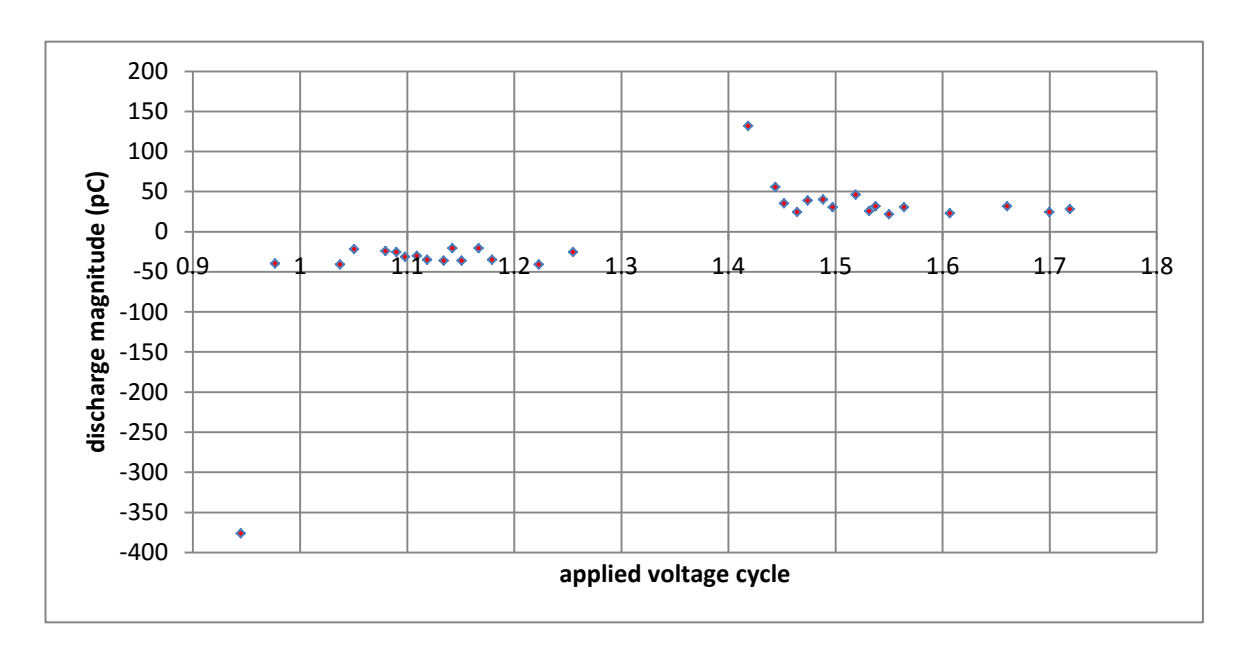


Figure 4-3: typical pulse sequence for degradation stage 2 – "rabbit-like" discharge.

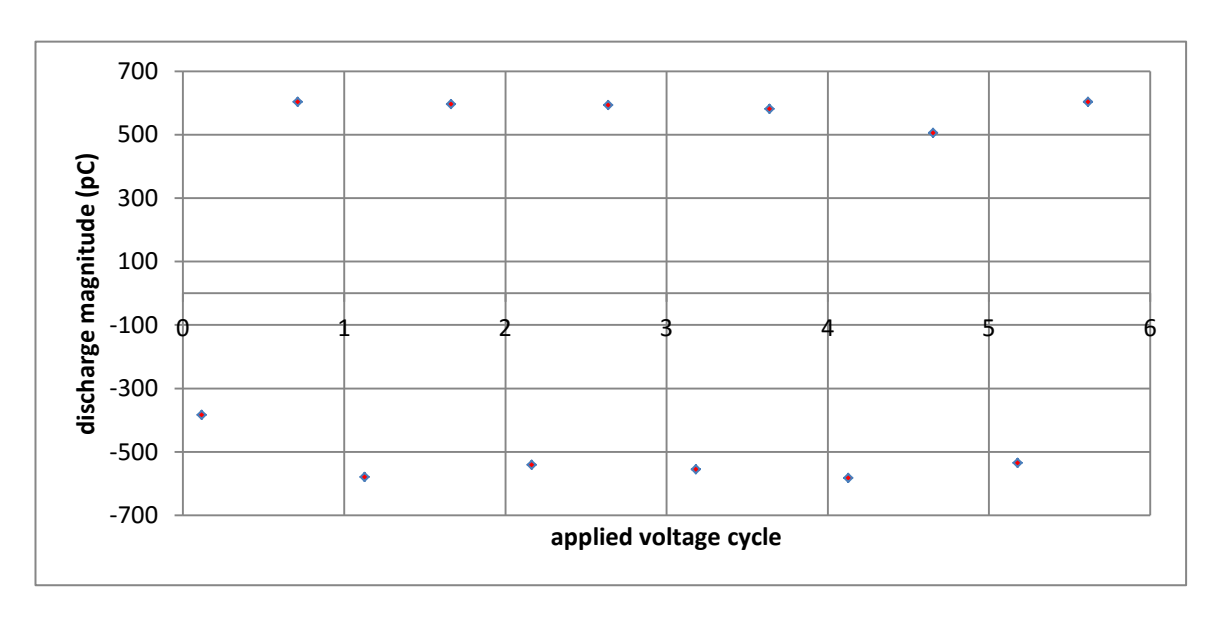


Figure 4-4: typical pulse sequence for degradation stage 3 – "detached rabbit ear" discharge.

All four samples in group B showed a very high level of consistency in not only the typical patterns observed, but also the elapsed time into the degradation process when the typical patterns were first detected. Table 4-1 shows the inception time of each degradation stage for sample group B. The only exception was sample B1 starting with "rabbit-like" stage, due to the fact that in early stage of degradation, "turtle-like" patterns and "rabbit-like" patterns are triggered with quite similar surface conditions at the interface, thus at the beginning of degradation, surface conditions across the entire surface are quite similar so the triggering chance of both discharge types are very close to each other.

Table 4-1: Inception time of each degradation stage, sample group B.

	B1	B2	В3	B4
"turtle-like" stage	N/A	0 hours	0 hours	0 hours
"rabbit-like" stage	0 hours	150 hours	150 hours	150 hours
"detached ear" stage	500 hours	450 hours	500 hours	400 hours

Only the most representative parts of group B experimental results are discussed in this chapter as it was only a trial test with four samples. Detailed discussion will be included with sample group C experiments, which had consistent results comparing to group B tests. The full version of group B PRPD pattern results can be found in Appendix. A.

All samples after 1450 hours were only intermittently discharging above the noise threshold of 3pC, but under a few circumstances "detached rabbit ear" patterns could still be seen if the acquisition tool was allowed to capture data for hours. However, this long term acquisition function could not generate any data base for further analysis, but only generate an image of the PRPD pattern. Also, a possible stage of swarming discharge was observed with sample B1 during the quite period, for which type high density of low magnitude discharge events take place inside a narrow range of phase angles, as shown in Figure 4-5.

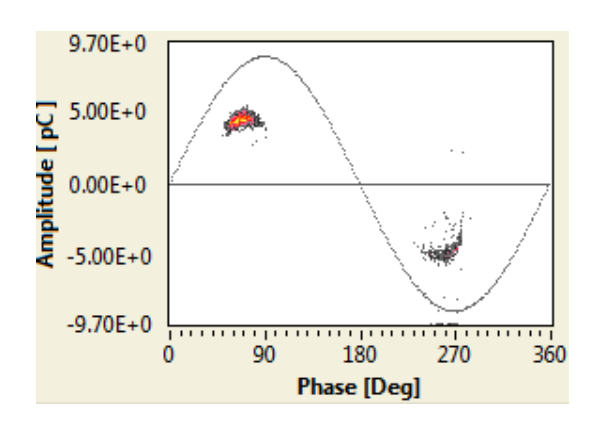


Figure 4-5: Possible swarming discharge observed with sample B1 at 1150 hours.

As far as the degradation level estimation is concerned, it is observed that with classic PRPD pattern features only repetition rate has shown the clearest trend along with degradation time. Other factors such as peak magnitude and average discharge magnitude have shown some trends, such as the rising trend from "turtle-like" to "rabbit-like" stage and "detached rabbit ear" stage, but it is hard to conclude any precise trending from them as they are controlled heavily by the stochastic time delay of availability of the first electrons required to trigger an electron avalanche. Figure 4-6 shows the trends of repetition rate, even though the decreasing trend can be seen, however it drops down close to 0 after the initiation of "detached rabbit ear" stage, hence it is still problematic to be based on for any precise calculation of degradation level for later degradation stages.

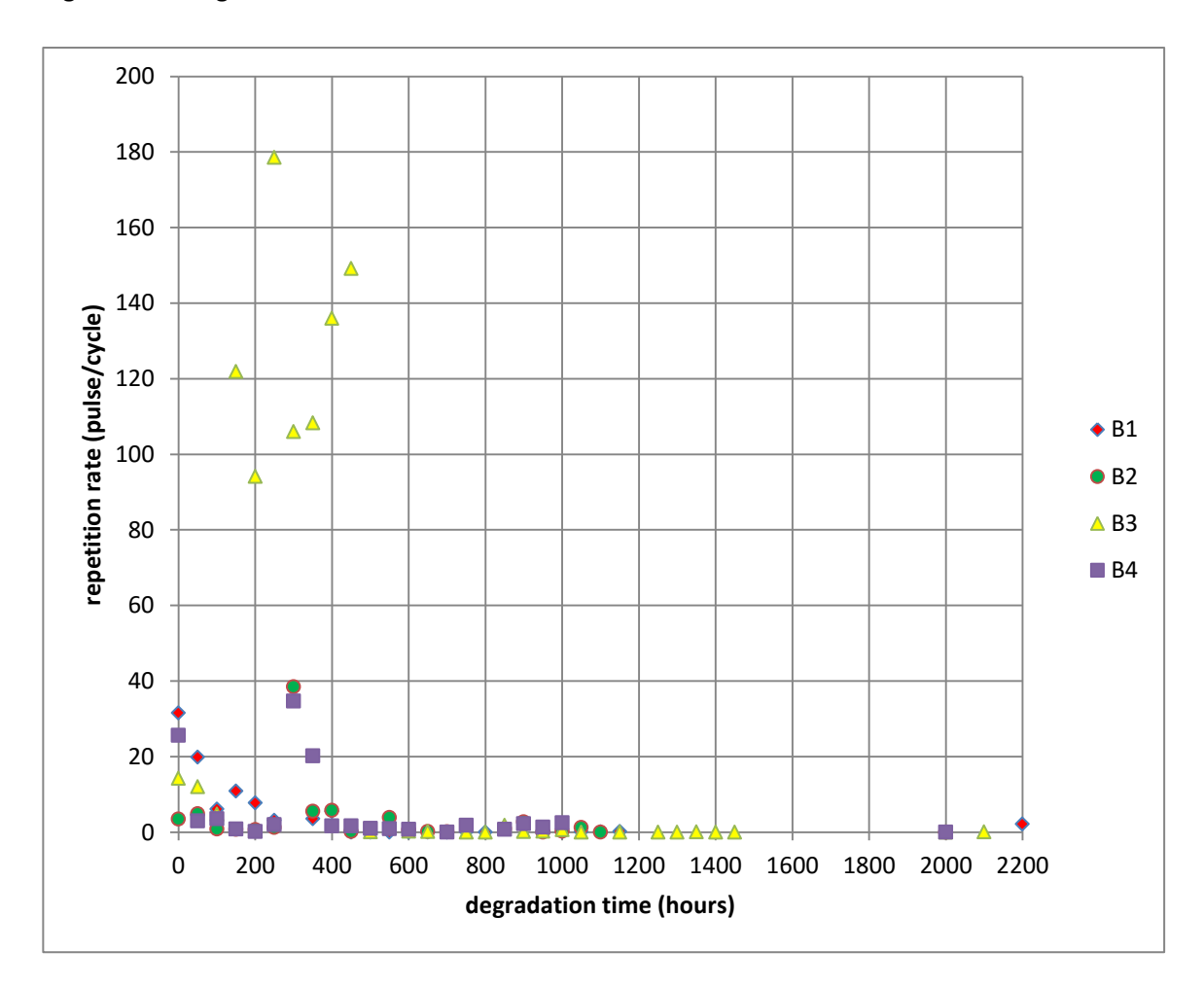


Figure 4-6: Group B PD repetition rate with degradation.

At the end of the experiments with group B samples, it was noticed that the PD feedforward capability was the major driving force behind PD stage transitions. Thus, it seemed the most effective to estimate degradation level by estimating PD feedforward capability level. For that purpose, the maximum data point limit and acquisition time limit must be removed, as 30s and a maximum of 20,000 data point were proven to be very insufficient after the attempt to extract PD

feedforward factors using group B data, it could represent only a minor part of the entire PD behaviour and could be heavily misleading.

4.2 16 epoxy resin samples degradation experiments

A new group of 16 samples were used in this further developed set of experiments, termed as group C. Unlike group B experiments, PD data acquisition for sample group C were set to be 10 minutes long without any limit on maximum data points. Mtronix MOD 600 was used as PDBase II could not serve the purpose. Also, Samples in group C were degraded and tested in two different locations. This was designed to maximize experimental efficiency in terms of time, and also to avoid possible air refill into the cavities, as it was claimed to be one of the major reasons for PD pattern transition, so this would be closer to realistic situations. Results from group C in general repeated group B findings. As expected this new method of constant stressing did bring some different features from what were observed in group B. The ability to obtain pulse sequence behaviours in the time domain was the main focus of experiments undertaken with sample group C.

4.2.1 Experimental method and PD data acquisition

4.2.1.1 Degradation rig and test rig layout

The degradation rig utilizes brass for both high voltage and ground electrodes. The high voltage electrodes were 15mm diameter, and the ground electrodes were 25mm diameter. All high voltage electrodes were connected to the same power source, supplying 20kV AC voltage at 50Hz. All ground electrodes were connected to a common ground joint. Samples were clamped in between electrodes within three sided walls, leaving one side for handling purposes, and fixed on spot by the weight of high voltage electrodes.

The test rig consisted high voltage and ground electrodes both made of brass, both were 15mm diameter. A suitable spring was used to ensure a firm clamp onto test samples.

4.2.1.2 Degradation and PD test method

Degradation and PD test took place in two different locations within the Tony Davies High Voltage Laboratory. Each sample was taken out of the ageing rig for PD and microscopic test and returned under degradation stress immediately afterwards. Thus, there was nearly no time for a sample to be not under stress, except for under 10 minutes for each test day, including the extraction and returning the sample at both test and degradation cages, and microscopic examination.

Thus, samples in group C were in a condition that nearly no atmospheric air refill could take place, for which case the air consumption theory as discussed in previous chapter could hardly find its application here in later stages of degradation, after initial consumption of air which was to be in a matter of hours.

The samples were constantly under an electrical stress of 20kV, and tested twice a week under the same voltage level. All samples should be degraded for 168 hours per week. However, extracting 10 minutes of handling time for each test, and 2 minutes when each sample was handled at the degradation cage so electric stress for all samples were turned off, all samples were assumed to be under degradation stress for at least 165 hours per week.

During the PD test, 30 minutes was given for each sample to produce settled signal instead of surface or corona signals, which "noises" could be seen at the beginning of the voltage application if the sample was not placed between the electrodes properly. Also, as the samples were transferred from the degradation rig to the test rig within nearly no time, it can be safely assumed that PD data collected is a good representation of PD behaviour under long time stress.

PD data acquisition was divided into 10 minutes intervals. For each 10 minutes, all PD pulses were registered up to a scale limit of 10nC. No PD exceeding 10nC was detected. Noise level altered from day to day in the testing Faraday cage, from 1pC to 3pC depending on the type of other experiments in the laboratory building on that day.

For the first 500 hours an automatic surge protection mechanism was used to prevent any unexpected breakdown which could cause damage to the acquisition unit. However, this mechanism alters the gain level of PD detector when a large discharge is picked up, thus low level discharge events can be flooded by the altering noise level. In order to gain a complete and clear data set, this mechanism was disabled after 500 hours as all samples showed no sign of defect that may cause any unexpected breakdown.

On each test day, optical microscopic images were taken for every sample after being PD tested. Each sample were marked and oriented to ensure microscopic images were taken consistently for the same area and orientation every time.

After 660 hours into degradation, 2 samples were to be sacrificed after every 330 hours for later scanning electron microscope (SEM) imaging and chemical examination. The rest were stressed and tested until 1970 hours, and then sacrificed for SEM tests.

4.2.2 PRPD behaviour with degradation and analysis

Results from group C provided significant confidence regarding consistency with group B. Identical key patterns for each degradation stage observed with group B were reproduced.

Due to the amount of samples involved in this experiment, only some representative patterns are shown in the following discussion. A full record of all samples throughout the experiment can be found in Appendix B.

Stage 1 is again represented by "turtle-like" PRPD patterns. All samples started with this featured pattern. This stage was observed from 0 hours to 70 hours. However, it did not mean that small "turtle-like" patterns would no longer be seen after this stage, in fact, they kept reappearing in later degradation stages. Thus, the degradation stages are to be defined with the starting of the typical featured patterns, instead of the ending of them. It is believed that most samples start with a good PD feedforward capability, which is determined by 2 major factors: cavity surface conductivity and average trap depth near the cavity surface. First electrons are essential to trigger PD avalanches when local electric stress exceeds PD threshold. Apart from volume generation by which mechanism the generation rate is very low, first electrons can also be generated by surface emission which is mainly sourced from surface charge accumulated by previous discharge events. Hence this mechanism is sometimes called "feedforward": previous PD events triggering future events. Surface charge accumulated can decay by charge recombination and moving into deeper traps in insulation bulk. Charge recombination is dominated by charge mobility along the cavity surface. In this case a virgin cavity surface is free from degradation by-products, such as carbonyl products which can greatly enhance surface conductivity. Thus virgin cavity surfaces can hold charges for a longer time before recombination takes place. Hence a greater electron emission rate is achieved. Also, charge traps are formed by electron bombardment damage and byproducts, thus there will be less deep traps for charges to fall into, which also leads to a larger source for first electron generation. To conclude, in this stage previous PD events are very capable of influencing future events, leading to "turtle-like" PRPD patterns. Figure 4-7 shows examples of stage 1 PRPD patterns.

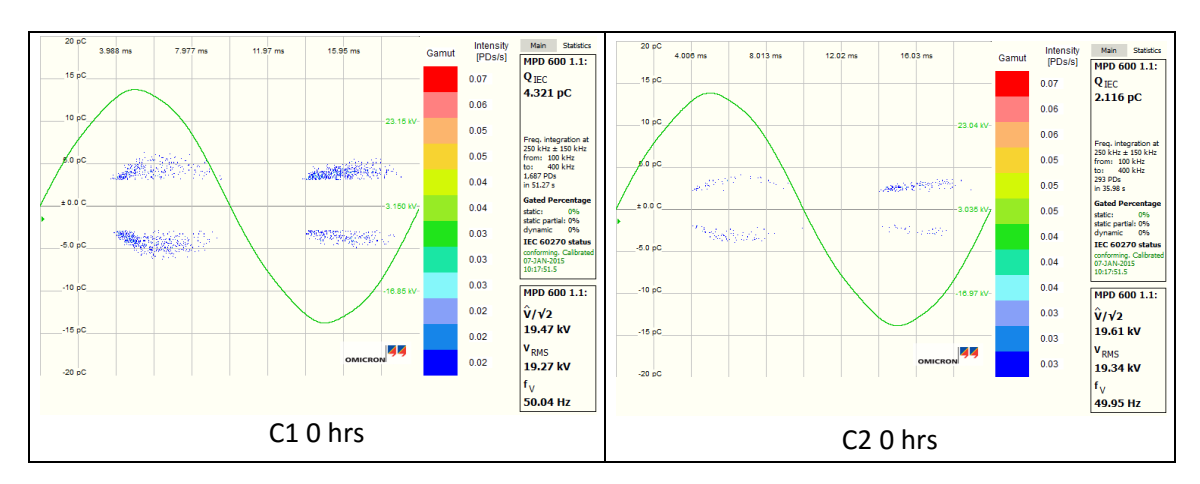


Figure 4-7: typical degradation stage 1 - "turtle-like" PRPD patterns from group C.

Stage 2 is the "rabbit-like" PRPD patterns, where "ear" like features were starting to be produced. This stage is observed with 16 samples out of 18, the most of them started this stage within 70 hours to 400 hours mark. Although PRPD patterns differ from sample to sample, but there is a common feature for all samples: "rabbit ears" are developed. Larger magnitude discharges in the ear part of PRPD patterns are not triggered immediately after PD inception voltage is exceeded, instead they are delayed due to the lack of first electrons. As discussed, increase of surface conductivity can accelerate charge recombination, and surface deterioration can create deeper traps which can cause a larger barrier for electrons to be released. Under both effects above, cavity surfaces are losing their PD feedforward capability. Thus first discharges after polarity reversal tend to enjoy a larger over voltage hence they are higher in magnitude. Again using C1 and C2 for example in Figure 4-8 for typical stage 2 PRPD patterns:

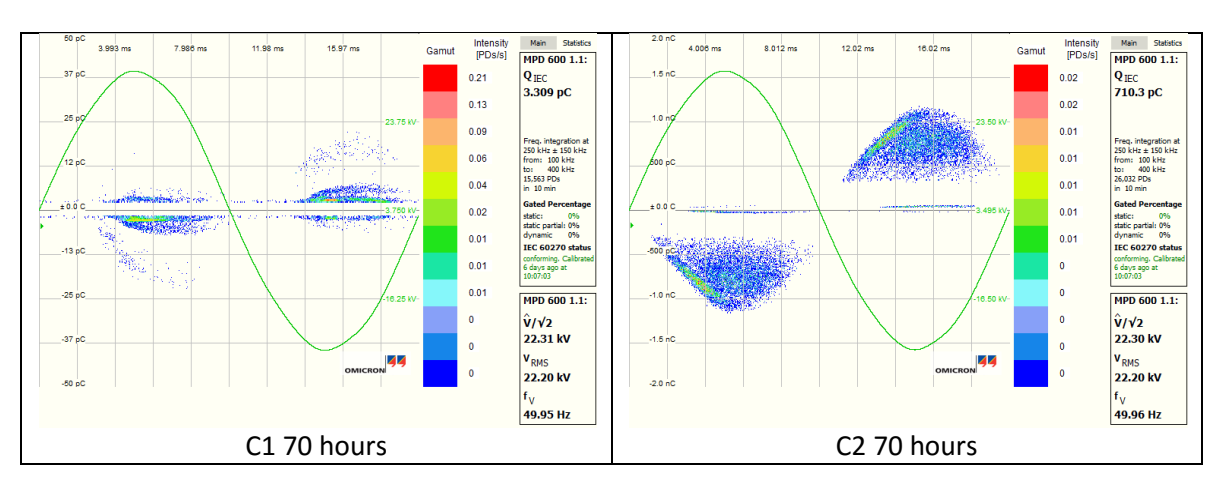


Figure 4-8: typical degradation stage 2 - "rabbit-like" PRPD patterns from group C.

The stage that came after the "rabbit" like stage, where there was nearly no pure "rabbit" like patterns observed since the initiation of this stage. "Rabbit" like patterns were either accompanied with "cloud" like patterns, or there was only "cloud" like patterns. 14 out of 16 samples showed clearly the existence of this stage, starting from as early as 300 hours, or as late as around 1000 hours. Typical "cloud" like patterns are shown in Figure 4-9.

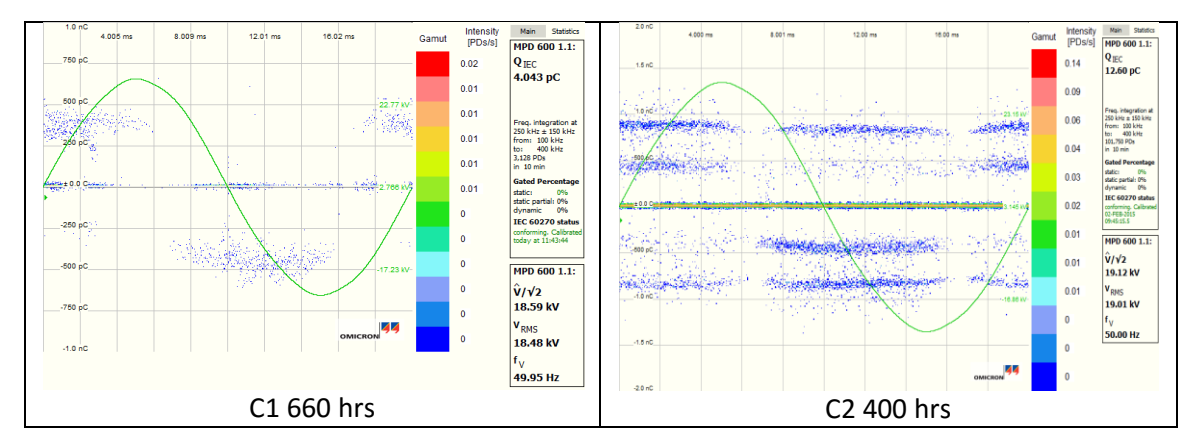


Figure 4-9: typical degradation stage 3 - "cloud-like" pattern from group C.

Detailed physics of discharge types in stage 3 and stage 4 will be discussed in the section summarizing the pulse train study, as they cannot be understood with PRPD patterns only. In stage 4, it is observed that the rabbit ears are detached from the body, and the body part of PRPD patterns are fading. This indicates a further loss of feedforward capability of cavity surfaces. Thus the cavities are returning to virgin state very quickly in terms of surface charge accumulation, which means the cavities are free from effects left by previous discharge events, so the first discharge events usually experience a longer delay, leading to higher magnitudes of them. As no other discharge events following the first one after polarity reversal, rabbit ears are detached from the body. For the same reason, the body part of the rabbit pattern disappears, leaving a very pronounced ear part. Figure 4-10 shows the typical degradation stage 4 patterns.

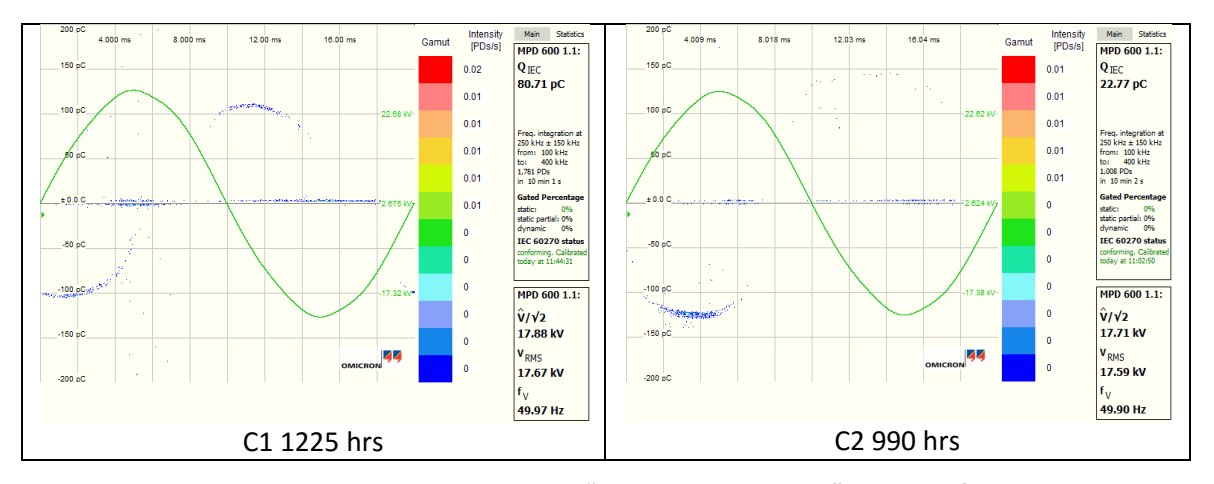


Figure 4-10: typical degradation stage 3 - "detached rabbit ear" patterns from group C.

As it was noticed, some of these ""detached rabbit ear"" patterns look fairly similar to the ""cloud-like" patterns". The difference can be found by analyzing pulse train sequence in time domain. The "cloud" type of events contains far more pulses in a single applied voltage cycle, sometimes hundreds; on the other hand, ""detached ear"" will have singular digit number of pulse in a single cycle, no more than 4 as the usual case. This will be discussed later in pulse sequence statistics section. Thus, although with similar appearance, the two discharge patterns

are in fact totally different from each other in terms of discharging physics, see Figure 4-11. Pulse sequence behaviour in time domain of the three discharge types are the same as found with sample group B, see Figure 4-2 to Figure 4-4.

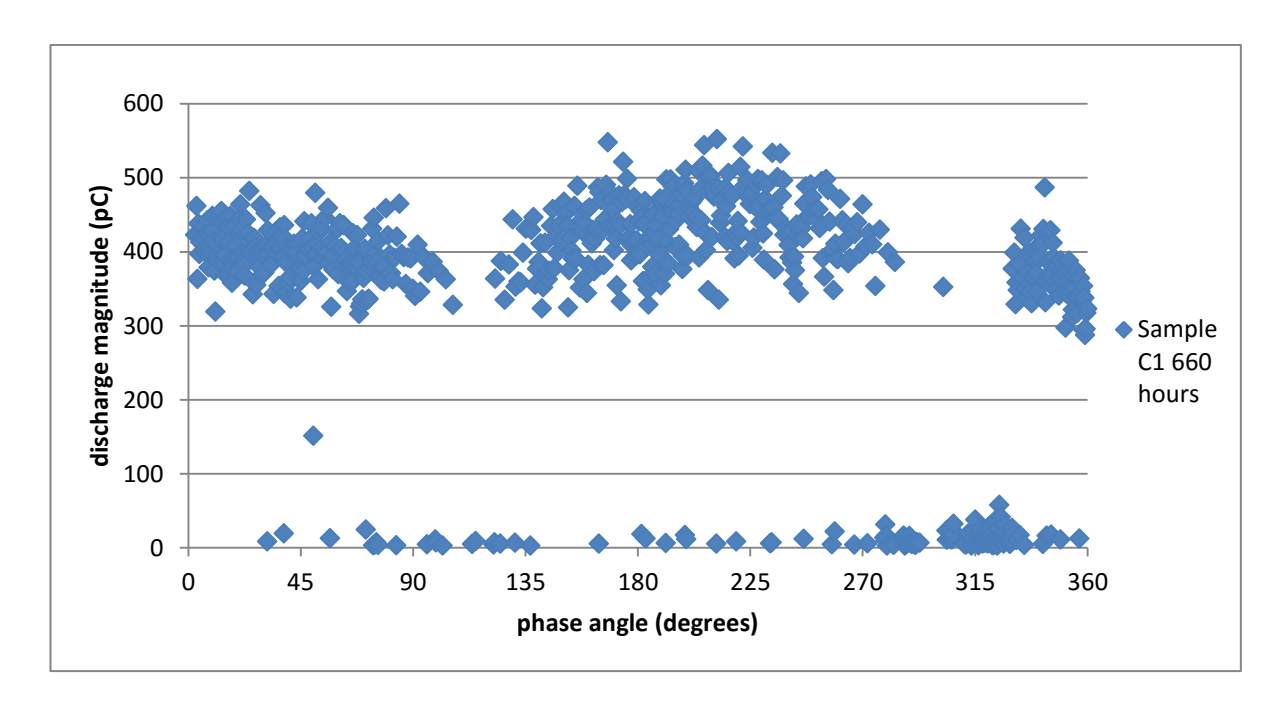


Figure 4-11: typical "cloud" discharge 1 power cycle pulse train.

According to initial PRPD patterns and pulse sequence results, 2 samples were sacrificed after every 330 hours, this process initiates at 660 hours, when initial signs of degradation stage 4 with "detached ear" patterns was about to start. In general, less active samples were chosen to be sacrificed and selected samples and ageing/degradation time are shown in Table 4-2:

Table 4-2: Sacrificed samples and time.

Degradation time (hours)	Sample No.
660	6, 8
990	3, 12
1320	9, 14
1650	5, 7

Finally, Table 4-3 shows the transition time in between adjacent stages of degradation, with 8 samples preserved until the end only.

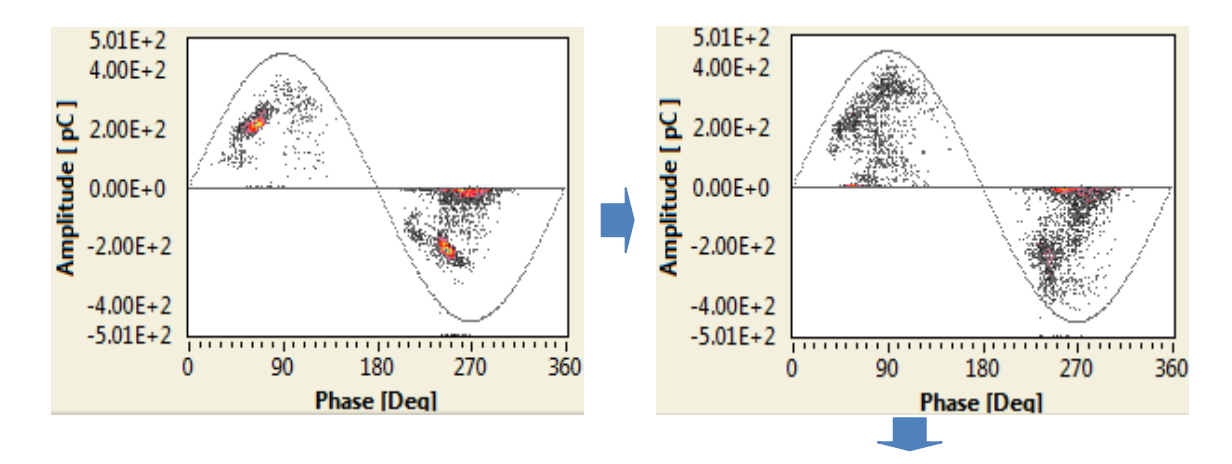
Table 4-3: group C transition time between degradation stages (8 samples held until 1970 hours).

	C1	C2	C4	C10	C11	C13	C15	C16
Turtle	0	0	0	0	0	0	0	0
Rabbit	70	70	70	400	235	165	165	165
Cloud	330	400	1060	565	235	235	165	565
"detached	825	990	N/A	1225	895	1060	1155	895

4.2.2.1 Discussion – General PRPD pattern features

Through the PRPD patterns recorded along PD degradation process, it is found that the PD feedforward capability is the most influential factor to change PRPD patterns. The PD feedforward capability of a cavity is reduced as degradation proceeds. This trend is driven by the increase of cavity surface conductivity, and also the deeper traps accumulated due to degradation by-products. PRPD patterns for virgin samples are generally "turtle-like" patterns, there is no rabbit ear due to the abundant supply of initial electrons eliminates the possibility of statistical delay. As surface conductivity increases, the reservoir for first electrons gets smaller, PD events after polarity reversal are usually delayed thus with higher magnitude to form the rabbit ear. With the further decrease of PD feedforward capability, discharge events are more independent, instead of being triggered by previous events. Thus the rabbit ear gets detached from the body.

Due to the increasing PD inception delay along the degradation process, peak magnitude of PRPD patterns increases. And as the feedforward capability drops, repetition rate drops with it. Also, space charge is getting harder to accumulate, thus the inception angle shifts to be more synchronized with applied voltage as the overall local field is less affected by space charge, and PRPD patterns are getting easier to settle without the process of space charge accumulation. The PRPD pattern settling process can be demonstrated with Figure 4-12.



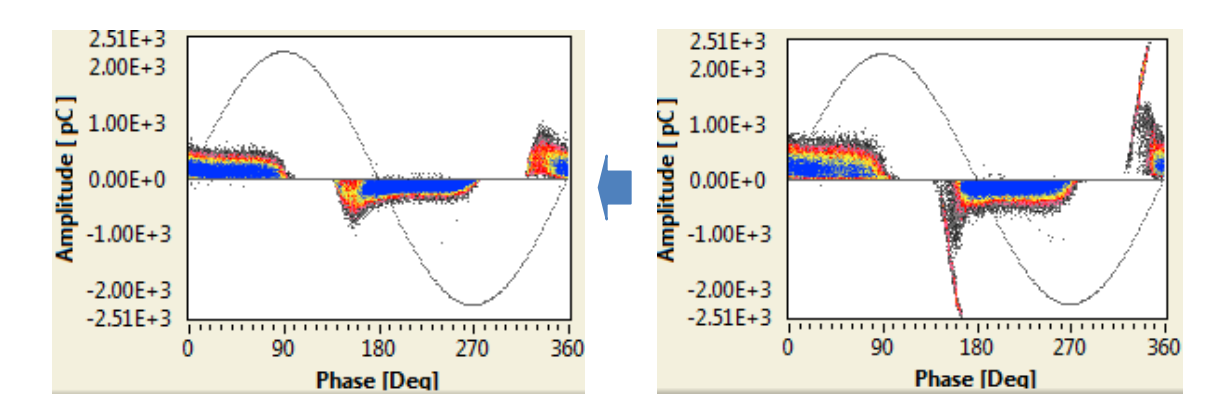


Figure 4-12: PRPD pattern settling process due to space charge build up.

Published literature has rarely covered PRPD pattern transitioning between degradation stages, especially for epoxy resin individual pulse type transitioning instead have drawn most of the attention as discussed earlier. Experiments conducted by Morshuis and many others found a transition from streamer to Townsend type of discharge in the beginning, after a few hours of stressing with epoxy resin [63], but the PRPD pattern was not included in those studies. Holboll [100] reported only one stage transition throughout 1000 hours of experiment for spherical cavities in epoxy resin, the transition from low magnitude Townsend discharge (~10pC) to high magnitude streamer discharge (~100pC) with a dropping repetition rate, which is similar to the case in this study. Also, PRPD patterns reported by Holboll [100] showed a transition from "turtlelike" to "rabbit-like" form which he believed was due to "the missing of initial electrons due to surface deterioration", which is also similar to the conclusion made in this study. An increase of surface conductivity was measured by Centurioni to study similar tasks [101]. However, due to PRPD patterns were only observed from a rather rough scale due to only long term accumulation was presented, more detailed degradation stages based on PRPD patterns were not possible to be defined. Other works such as the pattern transition by Mizutani [80], an initial transition indicated by the formation of a long rabbit ear was also reported, with the reason behind attributed to the production of electronegative gases to lower the initial electron generation rate due to the attachment process. This is not only proved by Mizutani when reopening the cavity to introduce fresh air indeed brought PRPD patterns back to its initial state, but also by [102] when raising the content of electronegative gas did trigger the transition from "turtle-like" to "rabbit-like" PRPD patterns with epoxy resin.

However, due to the fact that Mizutani used LDPE in his work, and experiments in [102] only reported the first 300 hours of observation, during such a short period of time surface deterioration may have limited effect on PD behaviours, or it has its affects in parallel with gas component change which makes the two hard to be distinguished from each other. Also, LDPE has very low melting point, thus a large percentage of surface deterioration may be induced during a

possible fast thermal runaway process instead of having a gradual affect throughout the entire degradation process. Suwarno and Mizutani also reported a transition not only in PRPD patterns, but also with pulse sequence behaviour in time domain [103], see Figure 4-13.

So, the transition from "turtle-like" to "rabbit-like" PRPD patterns is indeed widely found and reported. However, the "cloud-like" discharges has drawn much less attention. Similar "cloud-like" discharges were found by Wu, who reported a type of discharge events with similar rabbit ear only PRPD patterns with PE sandwich samples containing a cylindrical cavity [104], which can be found from Figure 4-14 (d) in the positive half cycle.

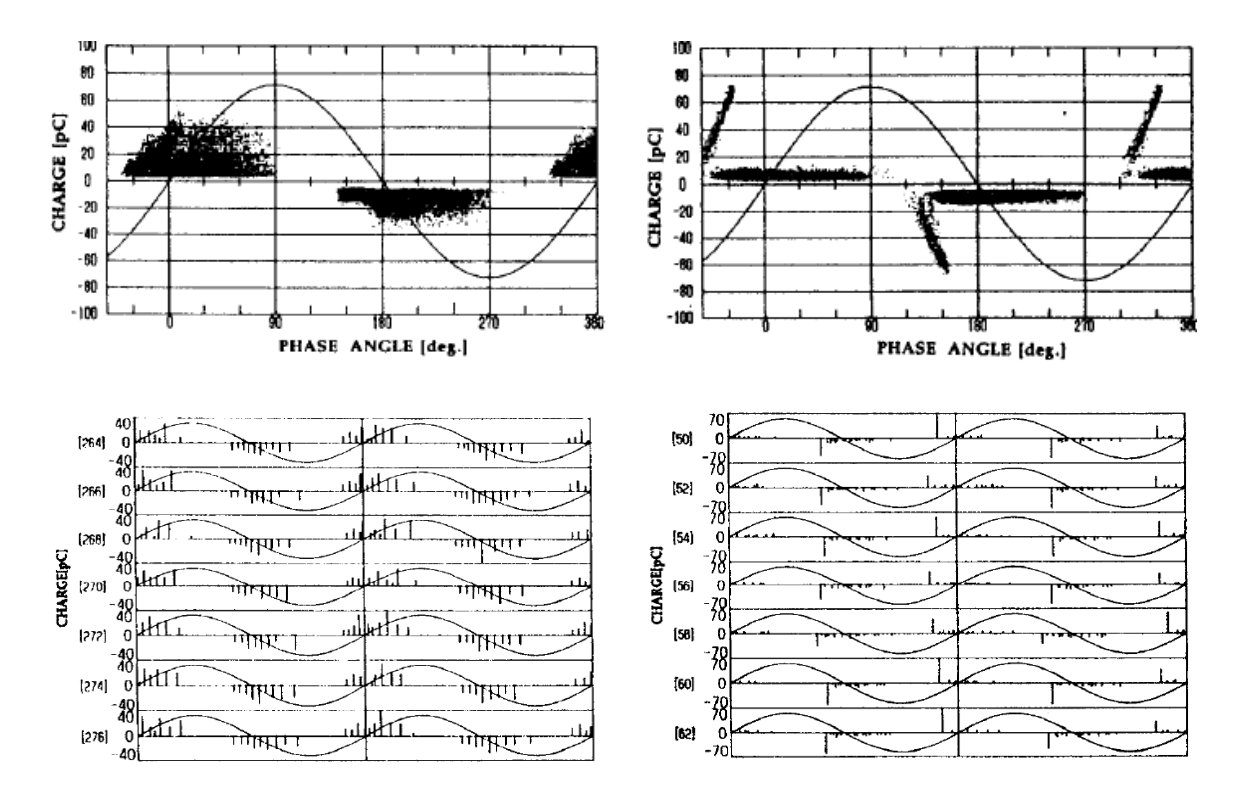


Figure 4-13: Similar "turtle-like" and "rabbit-like" pulse sequence behaviour observed by Mizutani, left: "turtle" at 0 min, right: "rabbit-like" pattern at 20 minutes into degradation [103].

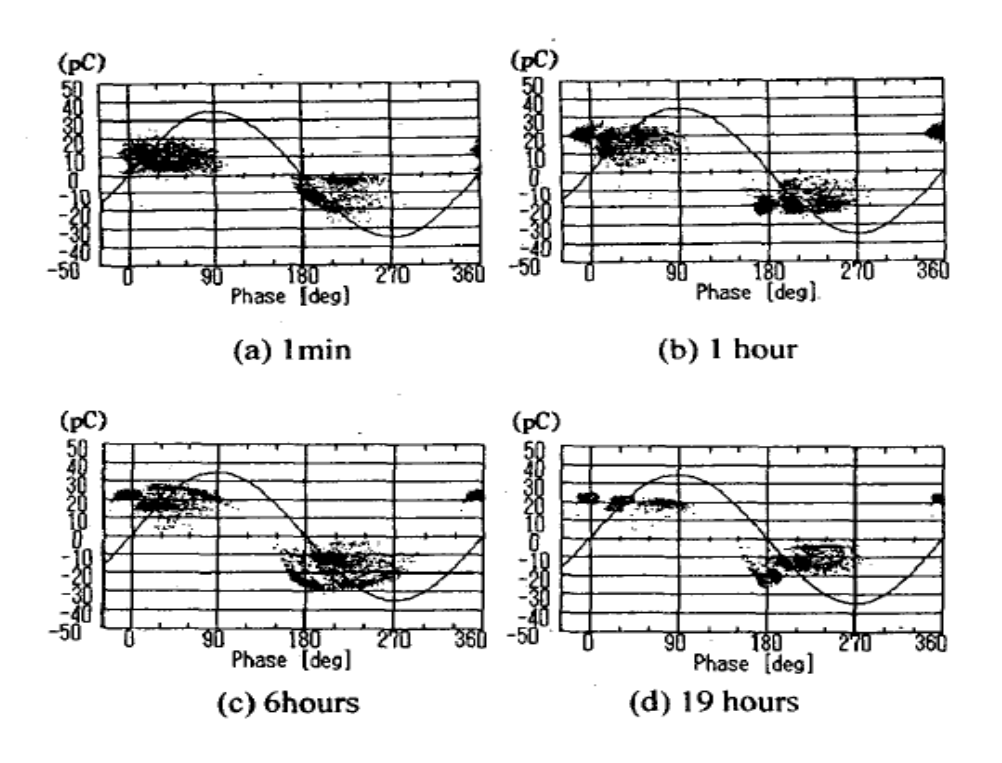


Figure 4-14: PD pattern transition with "cloud-like" discharge observed [104].

The reason for this type of discharge to happen is explained by Wu using the term "PD area", which is defined by him as "the area that charge carriers can defuse on the surface after PD events". It is explained that surface degradation increases conductivity along the surface, thus charge carriers can travel further as degradation time goes on. Initially, an individual discharge can only affect the connection path between two tiny spots on the two sides of a cavity, meanwhile electric field in other spatial areas is nearly unaffected, thus PD can still occur in other areas independently. With the conductivity raised by surface deterioration, charge carriers from a single PD can travel further along the cavity surface. Thus in order to cease the PD, initially only a small amount of charge carriers is needed to create the resisting electric field in a small spatial area, while when charge carriers can defuse further, a single discharge event must produce more charges to create a resisting field in a larger spatial area. Hence, if the charges are able to travel the full distance along cavity surfaces, only one discharge can happen at a time because the electric field in the entire cavity is reduced by the discharge. Based on this theory, Wu conducted an experiment with metal electrodes built in the PE sandwich sample as the two cavity surfaces. In this case, an abundant first electron source is provided by metal electrodes, thus there should be no stochastic issue, PD events should trigger as soon as the inception voltage is achieved, and cease when the entire cavity has its field dropped below extinction value. Indeed PRPD patterns turned out to be "the cloud type" defined by Wu, which is a strictly periodical type of discharge illustrated in Figure 4-15. A series of work done by Wu have also examined this theory with different voltage waveforms [105], and from the aspect of pulse current waveforms when charge defusing shows a different slop from discharge itself on the current waveform plot [106].

However, feedforward capability features of the "cloud" discharge in the actual PE cavity test were not examined.

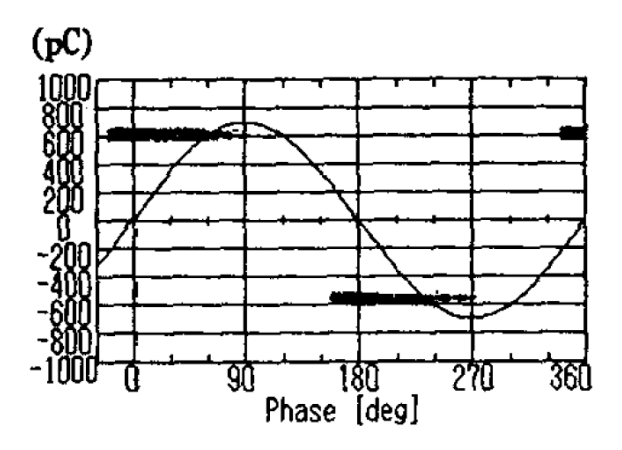


Figure 4-15: "cloud-like" discharge produced using metal cavity surfaces [104].

When considering "detached rabbit ear" and onwards in this work, a similar transition has been revealed by Bai with silicone rubber in TDHVL [107] as shown in Figure 4-16.

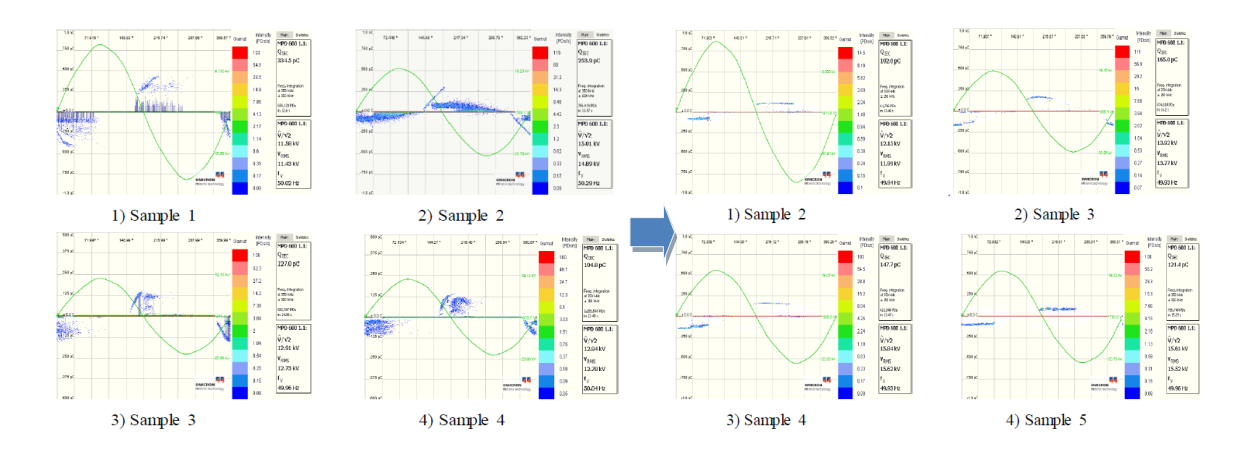


Figure 4-16: Transition from "rabbit-like" to rabbit ear only patterns with silicone rubber around 6 hours into degradation [107].

These published results may indicate that polymeric insulating materials have a similar degradation process under PD, and the rabbit ear detached from body patterns may indicate an important degradation phase before accumulated deterioration leads the material to destruction. In the case of silicone rubber, a couple of hours of no discharge period took place after "detached rabbit ear" patterns, and then thermal failure followed for all samples. PRPD patterns with only rabbit ears indicate that the cavity is now too conductive for continuous discharge events to take place, and only high magnitude discharges after a long statistical delay can happen. The most possible next stage to take over these discharges and they indeed stopped in both cases of epoxy resin and silicone rubber, is the development of conductive pits, which generates lower magnitude but high repetition rate discharge events, and act like a short circuit to ground to stop

other PD events from happening. And indeed for silicone rubber, during the period of no observable discharge events, severely carbonized degradation sites have been developed, which can confirm the hypothesis to a certain degree, as shown in Figure 4-17.



Figure 4-17: Carbonyl degradation sites produced under no observable PD condition [107].

Similar to this work, PD activity almost disappeared afterwards until a sudden rise was observed before final breakdown. Also, experiments carried out in Nagoya University, Japan have extended Mizutani's work with LDPE, defining a "turtle"-"rabbit"-"minor" discharge transition shown in Figure 4-18.

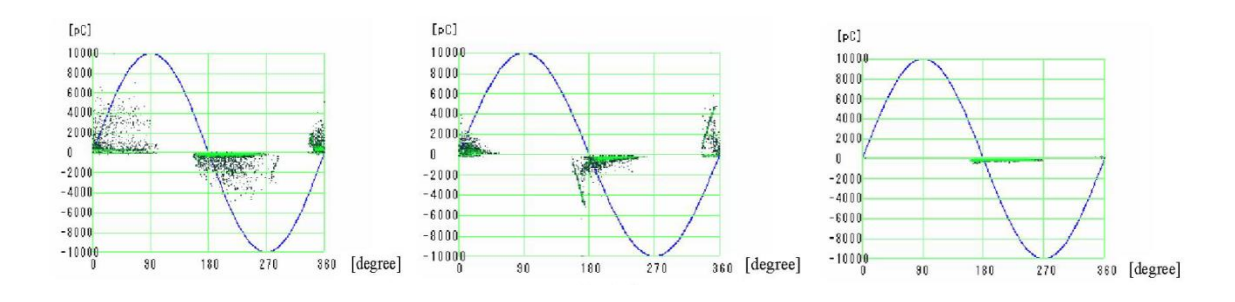


Figure 4-18: Degradation PRPD pattern transition with LDPE, left: 0hrs, middle: 0.1hrs, right: 2hrs [108].

Furthermore, rabbit ear detached from the body were also observed, such as Mizutani with LDPE and Montanari with XLPE in Figure 4-19. However, these "detached rabbit ear" patterns did not draw any attention from the researchers and were not discussed. In the case of Montanari's work, PRPD patterns were quite similar "rabbit-like" patterns throughout the degradation process, thus he used the trending of total electron number for the separation of degradation stages as discussed earlier. There is very little published work that discusses the precise feedforward capability level of PD activities, as works focused on individual pulse analysis use long term accumulated pulses, and the only few groups working with accumulated PD behaviours have

many different viewpoints when considering pattern transitioning, and yet the evaluation of PD feedforward capability is not getting any attention. However, it does seem to be a very important factor in this work for a more detailed degradation stage analysis.

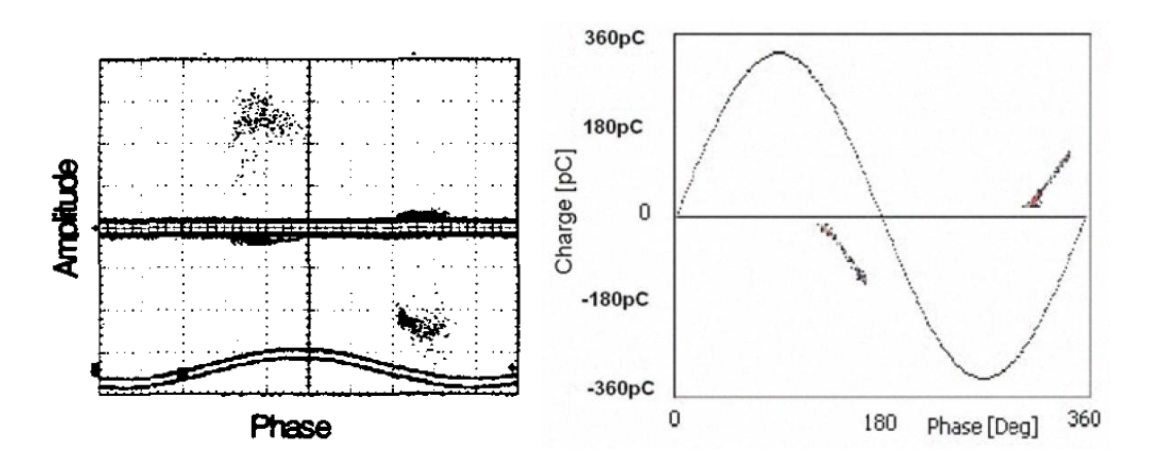


Figure 4-19: Rabbit ear detached from body observed by Mizutani [79] (left), and by Montanari [94] (right).

4.2.3 Pulse sequence in time domain and statistical analysis – evaluation of PD feedforward

Classic pulse sequence analysis is based on raw data of selected PRPD patterns. Apart from the classic statistical figures, the continuity features of selected data sets were examined by a number of characteristic parameters. Accumulated PD data is mainly represented in two major forms: ϕ -q-n patterns and Pulse-Sequence-Analysis (PSA) patterns. ϕ -q-n plots including PRPD patterns utilize three parameters: phase angle, pulse magnitude, and pulse number to super-position accumulated pulse data onto a single power cycle. As heavily discussed in this work, information contain in such patterns can be used to recognize discharge types, analyze discharge characters, results of which can be used to study degradation induced affects.

The classic PSA method instead of super-positioned PD data which can lose a significant amount of information contained within the data as discussed in this report, studies the relationship between consecutive pulses [109]. This method was designed to focus on the effect that a discharge event can have on future discharge events. Phase angel difference and applied voltage difference between two consecutive discharge events [110] are used. In general, accumulated PD data analysis is mostly used to distinguish obviously different patterns in ϕ -q-n plots, but pulse sequence study is more effective at identifying the physics behind accumulated plots by showing the feedforward effect of PD events.

In this work, PD feedforward capability of a set of PD data is assessed by continuous discharging cycles and breaks. If magnitude is ignored, time resolved PD patterns will be a dotted straight line. Hence, to evaluate how dense a dotted line is, the dots and spaces can be considered, as equivalent to continuous discharging events and breaks in PD data series. There is no minimum length of a continuous discharging event defined in this work, such events can be from 1 cycle to as long as there is no empty cycle observed. On the other hand, a break is defined as the length of empty power cycles in between adjacent continuous discharging events. With such definitions, the active cycle percentage of a PD series can be defined, as the percentage of discharging cycles against the overall applied voltage cycle number. Furthermore, pulse count per discharging power cycles was found to be a very important factor to express continuity features of PD.

4.2.3.1 Trends between degradation stages – the statistics

As discussed earlier, three parameters were found to be the major factors describing PD feedforward capability level: the PD active level being discharging cycles divided by total applied voltage cycles; discharging cycle length being the number of discharging cycles before a non-discharging cycle is seen; pulse per discharging cycle being the number of pulses counted in a single discharging cycle.

As in different degradation stages the featured patterns have very different discharging physics, due to surface deterioration brought by accumulating discharge impact, PD feedforward capability was determined to be the main factor both showing and also causing the change in terms of both PD behaviour and surface degradation. Thus, the three parameters introduced should be able to show clear trends along with degradation stages.

Statistical distribution charts are shown for every parameter and every stage of degradation. These distributions are found from a data base containing all 8 samples that finished the full 1970 hours of group C experiment. At each degradation stage, the featuring PD type is examined to generate such a statistic distribution.

First of all, PD active level contains similar information comparing to repetition rate. Repetition rate shows an average pulse count per second which can be misleading when assessing the continuity features of PD, for instance a very short but bursting "cloud" discharge event can have the same repetition rate as a long term "turtle" type discharge, or the same "cloud" discharge can even have similar PRPD pattern shape and repetition rate as a long term "detached rabbit ear" discharge, giving the correct amount of observation time. On the other hand, PD active level eliminates the influence from the number of pulses, it purely focuses on the active level of PD on

a cycle to cycle base. Figure 4-20 shows the distribution of PD active level for every degradation stage featuring PRPD patterns.

From Figure 4-20 it can be clearly observed that PD is getting less active as degradation progresses. "Turtle" type discharges in stage 1 almost hold an even distribution across all active levels, whilst a clear increasing trend can be found for at lower active levels from 0% to 5% of overall power cycles observed, and a decreasing trend can be found for higher active levels. For later degradation stages 3 and 4, nearly 50% discharges have the active level of less than 1% of total applied voltage cycles, and very low percentages can be seen for active levels higher than 5%. This states that the cavities are growing to be less and less active as anticipated. Also, cloud type and "detached rabbit ear" type of discharges are not yet generated from vast initial electron sources such as sharp carbonized edges of by-products, as if that is the case the active level shall be much higher as the electron source will release when the local electric field level exceeds the threshold in every power cycle.

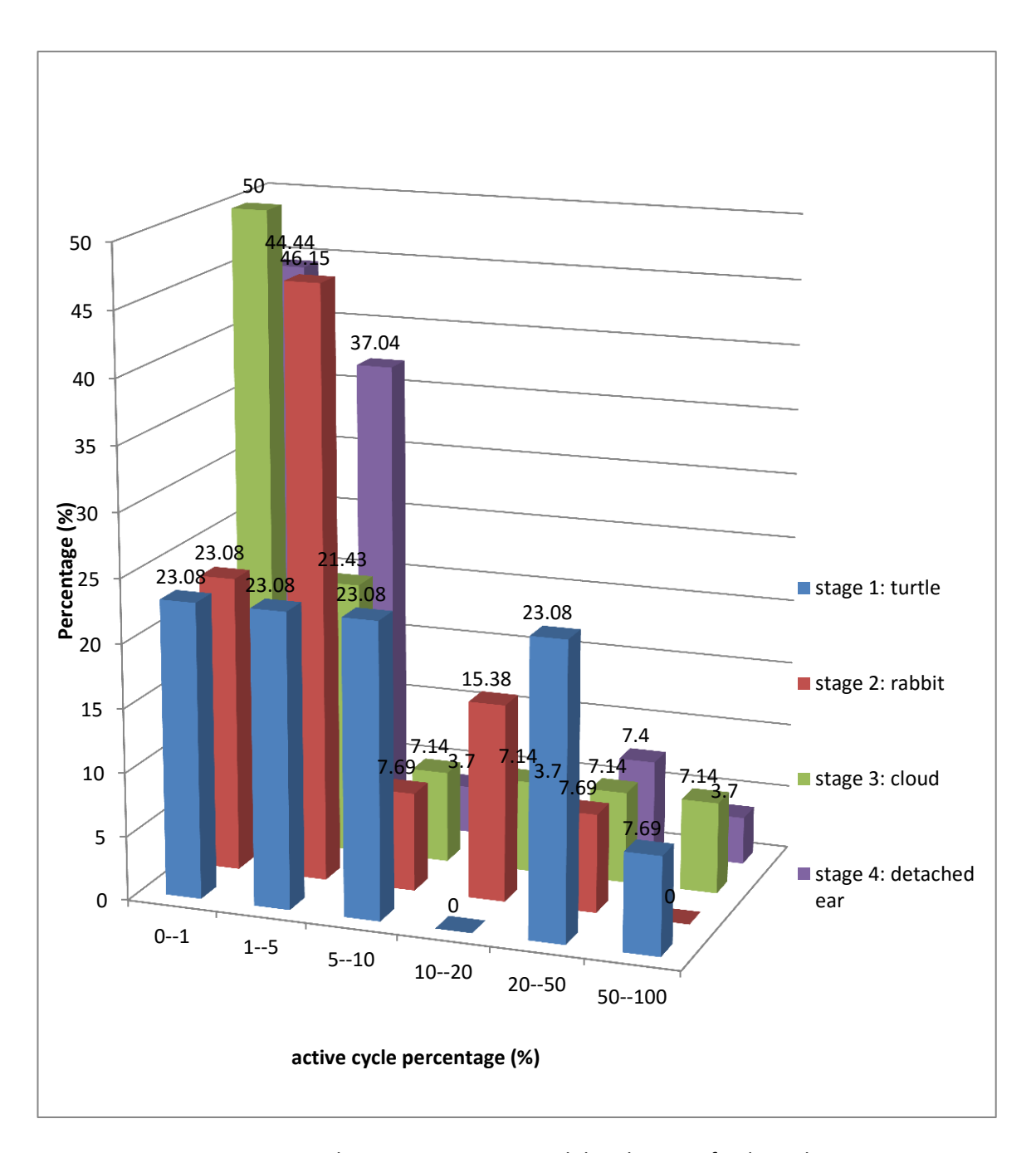


Figure 4-20: Active cycle percentage statistical distribution of 4 degradation stages.

Apart from PD active level, continuous discharging cycle length and pulse count per active cycle are also good indicators of the feedforward capability level of degraded cavities. Continuous discharging cycle length examines the continuity of PD events on a cycle to cycle level. PD events will be less continuous when the cavity surface cannot hold charges as long as before, leading to a smaller chance for future discharges to be generated by initial electrons from residual charges. Figure 4-21 shows the distribution of discharge continuity level for all four degradation stages.

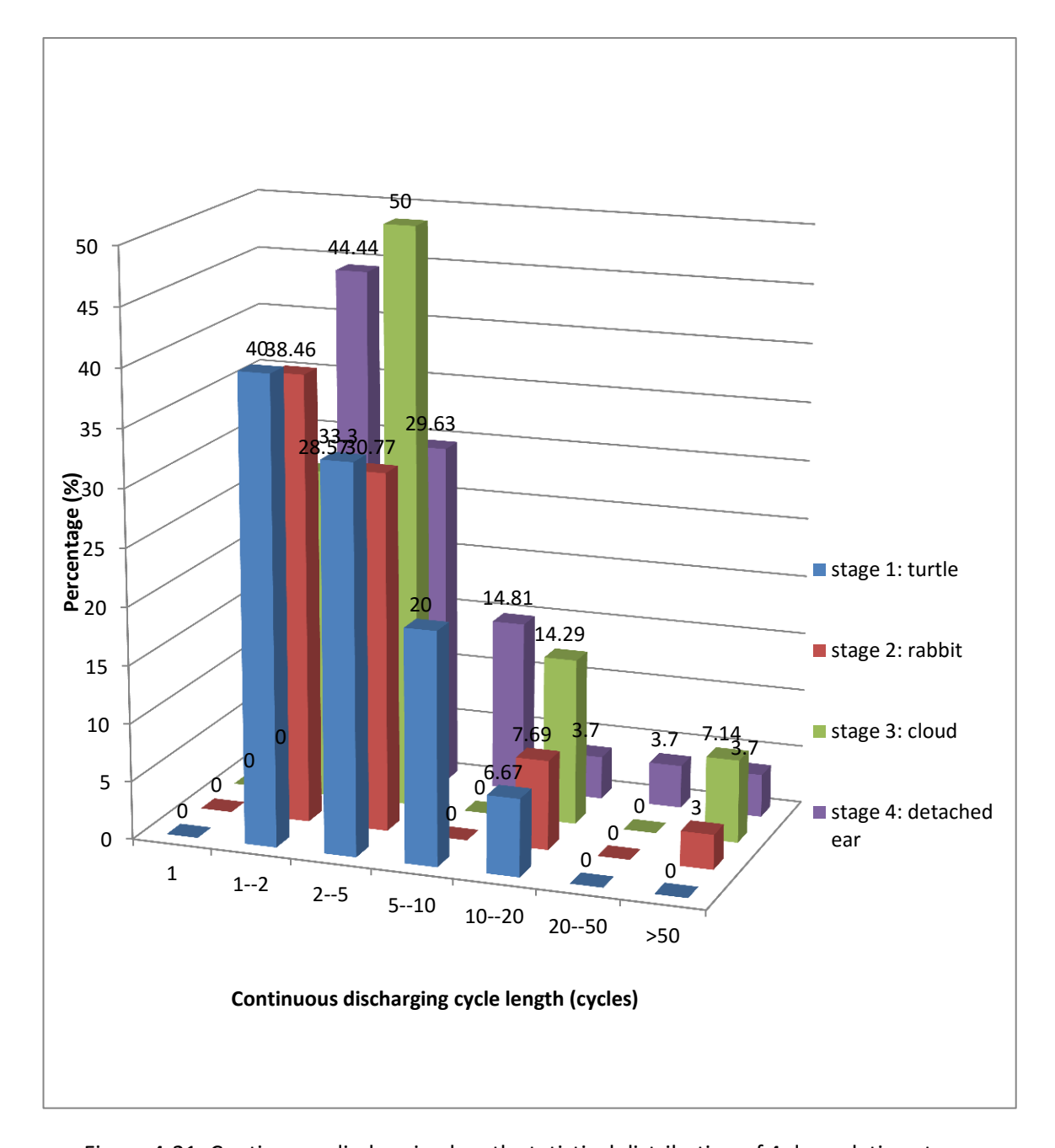


Figure 4-21: Continuous discharging length statistical distribution of 4 degradation stages.

From Figure 4-21, the most noticeable finding is that later stage discharges such as cloud and "detached ear" discharges can have continuous discharges exceeding 10 cycles or even 50 cycles, while "turtle-like" discharges have fewer long events, with none exceeding 20 at all. This is due to "turtle-like" discharges are low in magnitude, thus the chance for residual charge to cause future events is relatively low as well. However, stage 1 "turtle" discharges can occur across the entire cavity surface, thus there will be a great chance for another event to take place at another location after the cease of the previous one. So the "turtle-like" discharge are as Figure 4-20 and 4-21 suggest: a discharge type that is more active but a single event does not last very long. On the other hand, cloud and "detached ear" discharges can only happen at a few selected locations, but they both can generate a large amount of residual charges after a single event. Thus "cloud"

discharges act like high magnitude "turtle" discharges: when activated by a small chance of volume electron generation, it can survive relatively longer periods in terms of continuous discharging length due to the amount of residual charges available for PD feedforward, but can only happen at a few heavily degraded locations. Thus they are rarely seen and most likely with low active level as the two distribution charts showed. "detached rabbit ear" events are from the locations of "cloud" discharges, but further degraded. Local decay speed of residual charges is further increased, thus discharge events in general takes shorter period. On the other hand, volume generation rate is increased due to the more severe surface deterioration, so they are more frequently self-triggered thus more frequently seen. Discharge locations are confirmed by Morshuis [83], and also reported by Kato [108] that discharge events gets very concentrated since the initiation the transition from "turtle-like" to "rabbit-like" PRPD patterns (transition at 0.1 hours), see Figure 4-22. Further discharge location and surface deterioration will be discussed further in later sections with optical and scanning electron microscopic images in later chapters.

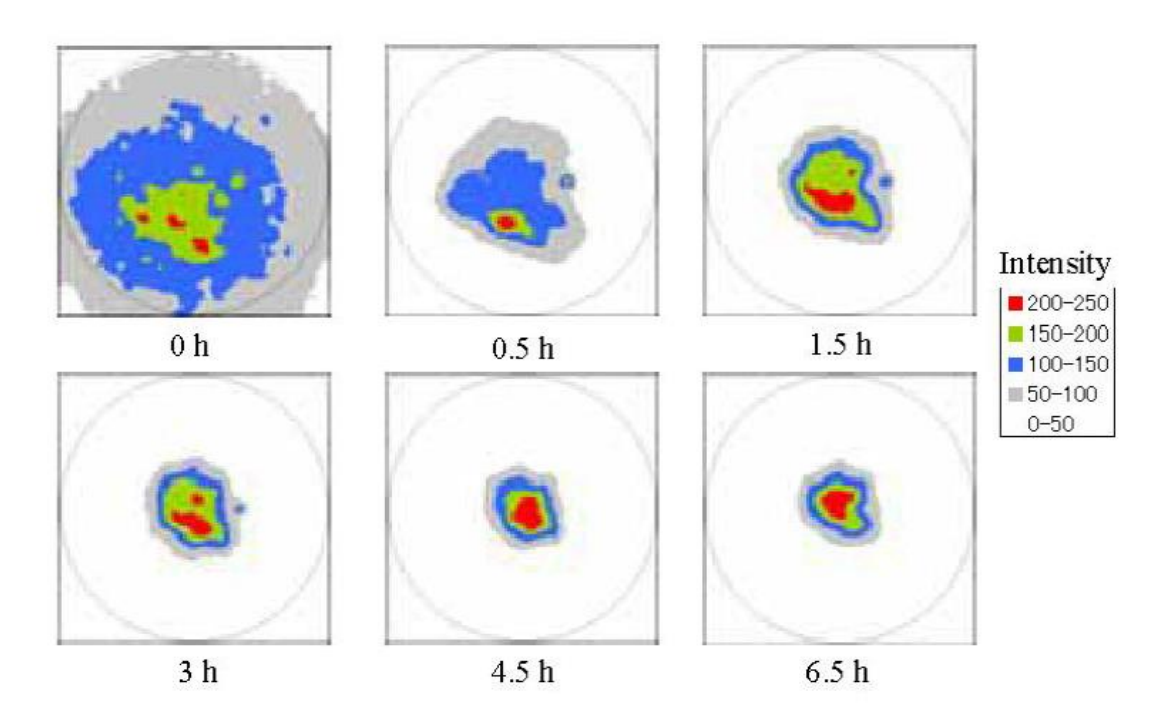


Figure 4-22: Discharge area change in a cavity in PE during PD degradation by Kato, 20 minutes transition from "turtle-like" to "rabbit-like" PRPD behaviour [108].

Pulse count during discharging cycles in the first place confirms the definition of the four degradation stages, as it can be observed in Figure 4-23. The transition from stage 2 to 3 and 3 to 4 is very clear, as "cloud" discharges in stage 3 have high numbers of pulse count only, while stage 4 "detached ear" discharges have low numbers only. This again confirms that "cloud" discharges relies on PD feedforward heavily, once triggered the vast amount of residual electrons can sustain the discharge well. In the case of "detached ear" discharges, the feedforward capability is

relatively low, as it can be seen in the chart only less than 4 pulses can take place during a single power cycle.

Furthermore, theoretically any type of discharge events will show the trend of being less continuous as degradation progresses, which means less active cycle percentage, shorter continuous discharging length, and also less pulses in a single discharging cycle. However, from the discussion above it can also be seen that the comparison should be limited between same type patterns only, as the step change can only be used to define degradation stages, but not very useful to build up any trends across the stages. This will be discussed in the next sub-chapter.

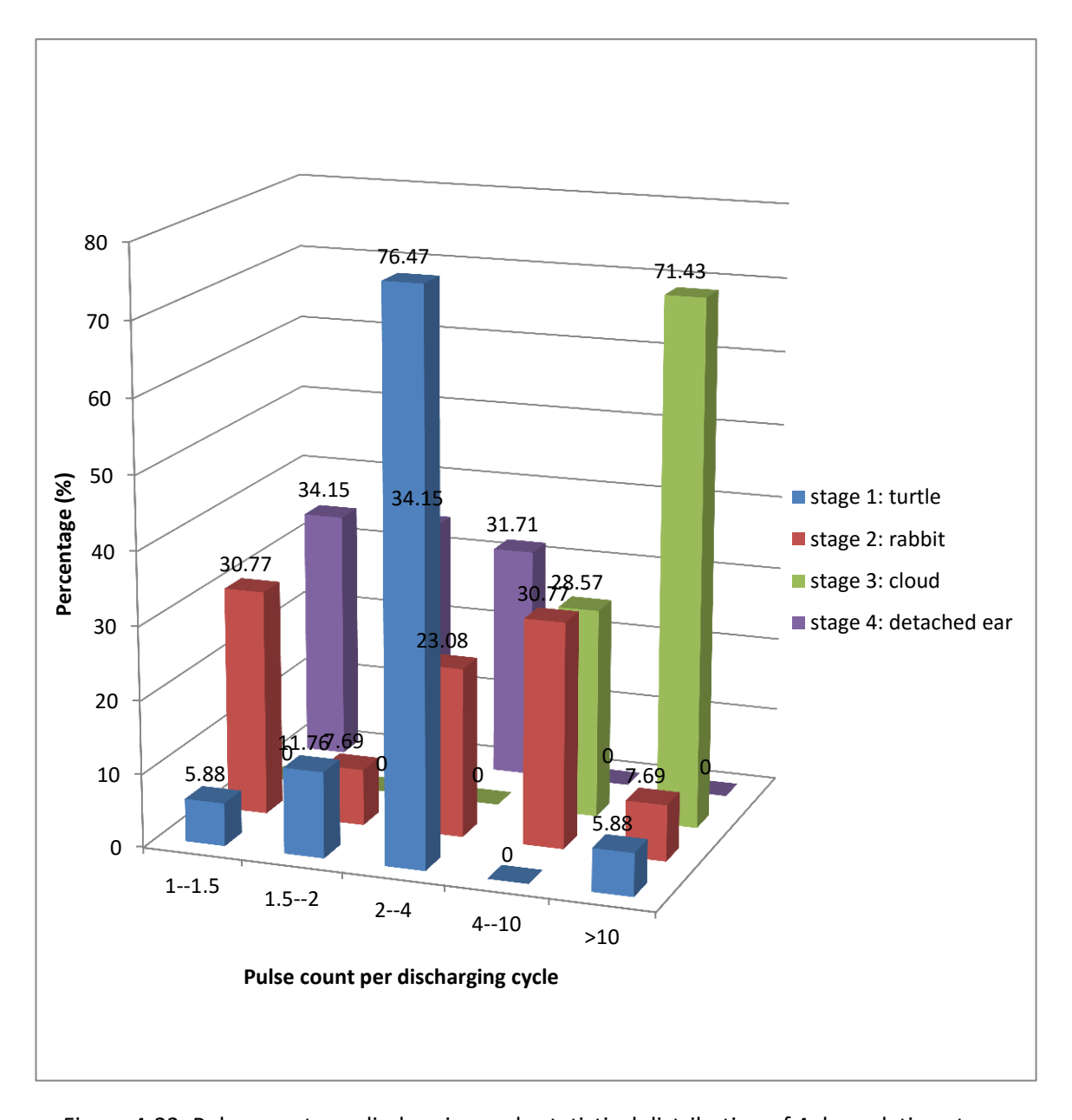


Figure 4-23: Pulse count per discharging cycle statistical distribution of 4 degradation stages.

4.2.3.2 Feedforward capability evaluation between similar patterns – the importance of "turtle-like" discharges

When it comes to evaluating the level of degradation cavities have suffered, randomness of PD behaviours is one of the trickiest problems to solve. Obviously the featured patterns from different stages can be compared to give a qualitative assessment of degradation level expressed by degradation stages, but for quantitative assessment of degradation in each stage, similar patterns shall be compared to provide a better understanding of surface degradation level.

Similar patterns are generated by similar mechanisms and by similar degradation sites, even there are multiple sites on the surface, which could be very likely under similar degradation conditions. Thus, through the continuity analysis, trending of feedforward capability of such sites can be examined, and used for quantitative analysis and prediction of PD degradation.

Ideally, all featured patterns from each degradation stage if compared with their own kind, can provide information of how feedforward capability decreases as degradation time goes on. However, "rabbit-like" patterns stops reviewing themselves in an early stage into degradation, and "cloud-like" patterns are too random to build any data set with, not to mention they generally stop reviewing themselves before stage 4 as well, they will not be suitable for the object. "detached ear" patterns occupies a longer time during the entire degradation process, however, average pulse per discharging cycle as the most important factor to evaluate feedforward capability randomly alters between 1-4 with a quite random manner even though it entirely depends on feedforward capability, because there is simply not enough sample cycles as the active period is usually around only 1% of observation time. Thus, trying to extract information with such a small data base is not ideal. However, if given more time and "detached ear" stage can last long enough, a drop in both average pulse/cycle and active percentage level may be found to indicate degradation level, especially when average pulse/cycle drops down to 1.

Up to now, the "turtle-like" pattern is the most promising type for the purpose of assessing the feedforward capability of the cavity. The main reason is "turtle-like" discharges never disappeared as degradation proceeded. They show up once in a while between other discharge types during later degradation stages. Also, "turtle-like" discharge is a less random type comparing to later types of discharges, which are very heavily depending on the feedforward capability of very limited surface areas. "turtle-like" discharges happens across the entire surface instead, its occurrence at multiple sites eliminates a large proportion of the randomness. Thus, if plotting against degradation time, the continuous discharging cycle length of "turtle-like" discharges generally shows a decreasing trend towards 1, and so does the pulse count per discharging cycle. Also, the active level percentage shows a dropping trend towards 0.

Figure 4-24 shows the converging of PD active level towards 0 for "turtle" discharge only along with degradation time. If focused into the area where PD active level is below 5% (Figure 4-25), it can be seen that there is still some space for PD active level to converge even at the end of 1970 hours, and below 5%. Thus, it is possible to be used for quantitatively predicting feedforward capability loss, and then degradation level.

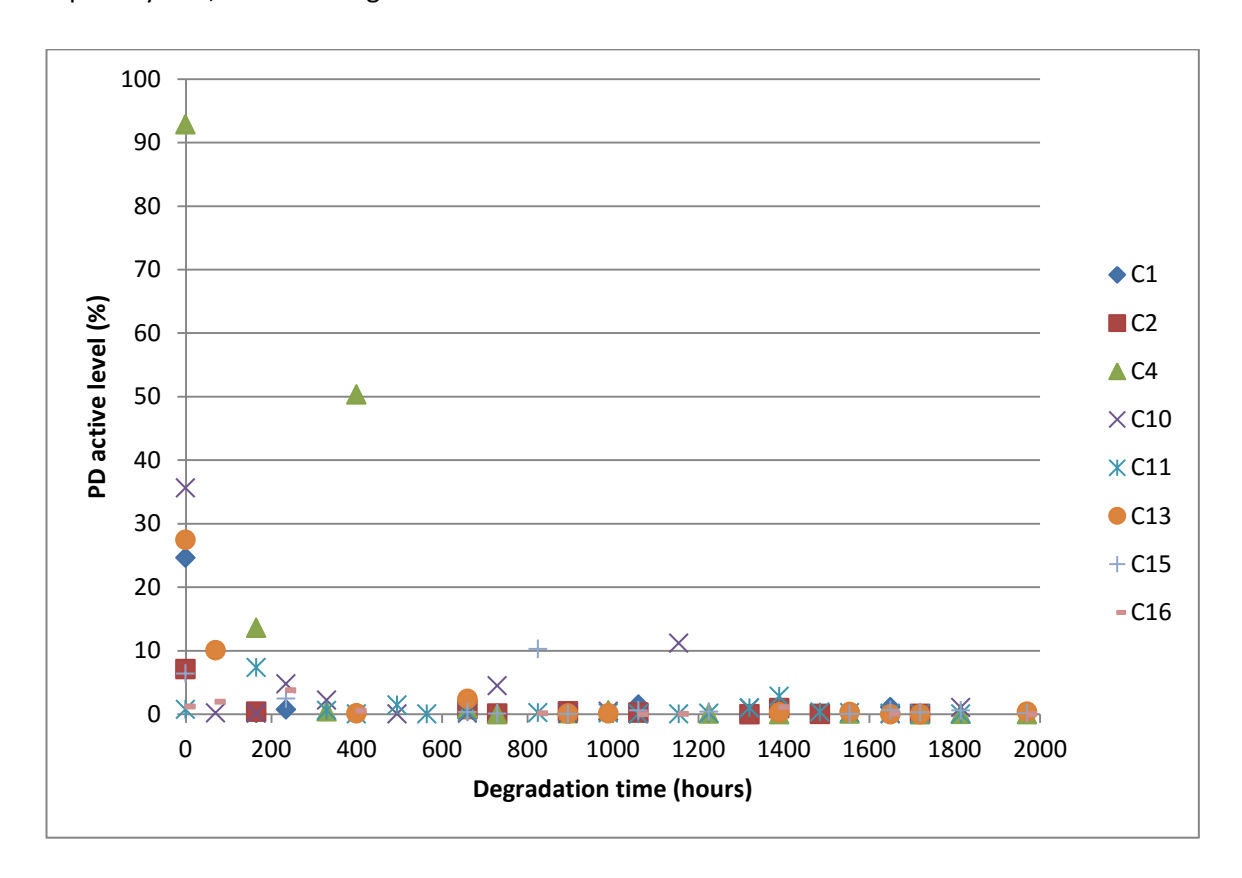


Figure 4-24: "turtle" discharge feedforward capability loss - PD active level.

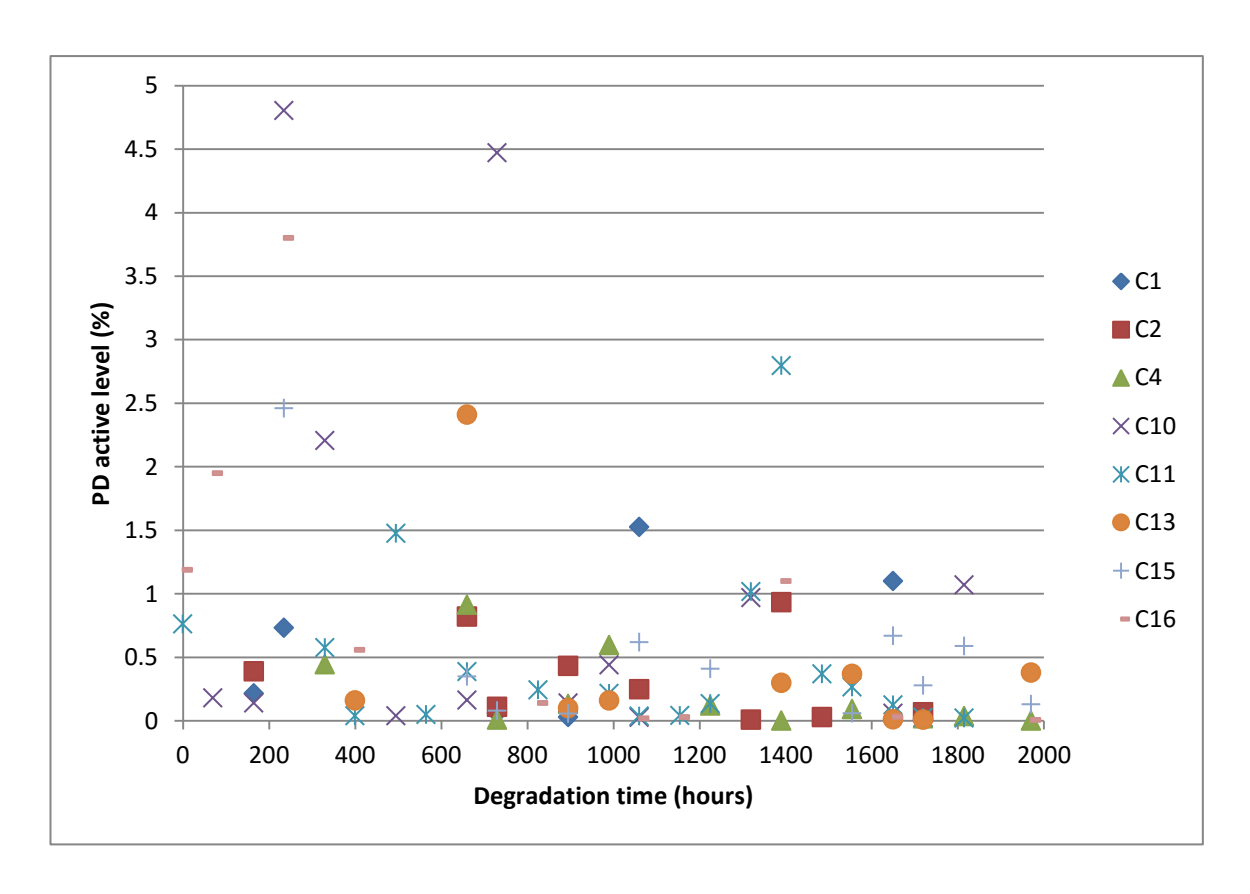


Figure 4-25: "turtle" discharge feedforward capability loss - PD active level below 5%.

As discussed above, continuous discharging length along with degradation time should also converge, to a value of 1 where each cycle of discharge event cannot trigger any activity afterwards. Figure 4-26 shows the convergence of continuous discharging length of "turtle" discharges.

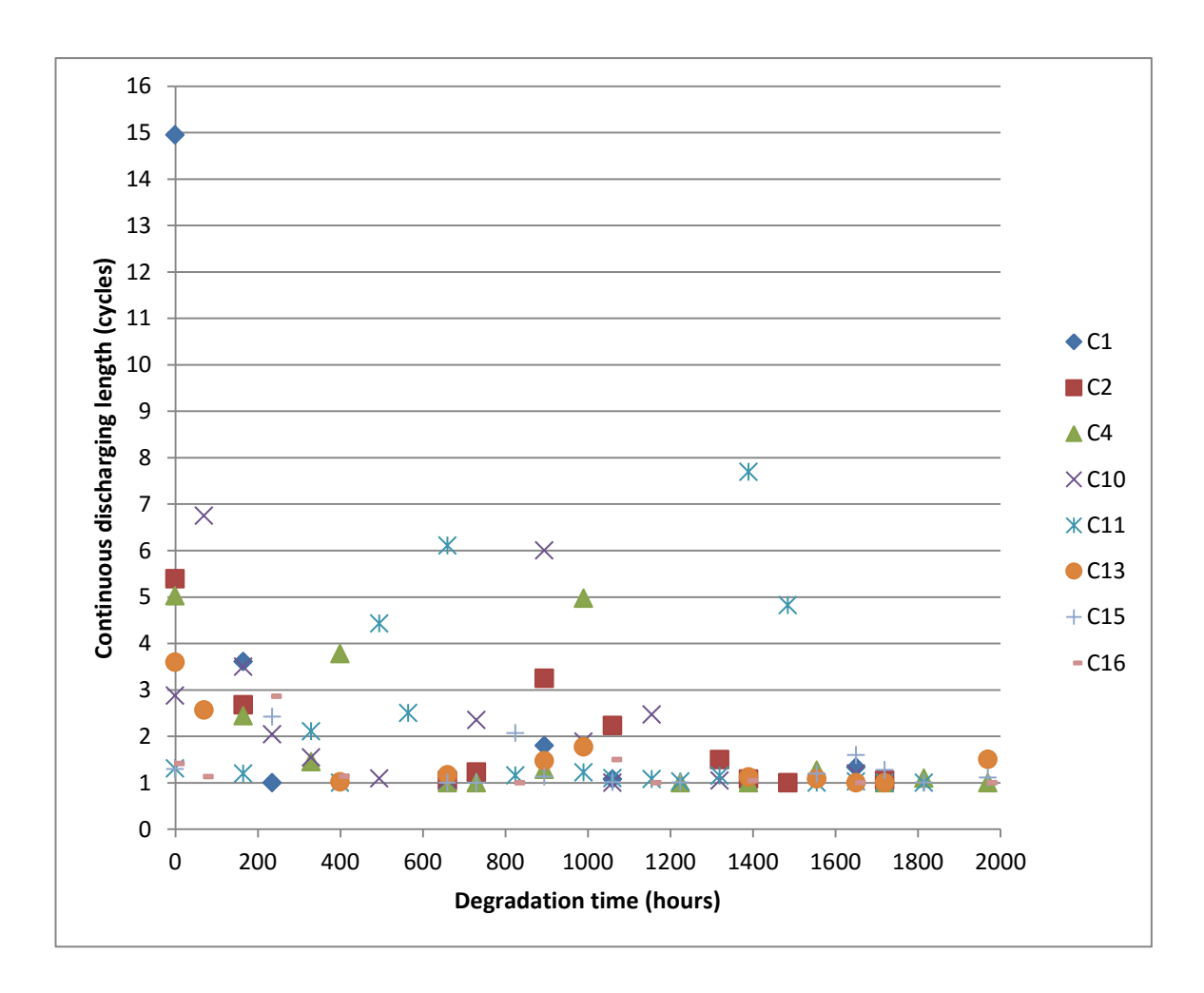


Figure 4-26: "turtle" discharge feedforward capability loss - continuous discharging cycle length.

Under the same theory, the number of pulses in each discharging cycle should also fall down to 1, where each pulse of PD is an individual that has no feedforward relationship with others. Figure 4-27 shows such trend of pulse number per discharging cycle.

Furthermore, by employing appropriate weighting factors, these representative continuity parameters could be combined to quantify the level of degradation suffered by cavity surfaces, if given a full life cycle of the material and corresponding PD data. However, the current group of epoxy resin samples showed no sign of failing until the end of this experiment.

The same principles should apply for any possible featured PRPD patterns, with decreasing trend of the continuity factors. This theory could be utilized if another featured pattern is observed in later degradation stages, when there are enough data samples to perform the analysis.

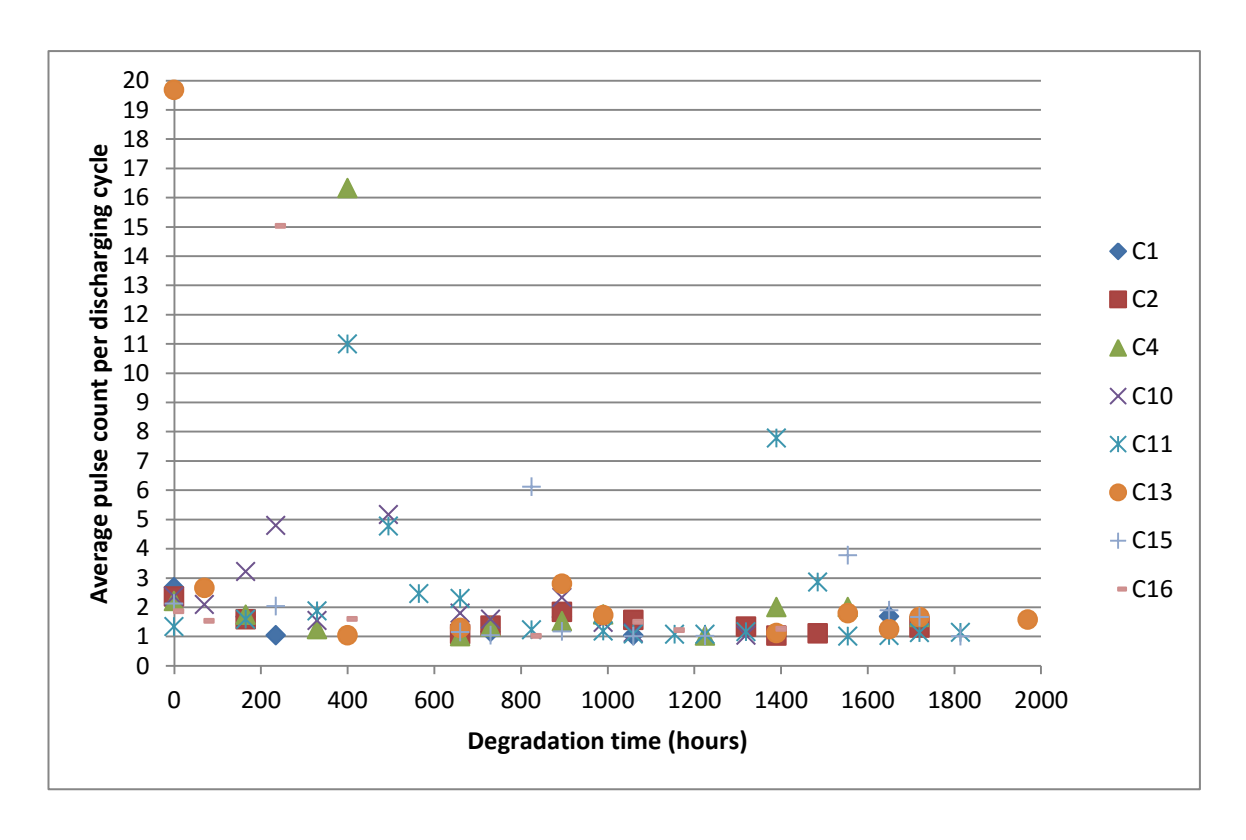


Figure 4-27: "turtle" discharge feedforward capability loss - average pulse count per discharging cycle.

4.2.4 Possible indication of future degradation stages – below the hard threshold

It has been found that after stage 4 with "detached ear" patterns, most samples did not generate detectable PD in between adjacent surging discharges above the hard threshold of 3pC, which threshold was kept constant since the beginning of experiments. However, during experiments since stage 4, the noise conditions in TDHVL were significantly improved due to the finish of most commercial impulse and breakdown tests, a noise level of only 1pC could be obtained. This lowering of noise level enabled the finding of a new degradation stage: stage 5 with periodical, low magnitude discharges as shown in Figure 4-28.

Pulse sequence analysis returned that most of these are very stable discharge events during their occurrence. With most applied voltage cycles only 1 discharge event takes place, either on the positive or negative half cycle, within very limited span of phase angle, resulting in an average pulse/cycle between 1 and 1.1. Continuous discharging length is significantly increased to tens of cycles, and PD active level is also back up to around 50%. Figure 4-29 shows a typical pulse train sequence from sample C16 at 1650 hours.

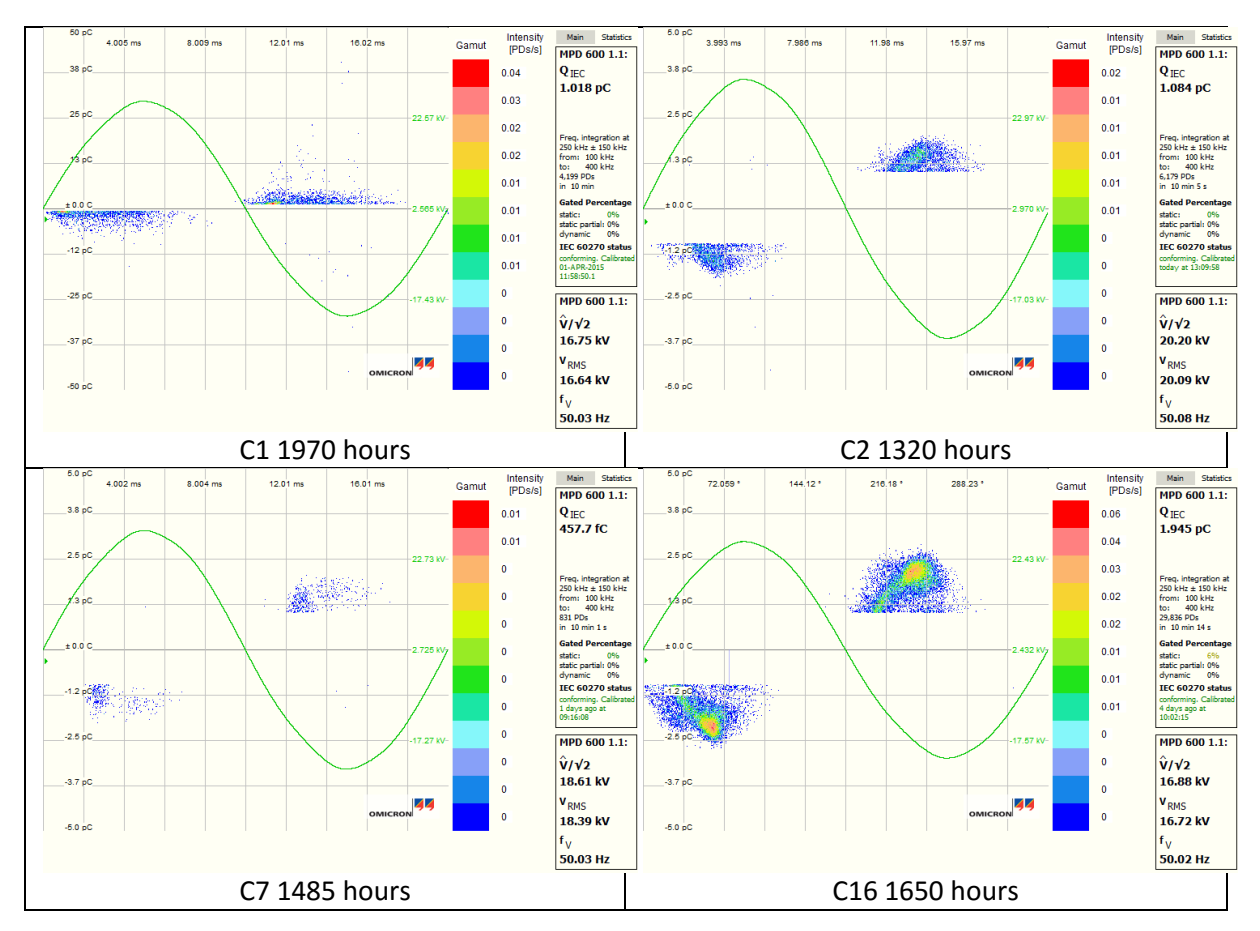


Figure 4-28: Typical degradation stage 3 patterns from group C, low magnitude periodical discharge.

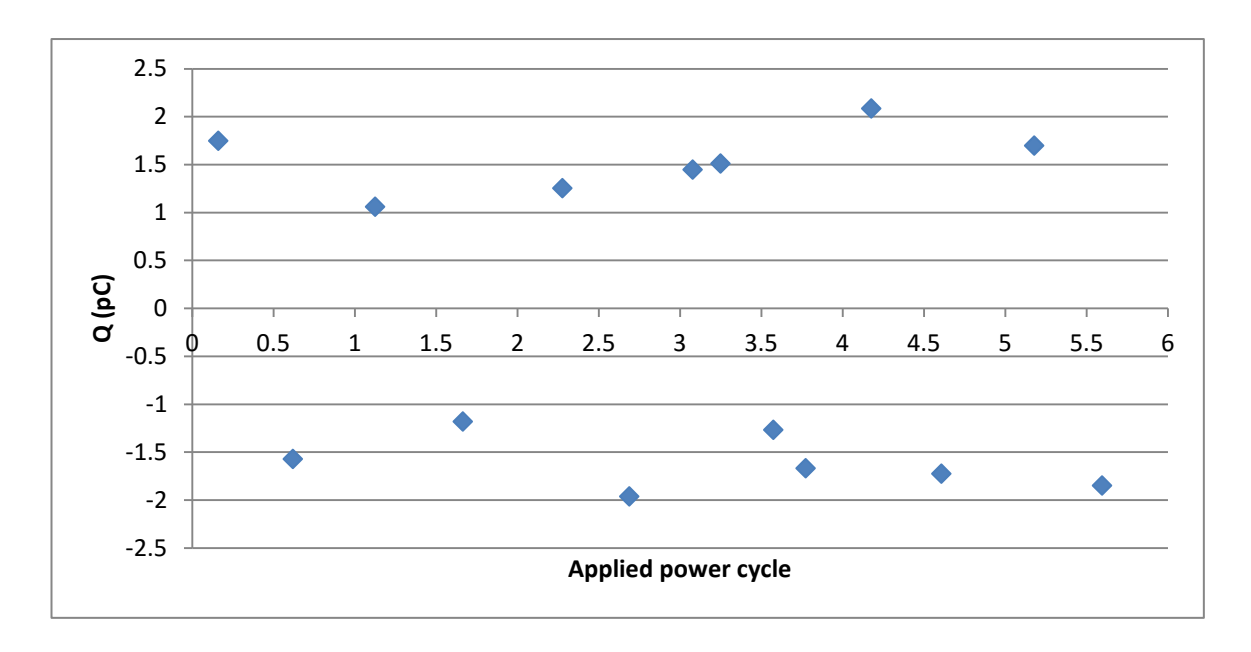


Figure 4-29: Typical swarming discharge pulse sequence from sample C16 at 1650 hours.

To conclude, this is a type of discharge with very low and consistent magnitude, happening in limited phase angle span, not very much relying on feedforward capability from previous events, but can frequently produce itself through volume electron generation from the surface material. All above statements indicate the discharge is happening within a very limited area on the surface

(limited span of magnitude and phase angle), the area is highly conductive (not relying on previous events), and possibly with some sharp carbonized structure formed (being able to frequently produce first electrons).

Peter Morshuis [111] had observed similar discharging events, it was claimed to be discharge activities "below the noise level of electronic acquisition tools, only picked up with a CCD camera by the illumination produced, which is within only very few tiny points on the surface". The type of discharge was termed as "swarming discharge" by Morshuis for both epoxy resin and polyethylene [112, 113, 114]. Furthermore, Morshuis utilized phase resolved classification to distinguish changes between possible degradation stages [111, 84, 83], and observed the localization of PD events from each discharge type [63].

There are still questions about discharge under the current noise threshold of 1pC. Methods published claiming successful noise removal without hard thresholding are generally based on wave shape, frequency and time related features of the pulse signals. A widely studied and applied method is the wavelet transform, which can decompose a pulse signal, then represent its features using a limited number of parameters [115, 116]. This method is also used in TDHVL claiming a high recognition rate when tested to achieve signal classification [117]. PDBase II as the data acquisition and processing tool used for group B samples in this work also offers a simple cluster mapping using basic equivalent time length/frequency approach [118, 119, 120]. However, these methods were applied but not found to be successful in this case.

Considering the assumption that electrical trees form and propagate through the insulation material before final breakdown, as well as all PRPD patterns produced by electrical trees are periodical behaviours with nearly no feedforward capability (needle tip trees), it can be seen that treeing patterns are "detached ear" patterns or swarming patterns with better first electron generation rate from the surface itself, and less effect from feedforward capability. Thus from "detached ear" patterns to swarming patterns, if local conductivity around the swarming discharging area can be further increased, and initial electron generation rate can be further enhanced, the treeing PRPD pattern can be achieved. Mizutani constructed an artificial channel in LDPE [121], discharge events from such channel reported are similar to the late stage PD behaviours, especially if compared by their pulse sequence behaviours: periodical events with minimum effect from surface charge accumulation. Figure 4-30 shows such events found by Mizutani. Figure 4-31 shows the typical treeing PRPD and pulse sequence patterns reported by Suwarno [122], which is generated by needle tip treeing in polyethylene.

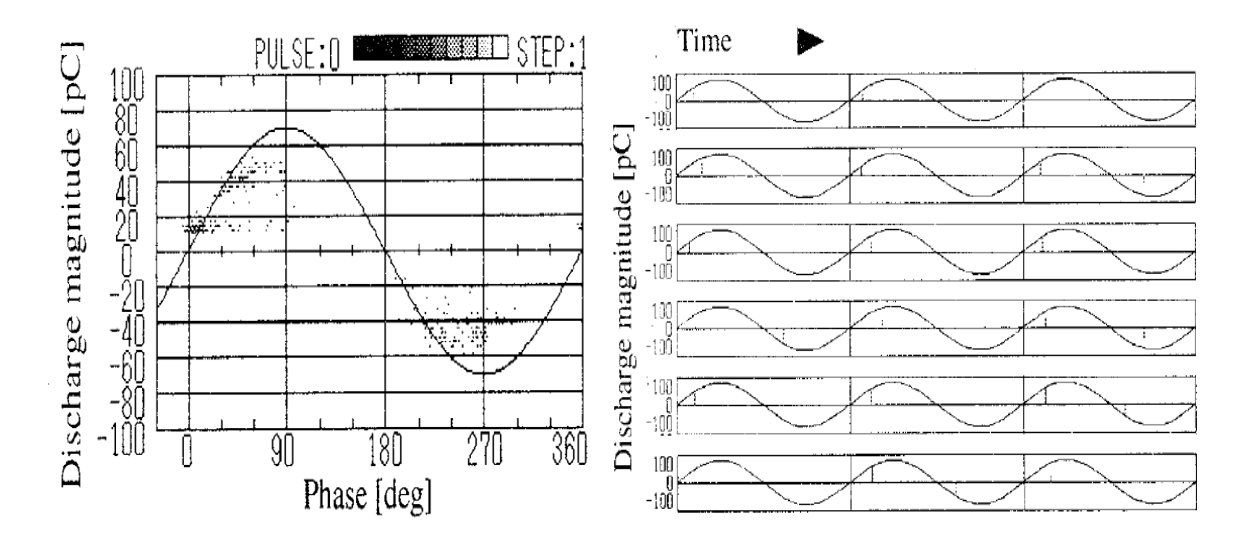


Figure 4-30: PD in artificial channel in PE, left: PRPD pattern; right: pulse sequence [121].

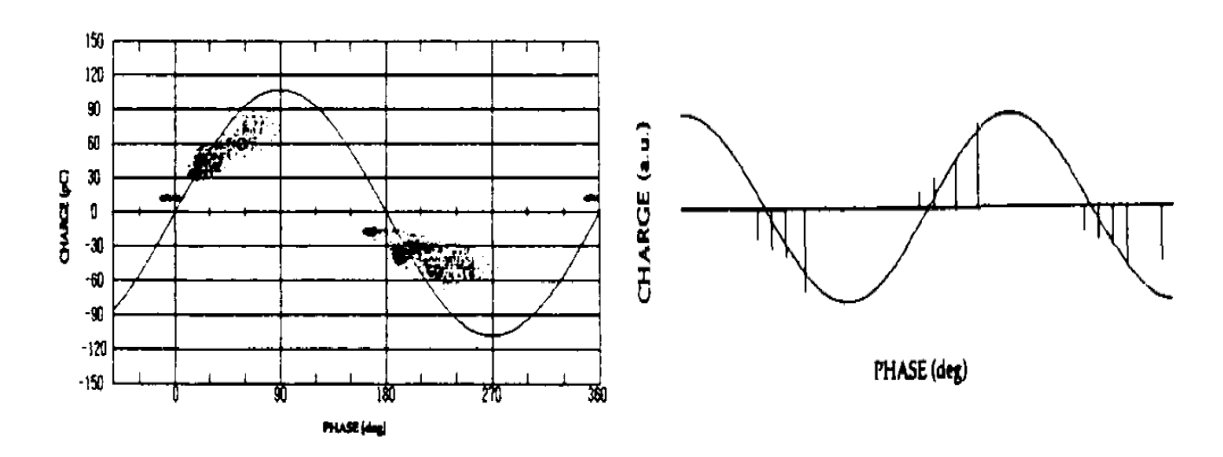


Figure 4-31: PD from needle tip treeing in PE, left: PRPD pattern; right: pulse sequence [122].

4.3 Microscopic observation of deteriorated surfaces

Although it has been reported that discharge events already start to focus onto a concentrated area since the transition from "turtle-like" to "rabbit-like" patterns inspected by discharge illumination [108], experiments in this work shows that degradation sites, especially concentrated spots appear mostly around the time when "detached ear" patterns are taking over, which is the start of degradation stage 4. See Table 4-4.

Hence, it is reasonable to conclude that the formation of concentrated degradation site is the driving force behind the occurrence of "detached ear" like discharges, if combined with the theory behind such discharge events as discussed earlier. Also, such discharge events in return bring further damage to the degradation sites.

Table 4-4: Surface degradation site formation vs. degradation stage 4 starting.

Sample No.	Degradation stage 4 starts at	First degradation site seen at
C1	895 hrs 895 hrs	
C2	990 hrs	990 hrs
C4	No "detached ear" after cloud	1720 hrs
C10	1225 hrs	1060 hrs
C11	895 hrs	895 hrs
C13	1060 hrs	1155 hrs
C15	1155 hrs	730 hrs
C16	895 hrs	895 hrs

The above 8 samples were stressed and tested up to 1970 hours, and are the ones carried observable degradation sites under the optical microscope utilized. Others were chosen to be sacrificed, not only because they did not carry observable degradation sites, but also due to they were generally less active in terms of discharging comparing to the 8 left. A full microscopic imaging record for the 8 samples with observable surface degradation can be found in Appendix C.

In this work, cavity surfaces were further deteriorated in two major ways: with or without the formation of liquid droplets. Liquid droplets as a term was used by Morshuis [65], However, there is no physical evidence that they are liquid in this work, instead their later survival of the vacuum process before gold-coating sacrificed samples suggest that they are actually solid. Their formation on polymer surfaces under partial discharge are widely reported [123, 54, 89, 66]. H, C, and O are all determined to be essential for the formation of such droplets. In the case of droplets being formed, including sample C2, C4, and C16, among which C16 was shown in Figure 4-32.

As it can be seen in Figure 4-32 that there were already a few concentrated degradation sites 895 hours into degradation, which are shown as black spots in the microscopic image. The colour black possibly indicates carbon from epoxy resin side chains. At the same time, "detached ear" patterns started to appear as a dominant discharging type, whilst other types of PD events were still not extinguished. Hence, droplets and carbonize sites all grew with time, eventually forming the very obvious carbonized spots in later images, which could be the source of swarming discharge detected towards the end of this 2000 hours experiment.

The other type without droplets including sample C1, C10, C11, C13, and C15, among which C15 is shown in Figure 4-33.

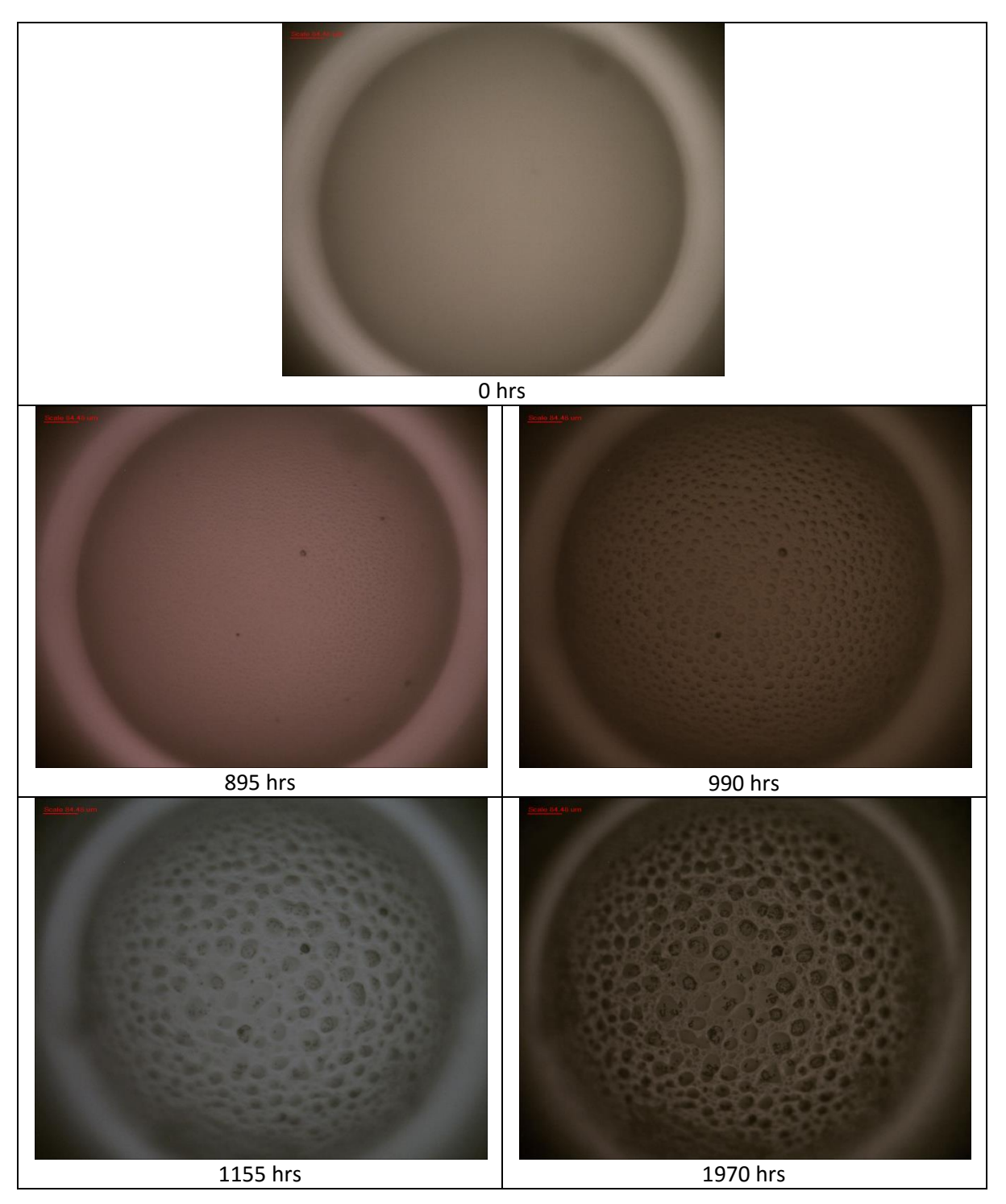


Figure 4-32: Sample C16 - formation of concentrated degradation sites with droplets.

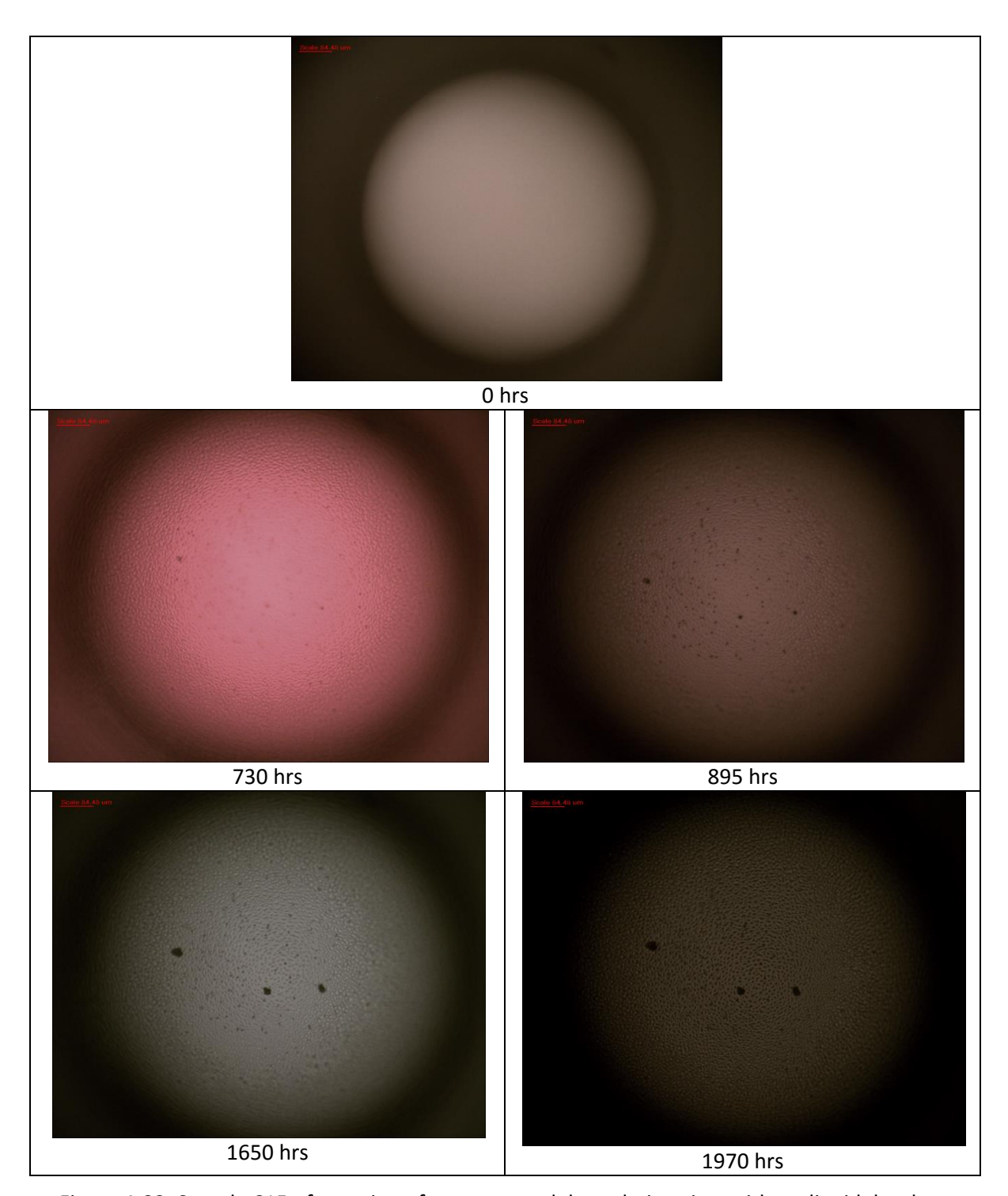


Figure 4-33: Sample C15 - formation of concentrated degradation sites without liquid droplets.

In the case of degradation without droplets in Figure 4-33, the initial carbonized sites can be seen to have greatly enhanced as degradation time progresses. At the same time, new sites started and grew. In fact, with or without droplets showed little effect on PD behaviours. Concentrated degradation sites with conductivity enhancing carbonized by-products were instead the major driving force behind the transition between later degradation stages. Such development of concentrated degradation sites are also reported by Morshuis [83], PD illumination location shift

recorded in which are similar to the physical degradation site development in this work. See Figure 4-34.

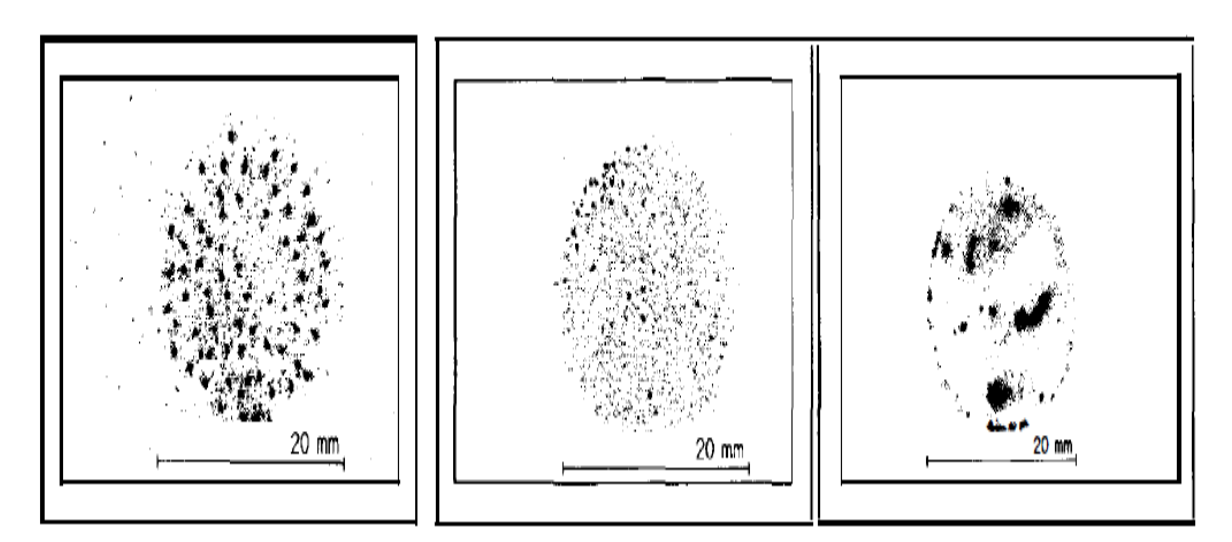


Figure 4-34: Discharge location in a cavity in PE, from left to right: 0-1 hrs, 1-25 hrs, >25 hrs [83].

To conclude, microscopic images confirm the formation and physics behind periodical discharge events in stage 4 with "detached ear" discharges, by the correspondence in terms of occurrence time of each other. Carbonized sites produce periodical discharges, and the discharges in return further damage the sites. Whether it is possible or not that carbonized sites can later grow into the start of electrical treeing will be further examined by SEM imaging in the next chapter.

Thus, by evaluating the feedforward capability of late stage periodical discharge types especially swarming discharge, the damage level of the exact location of such PD events can be estimated. Compared with other degradation life models, this method avoids the calculation of accumulated damage and the distribution of calculated damage across the degradation surface, instead it helps understanding the conditions of the exact locations suffering damage as the alarming type of discharge is only generated from such locations.

4.4 Summary

This chapter reports the experimental results from epoxy resin sample group B, for a 2000 hours degradation trial test. The methods in the trial test were then adapted, and utilized on 16 samples in group C. Samples were put through a degradation test which lasted 1970 hours, 8 samples were sacrificed along the way, and the other 8 were preserved until the end of the test. All samples were to be tested under SEM for more detailed optical and chemical examination.

PRPD results confirmed the conclusions from sample group B study, defining 4 degradation stages with clear PRPD pattern features. After more detailed pulse sequence study, which mainly

focused on the feedforward capability of discharge events, the degradation process under cavity PD with epoxy resin can be concluded.

During early degradation stages strong PD feedforward influences can be found, as later PD events heavily rely on the previous ones. These types of PD behaviours include "turtle-like" patterns which indicates stage 1, and "rabbit-like" patterns which indicates stage 2. Stage 3 is marked by "cloud" discharges, where discharge events still heavily depends on previous events once the cavity is activated, but there can hardly be any first electrons generated if there is no surface charge left. Stage 3 indicates a localized surface conductivity level that is high enough to disperse electrons for further feedforward effect, but not yet generated any sharp carbonized site to enhance first electron generation from the material bulk. Stage 4 marked by "detached rabbit ear" discharges and 5 by swarming discharges are both with periodical PD activities, which indicates a further decrease of feedforward capability, and a further increase of bulk electron generation ability.

Three major parameters used to define PD feedforward capability level are PD active level, continuous discharging length, and pulse count per discharging cycle. These parameters were put through statistical analysis and showed satisfactory trends. It is possible to quantitatively evaluate PD feedforward capability level of degraded surfaces with such parameters, leading to a quantitative evaluation of degradation level.

Microscopic images confirmed the theory, by showing the birth and growth of carbonized sites being very timely correspondent with the start of degradation stage 4 of "detached rabbit ear" discharges. With or without droplets, PD behaviours were similar according to the observation during experiment.

SEM optical and chemical analysis will be discussed in the next chapter, to confirm the chemical aspects of degradation sites, and also surface roughness before massive carbonized deterioration, which was not successfully captured using an optical microscope as utilized in this chapter.

Chapter 5: Cavity Surface Analysis

This chapter reports the effects from cavity surface deterioration on PD behaviour. This part of the study was undertaken to confirm the hypothesis that localized degradation sites dominate the latter stages of PD activity, and to further define the relationship between degradation sites and PD behaviour in details. RAMAN spectroscopy (RAMAN), Scanning Electron Microscopy (SEM), and Energy Dispersive Spectroscopy (EDS) were utilized to perform optical and chemical examinations on degraded cavity surfaces. Also, a set of UV degradation experiments was conducted to confirm the importance of geometrical modification of cavity surfaces. Results discussed in this chapter support the theory of degradation from PD data analysis and optical microscopic image analysis, by confirming the geometry of degradation sites, the existence of C and O at such sites, and also the role of such sites in the generation of periodical PD activities.

5.1 RAMAN spectroscopy

RAMAN spectroscopy works with a monochromatic light source, in the case of this experiment a red laser beam is used. It utilizes inelastic scattering to distinguish matters scanned, as the energy of laser photons will be shifted when interacting with molecular vibrations or other excitations. While scanning, laser wavelengths being elastically scattered from the matter examined will be filtered out, leaving wavelengths that are inelastically interacting with the matter to be recorded as a material feature of the scanned object.

In this study, RAMAN spectroscopy was used to observe chemical components of degradation by-products. Carbonyl groups were anticipated to be discovered as a result of electrons breaking side chains of epoxy resin. In this case it was very important that the system could be focused onto cavity surfaces precisely. The RAMAN system used in this study could operate under Confocal mode (C mode) and Non-Confocal mode (NC mode). C mode can focus onto an exact spot, while NC mode picks up all data along the travelling path of laser beam. Theoretically C mode suited the purpose of this study better, however, focusing onto exact cavity surfaces was quite difficult, thus NC mode was also tested and both modes returned very similar results.

5.1.1 Experimental method

The RAMAN system must be warmed up and calibrated after every system restart. The laser used in this study should be warmed up for at least 30 minutes, 4 LEDs turning all green indicates the laser being ready to use. Calibration should be carried out with a fixed silicone sample, it should produce a frequency response peak at $520 \, \Delta \lambda / \text{cm}^{-1}$ ($\Delta \lambda$ is the wave number). And the laser power

used must not saturate its range, if saturated the response peak will be blunt instead of sharp. When all calibration standards are met, response peak position, silicone peak intensity, actual laser intensity, and operating mode used must be recorded.

For actual measurement, the following procedures apply:

- Switch the microscope under visible light mode, focus onto the point to be scanned. A
 clear and in focus hexagon indicates the microscope is in focus.
- Switch the microscope to laser mode.
- Select frequency response range. In this study a full range from $100\Delta\lambda/\text{cm}^{-1}$ to $3200\Delta\lambda/\text{cm}^{-1}$ was used to study all possible degradation products.
- Select laser power to be the same level as used for calibration.
- Select cosmic light removal to ensure background noise elimination.
- Select accumulation numbers, 100 accumulations was used for recorded degradation data.
- Start scanning, turn off all external light sources, and make sure there is no vibration to the equipment and sample being tested.

5.1.2 Initial tests and cavity surface focusing methods

Virgin epoxy resin samples were used for initial trial tests to establish a reference point for future degradation tests. It was found difficult to use just the microscope under visible light for focusing onto cavity surfaces. A frequency response was found for virgin samples that the existence of air/resin interface, this was used to locate exact cavity surfaces, as for virgin samples the cavity surface and sample upper surface are both air/resin interfaces, thus they should present identical frequency response.

To find the exact focus onto cavity surfaces, the following tests were conducted:

- Test of pure epoxy resin sample bulk (not include the cavity), take measurements for every 20μm into the sample bulk from the upper surface. If the response does not change along the distance into the sample bulk, then it can be used as a reference for the same test on cavity top.
- Conduct the same test on cavity top, the focus point should departure from an air/resin interface (sample upper surface), travel inside epoxy resin bulk, and reach another resin/air interface (cavity top surface). Thus the response should start from the typical air/resin interface, towards the typical resin bulk response, and then return to the interface response.
- All samples used in this test should be virgin samples, to ensure sample upper surface and

cavity upper surface are identical interfaces.

Pure epoxy resin bulk returned following response plots, due to the number of measurement point tested, only results for every 200µm are shown in Figure 5-1.

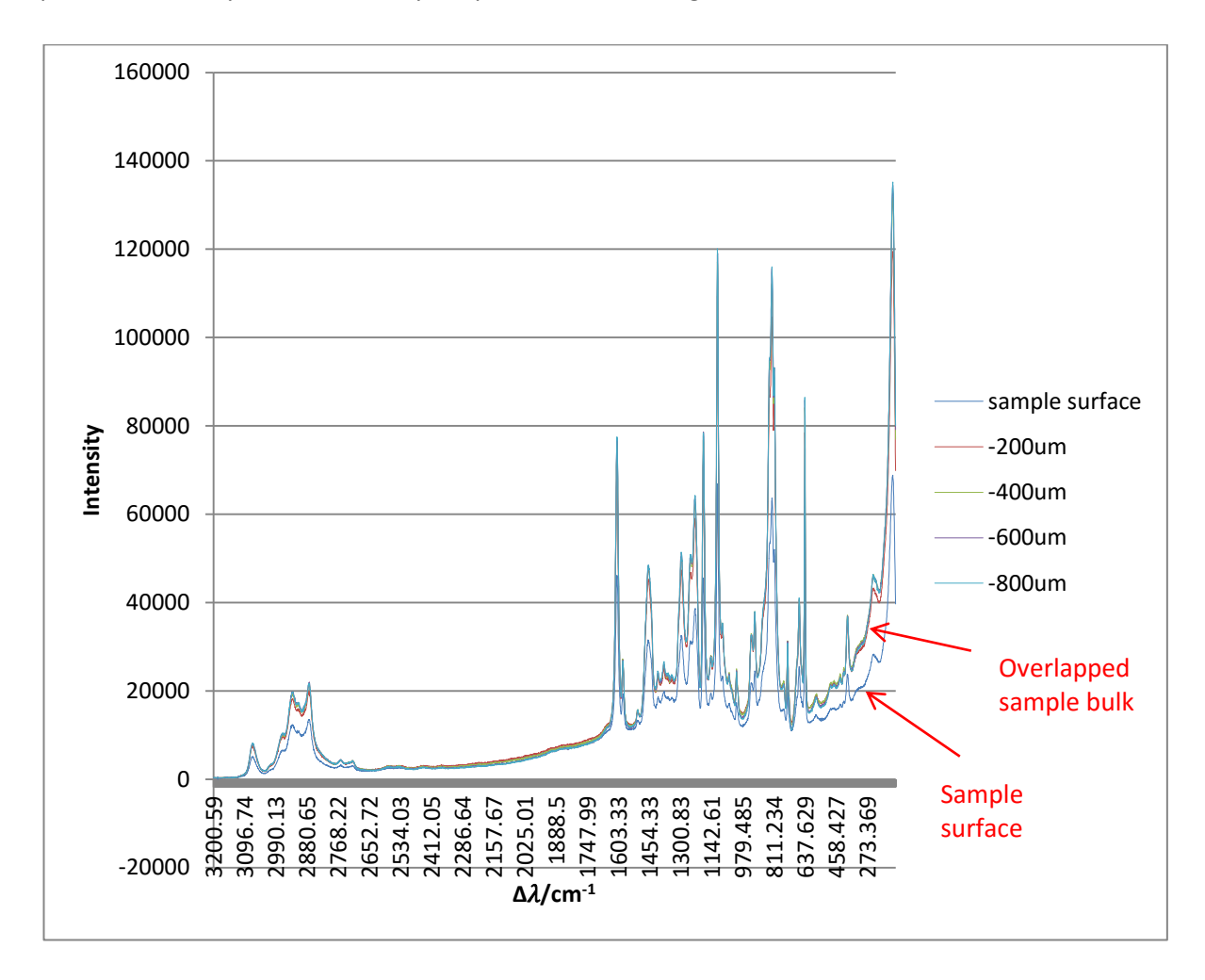


Figure 5-1: Epoxy resin RAMAN test, different depth into sample bulk.

From Figure 5-1 it can be observed that only the response plot on the sample surface has a lower peak intensity, whilst the rest almost overlap each other. This test again confirms that existence of air will change response intensity, and as it can be seen that the focus depth difference into the material bulk does not affect the frequency response.

The same test was repeated with the same virgin sample on top of the cavity, while the focusing point is exactly located on top of the cavity centre of gravity. The following result was returned in Figure 5-2.

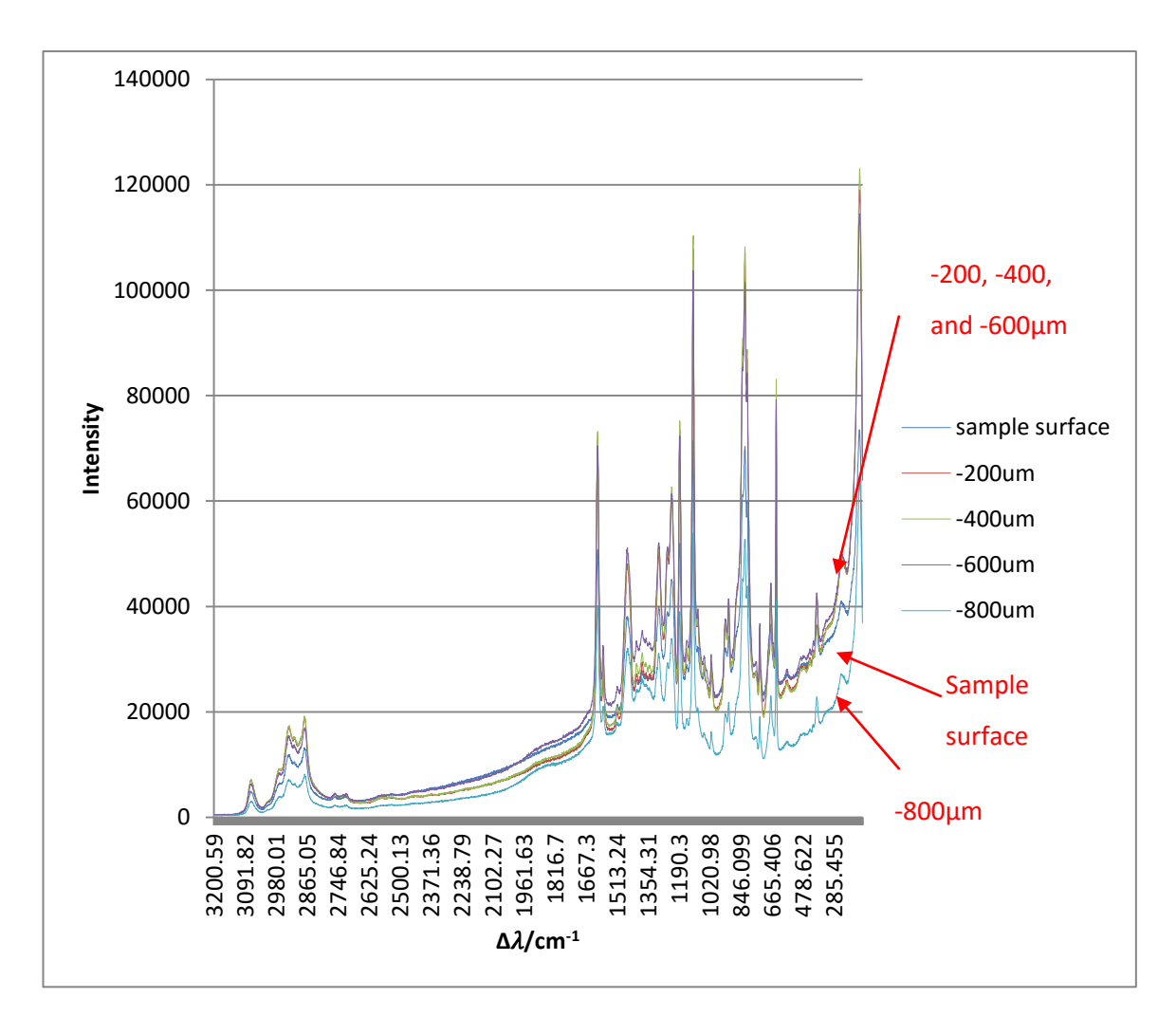


Figure 5-2: Epoxy resin RAMAN test, different depth into sample bulk through the cavity with 200µm steps.

As anticipated, peak intensity into sample bulk deviates from surface reading initially, readings from -200 μ m to -600 μ m overlap each other. Then at -800 μ m the focus point goes beyond cavity surface back into air, peak intensity drops back down again. Thus it can be determined that the cavity surface of this sample is located between -600 μ m and -800 μ m.

Smaller steps were used between -600 μ m and -800 μ m, it was found that peak intensity drop starts from beyond -780 μ m, and it was observed that the drop tends to be sharper across the depth step over the interface from all measurements as shown in Figure 5-3.

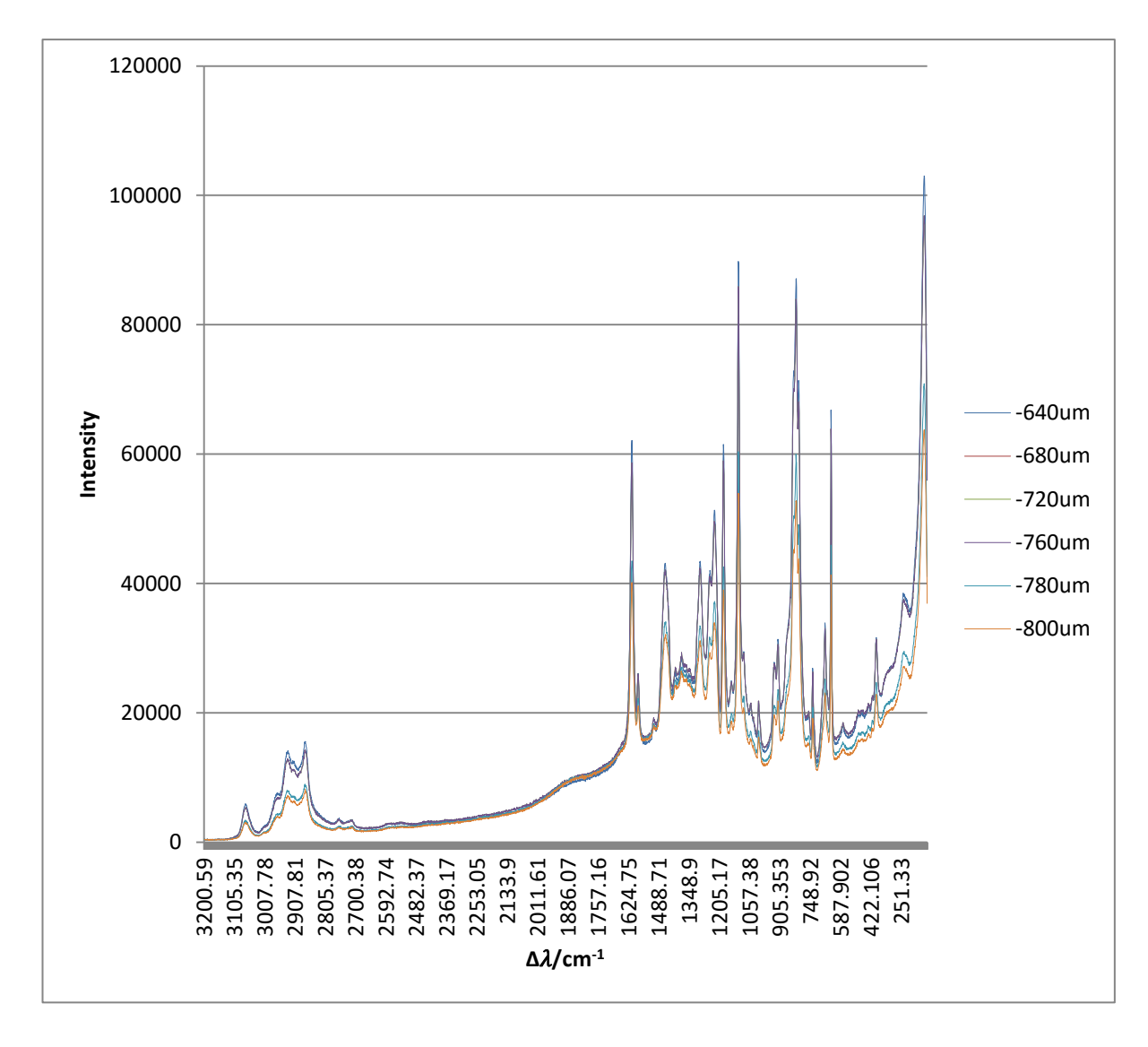


Figure 5-3: Epoxy resin RAMAN test, different depth into sample bulk above the cavity with $20\mu m$ steps.

It is now certain that the cavity surface is beyond the depth of -760μm but not more than 800μm. If taking laser focus intensity into consideration, a more precise cavity surface depth could be determined. It was found that if the microscope was in focus onto an interface, the laser beam in its scope would be shown by PC online monitor would be in better focus as well (slim and contracted). It would gradually lose its focus while moving away from the interface into homogeneous material. Thus the laser focus should act in a similar way with peak intensity while travelling between two interfaces through homogeneous resin bulk: from in focus to lost focus and then in focus again and Figure 5-4 shows the gradual change while moving from the sample upper surface into resin bulk, whereas Figure 5-5 shows the gradual change while approaching the cavity top surface.

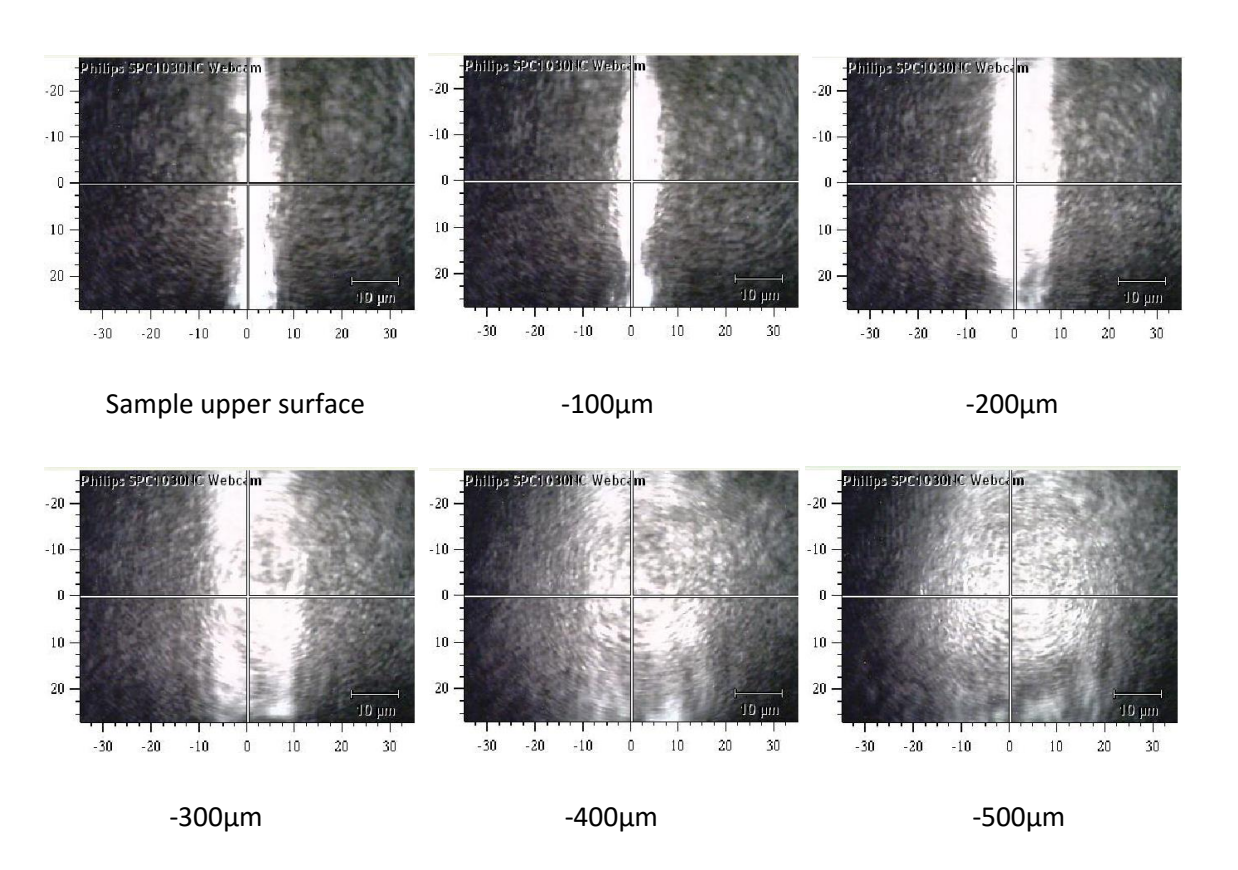


Figure 5-4: RAMAN focusing test, laser intensity at different depth leaving sample top surface.

By combining sharp peak intensity drop and laser focus intensity, -780 μ m was determined to be the depth of cavity top surface for this sample. Cavity surface focusing was with an accuracy of around 20 μ m only, as a depth step smaller than that could hardly make any observable difference with the current system used, both in terms of peak intensity and laser focus.

In summary, the cavity top surface can be located by the following procedures:

- Focus onto the exact geometrical centre of the cavity using the microscope under visible light mode.
- 2. Take a spectroscopic measurement for every 200μm into the epoxy resin sample, starting from its upper surface. Cavity top surfaces should all locate at around 800μm beneath sample upper surfaces, as all samples are made identical. This is just to confirm cavity location is roughly around normal level using peak intensity drop.
- 3. Take spectroscopic measurements for smaller depth steps around the cavity surface, every 20µm are used in this experiment.
- 4. During the 3rd step, also take laser beam images using the online monitoring system for every depth step measured.
- 5. Use combined information from peak intensity drop and laser focusing level to determine the exact location of the cavity top surface.

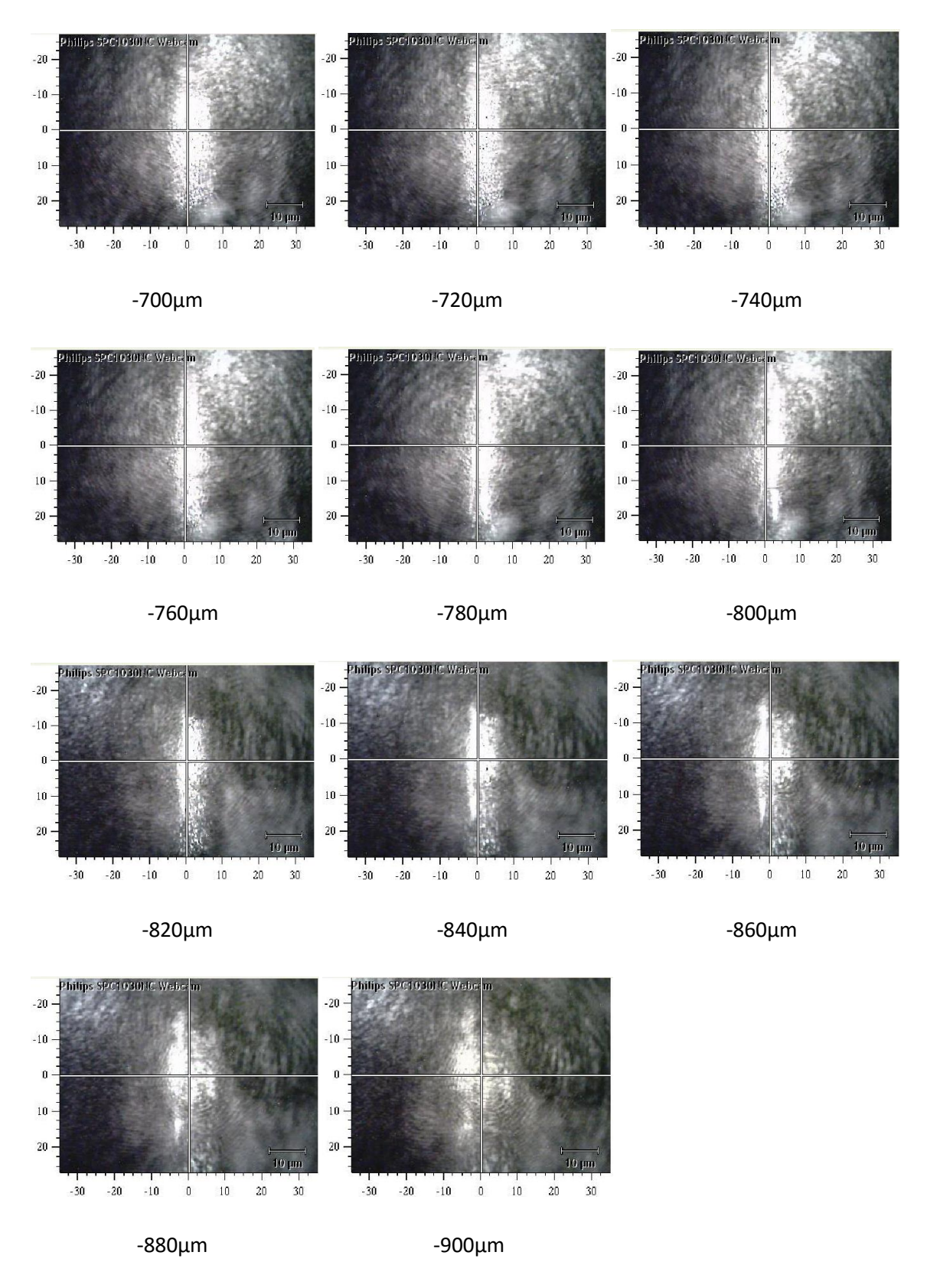


Figure 5-5: RAMAN focusing test, laser intensity at different depth when crossing cavity top surface.

5.1.3 Degradation test for epoxy resin samples – Group B

The cavity top focusing method introduced in section 5.1.2 was applied to all group B epoxy resin samples, finding the following cavity top surface locations for the 4 samples. Table 5-1 details the surface depths for the four samples.

Table 5-1: Cavity	v top surface	depth for ep	oxv resin sam	ple group B.

Sample	Cavity top surface depth
B1	-780μm
B2	-780μm
В3	-760μm
В4	-800μm

RAMAN spectroscopic scan was conducted for all 4 samples after full PD degradation experiments, however, no evidence of degradation by-products were found. According to previous experience from TDHVL, the RAMAN spectroscopic system was not sensitive enough to detect chemical accumulations until the amount of accumulation was significant (observable under visible light microscope by the RAMAN system). A typical result from 2000 hour degradation is shown in Figure 5-6. It can be seen that all response peaks from degraded cavity top surface are also produced by virgin epoxy resin sample bulk, which indicates that no new chemical accumulation was detected by the system.

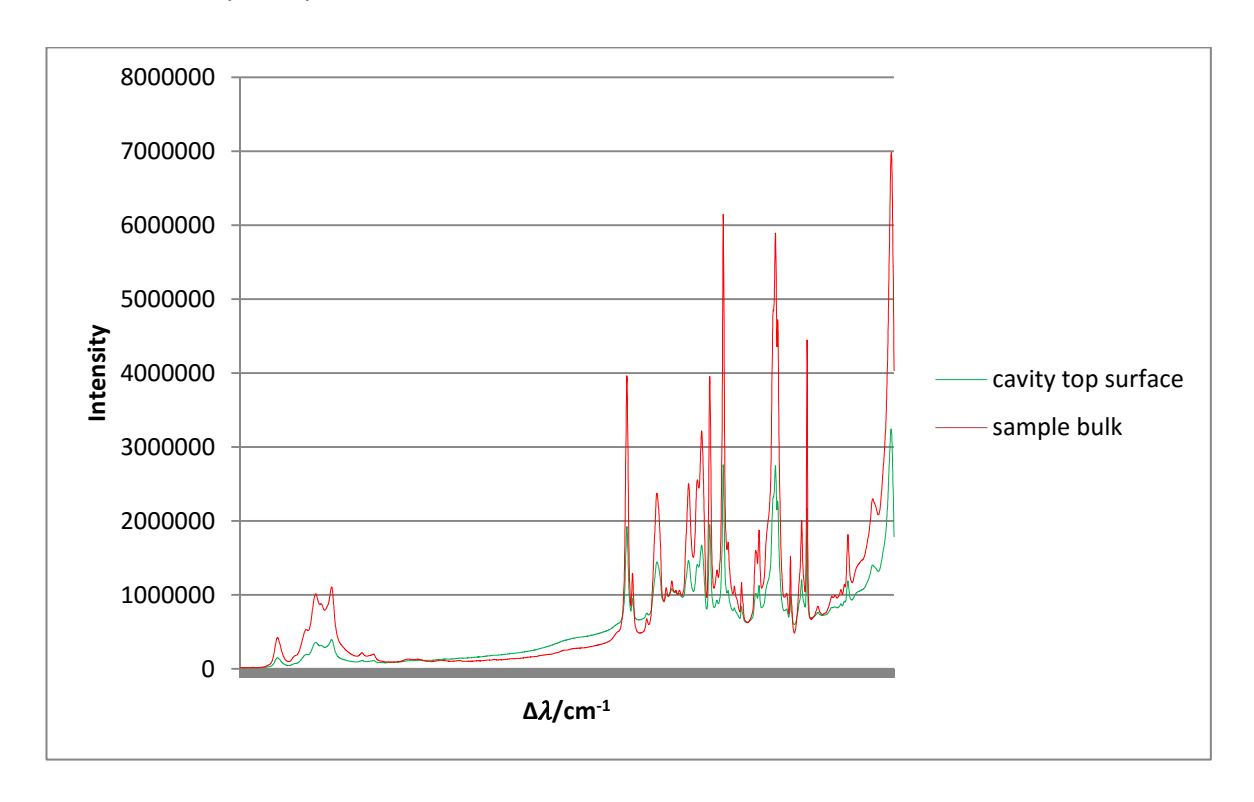


Figure 5-6: Typical RAMAN degradation test result, sample B2 at 1000 hours.

5.1.4 Summary

RAMAN spectroscopic scan was conducted, inspecting both virgin epoxy resin samples and degraded samples from group B. Through the tests with virgin samples it was found that a resin/air interface fed the signal back differently from how a pure resin region would do, but only the peak intensity is different, peak frequency locations are still the same. This was used to find the exact location of top cavity surfaces, also with the help from laser focusing intensity. Scanning of epoxy resin samples group B did not return any evidence of accumulated chemicals, due to the sensitivity of the RAMAN system and the amount of products produced during the experiment not being significant.

5.2 Scanning Electron Microscopy (SEM) and Energy Dispersive Spectroscopy (EDS)

SEM and EDS tests were conducted, inspecting both virgin epoxy resin samples and degraded samples. Advantages of a scanning electron microscope comparing to an optical one is that SEM works by shooting electrons against the surface of inspection and collecting scattering data, which makes the focus no longer an issue when the surface of inspection is uneven. An optical microscope against such an uneven surface like the ones in this work can only focus onto one depth at a time, thus SEM in this case can provide images with much better quality in this case.

A SEM is usually formed by an electron gun with fires electron beams against the surface of inspection. The beam is collimated by electromagnetic condenser lenses, focused by an objective lens. Based on the feedforward of electrons, an image is formed sequentially during a scan. Two types of signals are normally imaged in SEM: secondary and backscattered electrons. Second electrons are the ones emitted from sample top surface, which can be used to form the surface structure of the sample. Different depth on such a surface will result in different colour concentration on the image formed, the closer to the lens, the brighter the colour [124]. Backscattered electrons are the ones with higher energy, they are produced when the primary electron beam from the gun is bounced back by elastic collisions with atoms. The intensity of the beam being bounced back is determined by the mean atomic number of the area being focused on. Thus, the areas with larger and heavier atoms will have stronger signals. This feature is used to determine material composition, providing chemical information along with geometrical information.

The SEM used in this work can magnify up to x50,000, with a resolution level up to 1nm [125]. However, practical experience only returns a trustful resolution around 10nm. Electron beam

density and intensity of the SEM used in this work were adjustable, usually values applied from 5kV to 15kV for accelerating voltage, and beam current around 0.1nA. In this work, 5kV of accelerating voltage was usually applied, as the gold coated surfaces were not conductive enough so electrons could get accumulated in the area of inspection, resulting in burning effects. Also, for polymeric materials with lower atomic mass, higher speed electrons could penetrate into the surface, resulting in less effective surface image formation.

5.2.1 SEM samples preparation

SEM used in this work required sample surfaces to be conductive, thus samples were all gold coated with a coating current of 20mA, and a coating time of 3 minutes.

Before the coating process, degraded cavities were cut out of the original samples as small cubic blocks, and then remoulded into a bullet shaped epoxy resin tube which can fit into a microtome. Orientation of degraded cavities were ensured by adhesive rubber to make sure the surface of inspection was perpendicular to the SEM electron gun, also their orientation was marked and double checked after remoulding process.

The microtome utilized glass knifes, and ensured that samples could be cut from the top by tiny slices each time until the cavity was found and opened. Conductive tape was applied to each sample as the gold coating did not provide enough conductivity for electron dispersal during SEM tests.

A typical sample prepared for SEM is shown in Figure 5-7.



Figure 5-7: Sample made ready for SEM, cavity opened, gold coated, and conductive tape applied.

5.2.2 SEM imaging

One of the original purposes for utilizing SEM was to get better imaging results, as SEM might enable observation of rough surfaces which was beyond the limit of the optical microscope, especially for those samples sacrificed early before any surface degradation was found by optical microscope. Also, with higher magnification the size of all sorts of deterioration sites could be measured.

However for the early sacrificed samples, SEM did not return much more information with its superior magnification capability. Only sample C14 returned some readings from rough surfaces as shown in Figure 5-8.

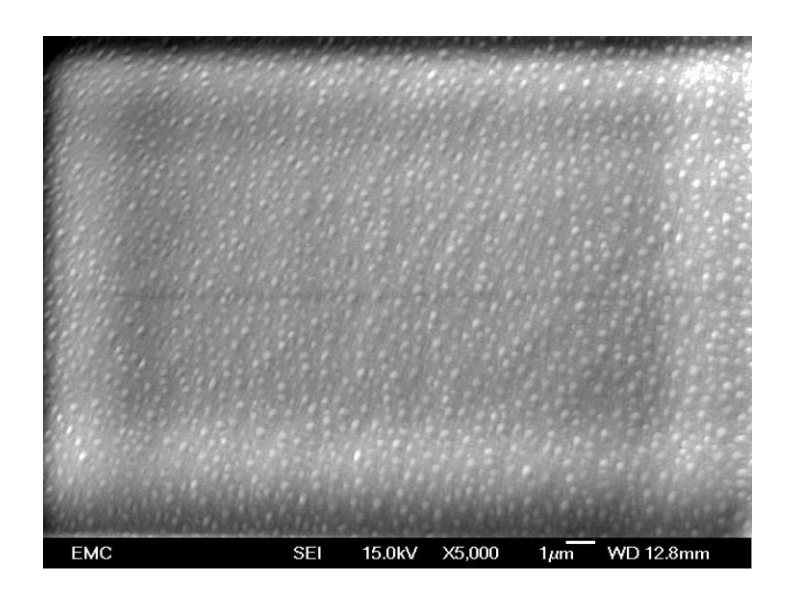


Figure 5-8: Rough surface of sample C14, sacrificed at 1320 hours under stress.

Although only C14 was found with rough surface, it still can be very indicative in terms of early stage degradation under cavity PD. As expected the degradation sites start to grow from an evenly distributed manner. More importantly, C14 was showing "detached ear" type of discharge at 1155 hours into degradation, which means "detached ear" discharge can already start with a much smaller scale of defect concentration. As it can be seen from Figure 5-8, the size of defect areas are around 100-300 nm, whilst for other samples with defects found by optical microscope, defects were observed with much larger scales, and in a far more concentrated manner.

Also as discussed earlier, "detached ear" discharge usually starts around the discovery of observable defects under optical microscope, before the defects started to concentrate on certain points. A very good example can be found with sample C1 between 1155 hours and 1555 hours of degradation time, "detached rabbit ear" patterns were observed during every data acquisition, and in the meantime, defect growth on its cavity surface can be viewed in Figure 5-9. As it can be seen, the initial defect points with a dark colour did not grow significantly in scale, instead a

"second layer" of deteriorated areas started to cover the entire surface of observation. It cannot be absolutely guaranteed that those defects were from "detached ear" PD events, however, it can at least be concluded that during heavy "detached ear" PD activities, the cavity surface is still damaged in a more evenly manner than the assumption that a few carbonized tips are involved.

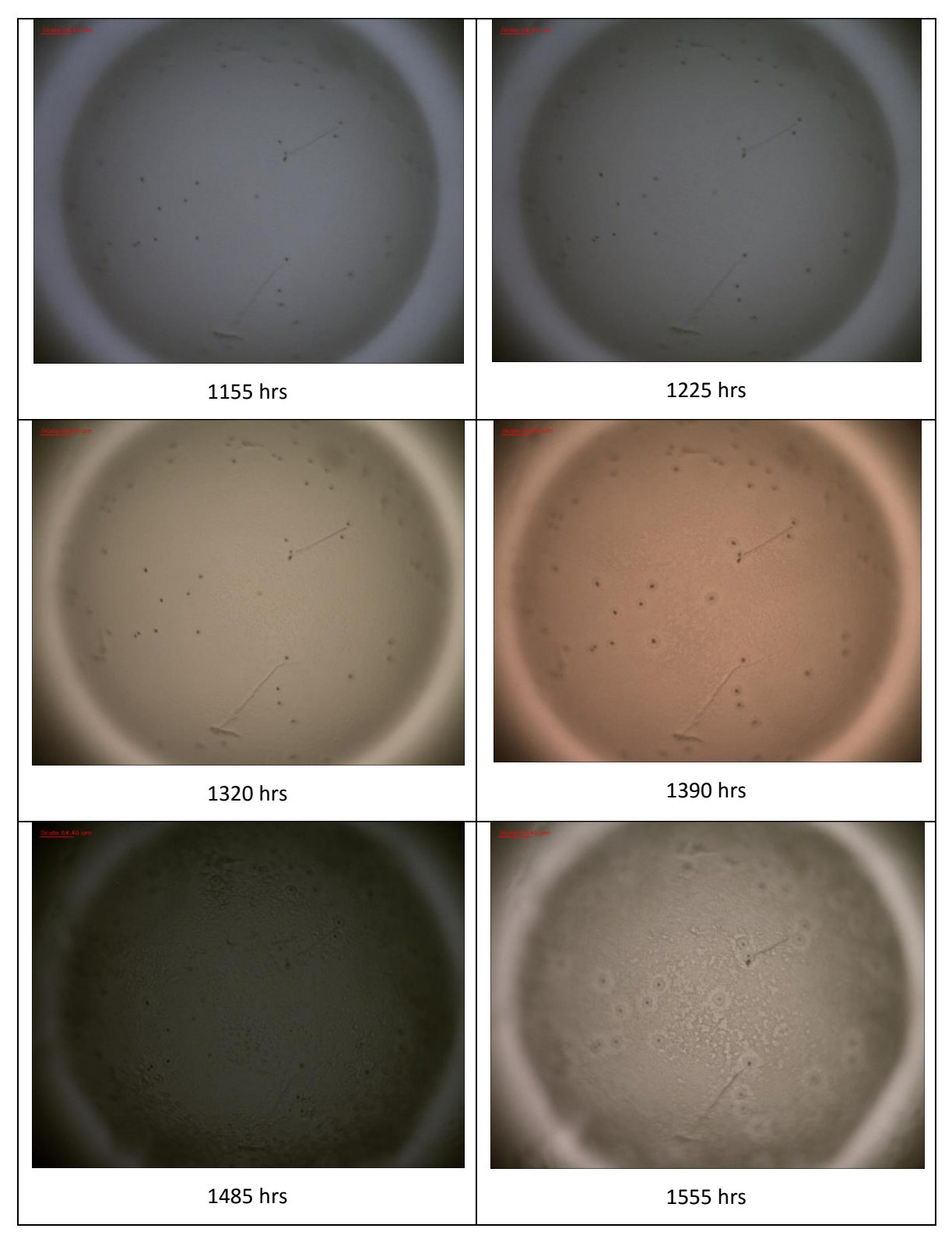


Figure 5-9: Defect growth on C1 cavity surface under "detached ear" PD.

The reason why it cannot be completely certain is that during the quiet period between "detached ear" discharges, low level discharge events were still happening as discussed earlier, which could also be responsible of the deterioration sites across the entire cavity surface. However, if considering the density of low level "turtle-like" discharges before and after the discovery of "detached ear" patterns, it is very likely that the defect sites were caused by "detached ear" discharges, as for the first approximately 1000 hours, other events including low level "turtle" discharges were dominant but imaged surfaces appeared undamaged.

So, "detached ear" discharges start with the initiation of concentrated degradation sites evenly distributed across the cavity surface. Those events will further deteriorate the sites across the entire surface, enhancing some of them to an initiation of heavily carbonized pits, which will then set the stage 5 discharge (pitting or swarming discharge) on the way.

Samples preserved to the end show a complete root towards pitting discharge on cavity surfaces. Under optical microscope μm level defect sites were already reviewed, thus under SEM, the major objective was to analyze the surface structure which could not be seen by optical microscope. The scan proved that large degradation sites were surrounded by smaller ones. All sites emerge as tiny rough areas on the surface, some of which preferred by PD events as landing sites develop into larger sites. These larger sites trigger "detached ear" discharges due to loss of their local PD feedforward capability, and in turn get further damaged and become the major sites seen under optical microscope, and become capable to trigger pitting discharge events as they are carbonized to a certain level.

Again this process has two paths: with or without droplets. Sample C16 can represent the type with droplets. From Figure 5-10, SEM images were captured from zones just beside droplets. It can be observed from the optical microscope image that droplets are generally larger than $10\mu m$ diameter horizontally. From the x10,000 SEM image clear altitude difference can be seen at the edge of a droplet, and degradation by-product clusters can be found both inside and outside of the droplet boundary. By-products in the image were identified as hydrated oxalic acid $(C_2H_2O_4.H_2O)$ by Hudon with epoxy resin [126]. Holboll also reported such by-products, an image of which is shown in Figure 5-11 [55]. The x30,000 SEM image in Figure 5-10 suggests the size of a by-product cluster being around $1\mu m$ and a pit is clearly in the middle. Also, smaller degradation sites less than 100nm can be found all over the surface, which have not grown as far as the others. Furthermore, similar pits were reported by Morshuis and claimed to be an initiation of electrical treeing in Figure 5-12 [68]. There are also other research works focusing on pitting and electric tree initiation, but mostly with needle electrodes [127, 128].

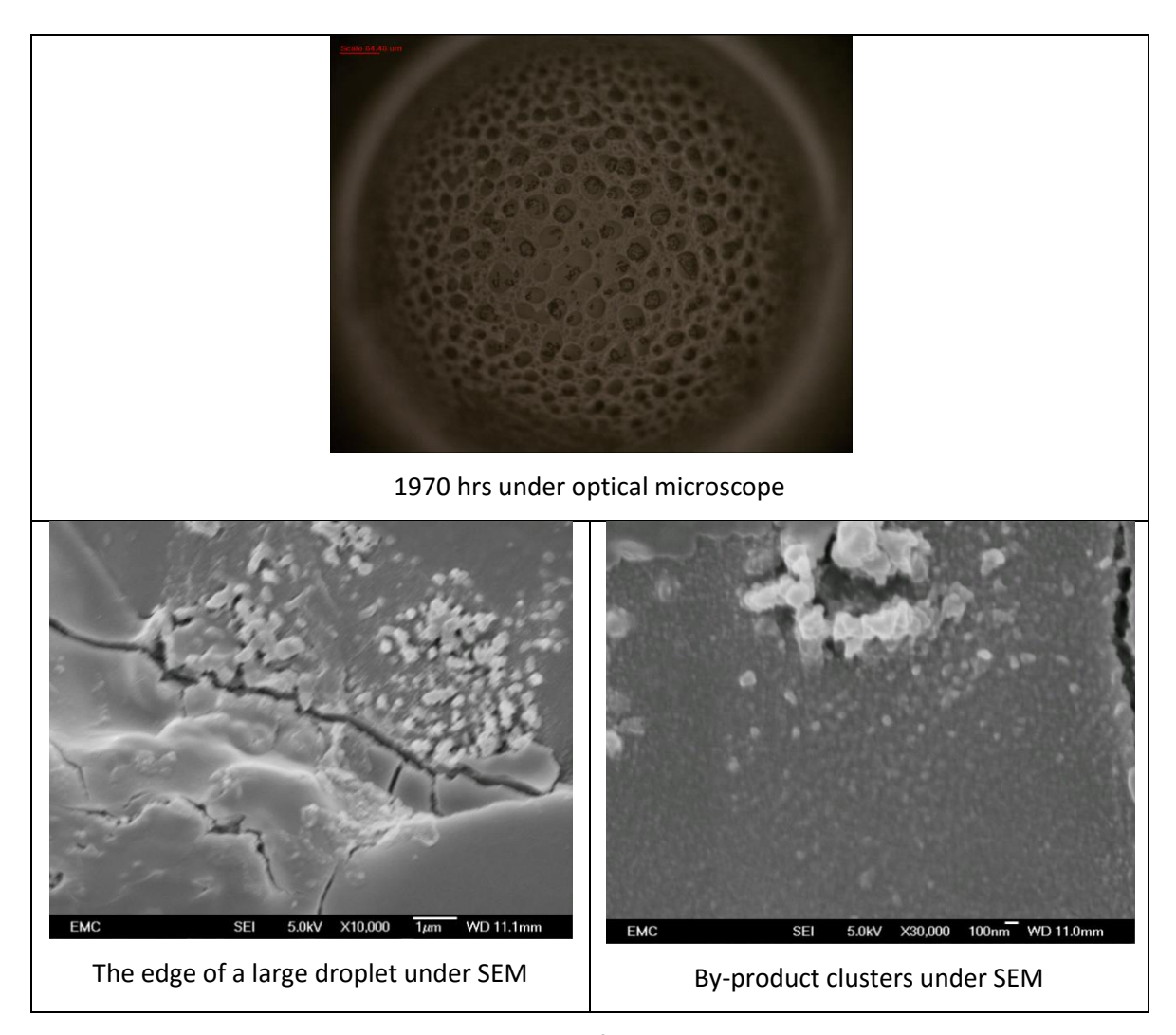


Figure 5-10: Sample C16 cavity surface, optical microscope vs. SEM.

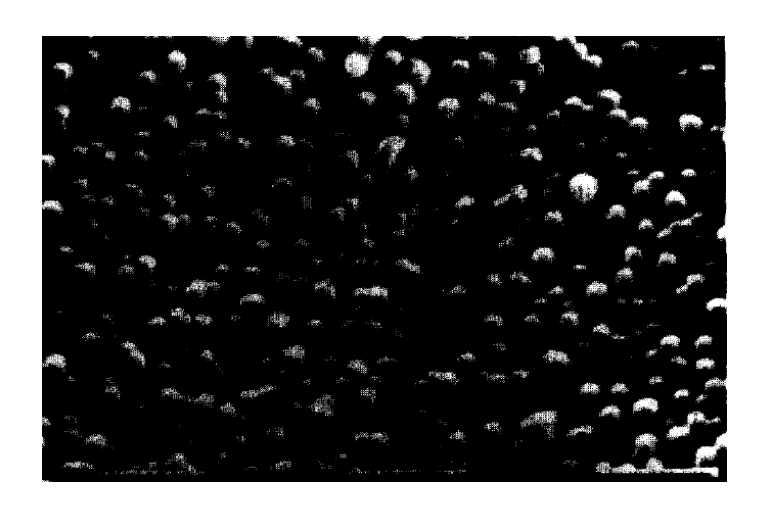


Figure 5-11: Surface of a spherical void (1.2mm diameter) in unfilled epoxy resin after 1200 hours

PD exposure by Holboll [55].

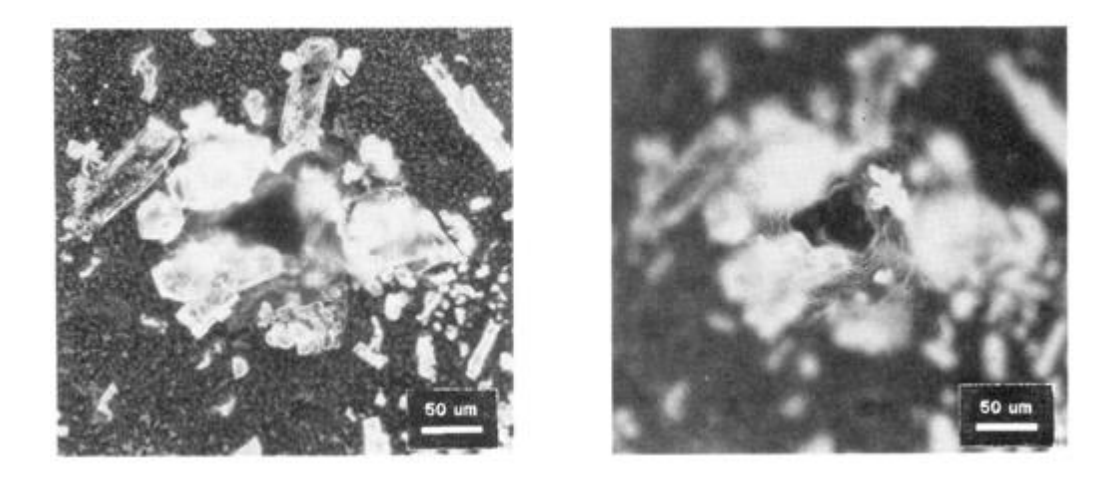


Figure 5-12: Pits on epoxy resin surface due to PD by Morshuis [68].

Sample C4 started late, but on the same degradation path of C16, thus it can be used to study the early process of this degradation process with droplet, see Figure 5-13.

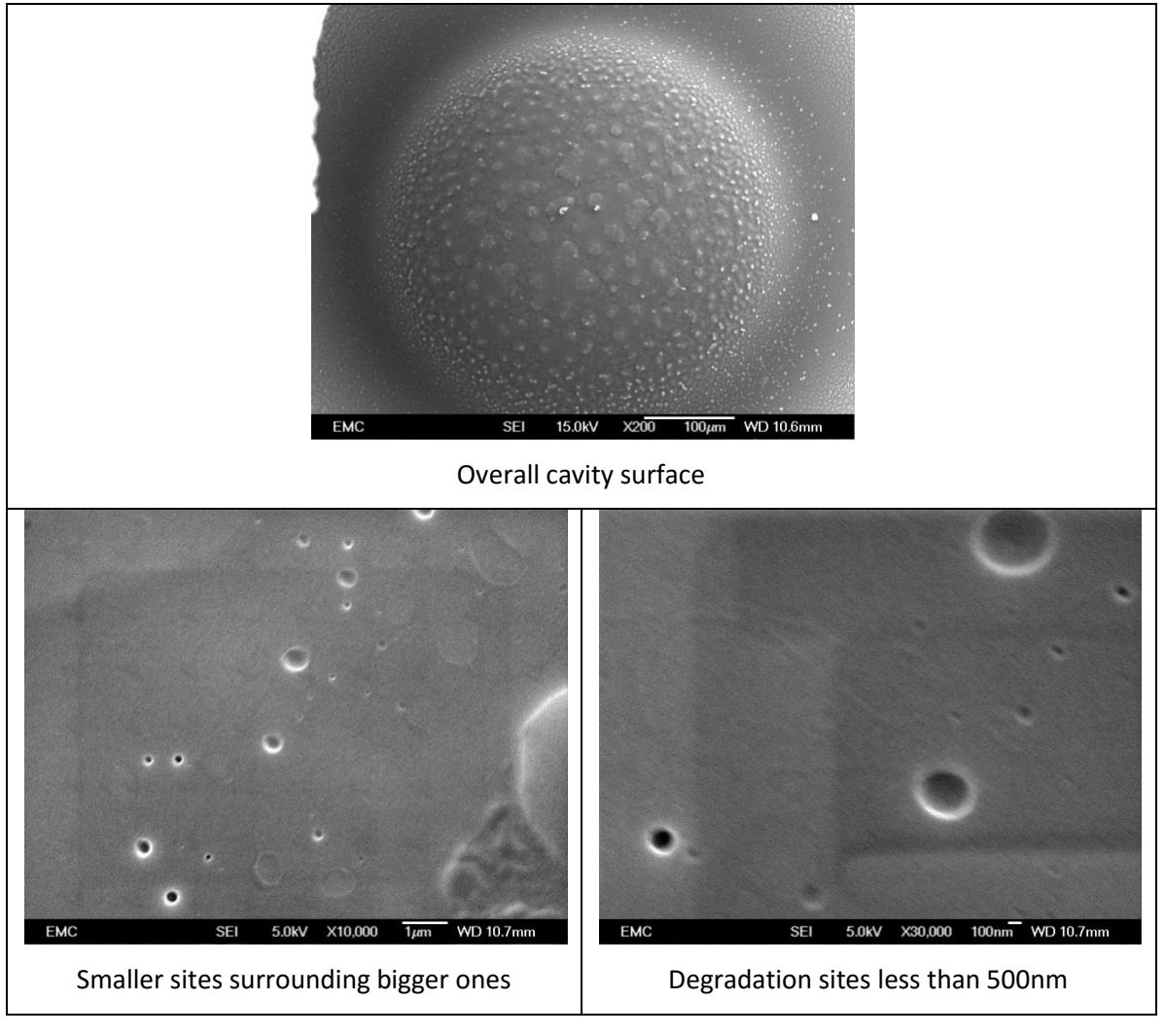


Figure 5-13: SEM imaging from sample C4.

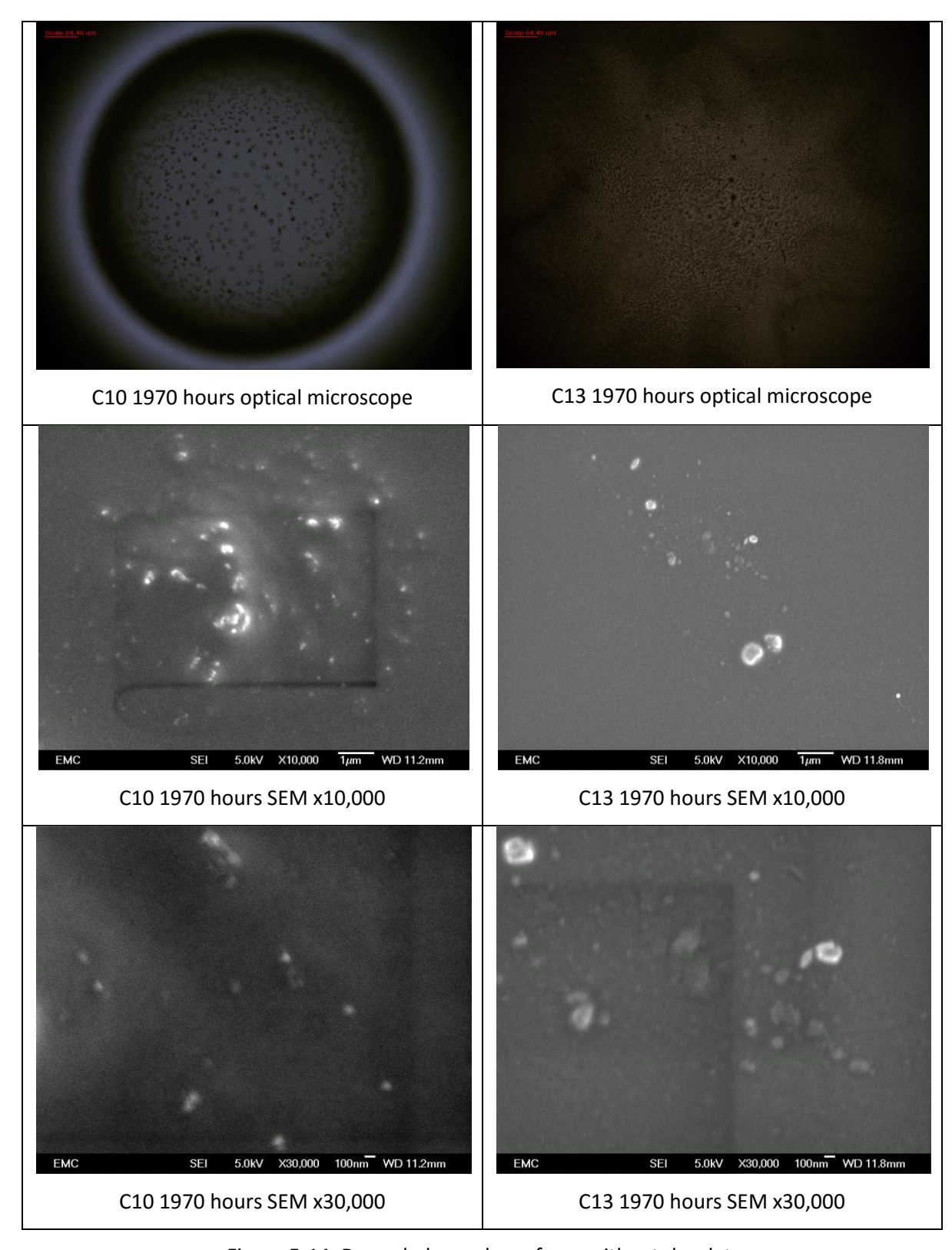


Figure 5-14: Degraded sample surfaces without droplet.

C4 can be considered a further stage of C14 in Figure 5-8, and has not yet produced that many by-products as C16 has in Figure 5-10. It can be clearly seen how droplets initiate and grow. Morshuis and Hudon have also observed this process. However, different from this work, they only studied individual pulse shapes along the process [82, 88]. It was reported by both researchers that a streamer to Townsend (termed by Morshuis, spark to glow termed by Hudon) pulse shape

transition was detected after the formation of such droplets. With reference to this work, the initiation of "detached ear" discharge occurs with the formation of droplets (mostly can be seen under optical microscope), before which the "rabbit-like" or "cloud-like" discharges would take a streamer form, and after which only discrete events would happen with very low feedforward capability available.

On the other hand, the degradation process without droplets also follows the building up process, during which the selected degradation sites grow in size and become more and more outstanding amongst the others with its also growing ability to attract PD.

From Figure 5-14 it can be found that degradation sites are also formed with by-products, however less dense and smaller in dimensions. As discussed before the formation of droplets are formed with essential elements of O, H, and C, thus air consumption and moisture experienced during sample handling may be the reason for samples taking different path of degradation. However, with or without droplets, PD characteristics were similar in this work as with those discussed in Chapter 4.

5.2.3 Energy Dispersive Spectroscopy (EDS)

EDS was employed in this work to examine the chemical properties of surface deteriorated sites as it was expected to out-perform RAMAN which returned very little useful information. As predicted, carbon and oxygen were both detected with most of samples which had been stressed for 2000 hours. On the other hand, carbon was generally not picked up by EDS for samples sacrificed early (no observable surface deterioration under optical microscope).

As mentioned above, O and C detected are mostly hydrated oxalic acid (C₂H₂O₄.H₂O) quality wise, but quantity wise the EDS was not useful. Although some research works utilize the colour difference on the image to determine quantitatively the chemical composition of a surface, the method relies on the scattering constants of chemical components being different, hence returning different colours, and a graphic analysis tool can be used to determine by percentage the component on a surface. However, in this work the surfaces were not flat, thus the altitude difference also returns colour change. Thus the method was not applicable. The author attempted to quantify C and O concentration by using gold as a reference value under an assumption that gold concentration should hold constant for every sample, as samples were gold plated in groups of six under the same current and duration time. However, concentration readings for gold vary beyond a tolerable range so this attempt was not successful.

Also, EDS was found to be not sensitive enough for picking up chemical composition readings single points in this case, as the author attempted to read off data from pits and carbonized sharp edges. Thus all readings taken were from consistent square areas covering the centre of cavities.

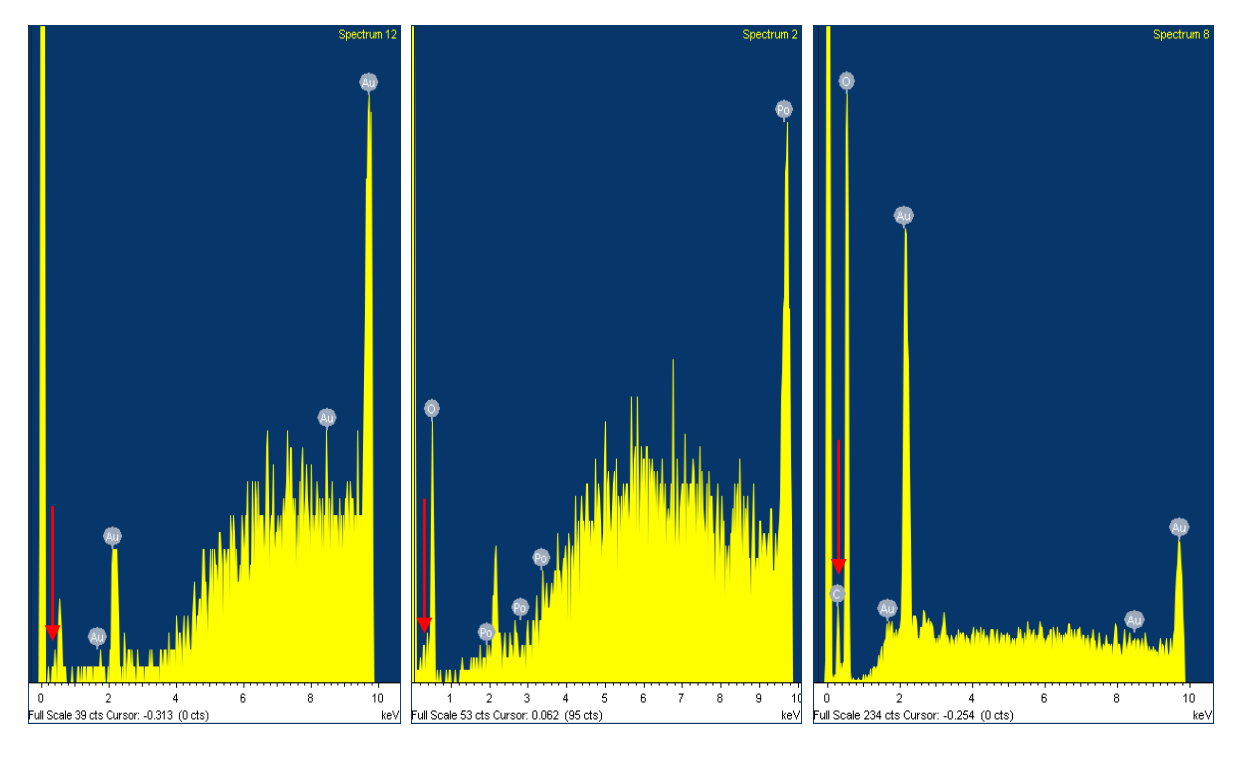
Samples with carbon found are shown in Table 5-2, all samples with carbon detected are the ones that experienced the full 1970 hours of degradation test, and with very pronounced degradation by-products accumulated across the surface.

Table 5-2: Samples with carbon found from degraded surface.

Sample No.	Degradation time (hours)	Droplet found
C1	1970	No
C2	1970	Yes
C13	1970	No
C15	1970	No
C16	1970	Yes

C4, C10, and C11 were missed out even though they all showed clearly observable degradation sites, as C4 was just into the formation stage of droplets, C10 and C11 were without droplets, and the concentration of carbon was not high enough for EDS to recognize automatically over the noise and other signals such as gold.

Referring to Figure 5-15, in general virgin samples have both C and O peaks too low to be recognized automatically by the system; samples sacrificed early had lower C and O peaks on their EDS plots, such as C6 sacrificed at 660 hours with no visible surface degradation under both optical microscope and SEM; and as degradation time proceeds, C and O plots both got more pronounced on the plot, such as C1 and all other samples with carbon peaks recognized automatically by EDS.



Virgin sample

C6 (660 hrs) with O peak C1 (1970 hrs) with clear C and O peaks

Figure 5-15: Typical EDS material composition charts with automatic chemical component recognition, carbon peak position marked by red arrow.

Figure 5-16 shows EDS scan results for samples with carbon existence automatically recognized by the system. Furthermore, carbon peaks can be observed from the three samples with significant degradation sites using an optical microscope, even though they were not automatically detected and labelled by the SEM itself, shown in Figure 5-17. Thus, all 8 samples with observable degradation sites under optical microscope have shown different level of carbon accumulation. Combining all readings from EDS, the degradation process started by accumulation of O in early stages by oxidation processes, then carbon from epoxy resin side chains started to be bombarded and react with H and O to form droplets or other carbonized by-products. The initiation of fast carbon accumulation should be relatively close to the start of "detached ear" discharges, which could be triggered by such carbonized sites and in turn enhanced those sites to form pits, triggering pitting discharges.

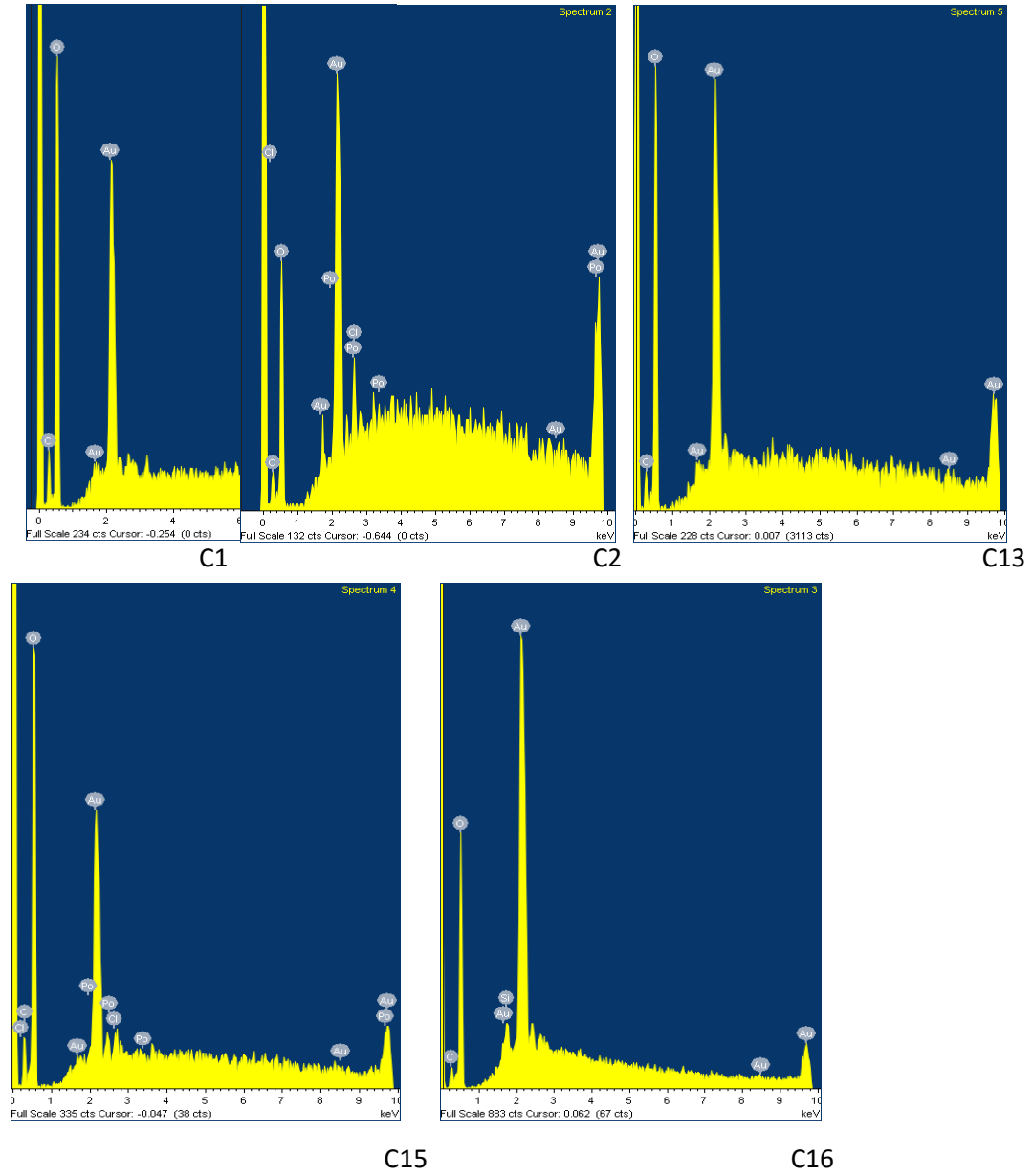


Figure 5-17: Carbon peak recognized automatically for C1, C2, C13, C15, and C16.

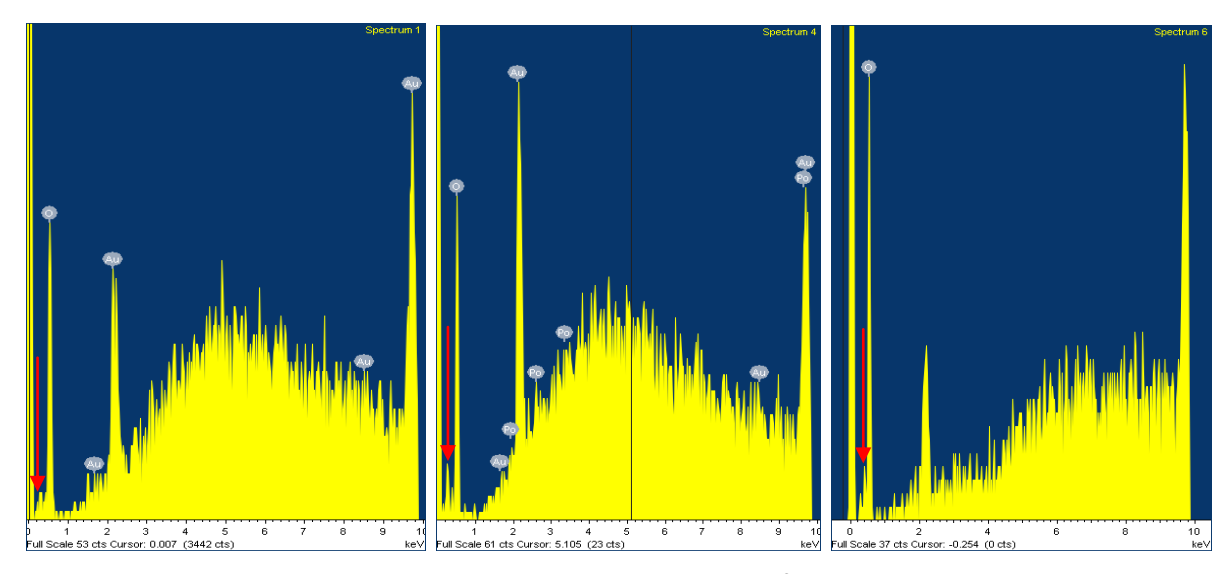


Figure 5-16: Carbon peak marked by red arrow for C4, C10, and C11.

5.2.4 Summary

SEM and EDS results revealed qualitatively the process of surface degradation under PD. In the first stages cavity surfaces trigger PD and get damaged by it evenly, with O products accumulating. As initial concentrated degradation sites formed, the sites get bombarded by PD with much higher volume due to its attraction for PD, causing periodical PD behaviours and in turn getting further damaged by it. From this stage, "detached ear" events appear and get enhanced, causing sharp carbonized sites to grow, and finally leading to pitting, resulting in periodical PD activities such as "detached rabbit ear" or swarming discharges.

5.3 UV degradation – surface conductivity enhancement on cavity surfaces without geometrical modification

Degradation of polymeric materials caused by internal PD is mainly due to electron bombardment against cavity surfaces, polymeric chains will be broken by high energy impacting electrons. In fact, polymeric chains can be broken by many other types of energy forms, such as energy conducted thermally, or by UV irradiation.

Samples exposed to UV irradiation will be uniformly degraded unlike under PD impact localized degradation sites will be generated. The objective of this experiment was to test UV irradiation against natural PD degradation in terms of the effect on PD behaviour change, in order to understand whether cavity surface geometrical modification is essential or not for the generation of the periodical PD activities discussed in chapter 4.

5.3.1 Experimental method

UV degradation test was conducted using an UV exposure unit (Mega Electronics Medium UV Exposure Unit model LV204), which operates on 15W * 4 UV lamps, producing 4 - 5 mW/cm² of power. Image of the UV unit is shown in Figure 5-18.

To achieve uniform exposure for all samples, only the area symmetrically in the middle of all UV lamps (marked by red in Figure 5-18) was used for exposure. Two extra ventilation fans were installed onto the unit to keep the temperature below 50°C while the UV exposure box is working with full power, which could ensure that no thermal degradation was introduced to epoxy resin samples stressed.



Figure 5-18: UV exposure unit used.

4 Epoxy resin samples were selected to conduct this experiment, labelled UV1 – UV4. UV1 started with "rabbit-like" PRPD pattern, and the rest started with "turtle-like" patterns. 4 samples were placed in the red area marked in Figure 5-18, stressed with full power with exposure unit lid closed. PD data acquisition was taken after every 50 hours of stressing.

5.3.2 Experimental results and discussions

PRPD patterns was anticipated to follow the trend from stage 1 "turtle-like" patterns to stage 2 "rabbit-like" patterns, as cavity surface geometrical and conductivity modification due to UV light should be similar to what PD degradation brings in the first 2 stages: uniform modification across the entire cavity surface. After stage 2, as anticipated due to the missing of localized degradation sites, periodical PD activities were not observed. Instead, cavities tend to cease discharging due to the enhancement of surface conductivity which leads to decreased PD feedforward capability. Typical transition of such behaviours can be observed in Figure 5-19.

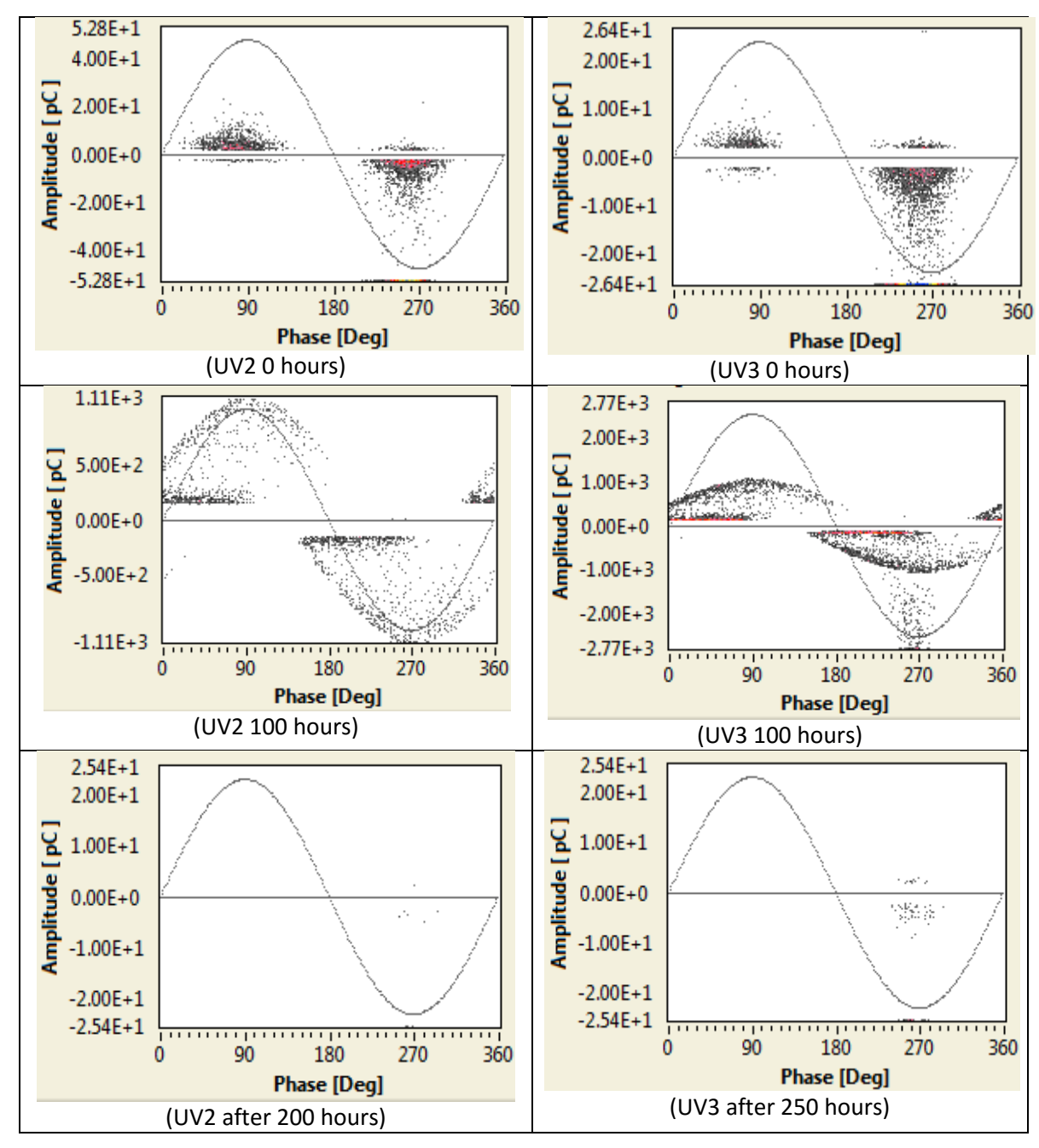


Figure 5-19: Typical PRPD pattern transition under UV stressing.

5.3.3 Summary

Up to this stage, if combining all experimental findings, a clear root of degradation under cavity PD can be summarized:

• The transition from stage 1 "turtle" type activities to stage 2 rabbit type activities is achieved by surface conductivity enhancement. Surface geometrical modification is not essential in this transition as shown from UV experiments. Surface roughness is indeed building up but small in scale as shown by sample C14 in Figure 5-8.

- The transition from stage 2 to later stage PRPD patterns cannot be achieved by surface conductivity enhancement only, as UV degradation results suggest. The timely correspondence between the first occurrence of "detached rabbit ear" PD and localized degradation sites shown in Table 4-4 confirms the physics of periodical PD activities.
- Swarming discharge and the detection of carbonized pits suggest the future behaviour of PD degradation.

5.4 Conclusion

This chapter reports the study on cavity surface conditions under degradation. RAMAN, SEM, EDS, and UV degradation experiments were conducted. Amongst the three RAMAN was experimented with group B samples and determined to be not sensitive enough for chemical examination in this case. SEM returned images with better quality than an optical microscope, revealing early stage surface degradation as an evenly distributed process but still promoting certain sites in each small area. Carbonyl group accumulation and pitting sites were also discovered under SEM. EDS showed that oxidation was the major chemical process during evenly distributed PD events and degradation site growth. Carbonized by-products start to grow rapidly since the formation of droplets or larger conductive sites, which will trigger and in turn get further damaged by periodical PD activities such as "detached ear" discharges. Eventually the selected sites of surface deterioration will grow into pits, triggering pitting discharge.

UV degradation experiments found that surface geometrical modification is essential in the generation of later stage periodical PD events, thus confirming the hypothesis of degradation stage transitioning under PD in this work.

Chapter 6: Simulation of PRPD Patterns

In this chapter, a simulation model based on Niemeyer's derivations is detailed. This model was used to study earlier experimental results, and to help directing future experimental work. By reproducing experimental PD results and combined with experimental observations (microscopic and chemical), it is possible to understand detailed and accurate changes of physical parameters induced by surface deterioration during the degradation life cycle.

The simulation model introduced in this chapter was developed under the co-operation of Vaibhav Thatte and the author. It was a part of an MSc final project named as "Aging and Degradation in the Epoxy Resin Using Partial Discharge Technique" [129]. The simulation code was developed by the author of this report, Mr Thatte took the code for boundary setting tests and minor corrections, and used it for the simulation of PD behaviour from UV degraded samples, for which work the experimental part was carried out by the author of this work and was included in Chapter 5.

6.1 Niemeyer's model

Niemeyer's model is chosen as the PD behaviour simulation model for this work. It is a mathematical model built to simulate free space PD behaviours. It calculates PD magnitude based on electric field collapse, at the same time it uses Pedersen's derivation to convert real charge calculated to apparent charge observed by PD measurement tools [17]. This model includes the stochastic behaviours of first electron generation by considering both volume generation and surface generation rate. Close matches were declared between experimental and simulation results by Niemeyer [23]. Also, Niemeyer's method was used by Illias combined with COMSOL utilizing FEA method to enhance the capability of the original PD model [16]. This COMSOL integrated model was used to study PD degradation with silicone rubber in TDHVL, comparison between the results from epoxy resin and silicone rubber is also discussed in this chapter.

6.1.1 Electric field calculation

Electric field in a free space is calculated with a field enhancement factor in Niemeyer's model. The field enhancement factor is derived depending on the shape of free space, gas type in the free space. For a spherical cavity [12]:

$$f_c = \frac{K\varepsilon_r}{1 + (K - 1\varepsilon_r)} \dots \dots (6 - 1)$$

where K is a dimensionless factor depending on cavity shape, depending on the ratio of axial diameter of the cavity a/b if the cavity is spherical or ellipsoidal [22]; ε_r is the relative permittivity of the insulating material.

With the field enhancement factor, applied electric field inside the cavity can be calculated:

$$E_i = f_c E_0 \dots (6-2)$$

where E_i being the electric field inside the cavity and E_0 is the applied field in the insulation bulk when the cavity is absent.

6.1.2 Streamer discharge inception

Inception of streamer discharge would take place when inception field is exceeded by internal field in a cavity, if ignoring the delay caused by first electron generation. The inception field as a threshold is derived as [69]:

$$E_{inc} = (\frac{E}{p})_{cr} p [1 + \frac{B}{(2pa)^n}] \dots \dots (6-3)$$

in which $(\frac{E}{p})_{cr}$, B, and n account for the ionization process of cavity gas, and p is the pressure in the cavity.

6.1.3 Statistical time-delay simulation

A first electron is required to start an electron avalanche after the inception field has been exceeded. First electrons can be generated from variable sources, among which volume generation and surface injection are considered as the major two sources.

6.1.3.1 Volume generation

Volume generation in Niemeyer's model considers electron generating rate by radioactive radiation [12]:

$$\dot{N}_v = \eta_i p V_{eff} = \eta_i p \frac{4}{3} \pi r^3 (1 - v^{-\beta}) \dots \dots (6 - 4)$$

in which p and V_{eff} are the gas pressure inside the cavity and the effective gas volume inside the cavity under the affect of applied field and radioactive radiation respectively, v is the over voltage ratio, β is an exponent in approximation for effective ionization coefficient, and η_i accounts for the ionization mechanism:

$$\eta_i = C_{rad} \emptyset_{rad} (\frac{\rho}{p})_0 \dots \dots (6-5)$$

where C_{rad} accounts for the interaction between radiation and gas, \emptyset_{rad} is the quantum flux density of radiation, and $(\frac{\rho}{p})_0$ being the pressure reduced density of the gas. Defined values for all three variables for air can be found in [12]. Niemeyer consider volume generation to be the major source of initial electrons for a virgin or inactive cavity, thus defining the statistical time-lag [130]:

$$\Delta t_{inc} \approx [(\frac{4}{3})C_{rad} \emptyset_{rad} (\frac{\rho}{p})_0 p \pi a b^2 (1 - v^{-\beta})]^{-1} \dots \dots (6 - 6)$$

6.1.3.2 Surface emission

Niemeyer declares that surface emission takes similar form of Schottky injection, which rate can be governed as [12]:

$$\dot{N}_{e} = \frac{A}{e} Sexp \left[-\frac{\phi - e\sqrt{\frac{eE_{i}}{4\pi\varepsilon_{0}}}}{kT} \right] = v_{0}N_{dt}exp \left[-\frac{\phi - e\sqrt{\frac{eE_{i}}{4\pi\varepsilon_{0}}}}{kT} \right] \dots \dots (6-7)$$

in above equation v_0 is the fundamental phonon frequency, ϕ is the effective work function for detrapping, $e\sqrt{\frac{eE_i}{4\pi\varepsilon_0}}$ is the Schottky term, k being the Boltzmann constant, and T is the absolute temperature. In addition, N_{dt} accounts for the number of detrappable electrons [130]:

$$N_{dt} = \xi(\frac{q}{e}) \exp(\frac{-t}{\tau}) \dots \dots (6-8)$$

where ξ < 1 is a dimensionless factor for detrappable electrons accounting the difference in efficiency when the surface is impacted by a positive ion (normal condition) or an electron (polarity reversal), q is the true PD charge, e is the elementary charge, t is the time interval since previous discharge event, and τ is the effective decay time constant.

6.1.3.3 Simulation of stochastic PD inception

By accounting the two first electron generating mechanisms, stochastic inception delay of PD events can be modelled. Mostly used methods are 1): calculate the probability of a first electron not being generated along with time, and compare with a random number between 0 and 1; 2): multiply a factor to the overall electron generating rate and compare to a random number between 0 and 1. Using these methods, the chance of a PD event inception can be stochastically decided for every time step when the inception field is exceeded during the simulation.

6.1.4 Discharge magnitude

Discharge magnitude in Niemeyer's model is calculated by the field collapsed due to the PD event, similar to the classic ABC model [14, 13, 15]. However, unlike the ABC model using extinction field as the end point which the internal field of cavity will collapse onto, Niemeyer's model defines a residual field which is related to the properties of cavity gas:

$$E_{res} = \gamma (\frac{E}{p})_{cr} p \dots \dots (6-9)$$

where γ is a dimensionless factor, and its value varies with polarity change. The field collapsed can be then determined:

$$\Delta E = f_c E_0 + E_a - E_{res} \dots \dots (6-10)$$

 E_q is the field induced by accumulated surface charge:

$$E_q = \frac{q_s}{\varepsilon_0 \pi a b^2 [1 + \varepsilon_r (K - 1)]} \dots \dots (6 - 11)$$

where $q_{\scriptscriptstyle S}$ is the surface charge magnitude which can be calculated by accumulating real PD charge landed onto the surface and the decay of it from previous PD events.

With ΔE , the real charge q and apparent charge q' induced by a PD event according to Pedersen's derivations can then be derived [17, 18]:

$$\pm q = \varepsilon_0 \pi b^2 [1 + \varepsilon_r (K - 1)] \Delta E \dots \dots (6 - 12)$$

$$q' = -\frac{4}{3}\pi a b^2 \varepsilon_0 \varepsilon_r K \Delta E \nabla \lambda_0 \dots \dots (6-13)$$

PRPD patterns are plotted with apparent charge q', and real charge q is used to calculate surface charge magnitude and induced electric field.

6.1.5 Surface charge decay

Surface charge decay may take place along the cavity surface [131], which can be governed by the following equation similar to Ohm's law [23]:

$$-\frac{dq}{dt} = \frac{\pi}{2} K_s E_i 2a \dots (6-14)$$

where K_s is surface conductivity, a being the radius of cavity along field direction, thus $E_i 2a$ is the voltage drop across the cavity along applied field direction.

6.1.6 Matlab simulation

A model Niemeyer's method is developed using MATLAB, simulation code can be found in Appendix D. A flow chart of the model can be viewed in Figure 6-1.

This model was examined by reproducing Niemeyer's experimental and simulation data reported in with the same parameters used by Niemeyer. Results showed good correspondence with Niemeyer's original work.

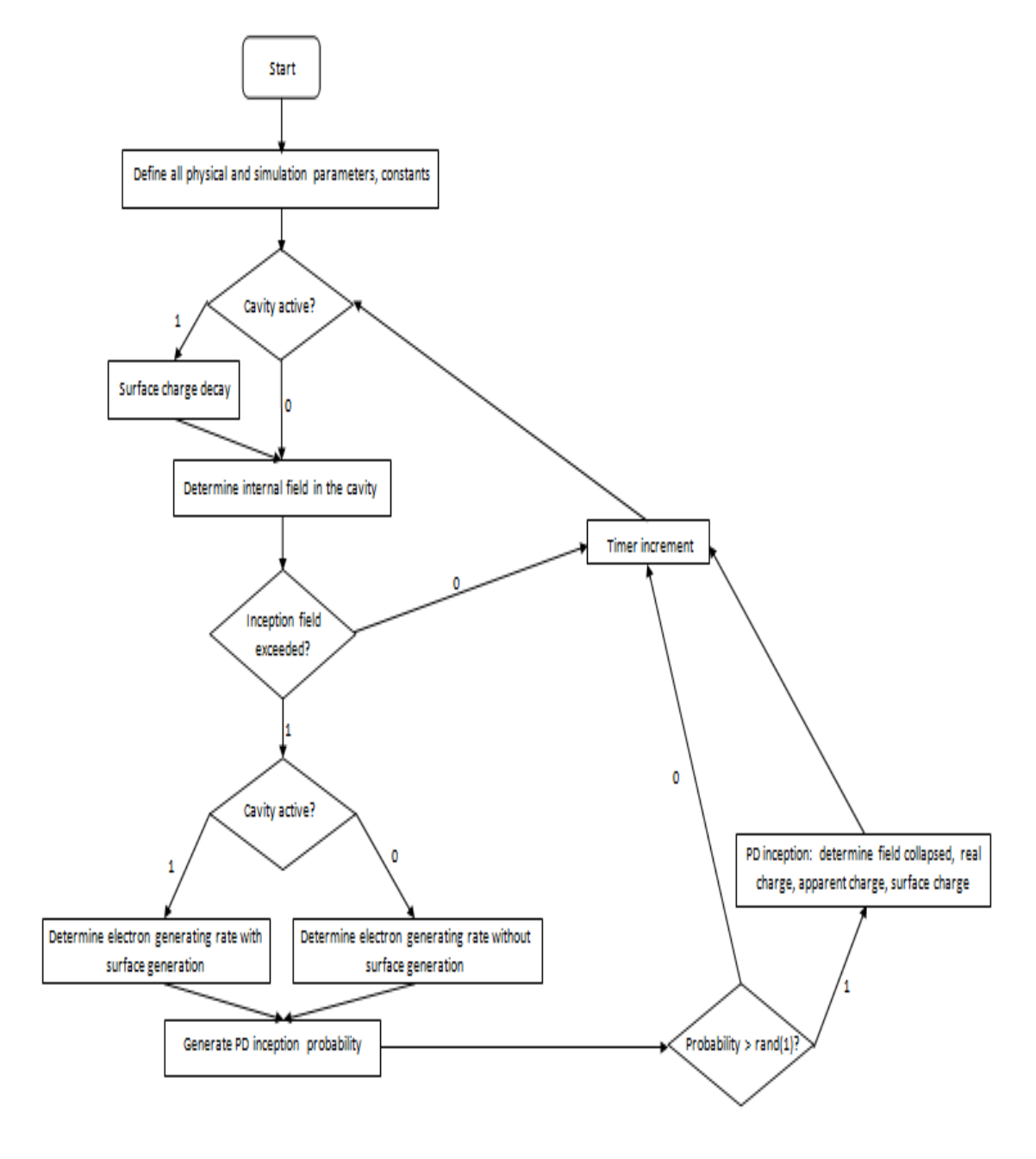


Figure 6-1: PD simulation model flow chart.

6.2 Variables related to PD degradation process

As discussed in earlier chapters, degradation induced by internal PD activities mainly happens at the interface between free space and insulating material. Typical cavity PD degradation in polymeric materials is achieved by electrons bombarding cavity surfaces, electrons that carry sufficient amount of energy can break polymeric chains, resulting in geometrical modification on the surface and chemical accumulation if by-products are produced during the bond breaking process. Geometrical modification in this case is very subtle in the beginning as shown by the microscopic images taken for degraded epoxy resin samples, thus it is not be included in the current model. On the other hand, chemical accumulation can modify electrical properties of the surface, and which is the major driving force of PD behaviour change in the case of this study.

In earlier discussions, it has been concluded that PRPD pattern changes significantly depend on PD feedforward capability of cavities. This PD feedforward capability is found to be governed mainly by surface charge decay speed and average depth of charge traps. In the case of Niemeyer's model, a work function ϕ is used to simulate the average depth of charge traps, it represents the average energy barrier for electrons to be detrapped and used as initial electrons for future PD events. On the other hand, surface charge decay in this model is governed by two parameters, the effective decay time constant and surface conductivity. Theoretically, surface charge decay can go through two different routes: charge recombination along the surface and charge moving into deep traps. In this case, charge moving into deep traps is covered by the average detrapping energy work function, and charge recombination is governed by the surface conductivity K_S and the effective decay time constant τ . Equations 18, 19, and 25 can describe how these 3 parameters can affect PRPD behaviour, by influencing the calculation of discharge probability and magnitude.

Also, an incremental test was conducted to find the most influential parameters. Parameters returned were the three mentioned above, plus cavity air pressure. Cavity air pressure is described by Niemeyer to be influential towards the residual electric field of PD events, thus it can directly affect the calculation of field collapse, then subsequently the calculations of discharge magnitude and space charge accumulation, and cause further influence to the probability for future discharges.

Boundary conditions for key parameters were reported by many previously published research works. Cavity gas pressure according to Paschen's law governs the breakdown electric field of air:

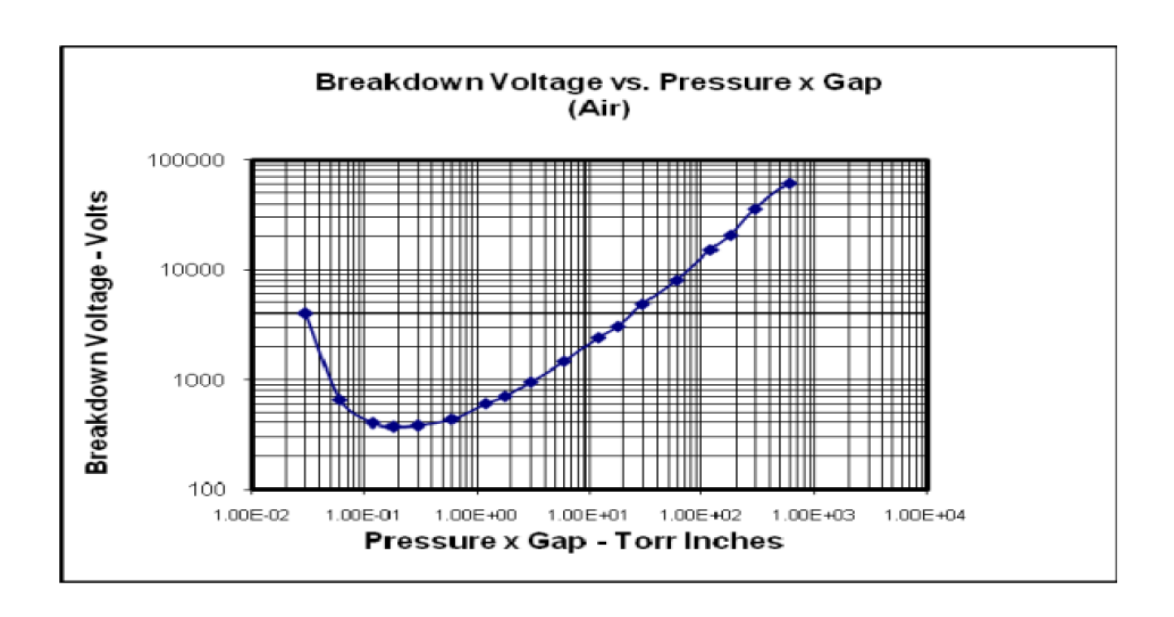


Figure 6-2: Paschen's curve [11].

Many researchers working in the area of partial discharge in polyethylene cavities have stated that a change in cavity gas pressure can alter initial electron generation rate [132, 72], however, the reason behind that statement is the production and consumption of electronegative gas, instead of the pressure itself. Le Wang observed the pressure throughout the degradation process of XLPE, and found the pressure drop was within a 25.5% range (Figure 6-3), this result is similar to Mizutani's work [132].

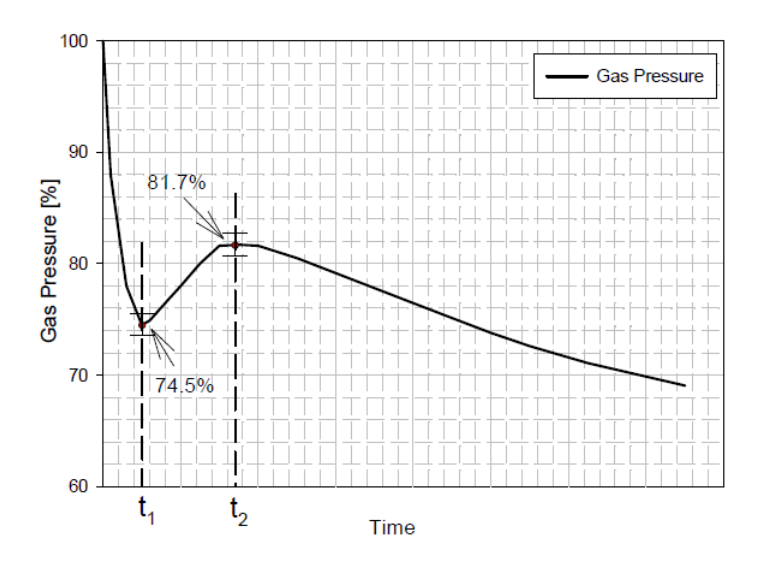


Figure 6-3: Gas pressure throughout PD degradation process [96].

Surface conductivity was measured by Morshuis and Hudon with epoxy resin as discussed earlier. A saturation was found around 1×10^{-10} S/m starting from a virgin stage less than 1×10^{-16} S/m which was the sensitivity limit of the measuring apparatus used, see Figure 6-4.

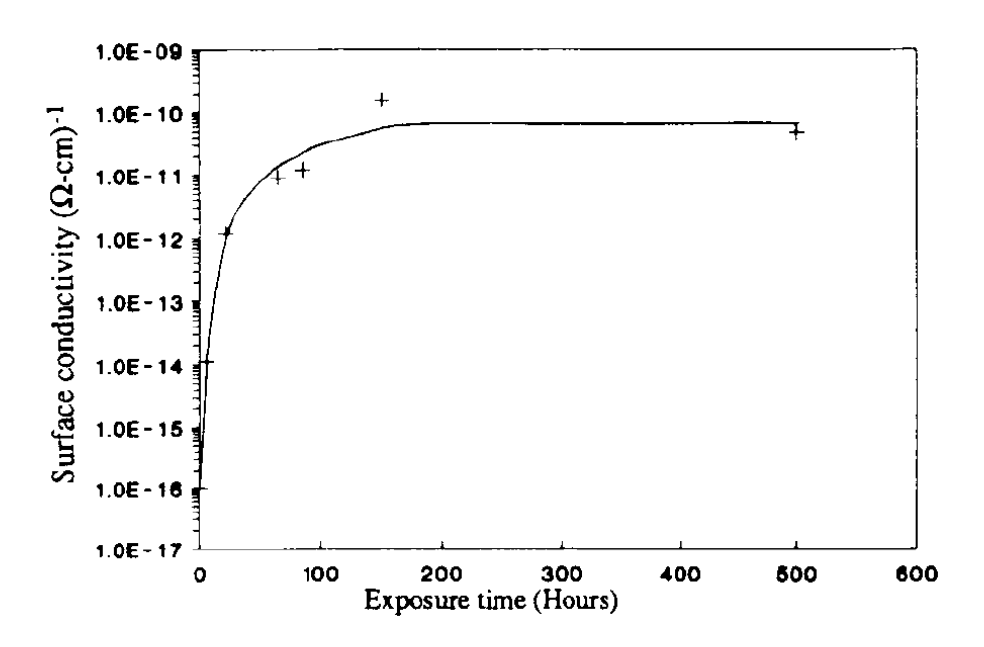


Figure 6-4: Conductivity curve under PD degradation with epoxy resin [85].

According to Niemeyer [12], a work function range was tested to be from 1eV to 1.3eV. Centurioni tested a large range of materials and confirmed that charge decay speed increases with PD ageing, and in most of reported simulation work regarding cavity partial discharge, the time decay constant is most commonly estimated using experimental results.

6.3 Simulation of PD degradation process

By varying the above mentioned parameters, experimental results for epoxy resin sample group B were reproduced using the developed model. According to the degradation stages observed, typical PRPD patterns for each stage were attempted.

Using all parameters in virgin state, a "turtle-like" pattern can be simulated, and by slowing decreasing charge decay speed, a growing rabbit ear can be simulated as in Figure 6-5.

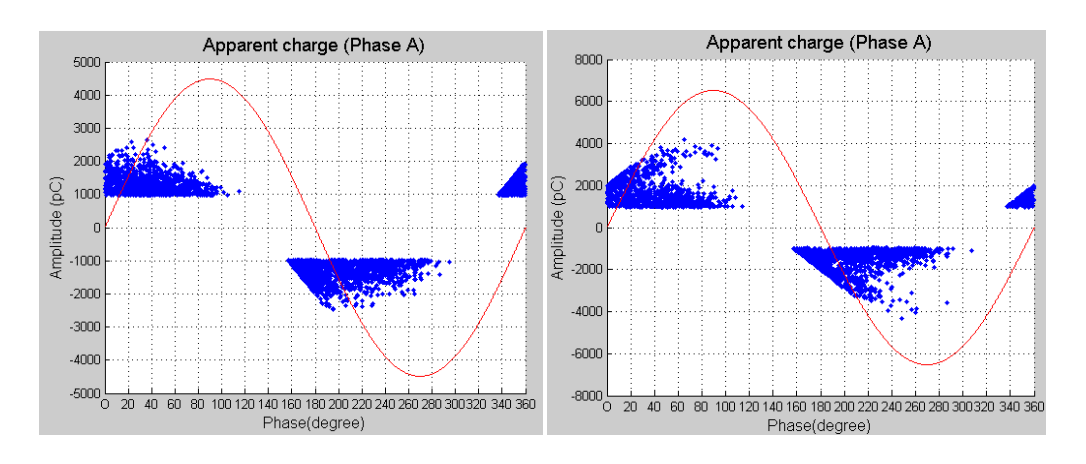


Figure 6-5: "turtle-like" to "rabbit-like" transition (left to right), surface conductivity 10⁻¹⁶S/m, pressure 101kPa, work function 1.0eV, polarity reversal coefficient 1, time decay constant from left: 10s, to right: 0.005s.

The creation of rabbit ear is due to charge decay during no discharge period, thus after polarity reversal, the first discharge has a much smaller source of initial electrons compared to other discharges. 0.005s as quarter of a power cycle is approximately the limit of discharge continuity in this model, further decreasing it will cause discontinuity during discharge events.

In Niemeyer's algorithm, initial electron reservoir decay is only governed by the decay constant, surface conductivity on the other hand only governs charge decay in terms of space charge induced field calculation [130]. For a typical "rabbit-like" PRPD pattern, Niemeyer utilized a proportionality factor $\xi < 1$ to account the difference in efficiency to emit an electron when the surface is impacted by a positive ion (normal condition) or an electron (polarity reversal). This factor ξ is widely used to control the height of first discharge events after polarity reversal [133, 134, 130, 31], thus a typical "rabbit-like" PRPD pattern with long ear can be simulated as shown in Figure 6-6:

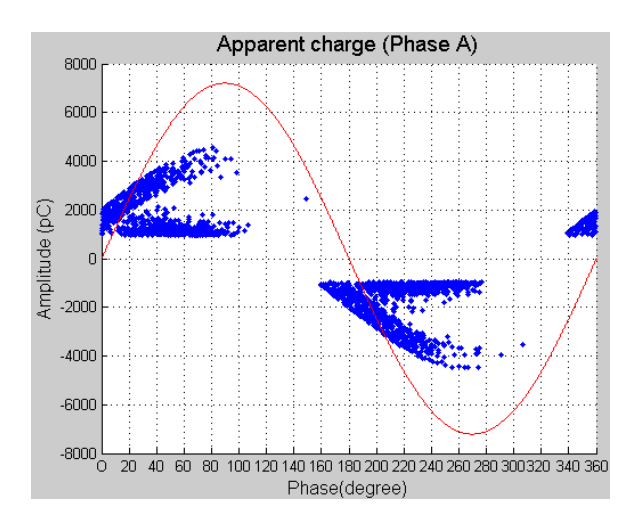


Figure 6-6: Long rabbit ear pattern simulated with the same parameters as figure 6-5 (left), only decreasing polarity reversal coefficient to 0.1.

If charge decay time constant is further decreased, it is possible to reproduce the featured "detached rabbit ear" patterns, with the rabbit ear detached from the body, see Figure 6-7. With the current charge decay rate, consecutive discharge events triggered by previous events are very rare. Thus for this stage, body discharge events are not much greater in number compared with ear discharge events after polarity reversal, unlike during earlier stages one delayed ear discharge event can trigger multiple body events.

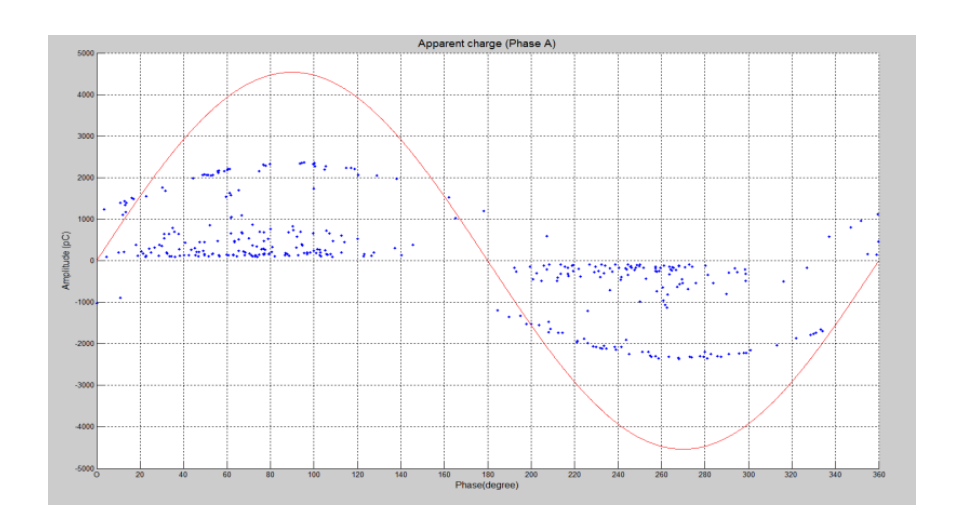


Figure 6-7: Rabbit ear detached from body pattern with τ =0.004s.

Also, as it can be observed from Figure 6-5 to Figure 6-7, the PRPD pattern under quicker surface charge decay rate has its firing angle more synchronized with applied voltage, which corresponds to experimental findings as the Poissonian field now receives no additional influence from space charge accumulation. If space charge decay rate can be further increased, the discharge pattern with ear part only shall be found. This is because the only way a discharge event can happen is through volume generation, which always experiences a long decay thus has higher magnitudes. And now space charge dissipation is too quick to trigger any future PD events afterwards. Simulation of this type of PD patterns usually needs manual triggering (forcing discharge to happen after polarity reversal), as discharge probability via volume generation is usually very low. On the other hand, the ear only PRPD patterns in reality are assumed to happen at localized degradation sites, with local field around the sites and local conductivity being severely enhanced to help generating initial electrons.

Furthermore, there are other parameters which at the moment can only be determined by experiments. These parameters also have significant effects on PRPD patterns simulated.

For degradation stage 1, the typical PRPD pattern was found with a decay time constant $\tau=10s$, surface conductivity $K_s=3^{-15}$:

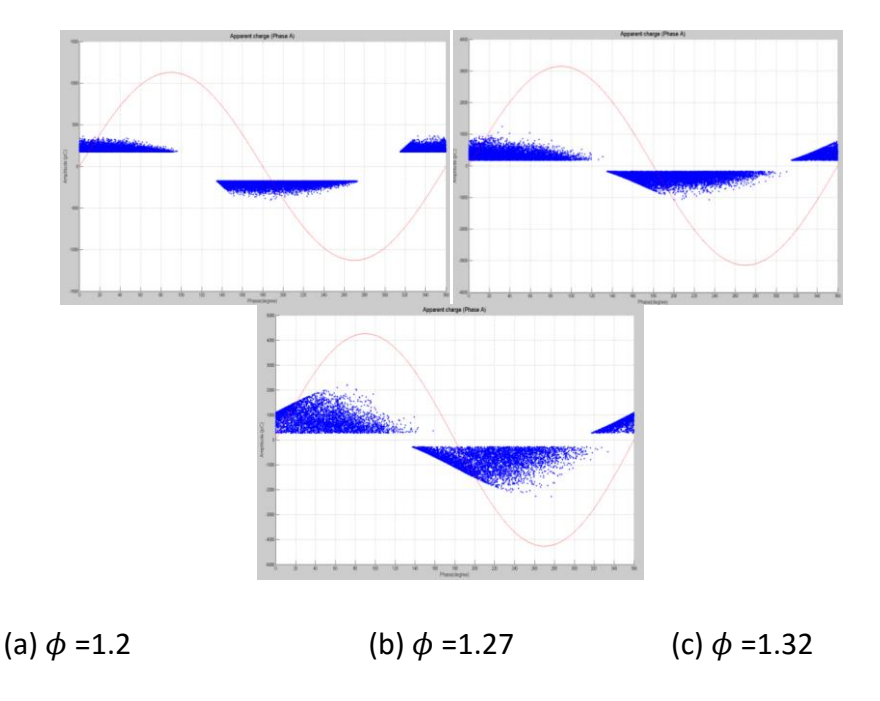


Figure 6-8: Degradation stage 1, "turtle-like" patterns with $\tau=100s$, and PD behaviour change due to detrapping work function.

All three PRPD patterns were generated with the same parameters apart from an increasing detrapping work function ϕ . A greater work function means a wider energy gap for electrons to be detrapped as initial electrons, thus increasing the work function results in a greater magnitude of first discharges simulated after polarity reversal.

If comparing surface conductivity to decay time constant, it can be seen from the equations that they both can affect the calculation of surface generation rate. However, surface conductivity decreases surface charge according to Ohm's law which is linear, and it does not have any direct affect to the calculation of discharge probability. On the other hand, decay time constant has direct affect to the final probability calculation, as it affects the calculation of real time initial electron availability exponentially. Thus, through various tests, surface conductivity does not significantly change PRPD pattern features, while decay time constant can significantly modify those features.

6.4 Future simulation directions

6.4.1 Simulation of pitting discharge

As discussed in this chapter, current simulation model considers the cavity surface homogeneously. Also, Niemeyer's algorithms can only be applied to simulate streamer type of discharge events. These hypotheses are suitable for degradation stage 1 and 2, and also partially applicable for the stage of "detached rabbit ear" patterns. However, with the assumption of

possible low magnitude high repetition rate pitting discharge, the current model is no longer suitable.

In theory, pitting discharge has an initial electron generation rate very different to streamer discharge events. Pitting sites are considered to be so conductive that can act as an infinite source of initial electrons. While on the other hand, current model calculates the probability of initial electron generation based on volume generation from insulating materials, and surface emission from accumulated surface charge. Also, streamer discharge events stop when opposing field due to space charge accumulation is raised to the level that the overall field drops below PD extinction threshold. The field collapse between inception and extinction fields is used to determine discharge magnitude. However, for pitting discharge, it may happen as a quite localized event, possibly quite similar to a needle tip treeing discharge event. Thus field distortion due to the geometrical shape of the pitting site may need to be considered prior to space charge accumulation of the entire cavity. Due to these considerations, pitting discharge possibly should be simulated using a mechanism closer to treeing discharge instead of streamer type.

6.4.2 Possible life model construction

As up to date experience suggests, pitting discharge should be very close to the end of insulation life. Thus, if a life model is to be built, the transitioning mechanism from "detached rabbit ear" stage to pitting discharge stage is more practical. This transition includes 2 important milestones. The first one is the start of "detached rabbit ear" stage when the entire cavity surface is conductive enough to cut off the feedforward between consecutive PD events, and the second one is when these discontinuous PD events finally created a pitting site and most PD events afterwards will be concentrated to this site.

6.4.2.1 Model based on "memory effect" parameters

Practically quantifying the damage induced by PD can be very difficult. In the case of this work, as it has been repetitively discussed in this report, the "memory" or feedforward capability of cavity surface plays a very important role to govern PRPD behaviour along the degradation process. Thus, quantifying the feedforward capability level of cavity surface may be more practical.

As discussed in Chapter 4, a number of parameters that can represent the level of memory loss were found, such as continuous discharge cycle length, pulse count per discharging cycle, and PD active level percentage. These parameters have potential to be used in a life model if accompanied with appropriate algorithm and weighting factors. For this approach to work, clearly a full life span data base should be needed.

However, this approach could be possibly limited due to the fact that all "memory" related parameters have a final value to converge towards. For instance, continuous discharging length and pulse count per discharging cycle converge to 1, and PD active level percentage converges to 0. It is possible that at the very late stage of cavity partial discharge that all "memory" parameters have converged to their respective values, however the degradation process could still last very long afterwards. A pitting degradation stage has been observed after "detached ear" stage, where some of the three parameters should experience a step change, for instance the pulse count per discharging cycle should be restored to 2 or higher numbers, and the other two parameters should departure from 1 as a significant source of first electrons is introduced by the pit. However, due to the hard threshold of the system can block some of the signals from pitting discharge as they are in general low in magnitude. In this case, the feedforward capability parameters measured can be misleading due to the missing part of signals below noise level.

Theoretically a reversed trend of all feedforward capability parameters could be seen after the initiation of pitting discharge, as the pit is assumed to grow into conductive sharp tips which can produce treeing discharge. Such discharges are continuous, thus they should have high values of continuous discharging length and PD active level. Also, a typical treeing or pitting discharge can have multiple pulses during one half cycle, thus an increase of pulse count during surging cycle can be assumed.

Even with such uncertainties, the reversed trending for feedforward capability parameters can be used to define degradation stage transition into the final pitting or treeing discharge stage, if considered qualitatively. The best case scenario is that the system breaks down before all parameters saturate: discharge being nearly 100% active, with very few empty power cycles, and very stable multiple pulses during each half cycle as it would be with a metal needle tip treeing experiment. If the system breaks down before saturation, an excellent life model can be built based on such data bases. On the other hand, if the system keeps going on after saturation, more details will be needed to study the saturation period quantitatively.

6.4.2.2 Model based on chaotic theory

Chaotic theory is a newly recognized tool to analyze partial discharge. Lyapunov exponents is currently the most common one used and studied, which recognizes the sensitivity to initial conditions for a dynamical system. A measure of divergence of two trajectories (time series) estimated by Lyapunov exponents can be used to describe the chaotic nature of their attractor. This method is used to recognize PD source [135, 136], and predict near future performance [137]. Yet cavity PD type recognition has also been attempted [138], by using Lyapunov exponent to

recognize the trajectory of applied electric field with potential a repeating manner under periodical PD behaviours.

Hurst exponent compares a time series with Brownian motion. As the distance covered by a random particle undergoing random collisions from all sides is directly related to the square root of time [139]:

$$R = kT^{1/2} \dots (6-15)$$

In above equations R is the distance covered, k is a constant, T is the time. Hurst proposed a generalization of Brownian motion that can be used to estimate the randomness of time series:

$$\frac{R}{S} = kT^H \dots \dots (6-16)$$

Where S is the standard deviation, and H is the Hurst exponent. Thus, by comparing the two equations it can be observed that H=0.5 represents a random Brownian motion. When 0<H<0.5 it means the system is covering less distance than a random walk, thus it tends to reverse itself often: if increasing, then it is more likely to be decreasing in the next time step, and vice versa. When 0.5<H<1 the system tend to go to the same direction as the previous step.

However, even with Hurst exponent, periodical discharges like pitting or treeing events can still be hard to manage. This is because the future events in such discharge behaviours are almost certain, thus Hurst exponent will eventually saturate similar to the case which has been discussed with feedforward capability parameters.

Never the less, either one of these possible life models will depend heavily on the successful detection of low magnitude PD events, as the outcome can be totally reversed if low magnitude periodical discharges are missing.

Work in using Hurst exponent to analyze partial discharge has been initiated by Lubo Petrov in TDHVL [140].

6.5 Summary

A simulation model has been developed based on Niemeyer's algorithms. Using this model the degradation stages for epoxy resin sample group B have been simulated in terms of PRPD pattern features.

It is found that during the degradation process of epoxy resin, the major physical parameters able to change PRPD pattern features are the ones which have effect on average charge trap depth and surface charge decay rate. This finding corresponds with experimental results.

Among the major degradation parameters, surface charge decay time constant has the most significant effect on charge decay speed in this model due to its direct and exponential relationship with PD probability. By altering surface charge decay time constant, feedforward capability between consecutive PD events can be controlled. In terms of PRPD patterns, this parameter has significant contribution to simulate the consequence of surface conductivity change and to decide the general shape of the pattern.

The charge detrapping work function in this model also has direct impact to PD probability calculation. It represents the production of deeper traps along the degradation process, however, this simulation raises the average trap depth as a whole instead of local accumulation of deeper traps due to chemical accumulation. Nevertheless, the average trap depth governs the probability of PD events in both the rabbit ear and body. It can be used to control peak magnitude of discharges in both parts, and also the repetition rate.

Other parameters are not as influential, but still can have considerable control to PRPD patterns. For instance, surface conductivity has only linear and secondary relationship to the final charge density used in probability calculation, it still can work as an extra tool to control charge decay rate. And also detrapping efficiency ξ , this factor only controls the probability of PD events right after polarity reversal, thus it can be used to independently control the rabbit ear length from the body.

With above mentioned parameters, the degradation process of epoxy resin samples was simulated. Major findings from the experiment was confirmed: degradation induced by PD up to this stage has changed cavity surface conductivity, created local accumulations of by-products, hence lowering the PD feedforward capability of the cavities which was the driving force behind PRPD pattern changes.

Future simulation potentials are also discussed in this chapter. Firstly the simulation of later periodical discharging events shall be conducted with models focusing on local geometry. Life span models are also suggested and discussed, by either feedforward capability parameters or chaotic theory. Completion of such life models requires a full life cycle data base, and requires clear detection of low magnitude periodical discharges.

Chapter 7: Conclusion and Future Work

The objective of this project was to study the link between physical/chemical degradation and partial discharge behaviours. In the field of high voltage asset monitoring, this subject at the moment has great potential to be further studied and understood. Currently most partial discharge activities detected are only roughly classified, located, and dealt with preventive measures which is beyond necessary. Especially for the case of internal discharge from cavities, it is concerned by most operators as a red sign for replacement immediately, without further consideration of the possible life time the asset could serve if the discharge signal was understood to a higher level.

A long term experiment was the main element of this project. A total number of 20 samples were put through around 2000 hours of high voltage stressing and tests. Unlike previous samples utilized in similar works in TDHVL or elsewhere, a syringe injected cavity was implanted in the very middle of every epoxy resin specimen. Under microscopic examination, these cavities were naturally spherical, and their dimensions were carefully controlled to be identical.

State of art in the field of partial discharge from a cavity and the damage suffered by insulating materials from it was carefully studied. Single pulse characteristics and accumulated PD behaviours are the two most up to date categories in the area. Single pulse characteristics are too limited to express the complicated process of degradation. On the other hand, when accumulated PD behaviours are concerned, accumulated PD patterns and pulse sequence analysis are the most popular aspects of interest. However, up to date research works usually focus on classification, location, and very rough identification of degradation stages only. It was noticed that all major aspects of degradation were studied with depth by other researchers, but not very much linked. Detailed degradation surface physical and chemical studies were only linked with single pulse analysis; accumulated PD patterns were usually found with short term experiments using materials with short life span, in which air consumption was determined as a major component of the reasoning; pulse sequence analysis were mainly used for location and classification of PD sources.

In this work, a link has been built between all three major components of the degradation process: surface deterioration, accumulated PD pattern, and pulse sequence behaviour. It was found that degradation in a cavity of epoxy resin used could be divided into stages, with clear features shown in all three aspects of observation. Physical principles behind PD behaviours in each stage, and transition between stages were also discussed. The feedforward capability is the main reason for the transition between degradation stages. Hence, the feedforward effect was studied further as

an indicator of degradation level, with a great deal of potential being shown that it could be used to qualitatively or even quantitatively determine the level of degradation suffered by the insulating system.

In general, PD activities start with continuous behaviours, such as "turtle-like" PRPD patterns, or "rabbit-like" patterns with the first discharges after polarity reversal having higher magnitude due to a slight loss of feedforward capability. Then periodical PD behaviours take over, such as "cloud-like" events, "detached rabbit ear" events, pitting events, and presumably treeing events afterwards. From the point of periodical events, PD activities are already localized onto concentrated degradation sites, which are the only places that can activate PD with its electric field concentration and enhanced first electron generation rate, but their local conductivity prevents the discharges to be continuous due to a quick decay of accumulated charge carriers.

Both optical and scanning electron microscopic observations confirmed such predicted surface conditions. C and O were found to be the main components in such degradation sites. Pitting was observed by SEM as well, accompanied with low level but concentrated PD events from electrical tests. At this stage all PD events become identical in terms of magnitude and phase angle. The periodical behaviour indicates a very strong first electron emitter, but also a very fast charge carrier decaying path. Also, an enhancement of cavity surface conductivity without geometrical modification by UV confirmed the essentialness of localized degradation sites in the generation of periodical PD events.

Throughout the degradation process, all featured patterns of each degradation stage were examined in terms of pulse sequence behaviours. Clear trends could be seen during the process. Some key factors were defined to describe the feedforward capability loss of cavities, such as PD active level, pulse count per discharging cycle, and continuous discharging length. These factors were proved to be following the trends, and could be used to determine the level of feedforward capability loss, hence the level of degradation suffered by such damaged surfaces. Possible life models based on such parameters can be more accurate compared to existing models, due to the parameters are only taken from discharging sites that generate the featured PD events, thus the model only focus on the condition of such sites instead of trying to calculate damage and distribute such damage across the cavity surface.

Although it was claimed by other researchers that electrical treeing could initiate from sharp edges of such degradation sites, especially crystal edges which were also found in this work. However, treeing was not observed in this work. Also the final breakdown of samples used was not approached. Hence, the life span after the 2000 hours tested remains unknown. Predictions

suggest a reversed trend of feedforward capability parameters as self-initiated periodical events should take over when pits and electrical trees are formed.

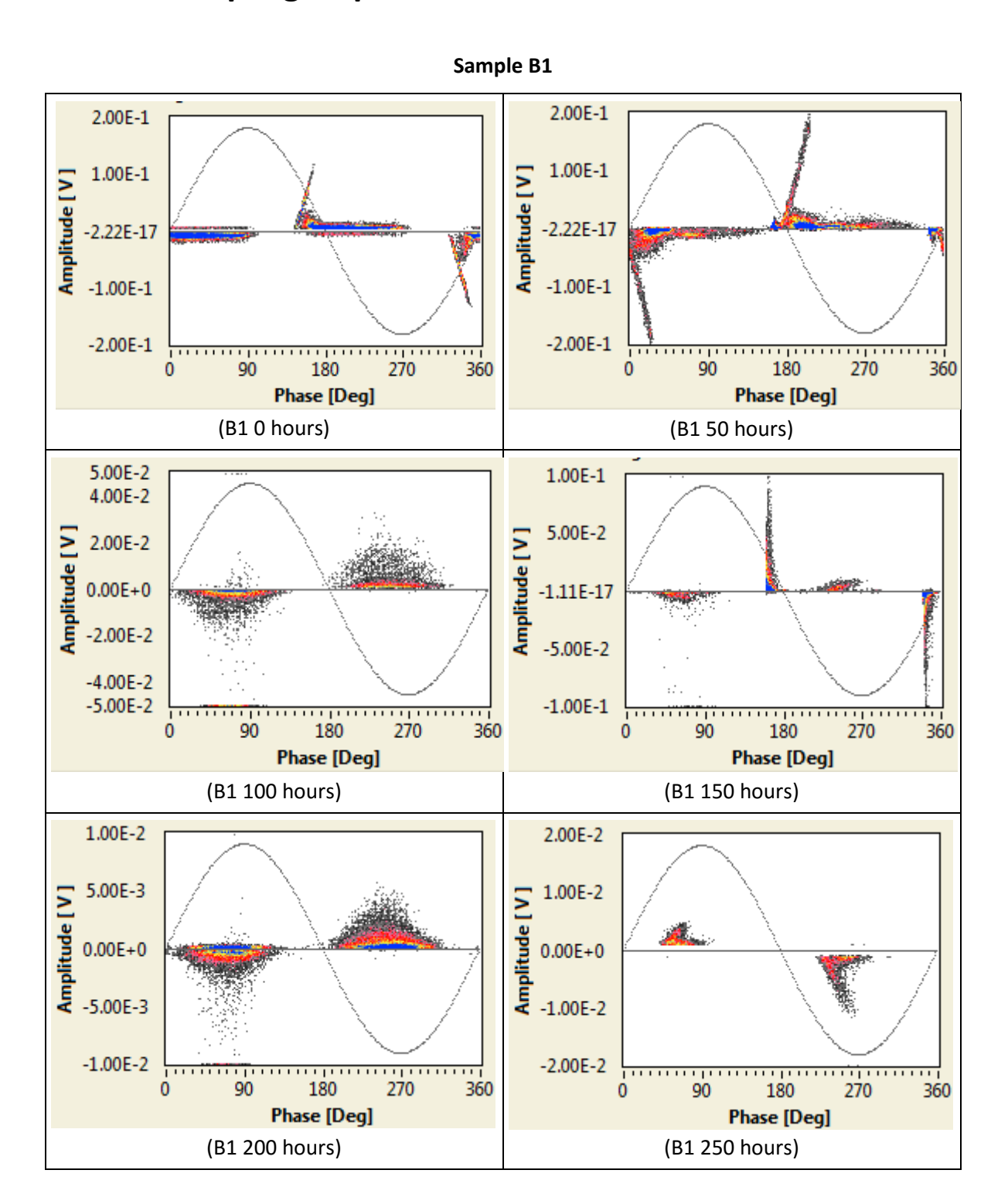
A simple PD simulation model based on Niemeyer's theory was used to reproduce the featured patterns of the initial degradation stages, including "turtle-like", "rabbit-like", and ""detached-rabbit-ear-like"" patterns. For pitting discharge and any possible degradation stage afterwards, simulation of such events would be a completely different model, with detailed and localized surface shape, and extremely field distortion and electron emitting capabilities, which are beyond the boundaries of the current model that was designed for streamer type of discharges only.

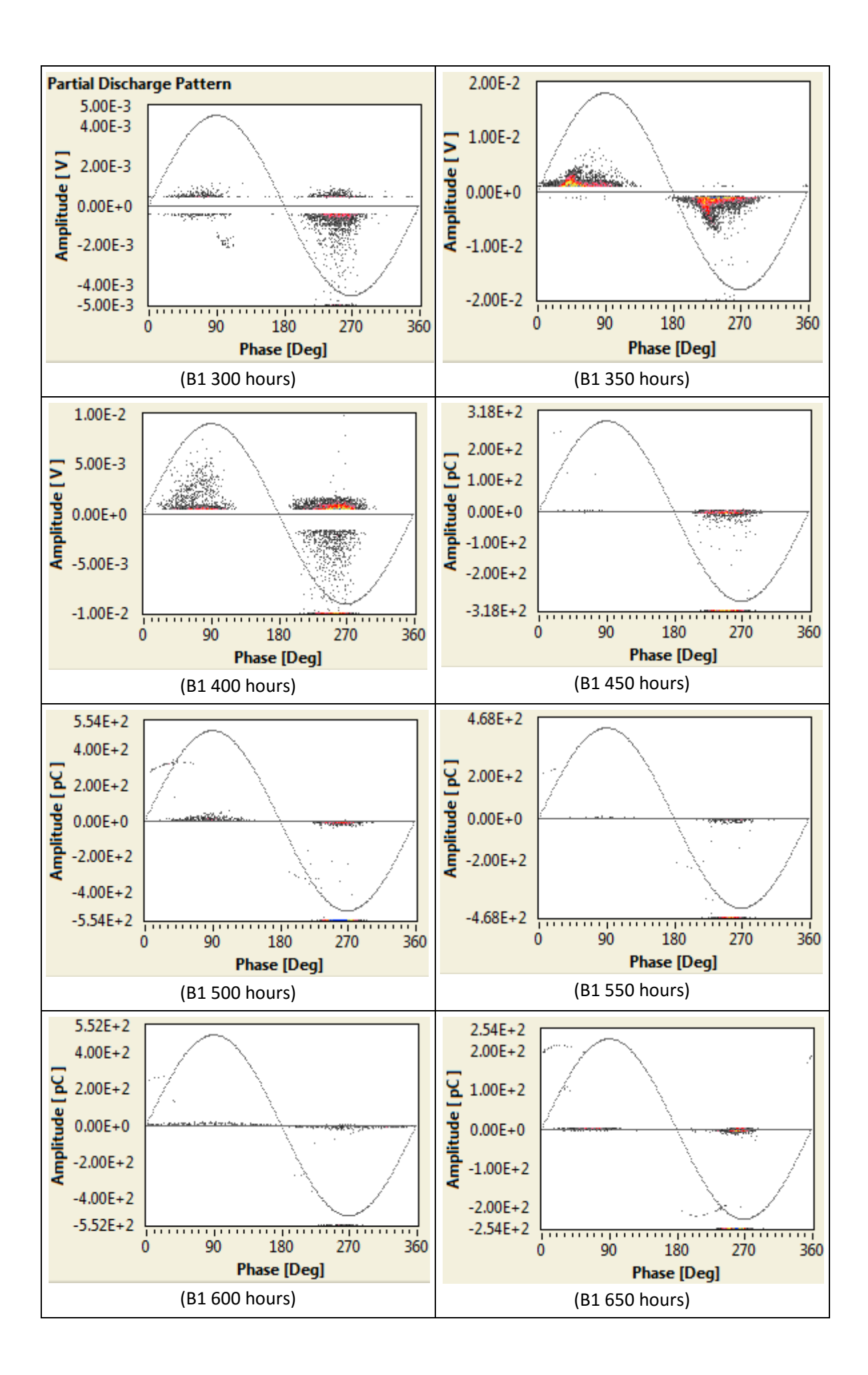
Nevertheless it is possible to bring simulation work of this study to another level, with much more detailed local parameters of degradation sites. However, it can be much simpler but more useful to simulate the feedforward capability effect instead of PD behaviour if degradation life is concerned. The proposed parameters from pulse sequence study can be further investigated if life experiment goes on until final breakdown, with such information the factors can be weighed and used in a life span model. Also, time resolved PD behaviour can be examined using chaos theory, especially Hurst exponent models, which may return clear trends as degradation time goes on. However, the two proposed methods can be hard to materialize, due to the fact that at the end of current experiments, many memory effect parameters have already dropped to their limit but the material is still far from final breakdown. Even if the predictions of reversed trends turn out to be true, the detection of low magnitude periodical events will still need to be fulfilled.

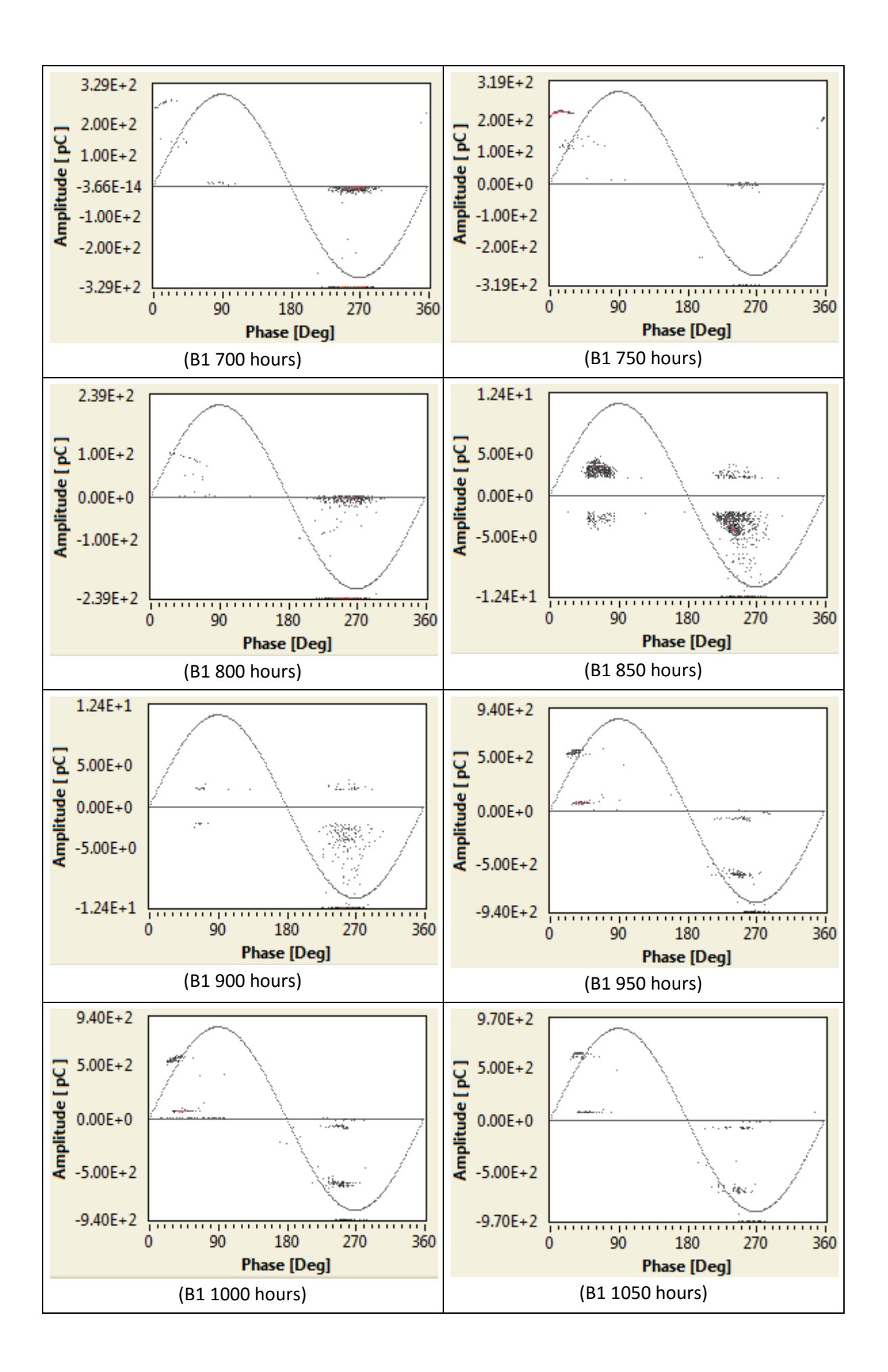
To conclude, this research work included all experimental anticipations that were initially set. Through 2000 hour long term degradation experiments of 20 successful samples, conventional analysis such as PRPD patterns were used to define degradation stages, and were interpreted by physical and chemical details behind. Both optical and scanning electron imaging and chemical analysis techniques were applied and productive during the process. A close loop relationship between cavity surface conditions and PD behaviours were established, leading to a method for degradation level assessment with the assistance from feedforward capability analysis. The author believe this method has overcame many disadvantages from traditional degradation models that attempt to simulate both PD and surface deterioration, such disadvantages are mainly caused by the random nature of PD itself.

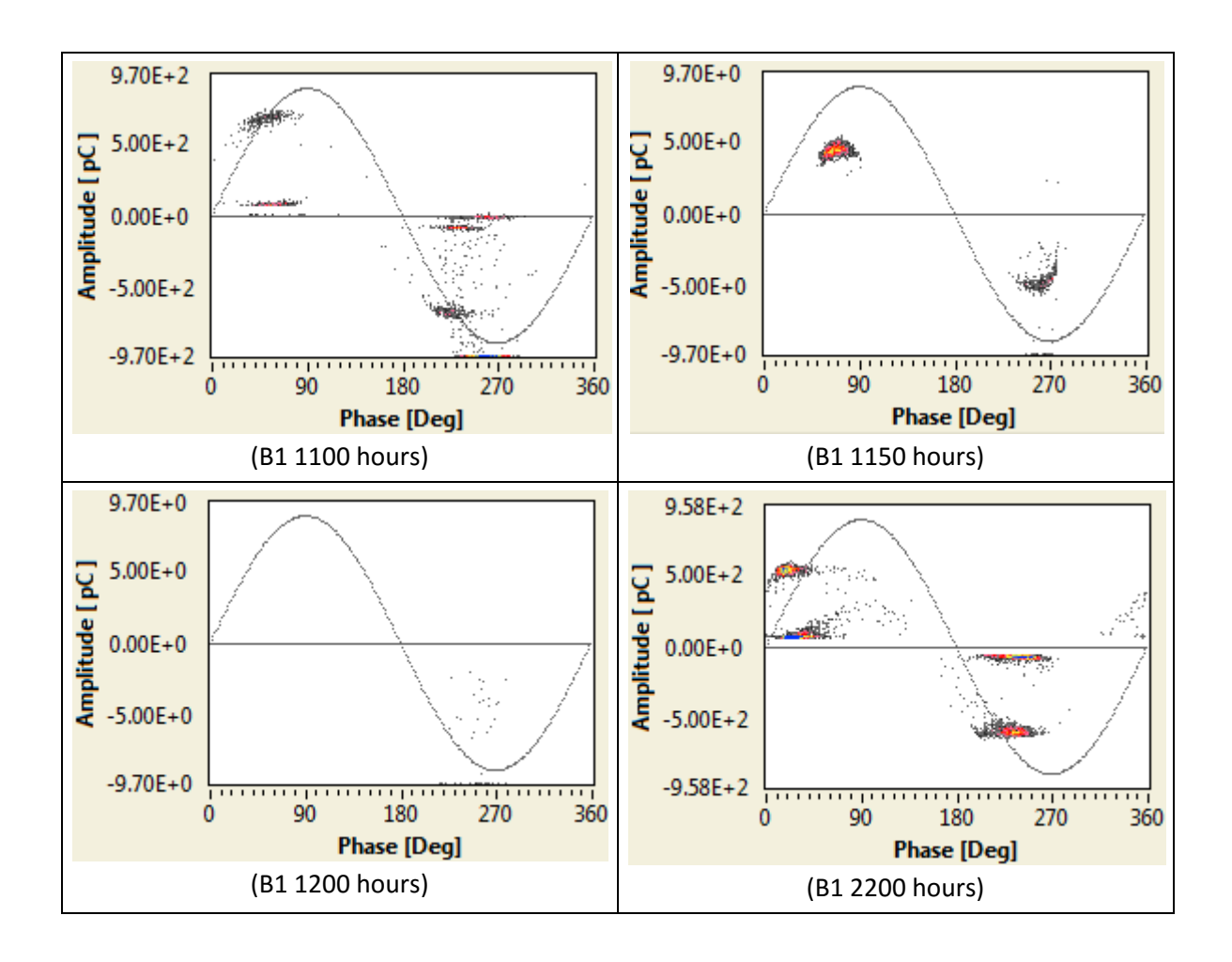
Appendices

Appendix A PRPD results of epoxy resin degradation test, sample group B.

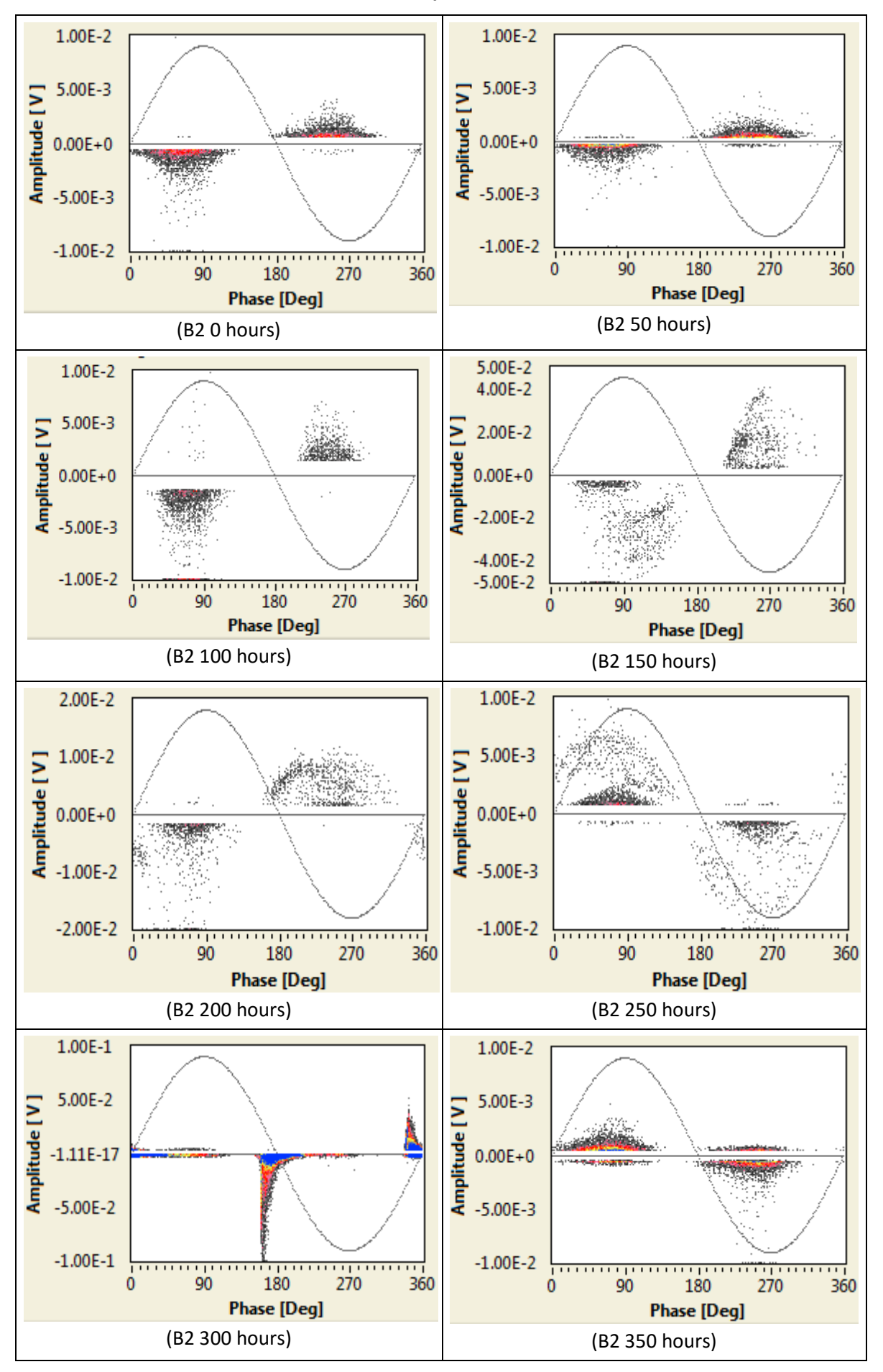


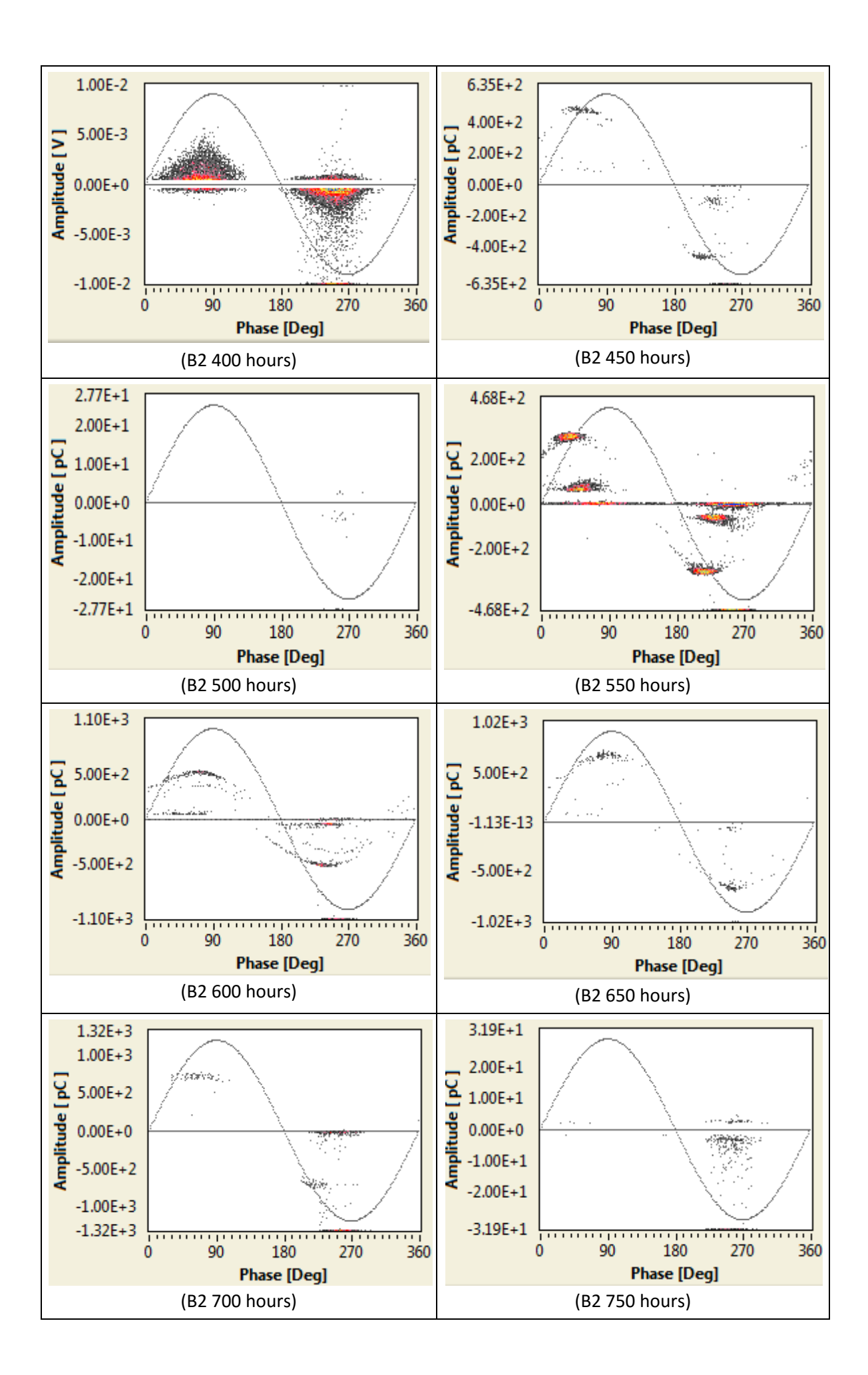


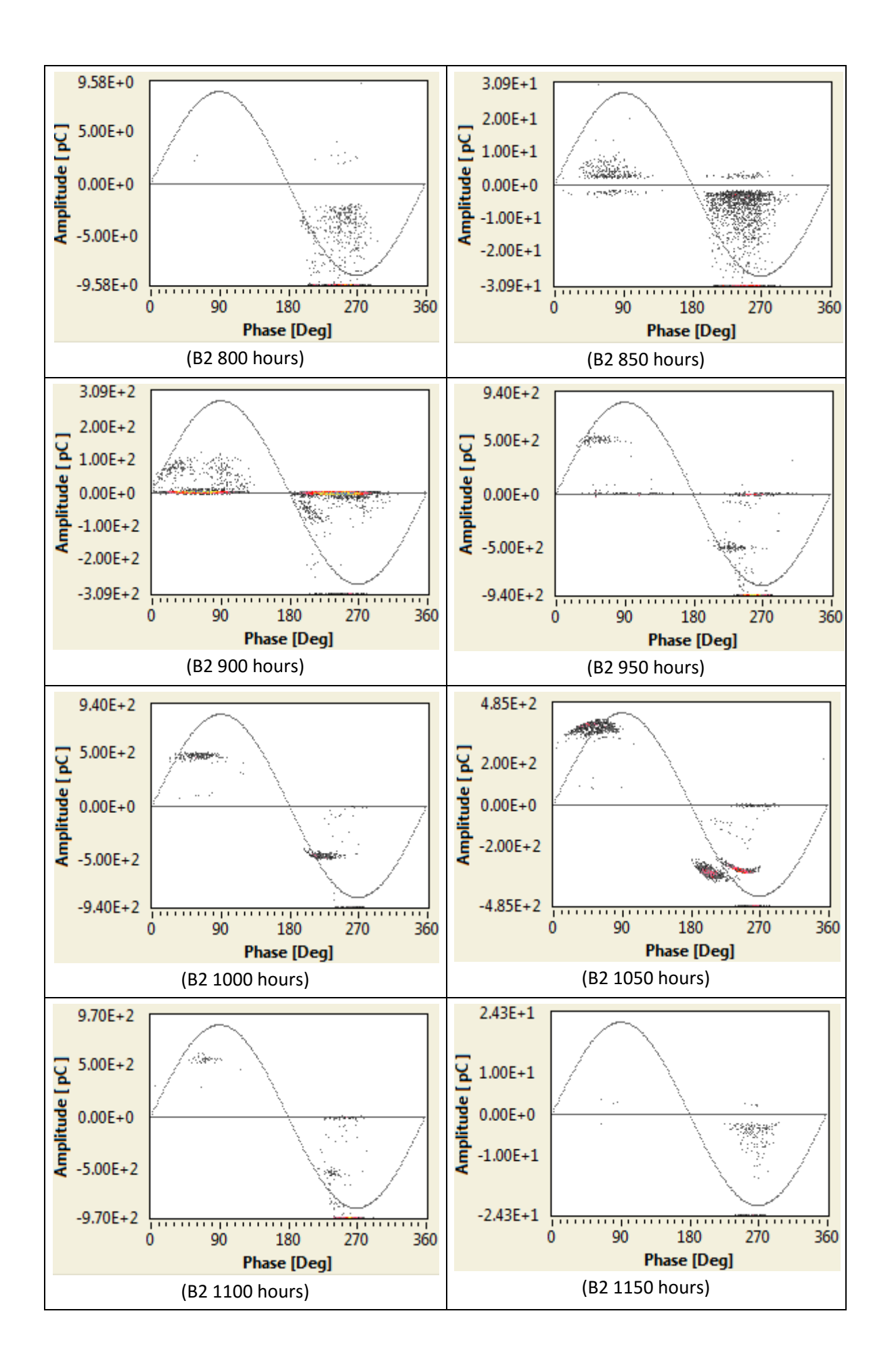


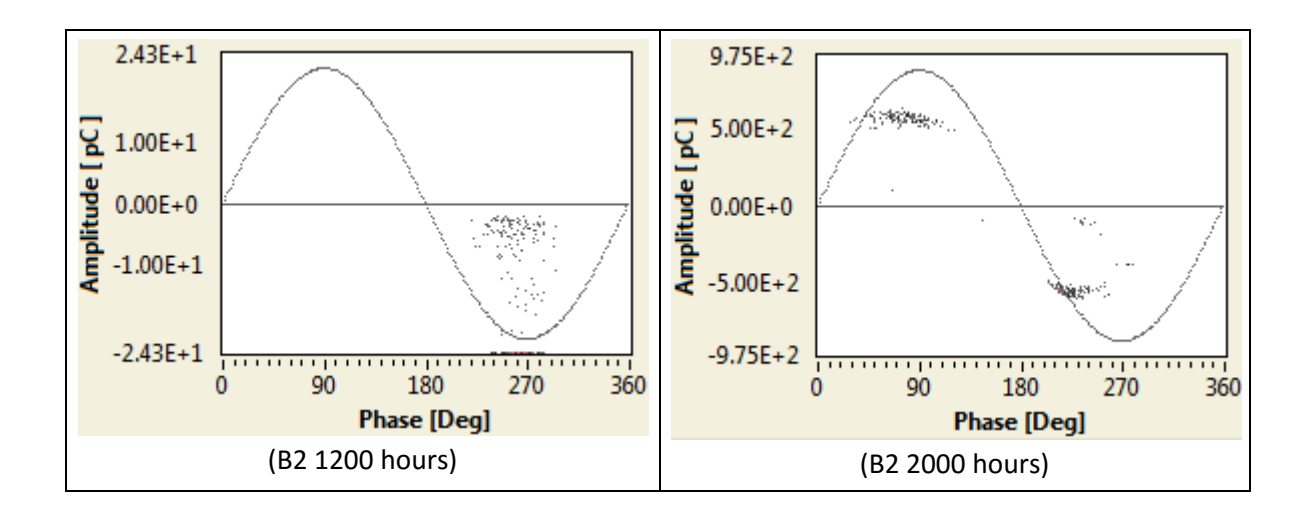


Sample B2

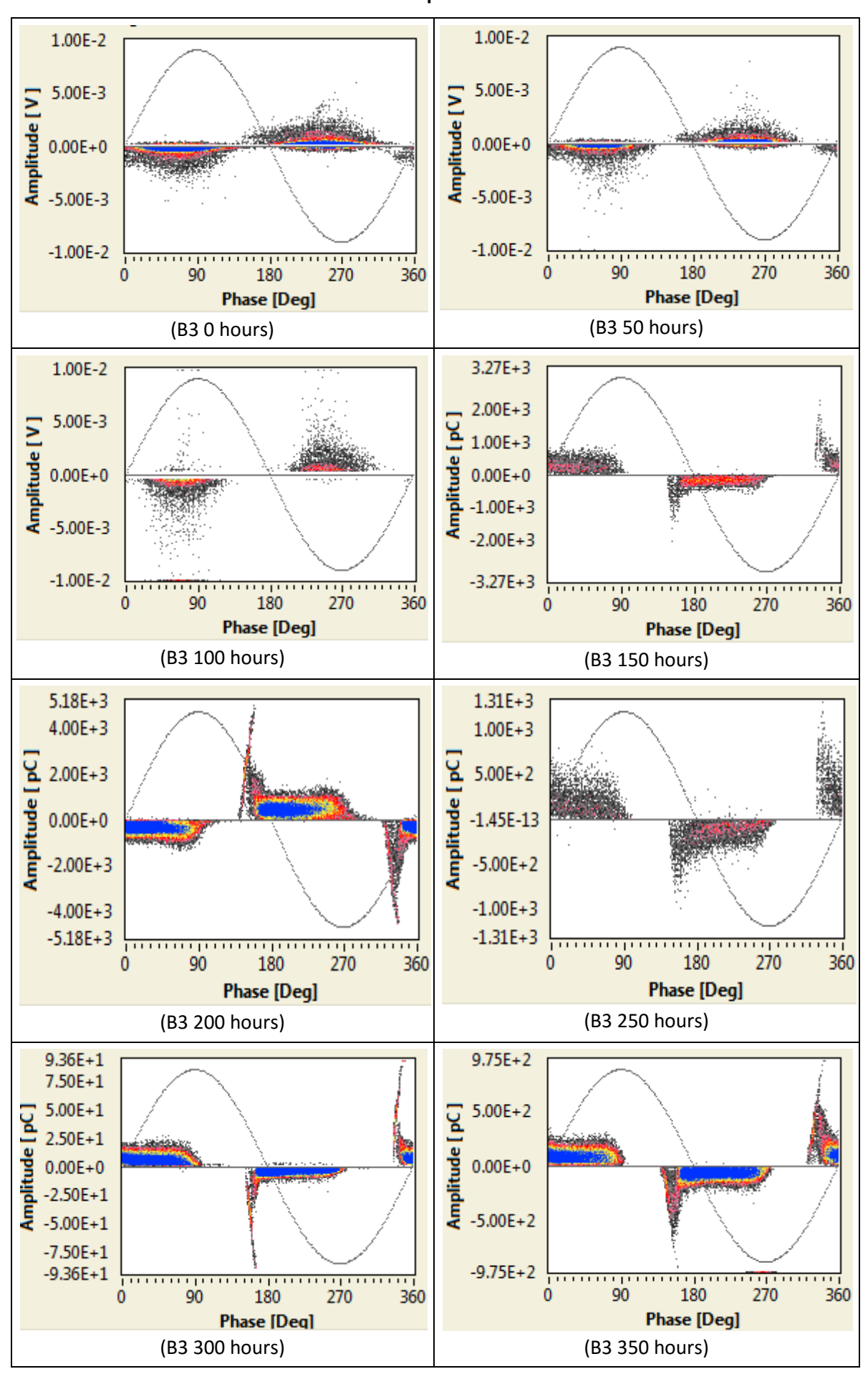


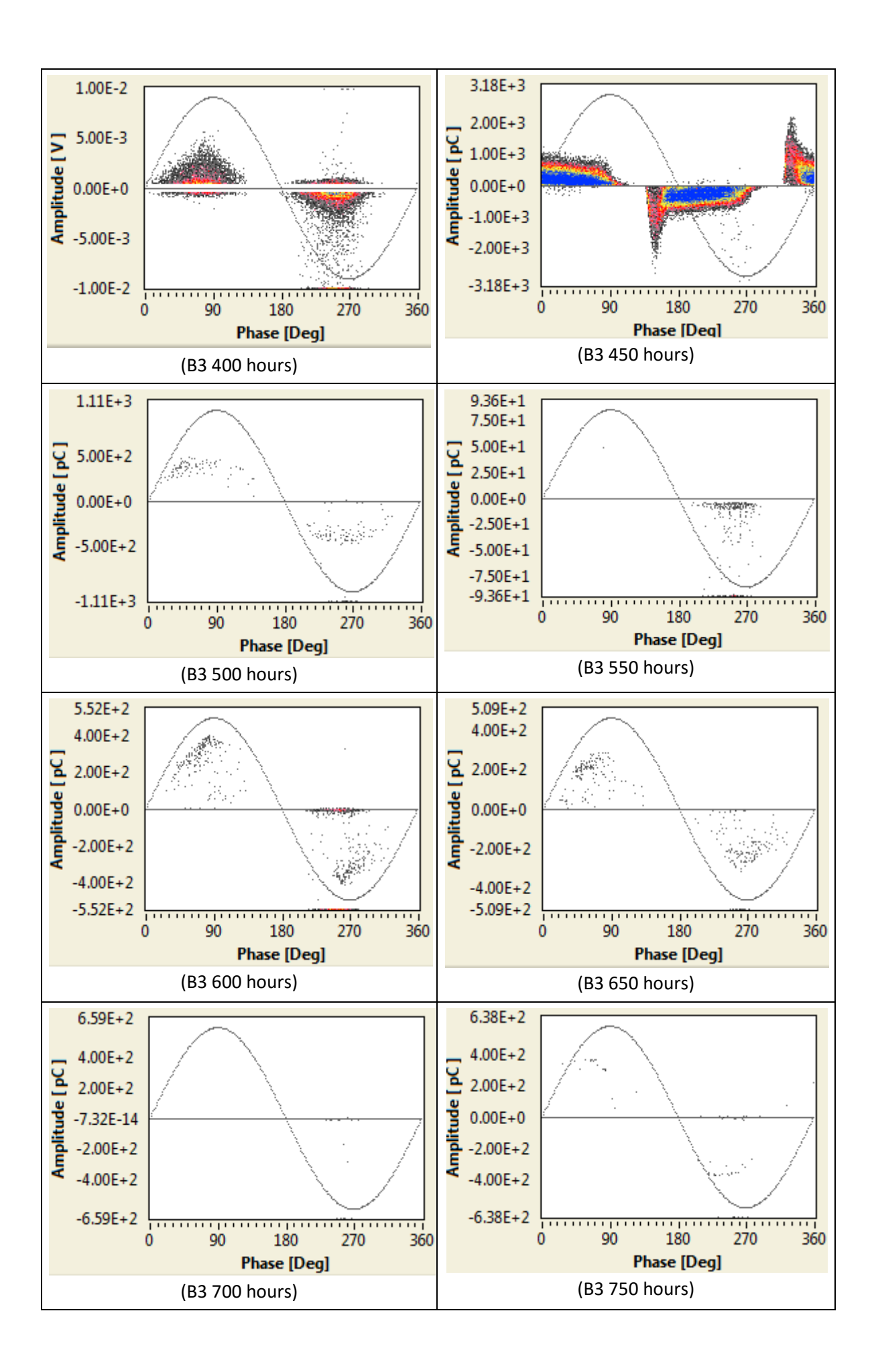


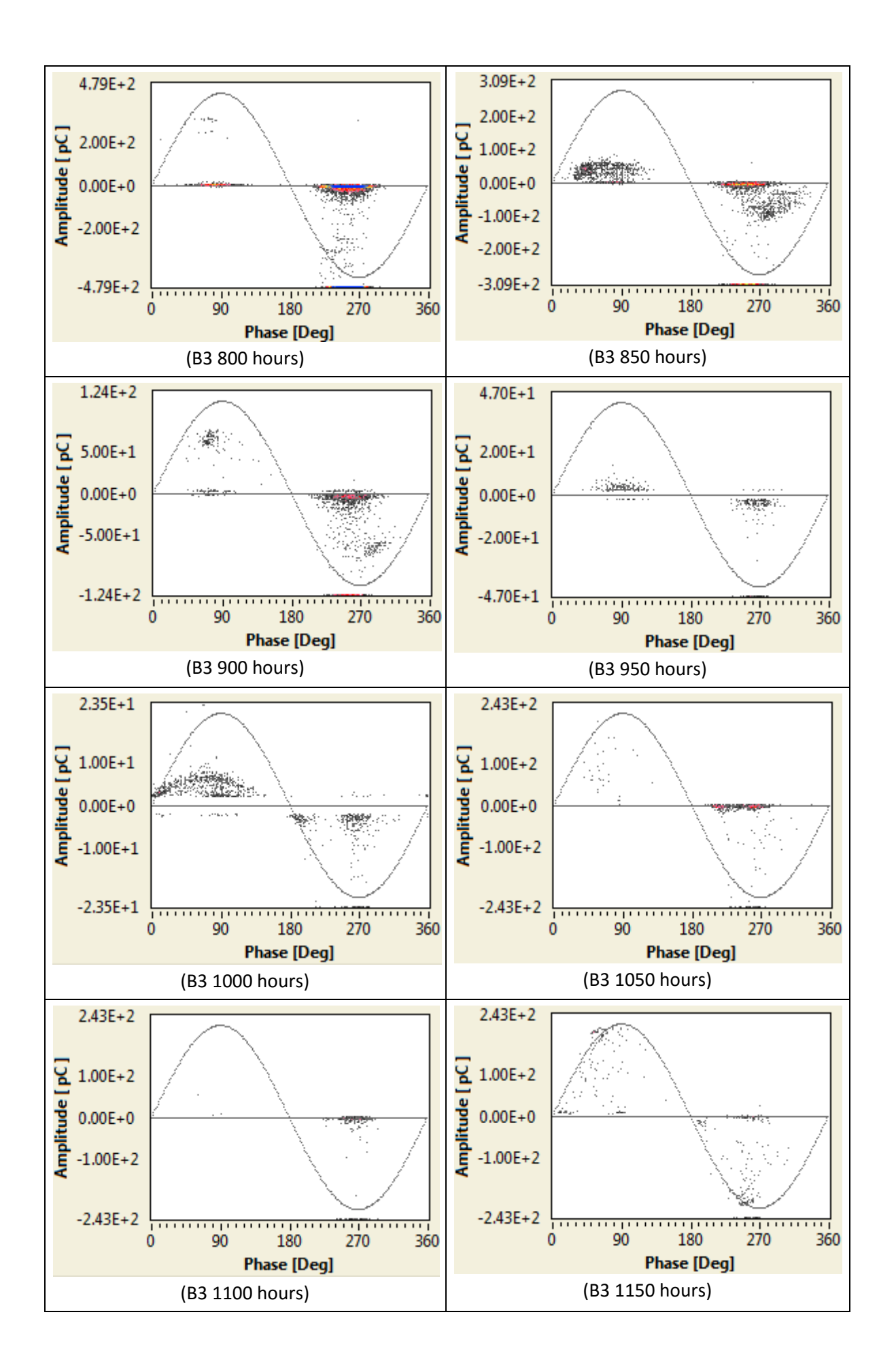


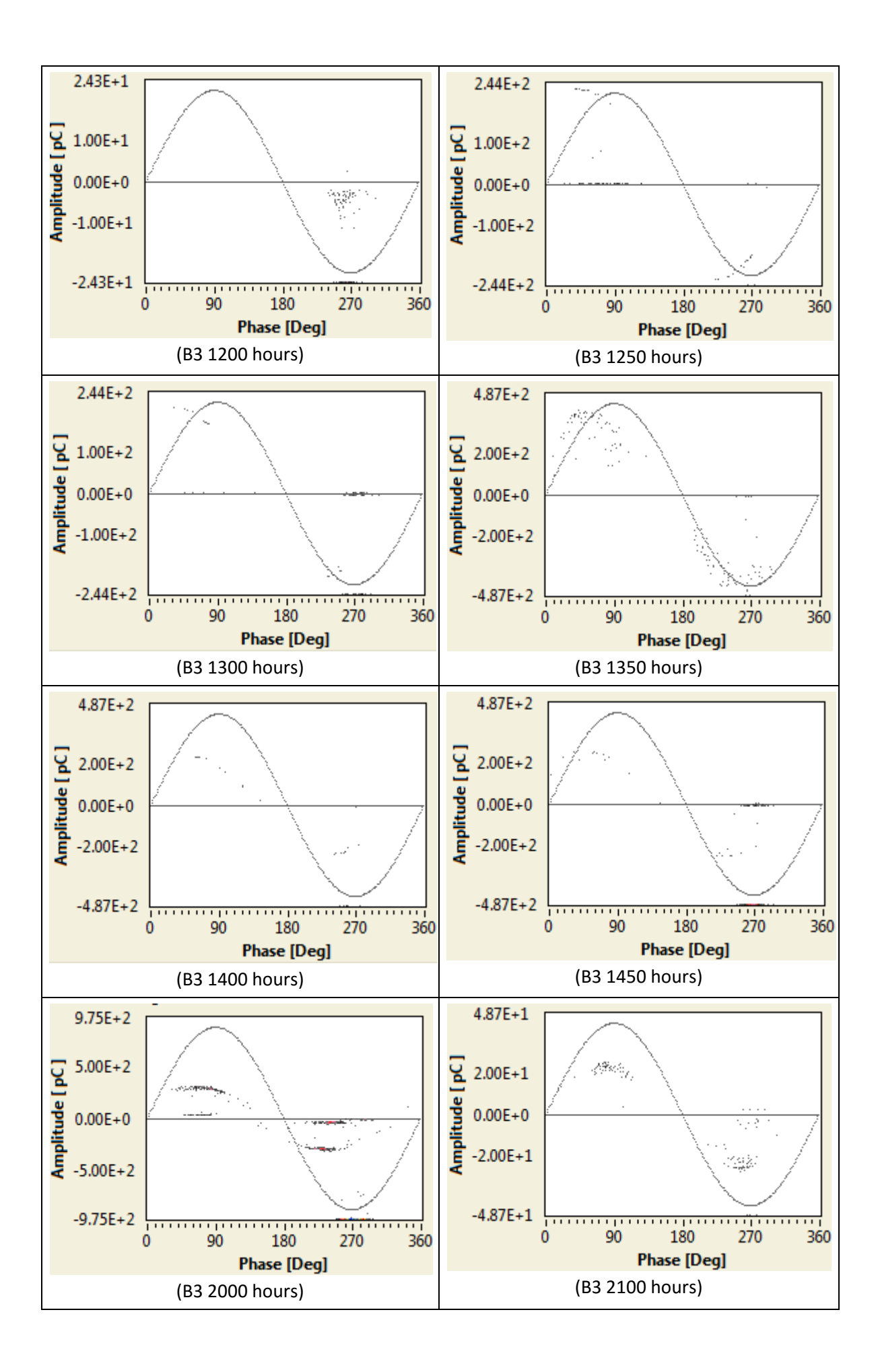


Sample B3

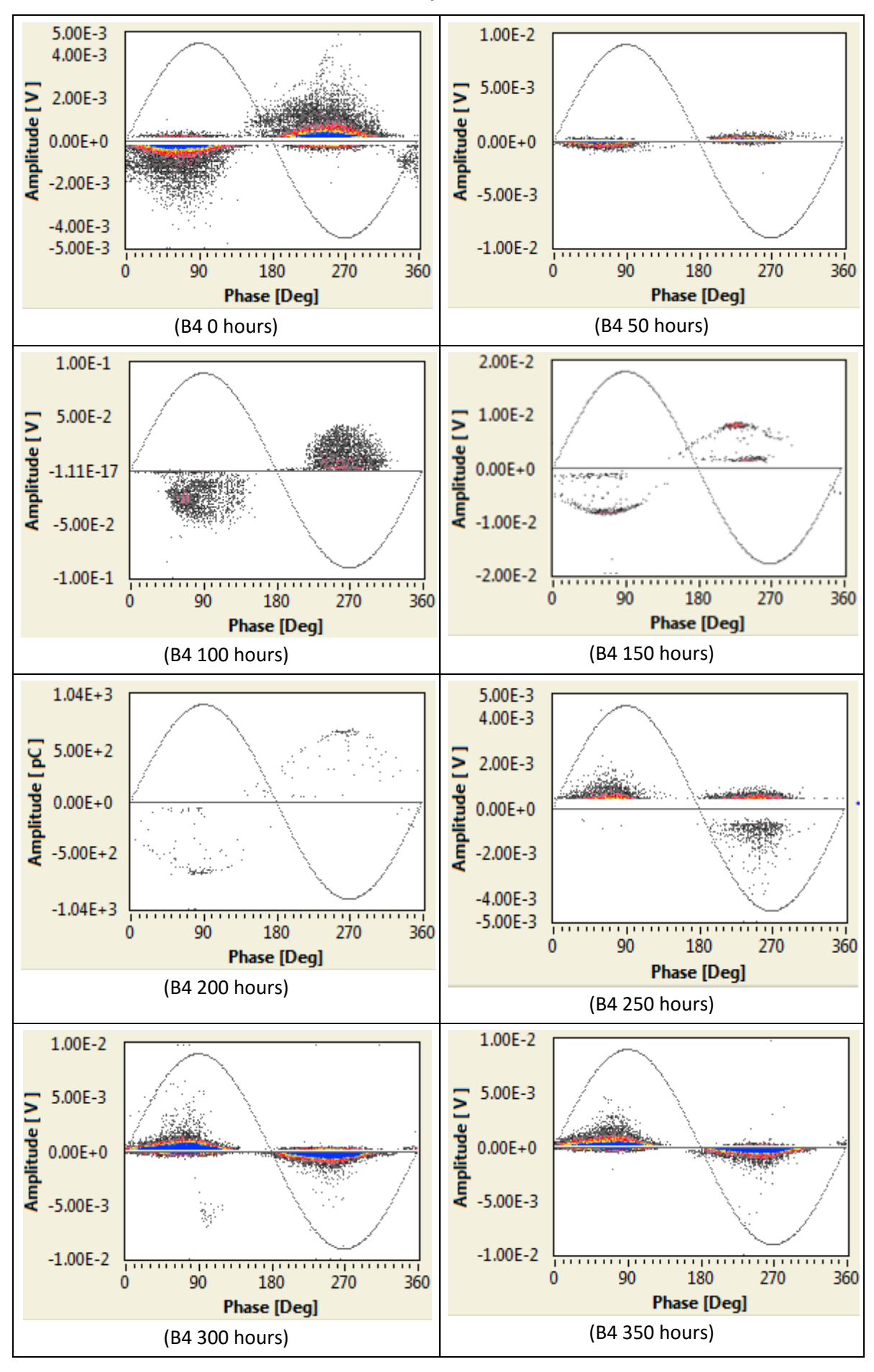


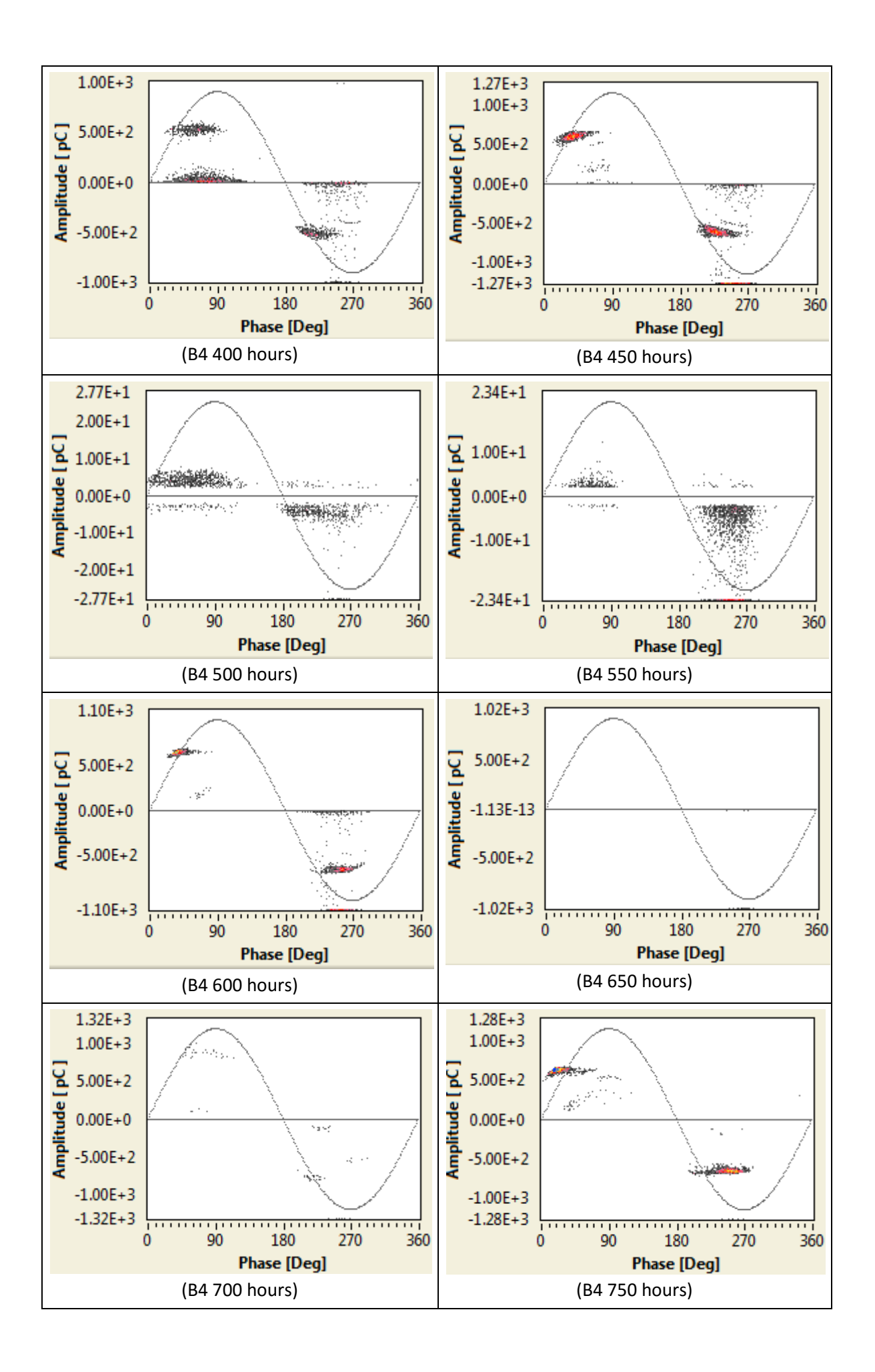


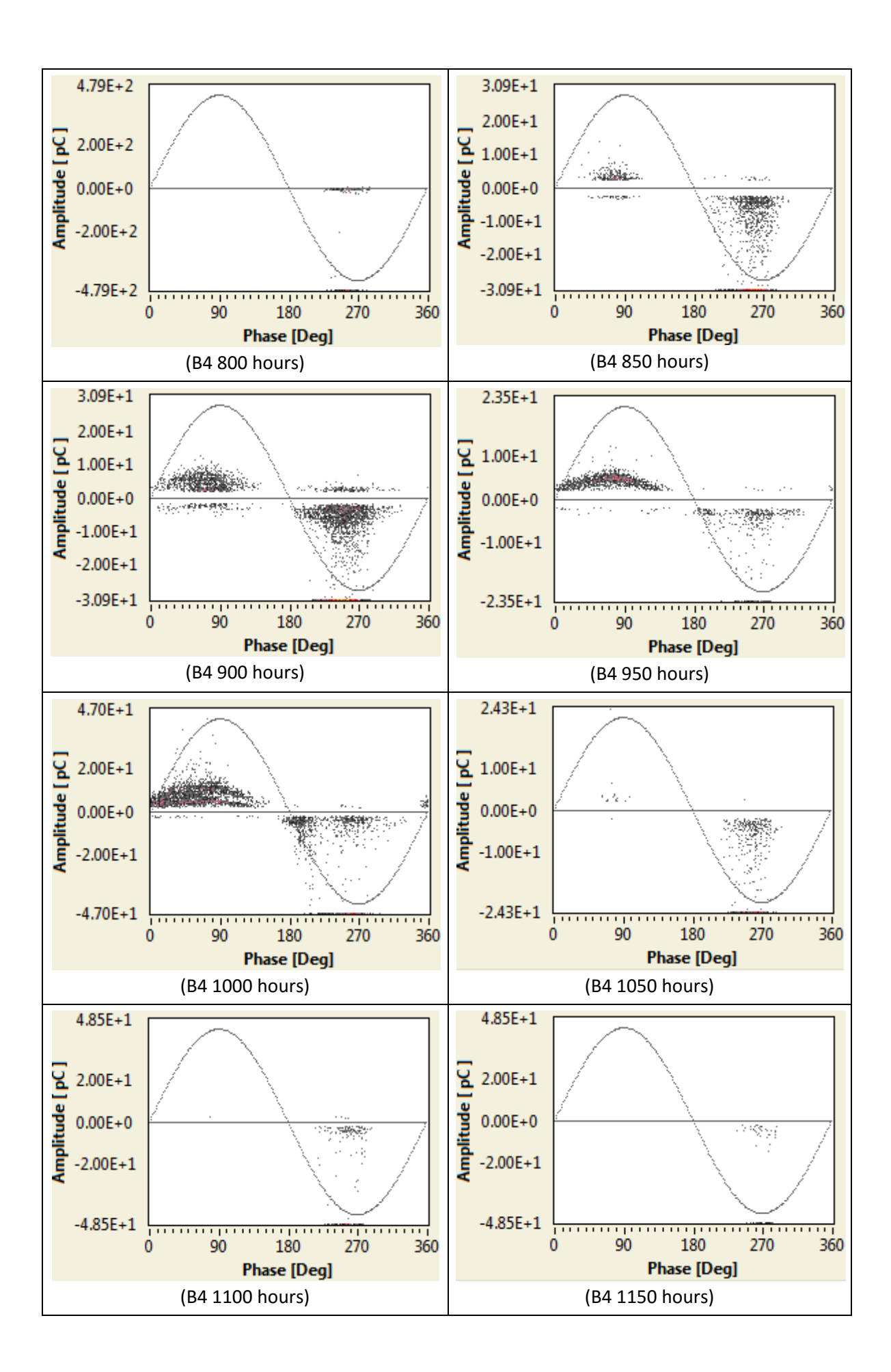


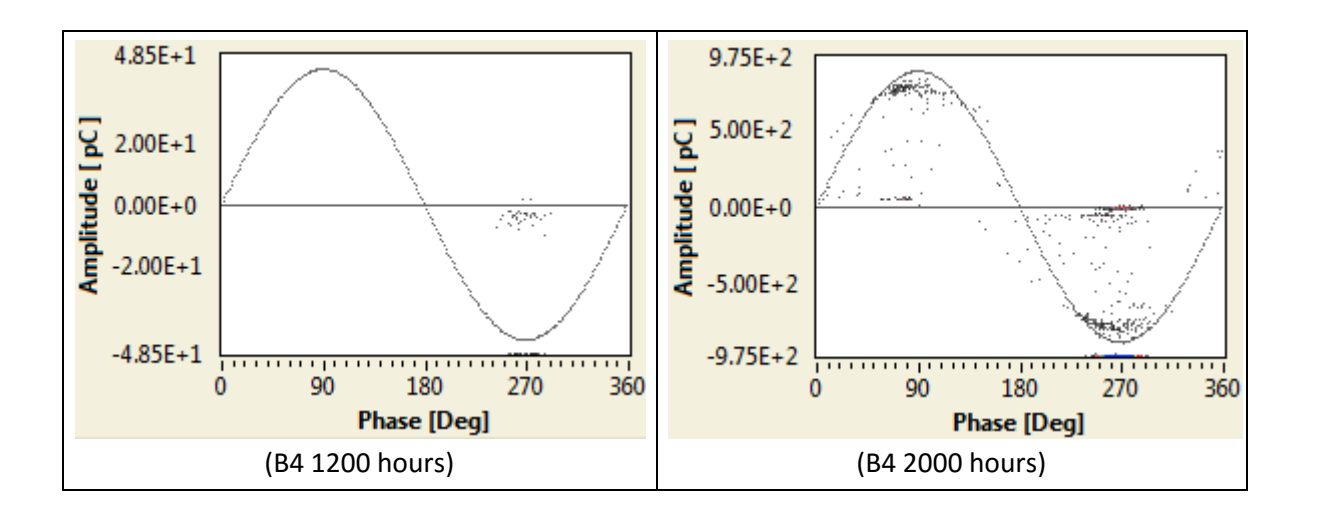


Sample B4

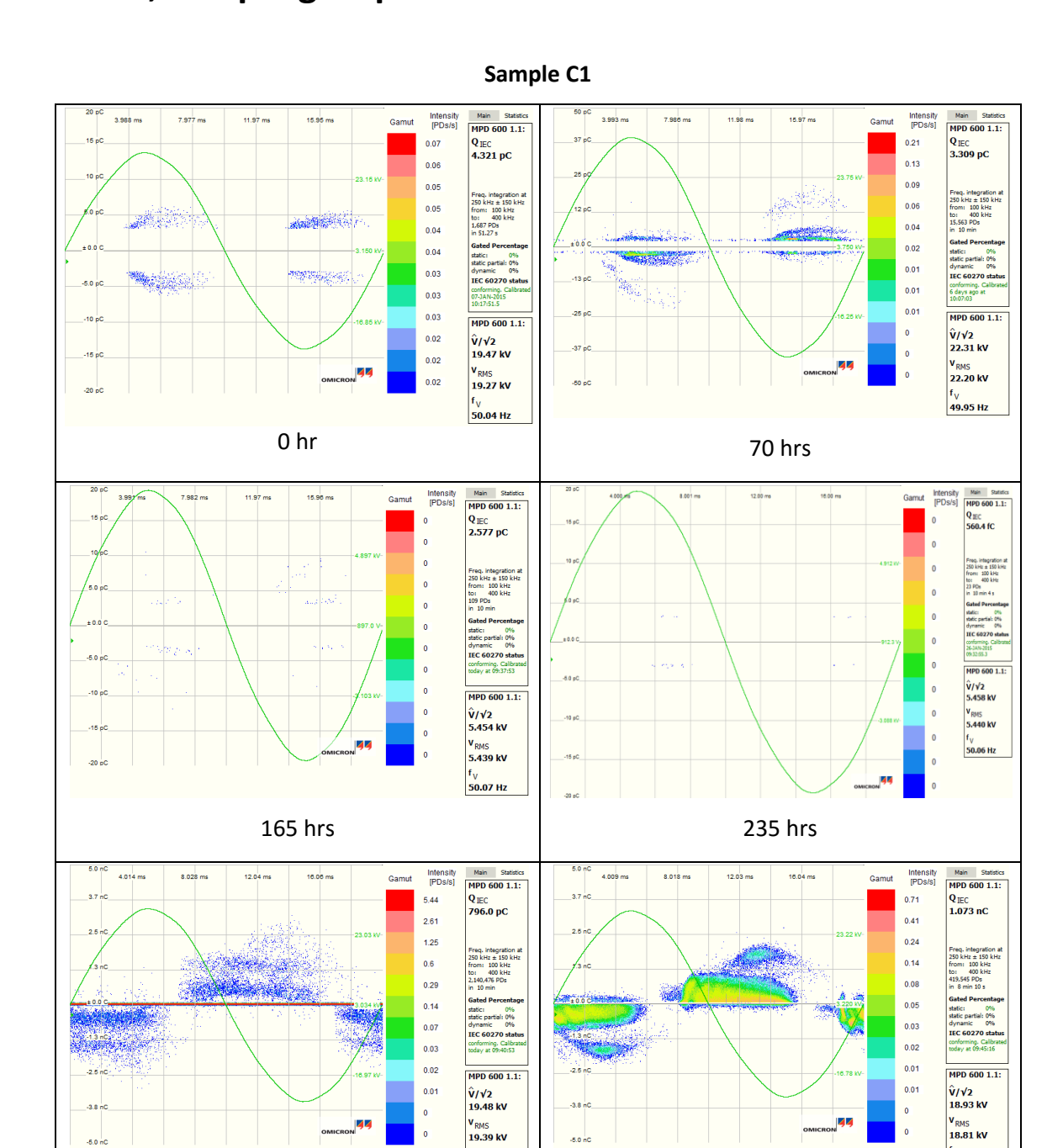








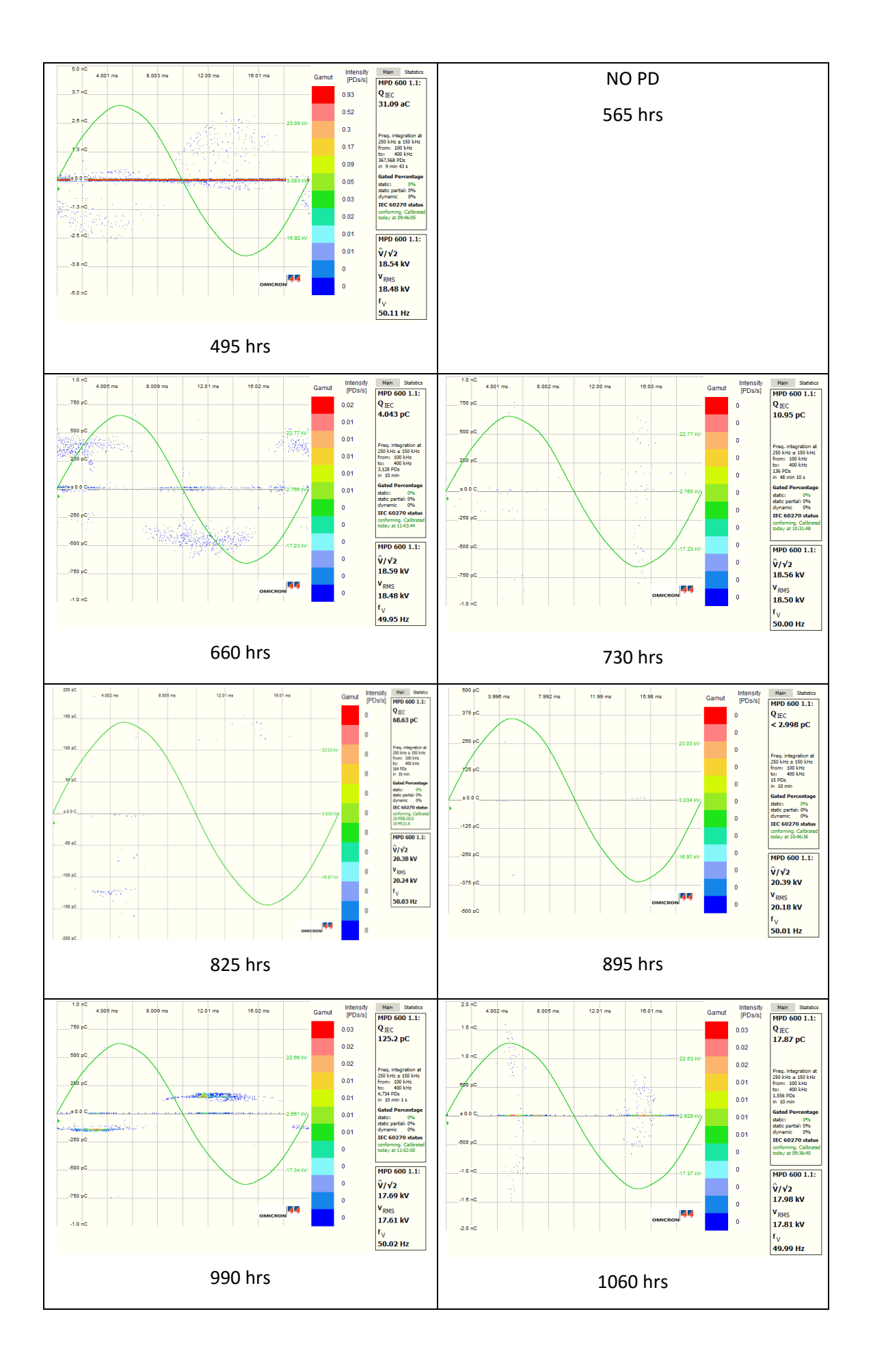
Appendix B PRPD results of epoxy resin degradation test, sample group C.

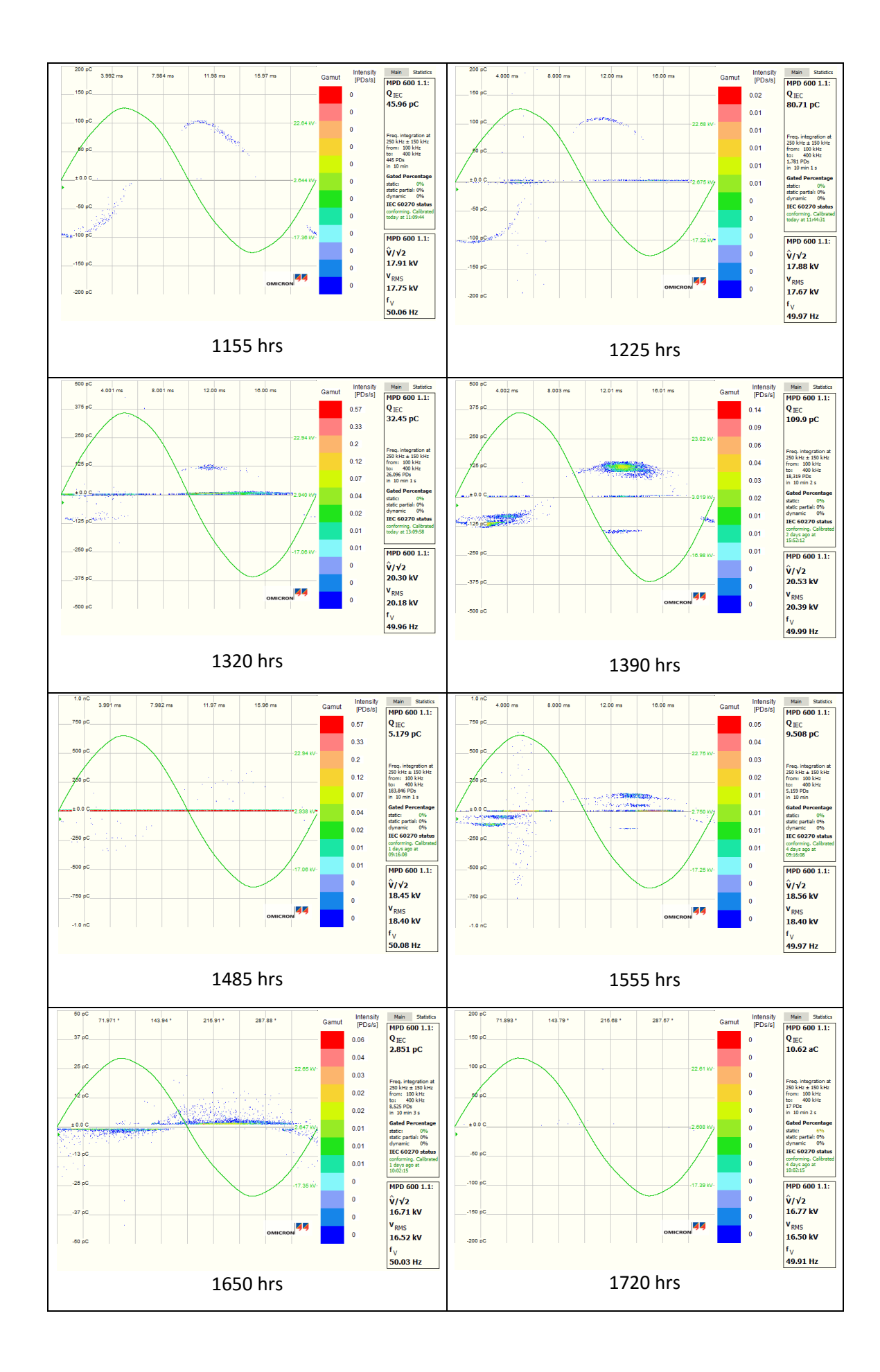


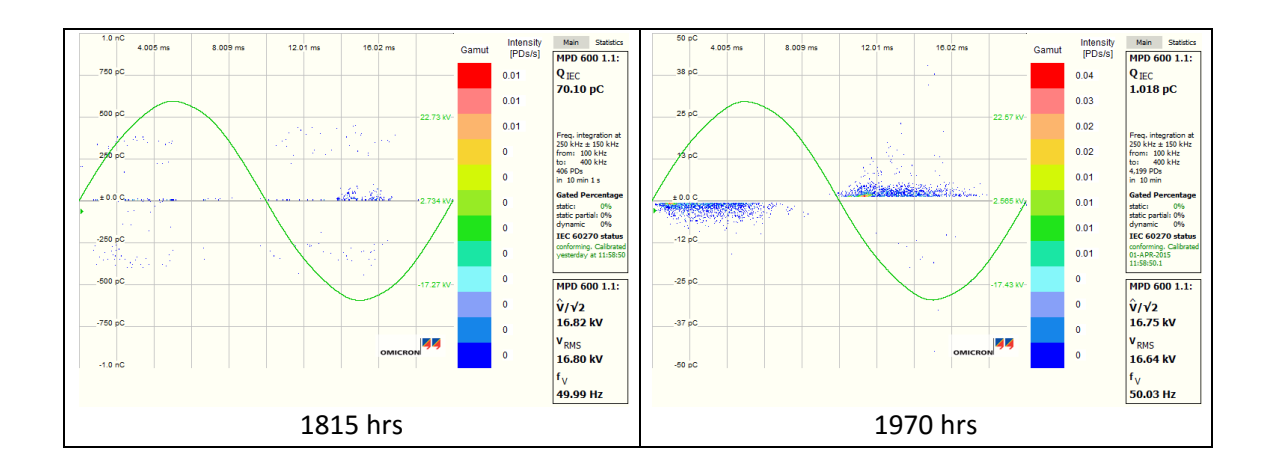
330 hrs

¹∨ 49.97 Hz

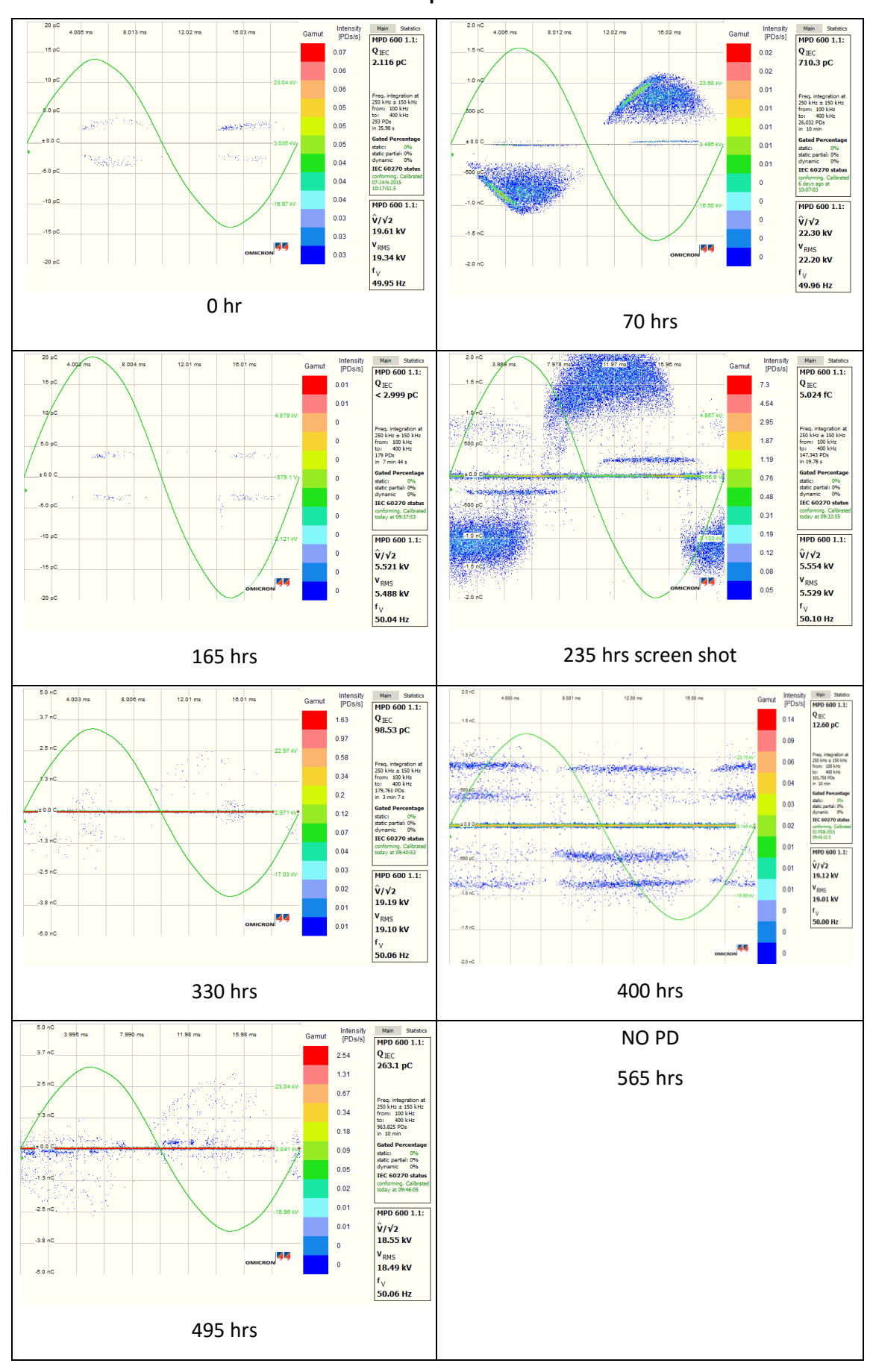
400 hrs

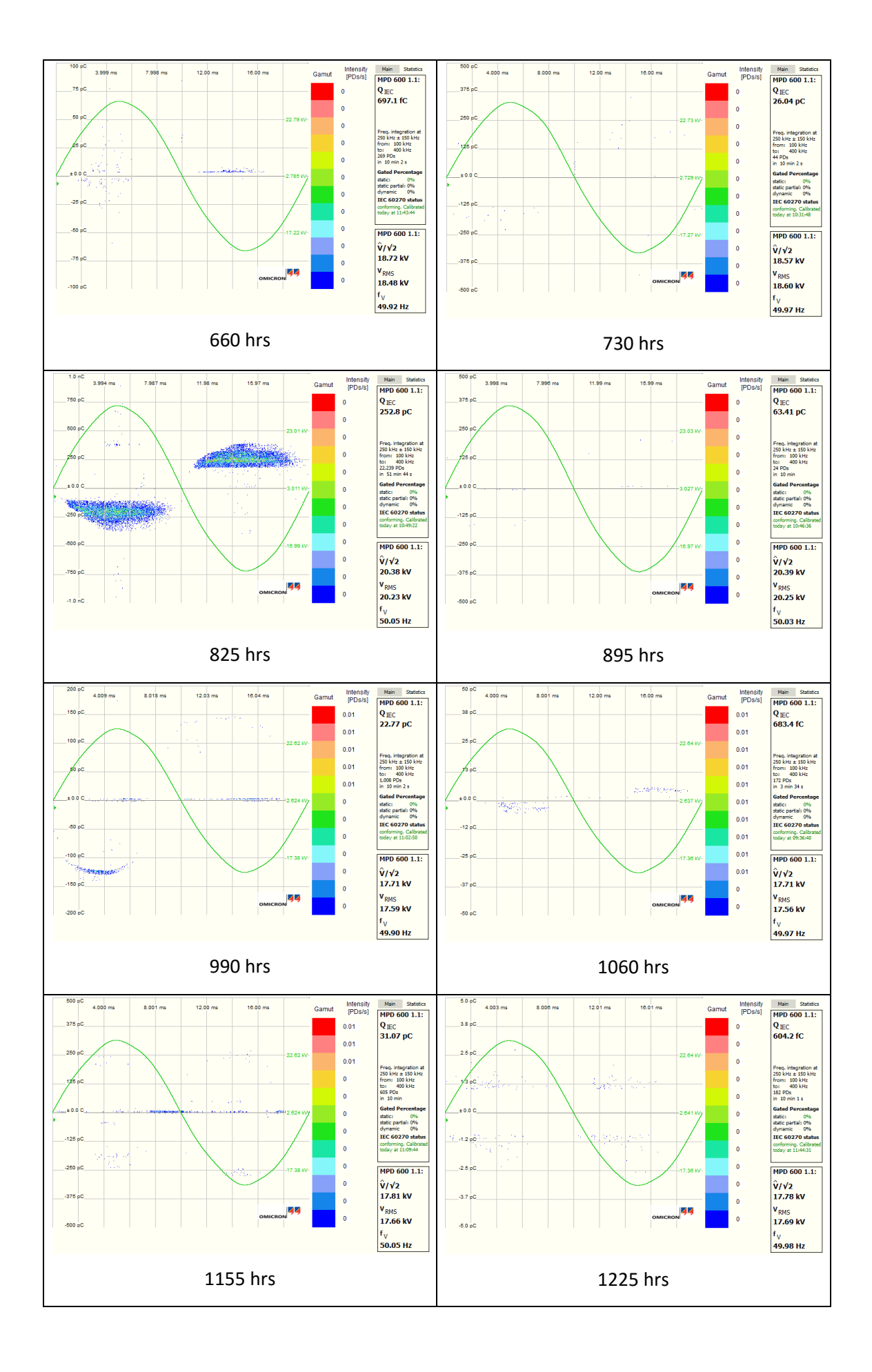


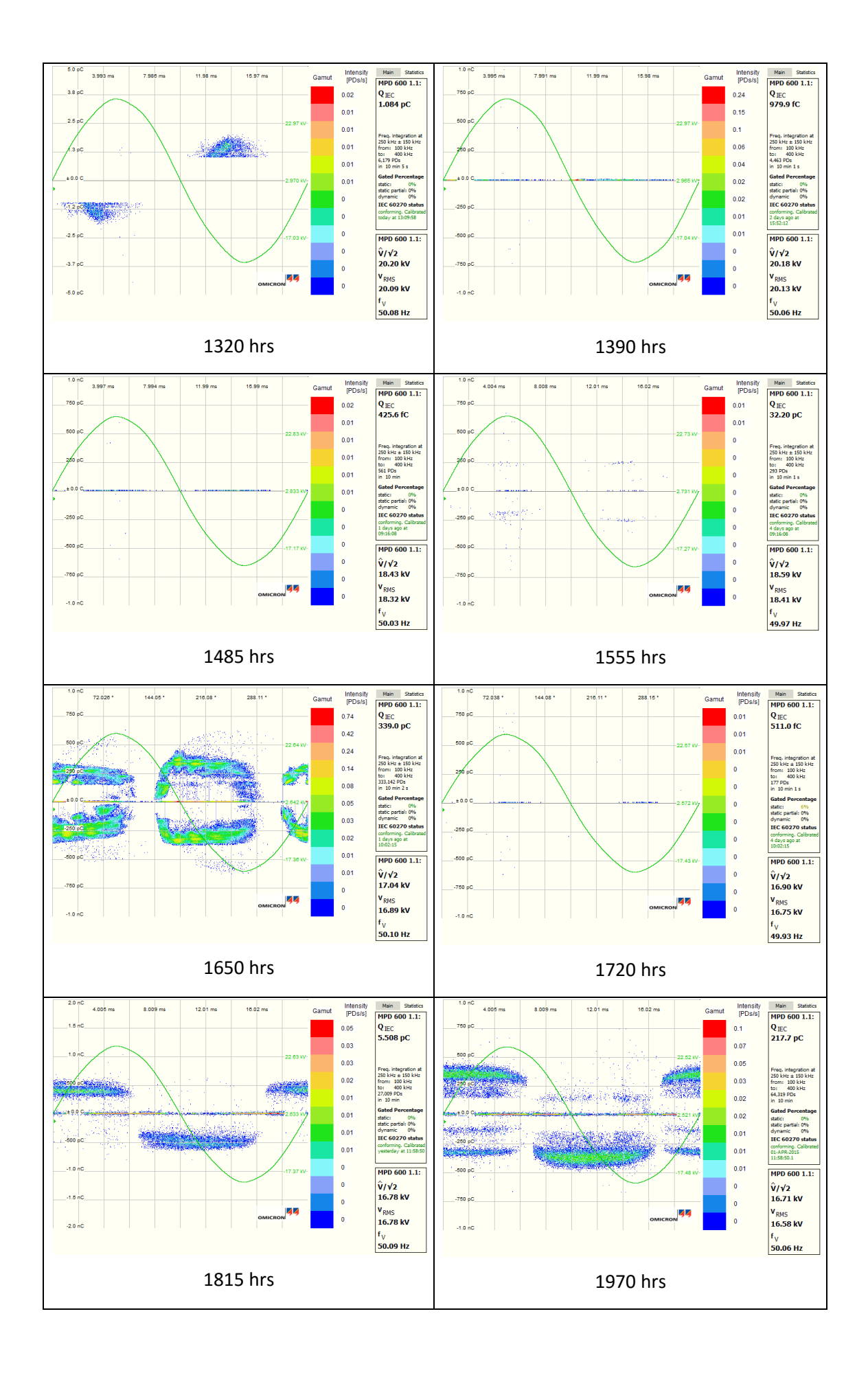




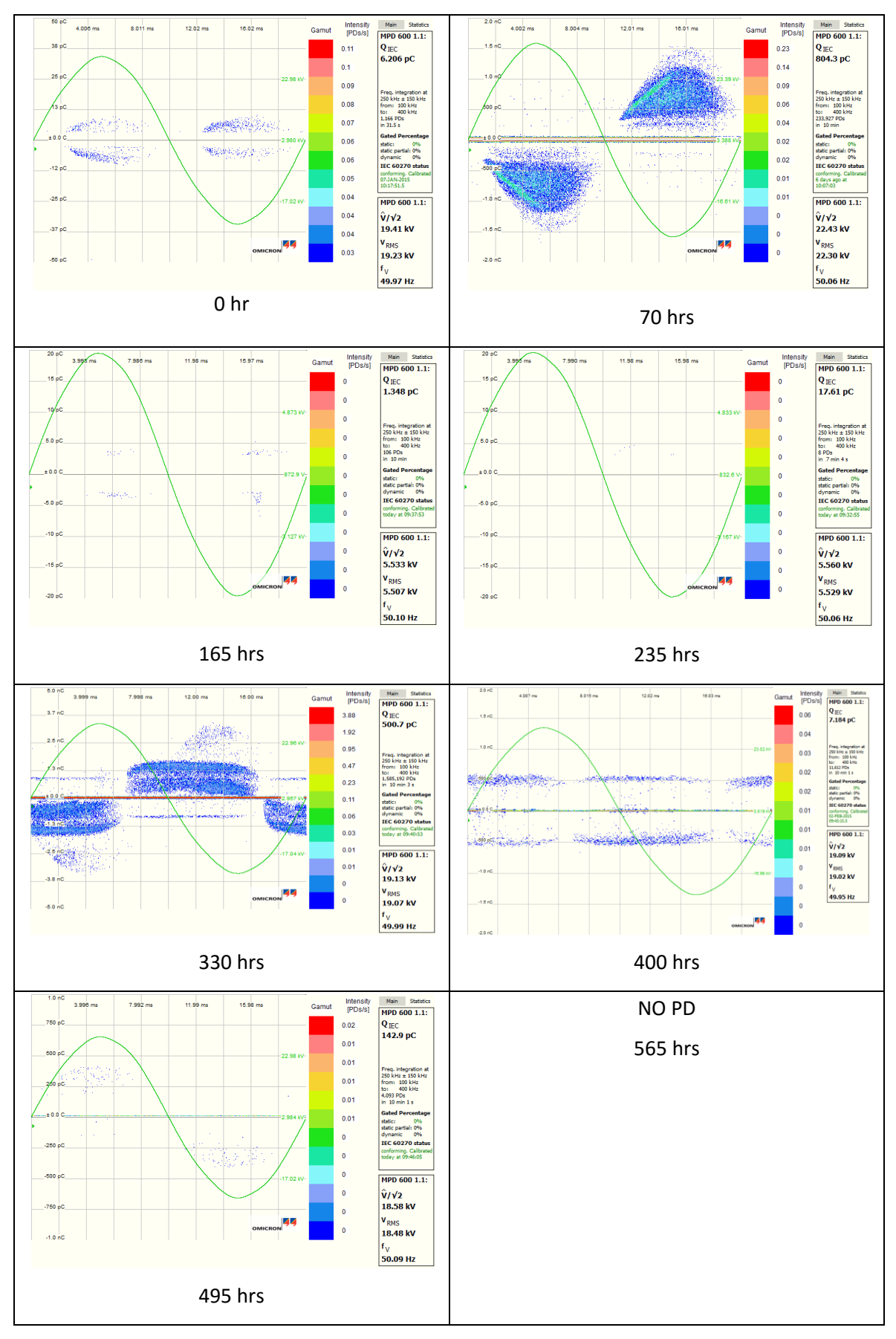
Sample C2

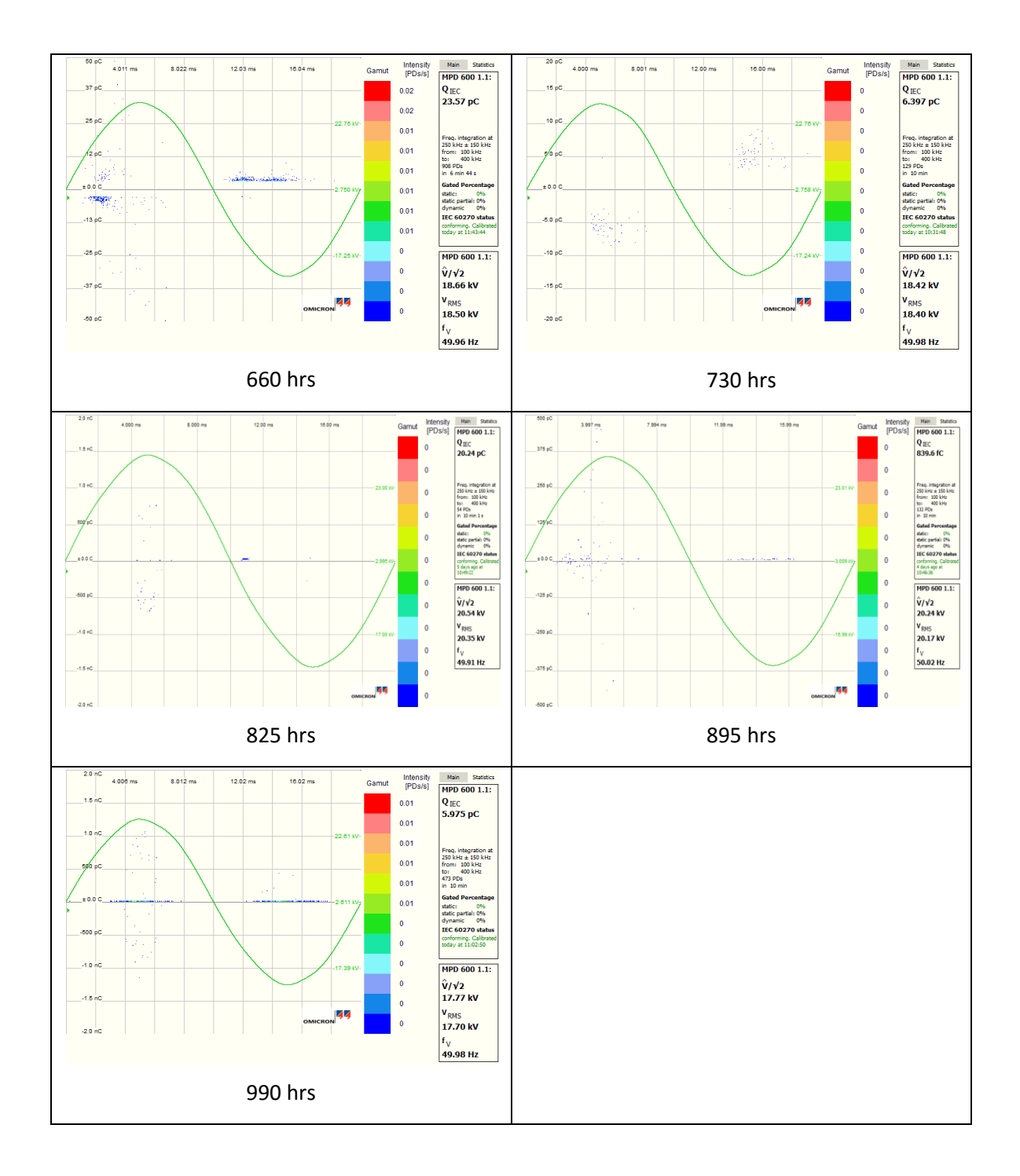




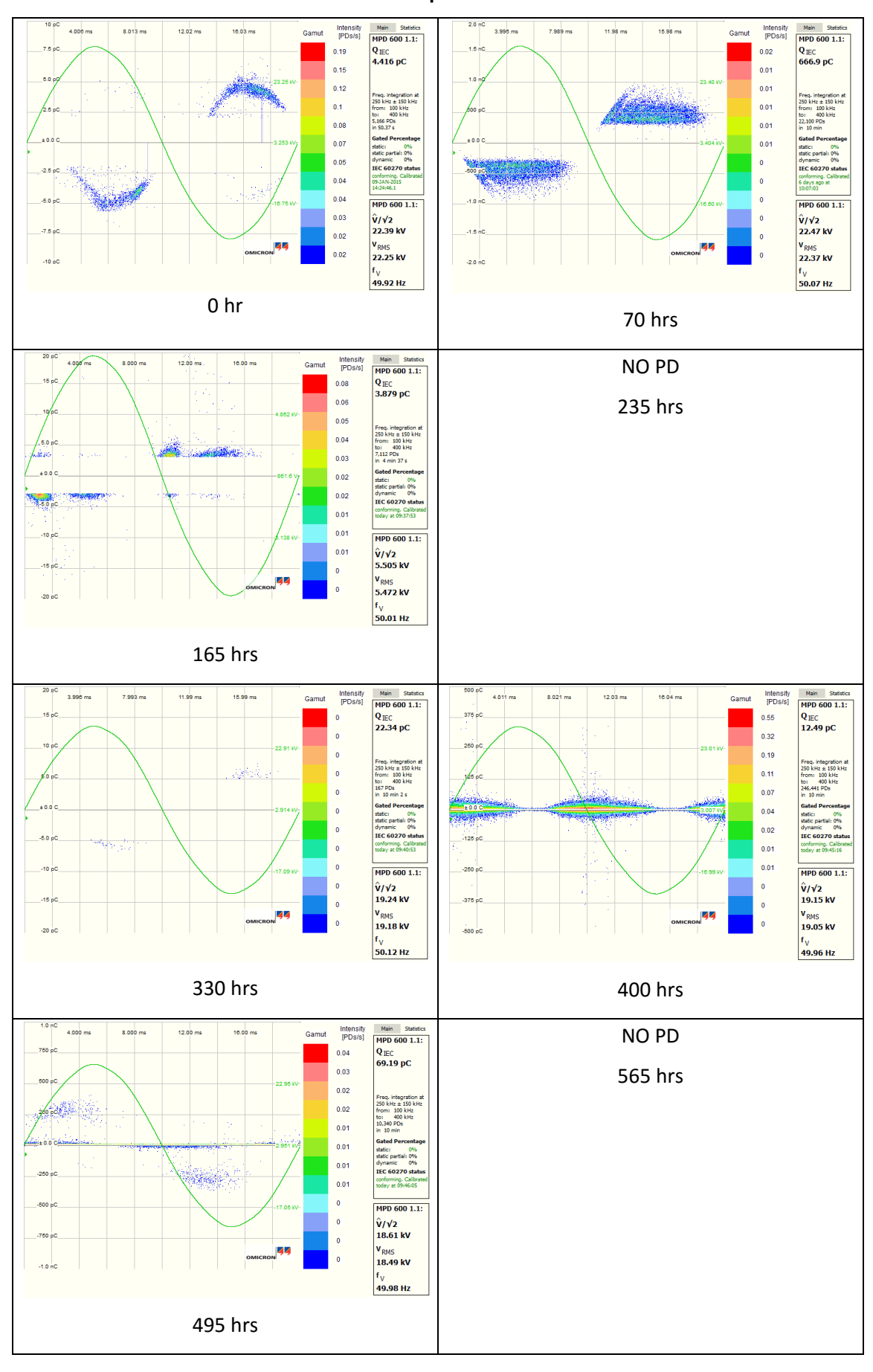


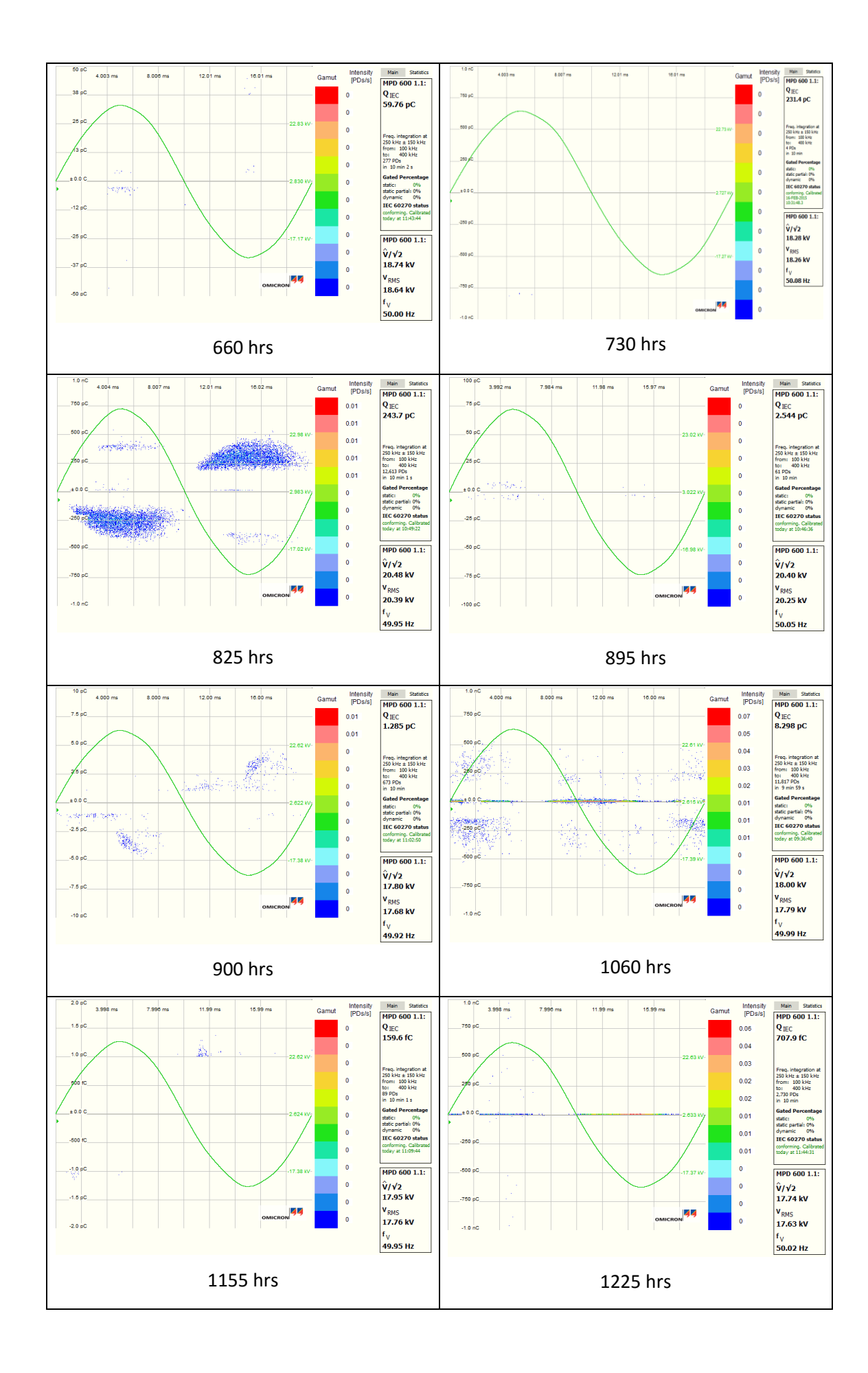
Sample C3

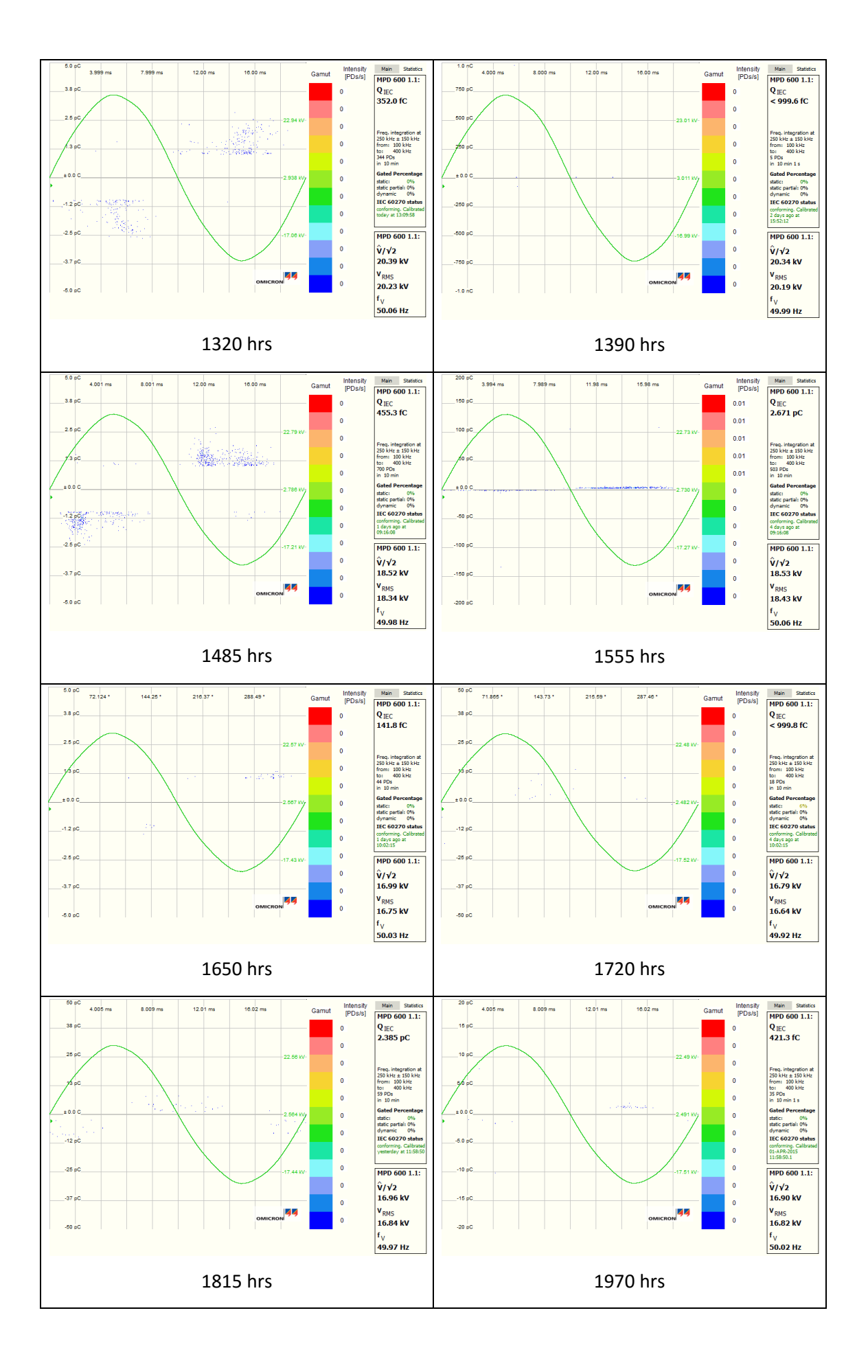




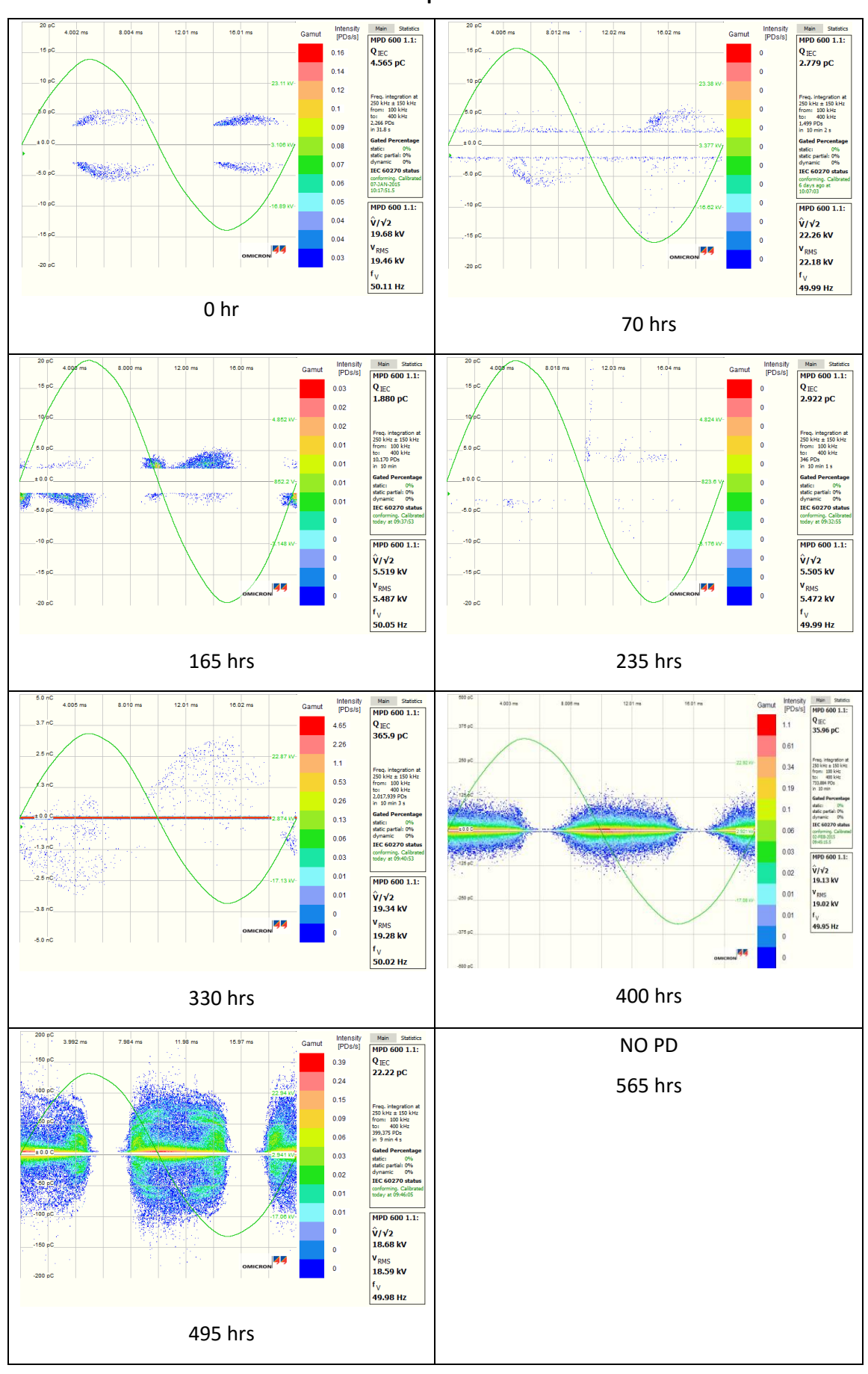
Sample C4

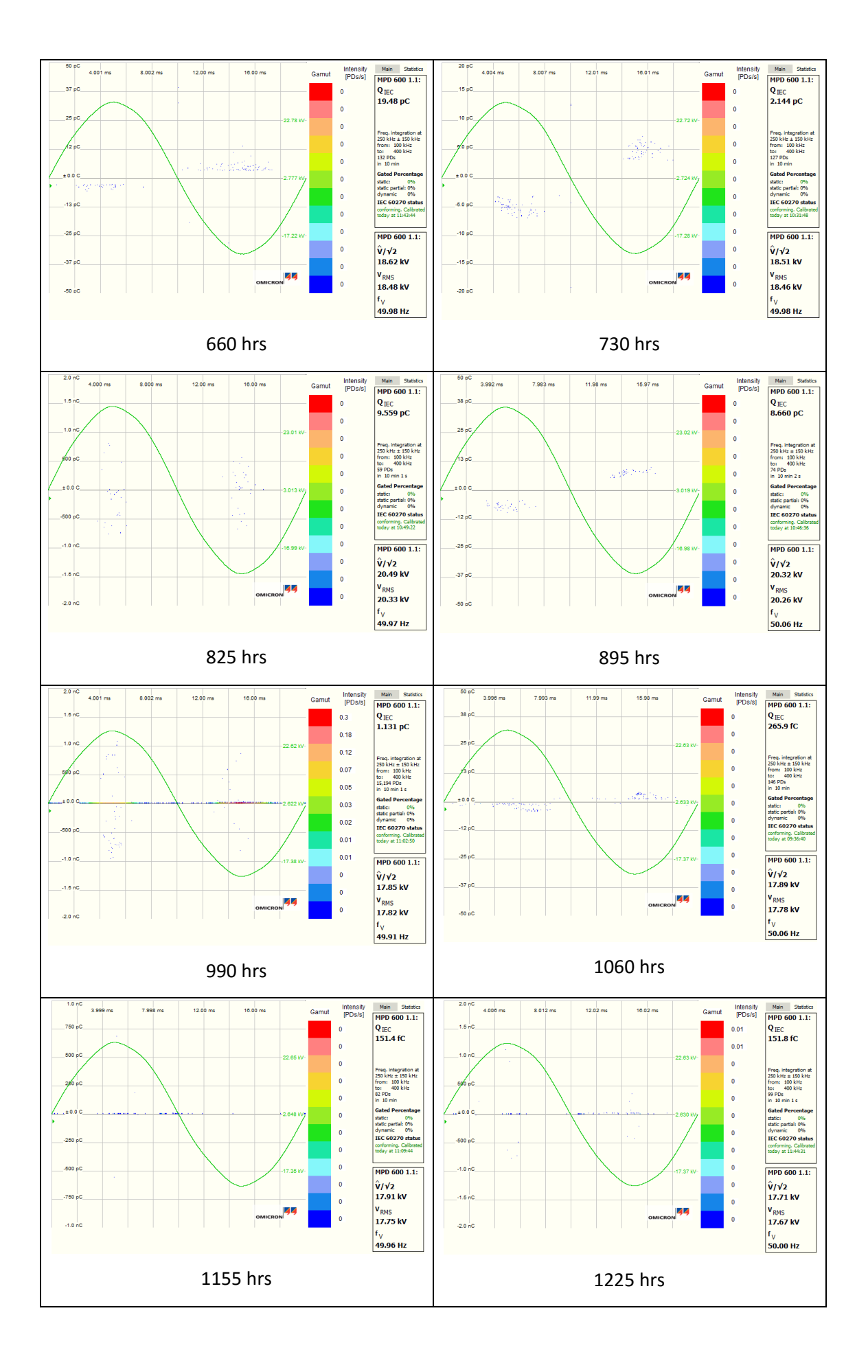


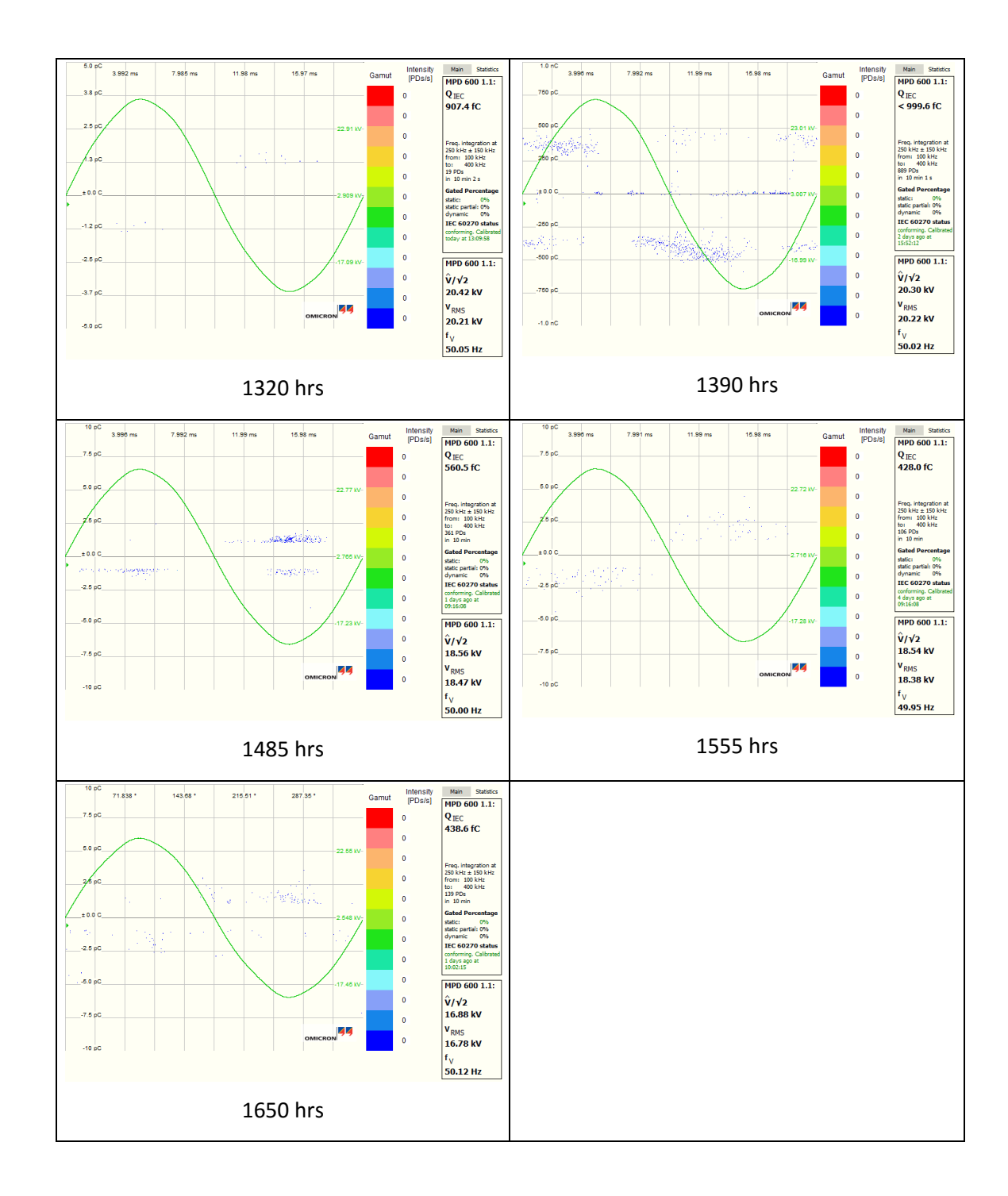




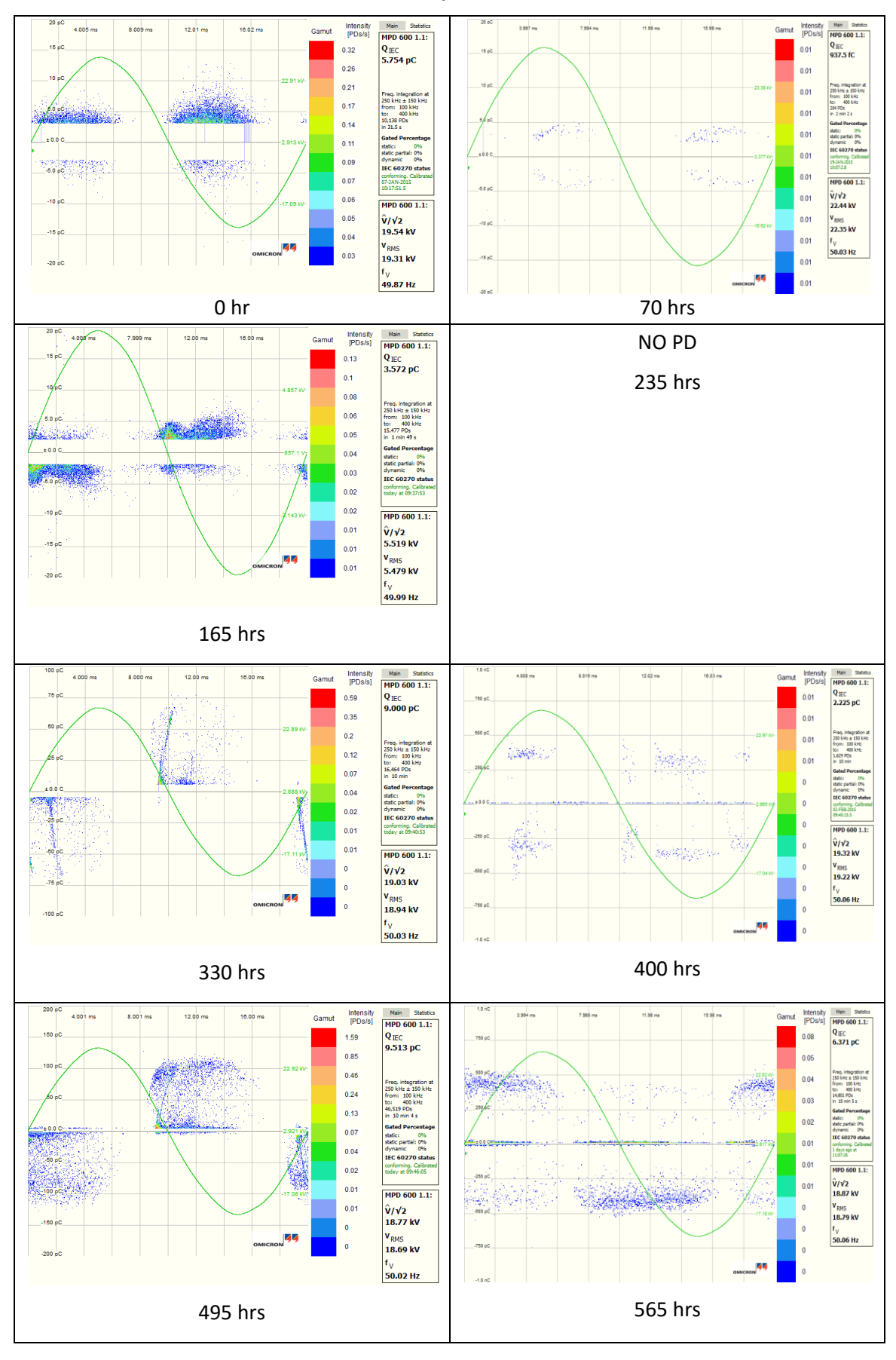
Sample C5

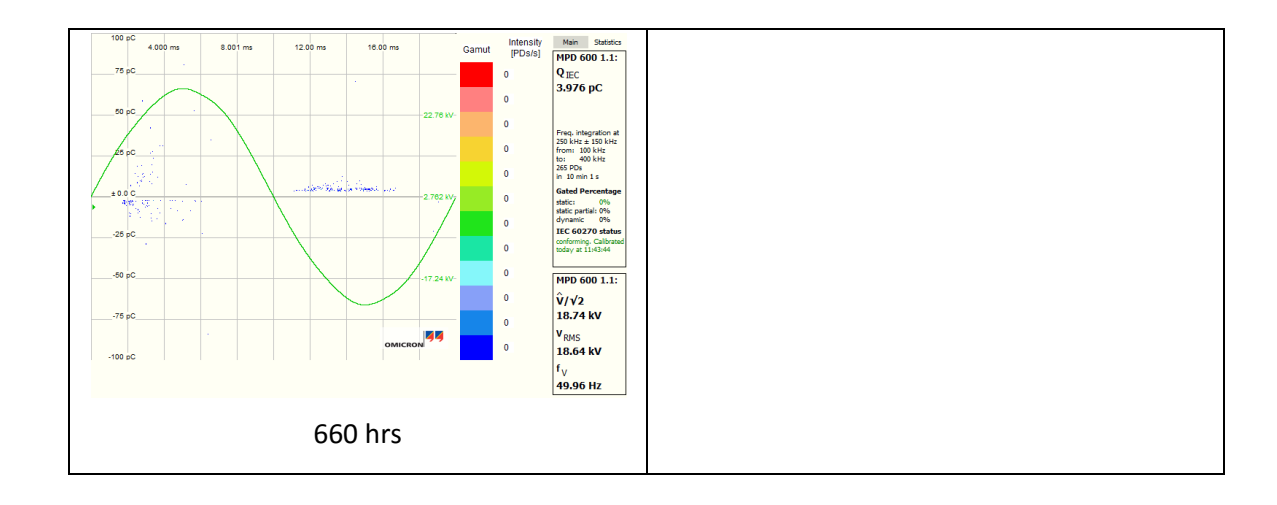




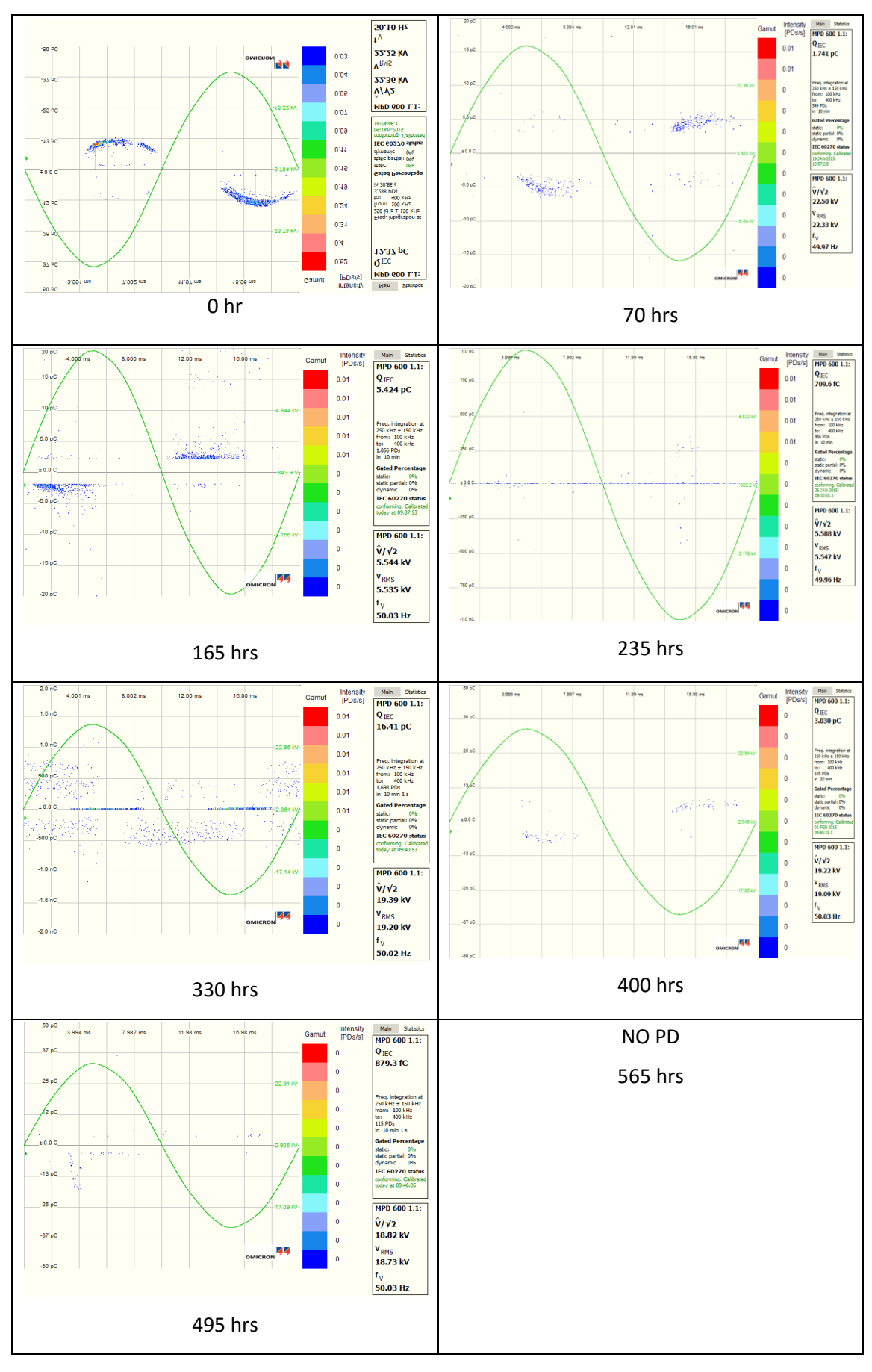


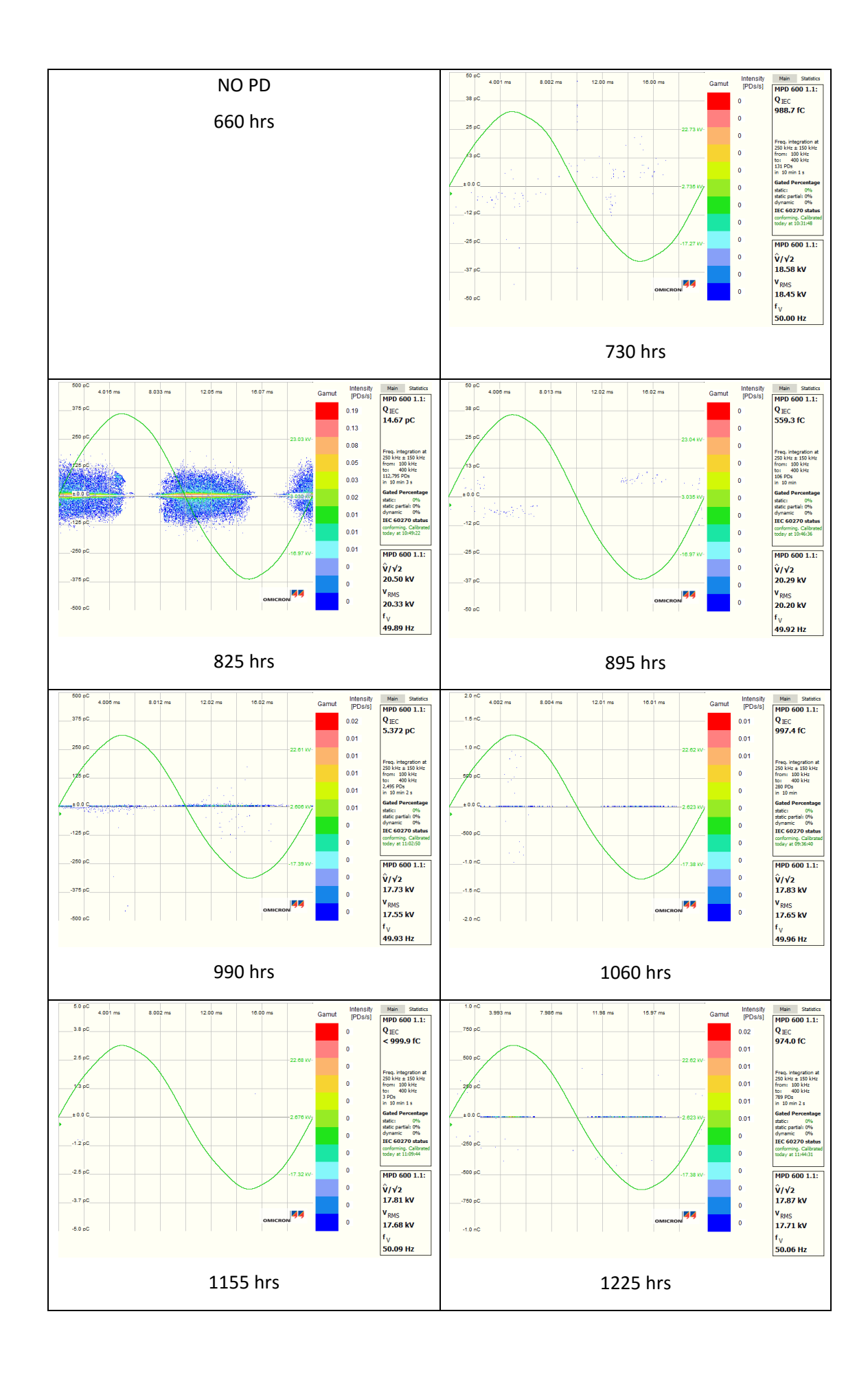
Sample C6

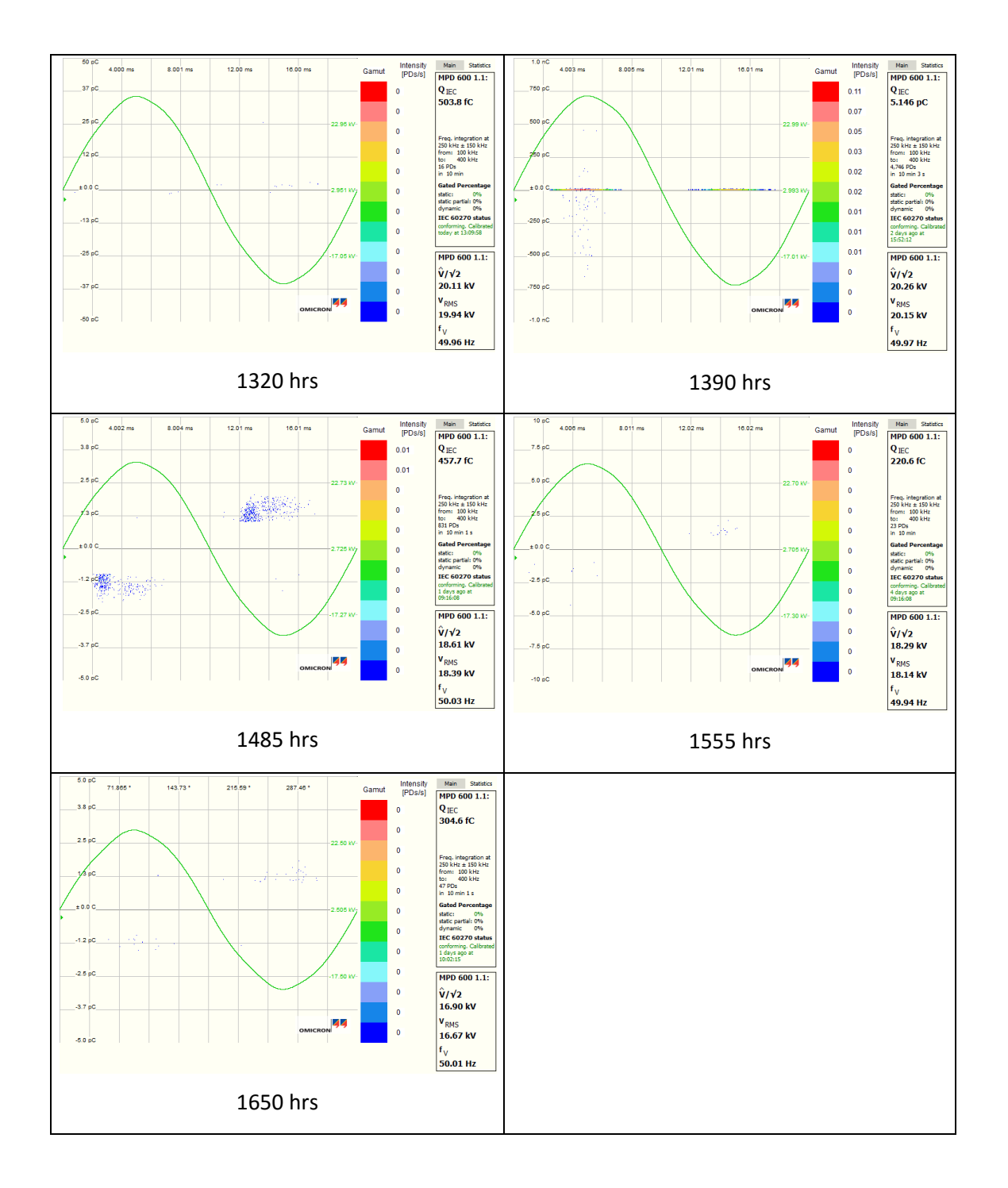




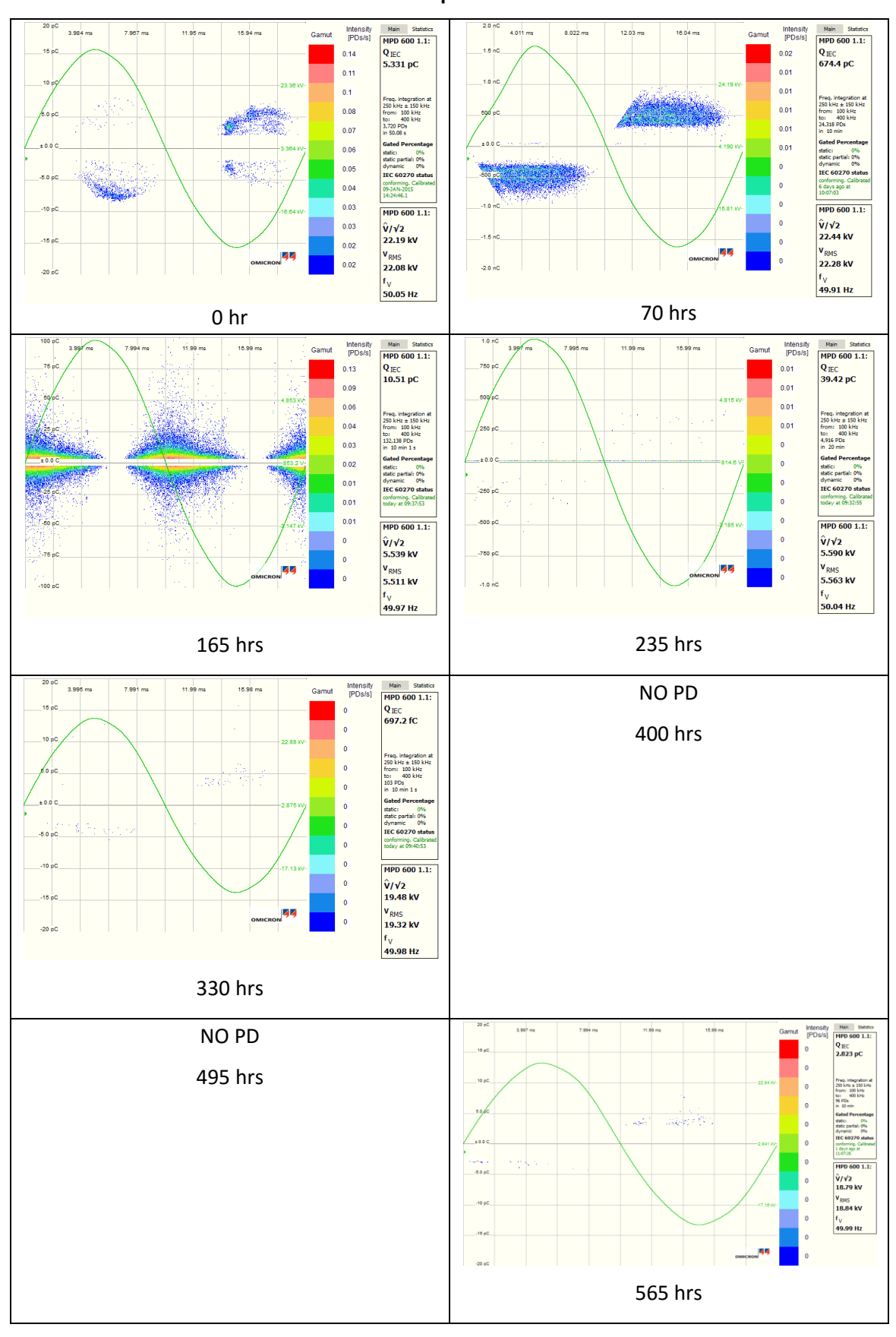
Sample C7

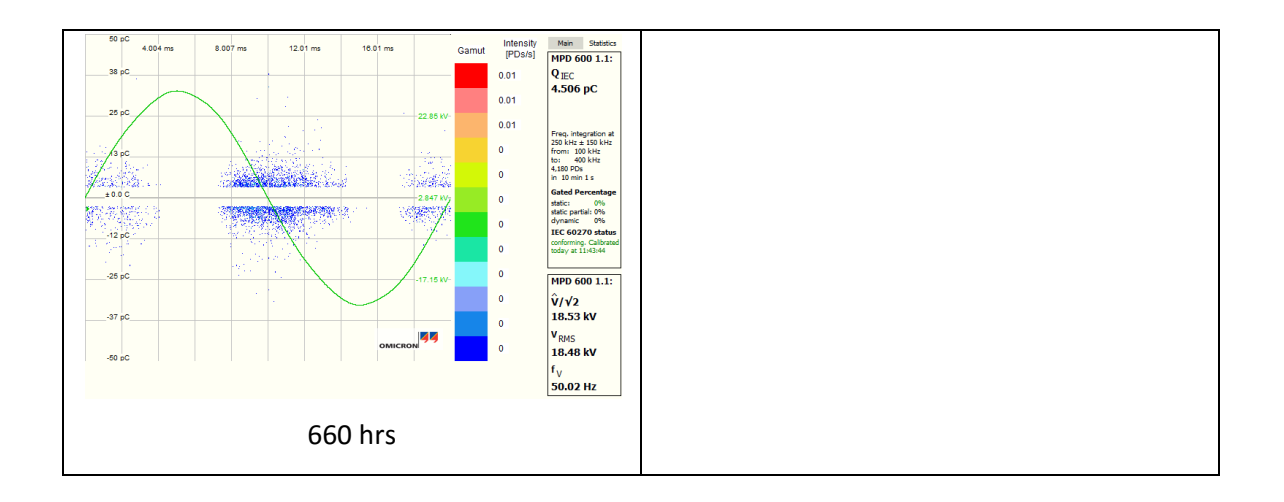




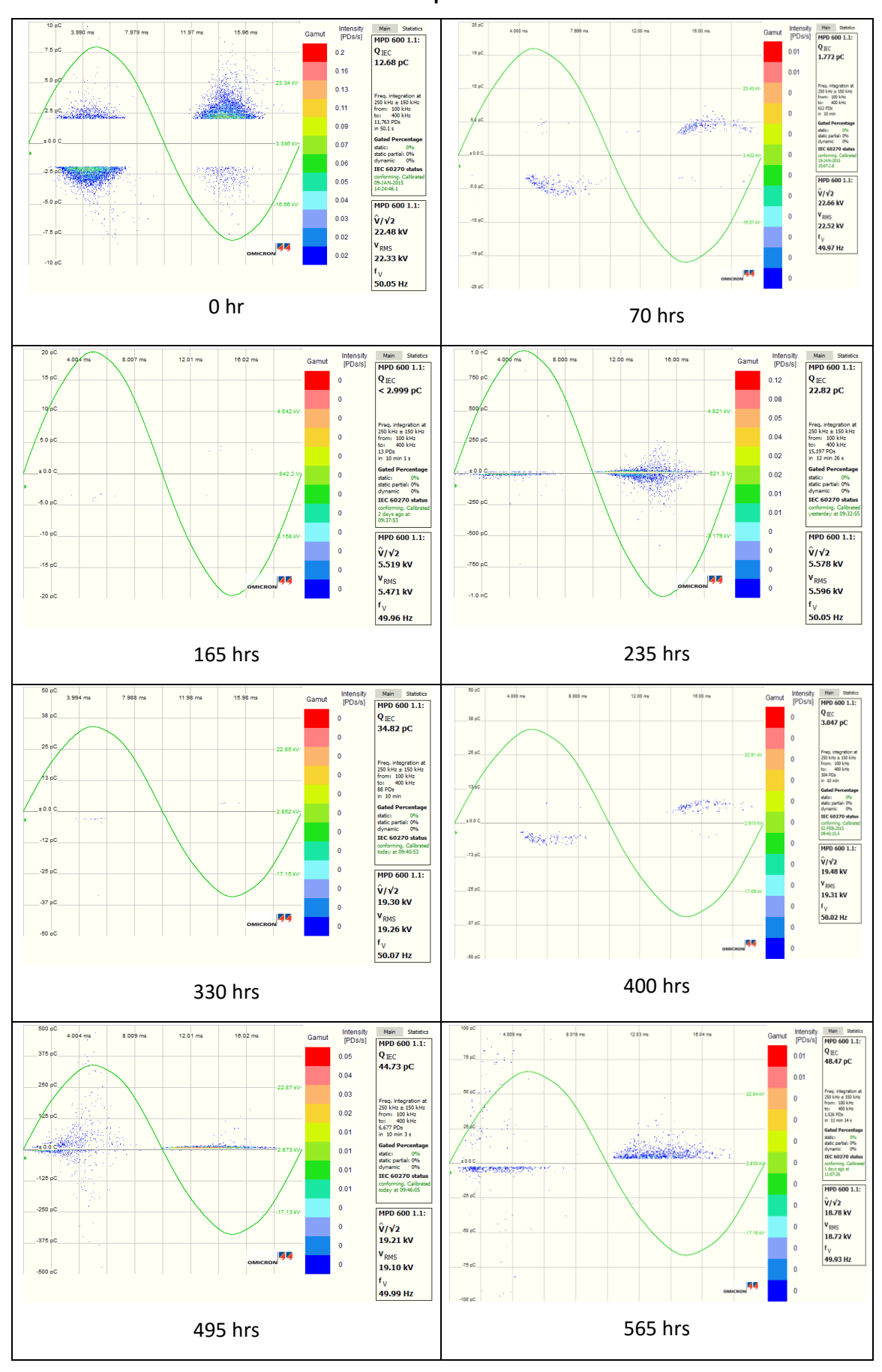


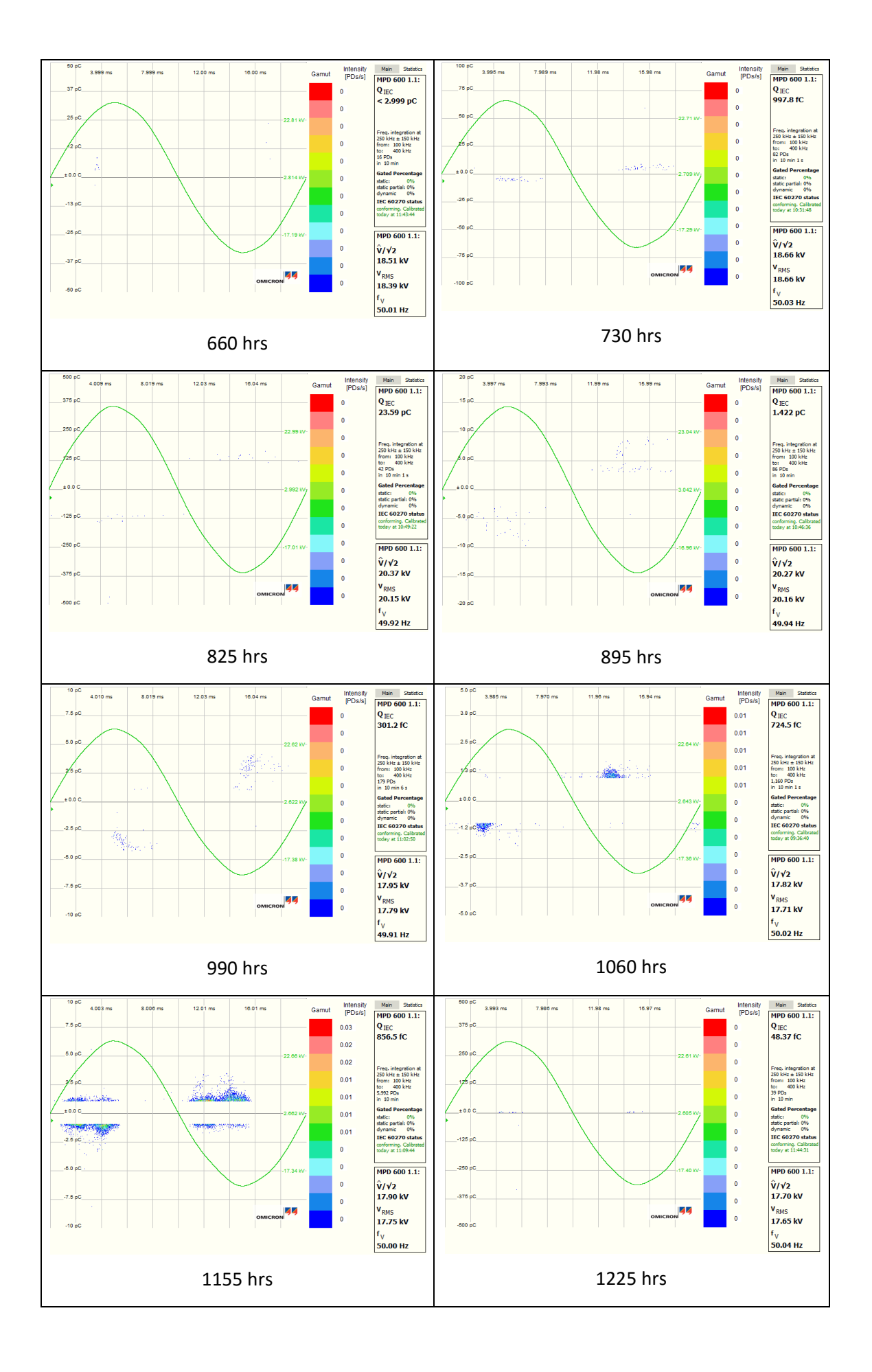
Sample C8

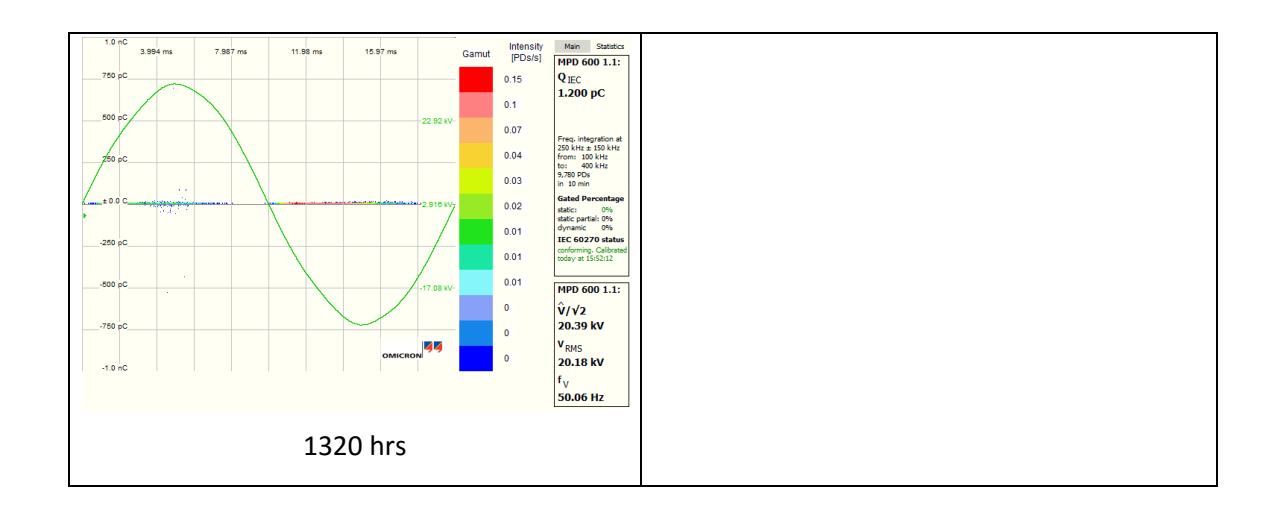




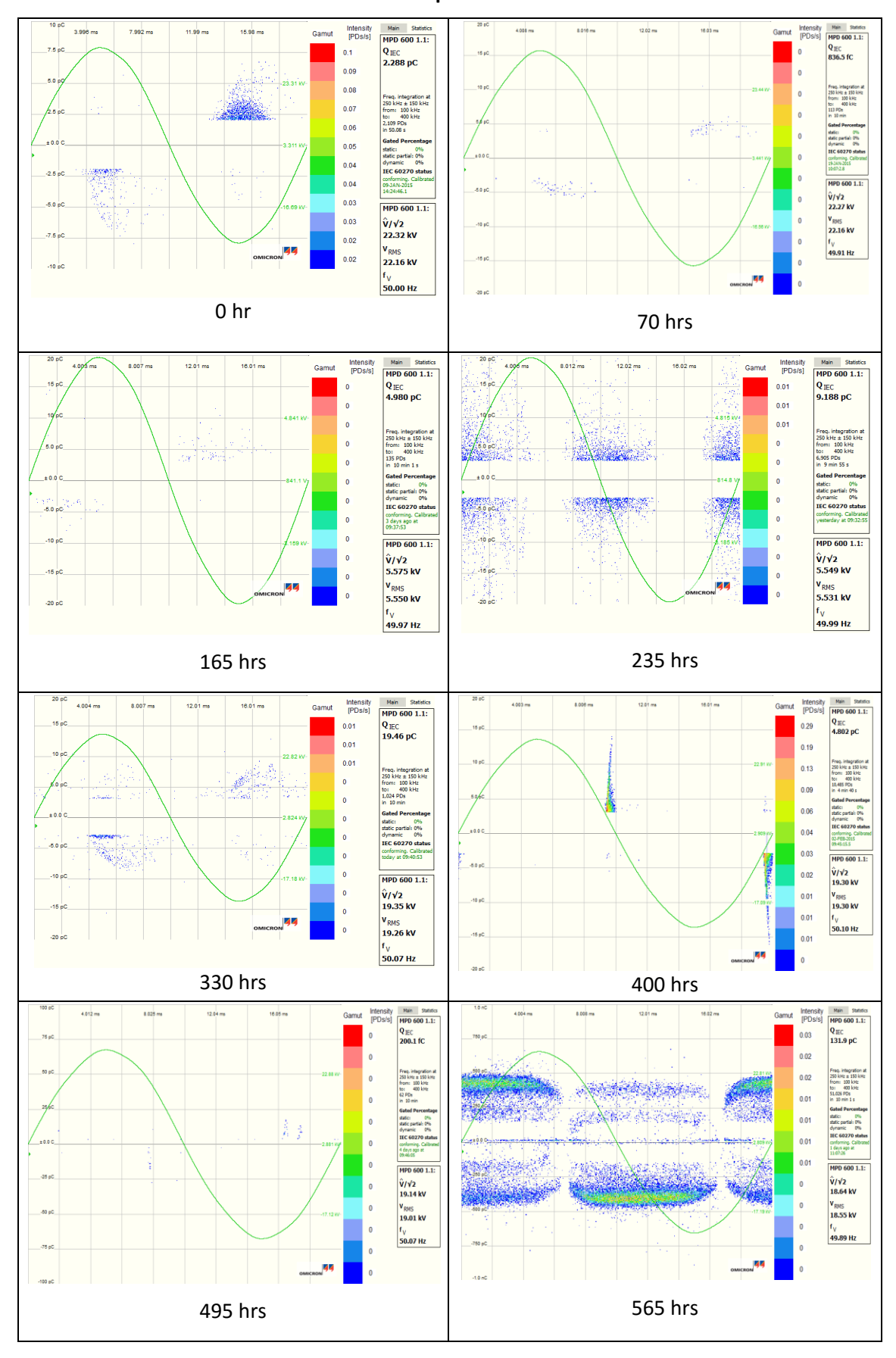
Sample C9

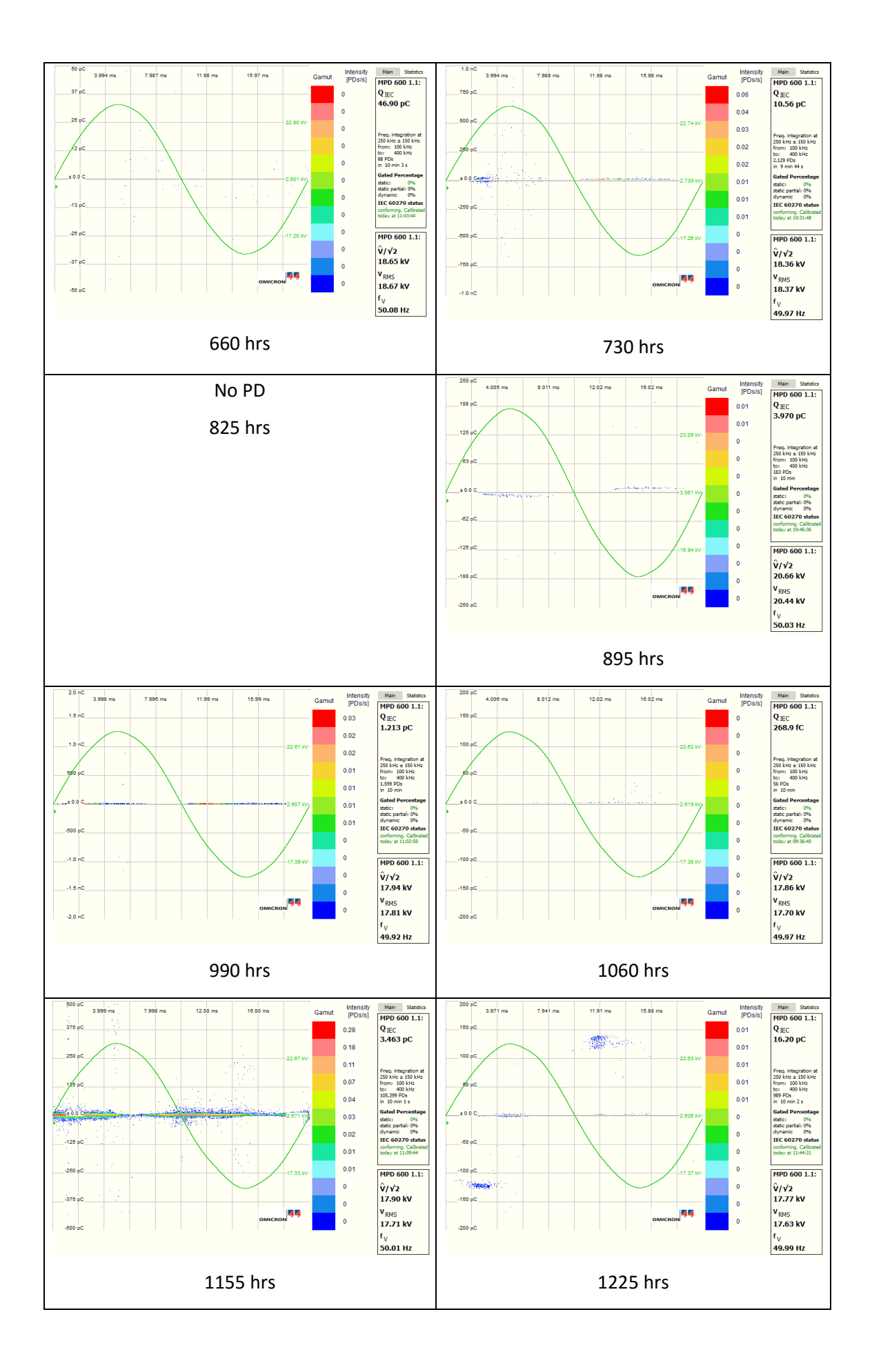


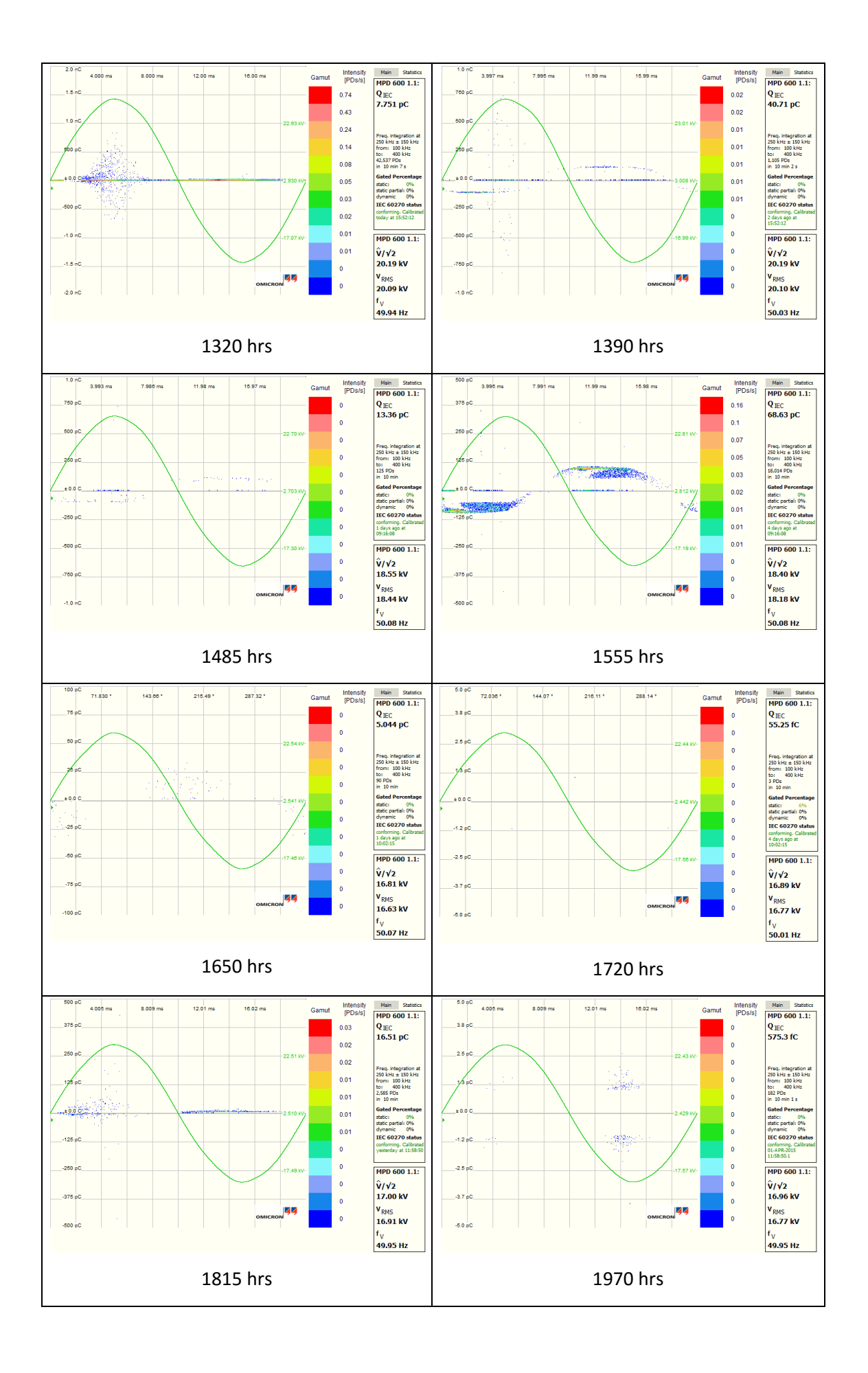




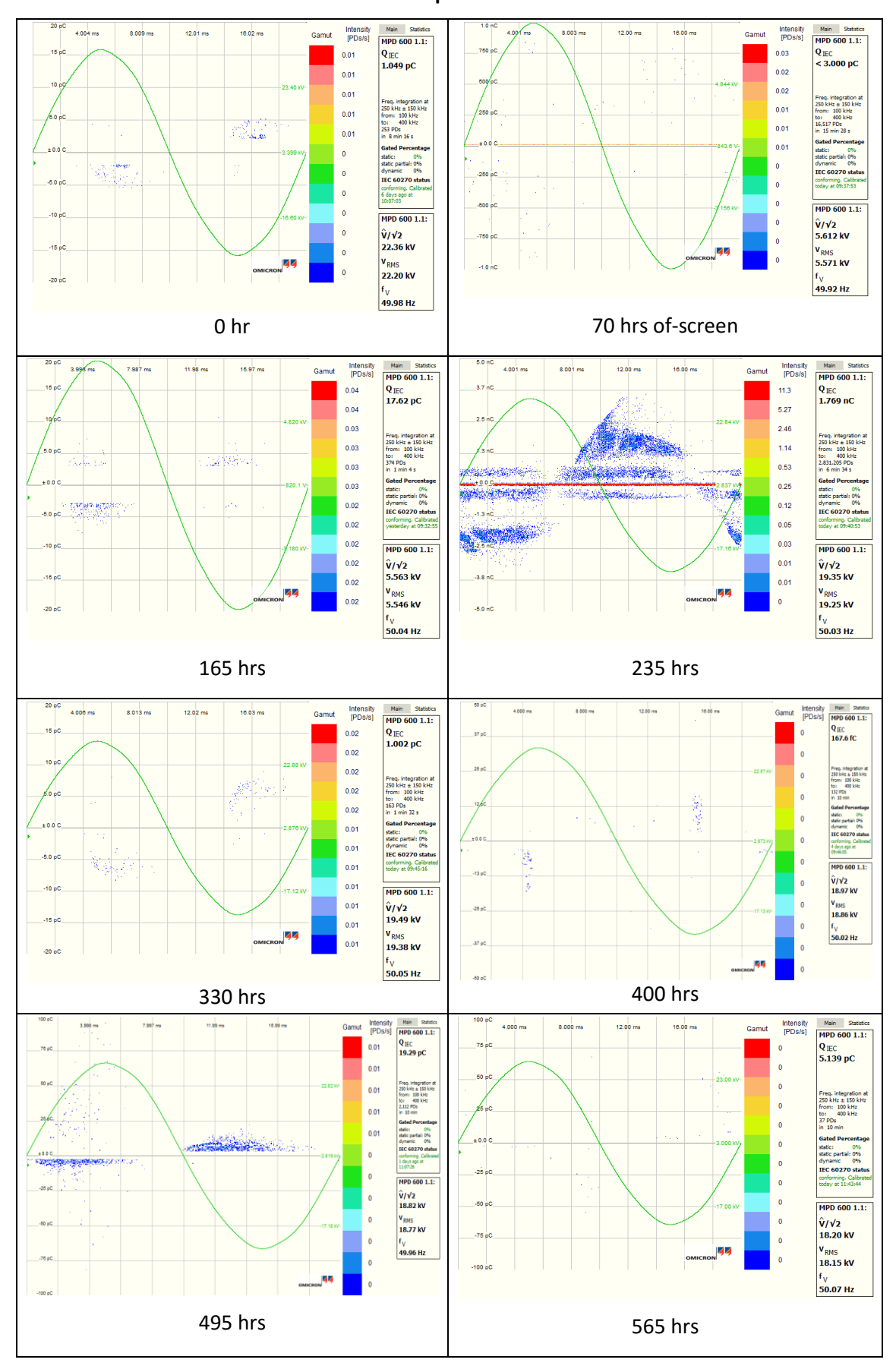
Sample C10

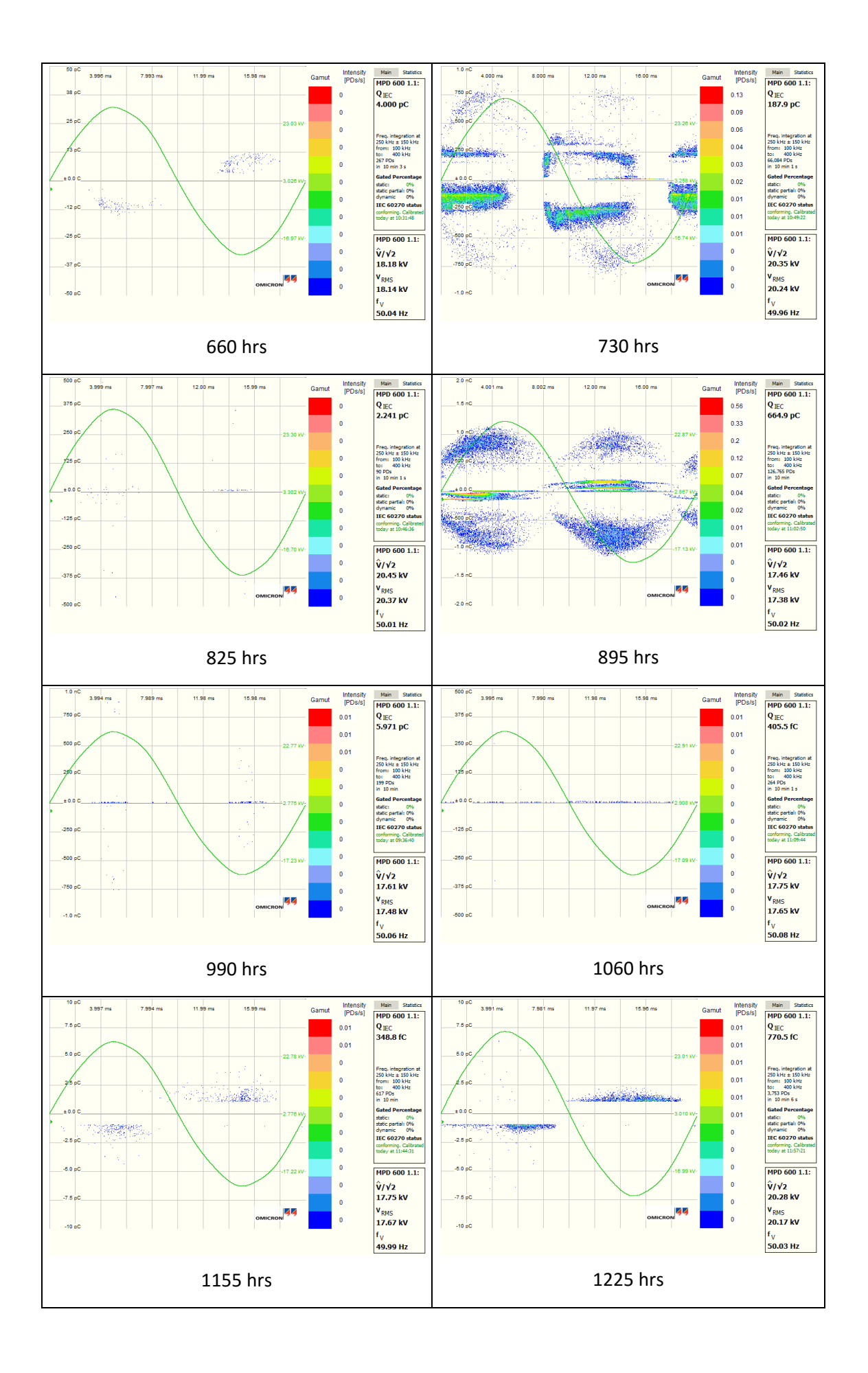


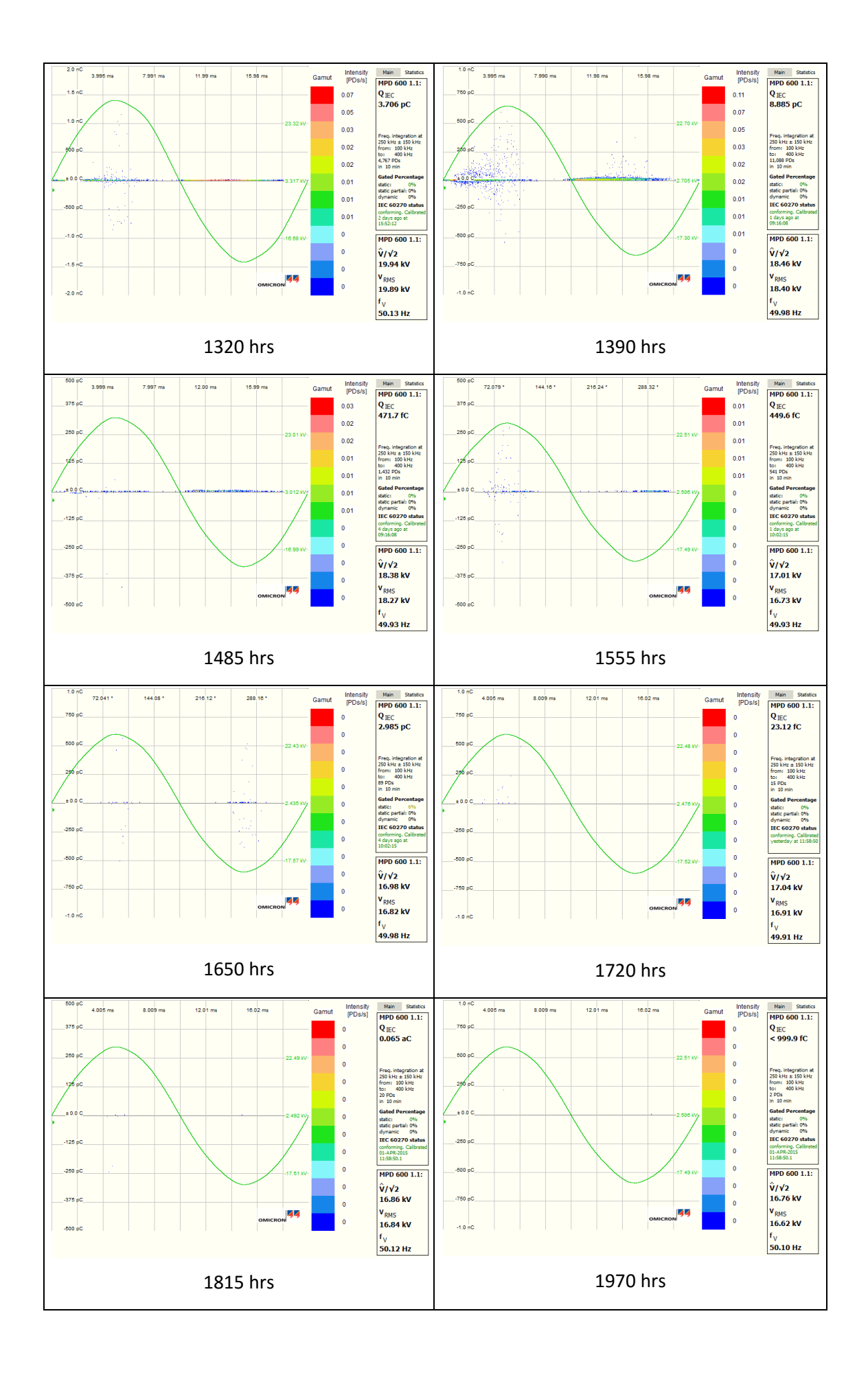




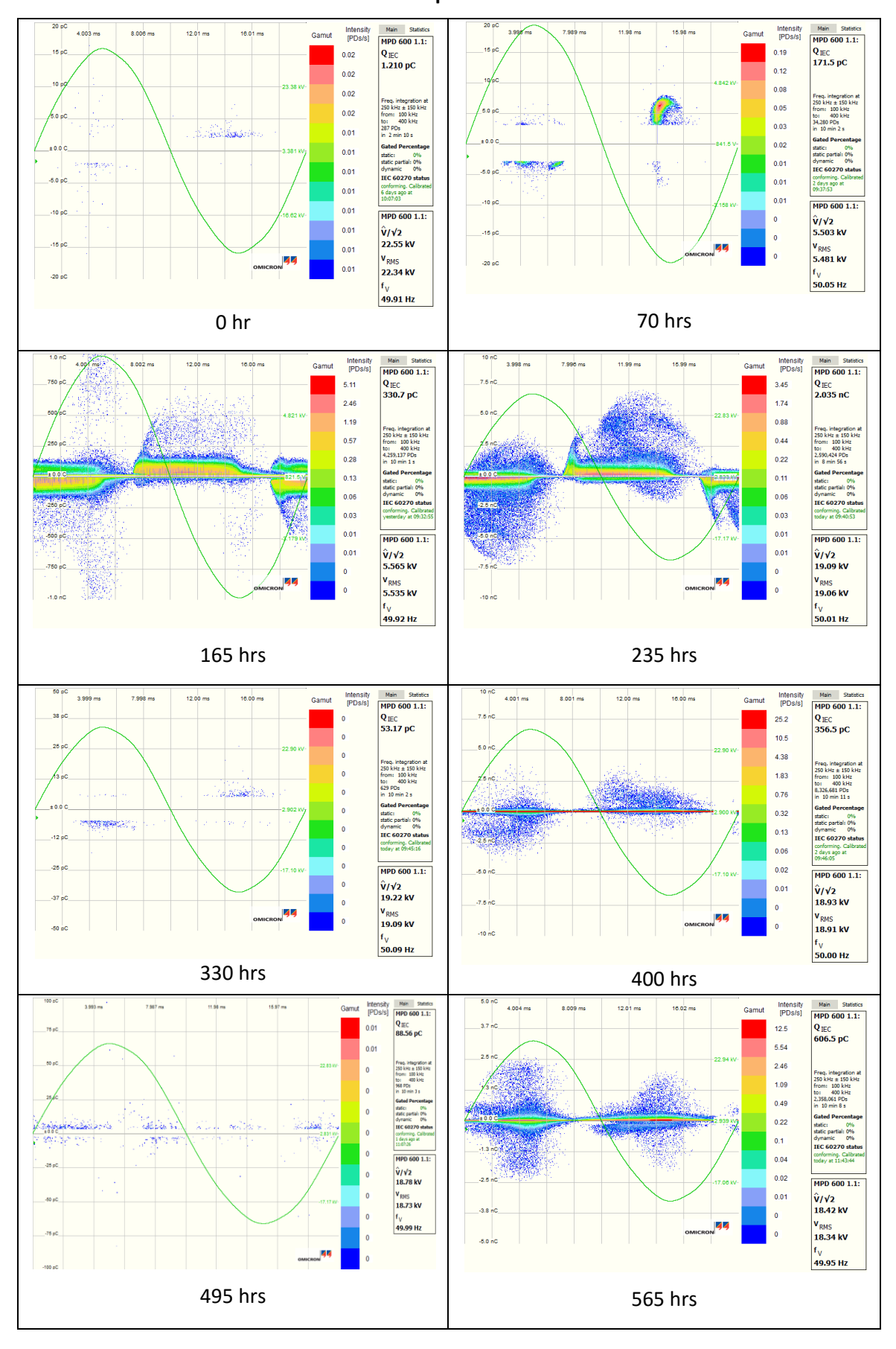
Sample C11

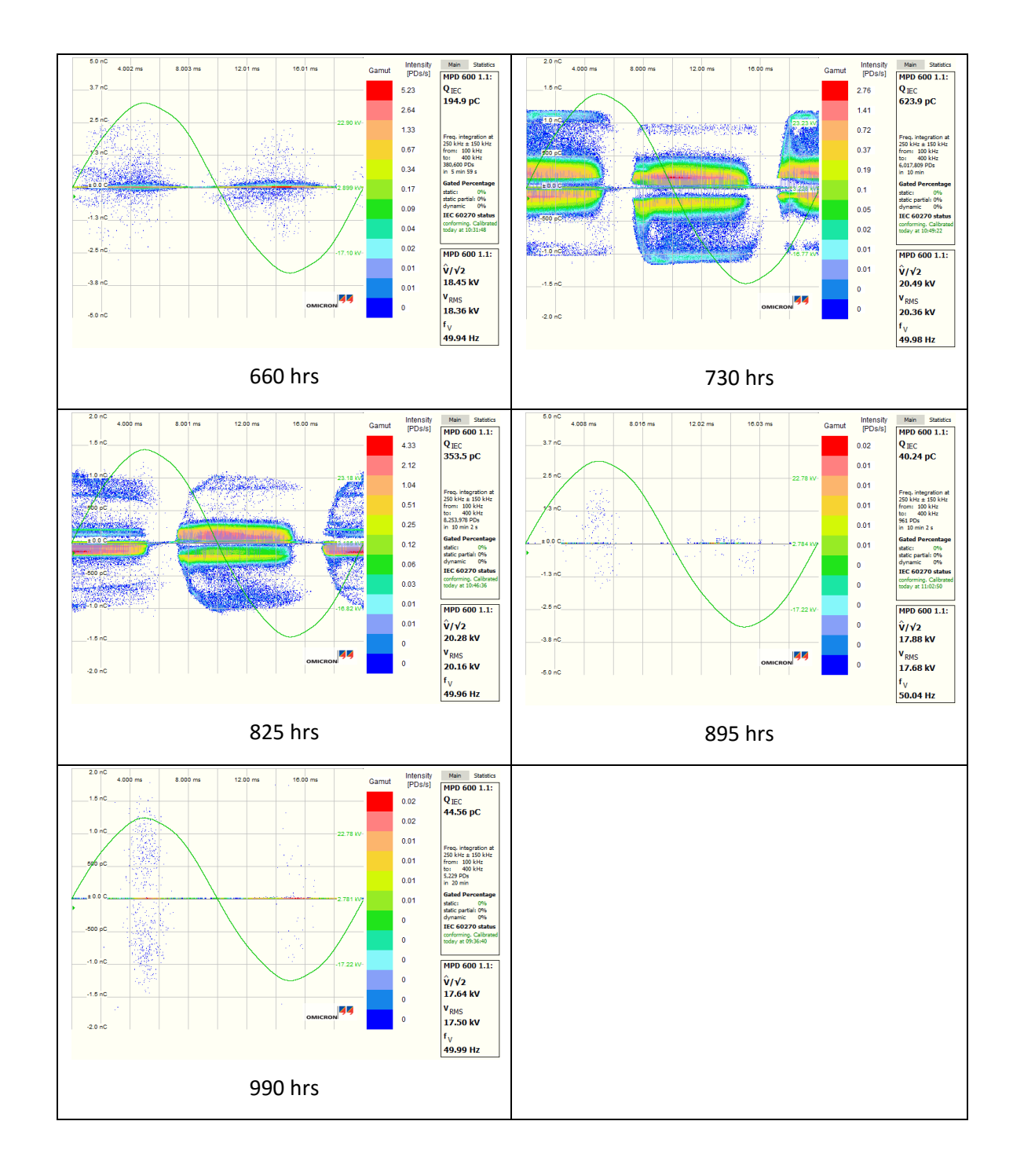




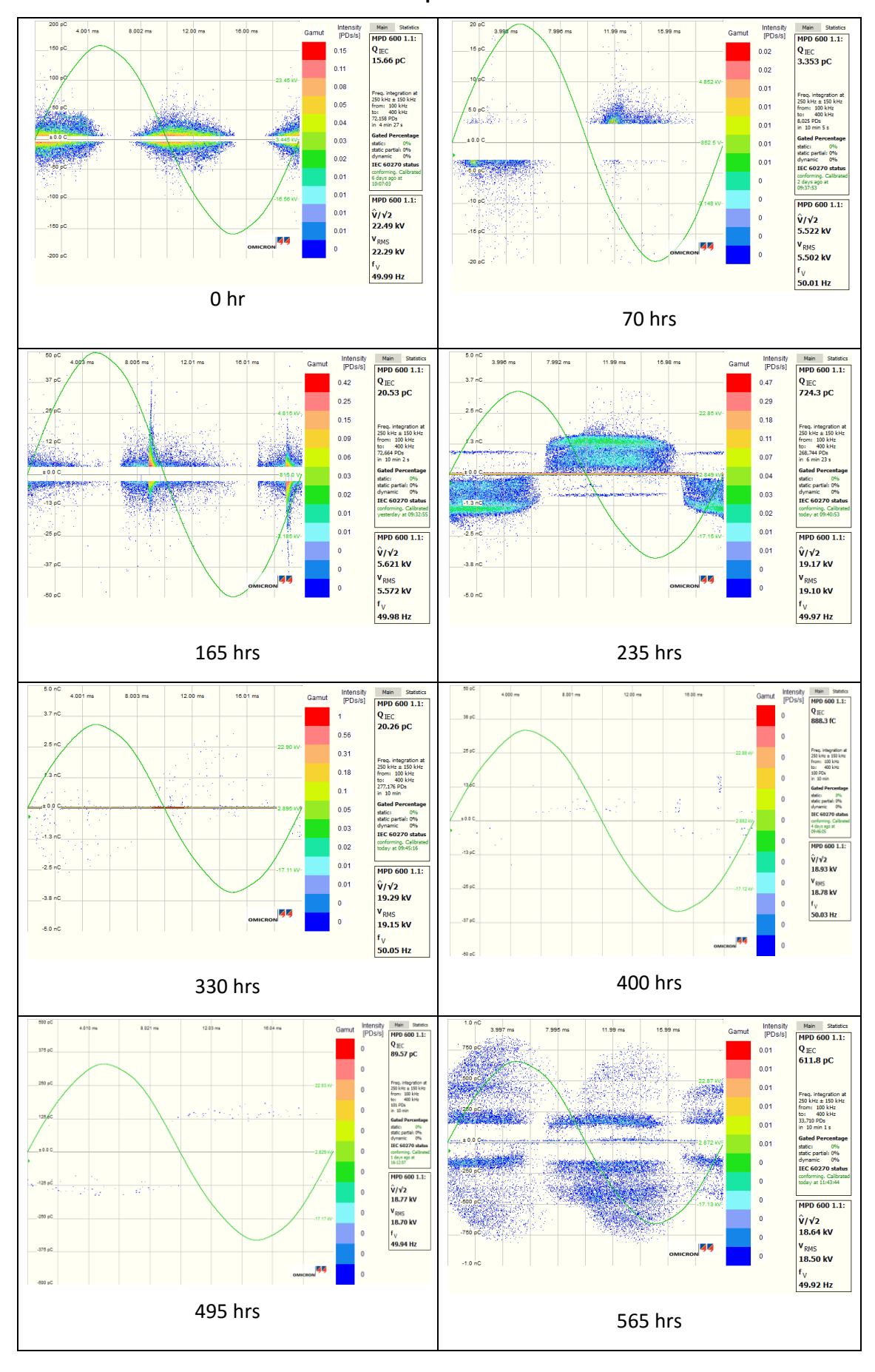


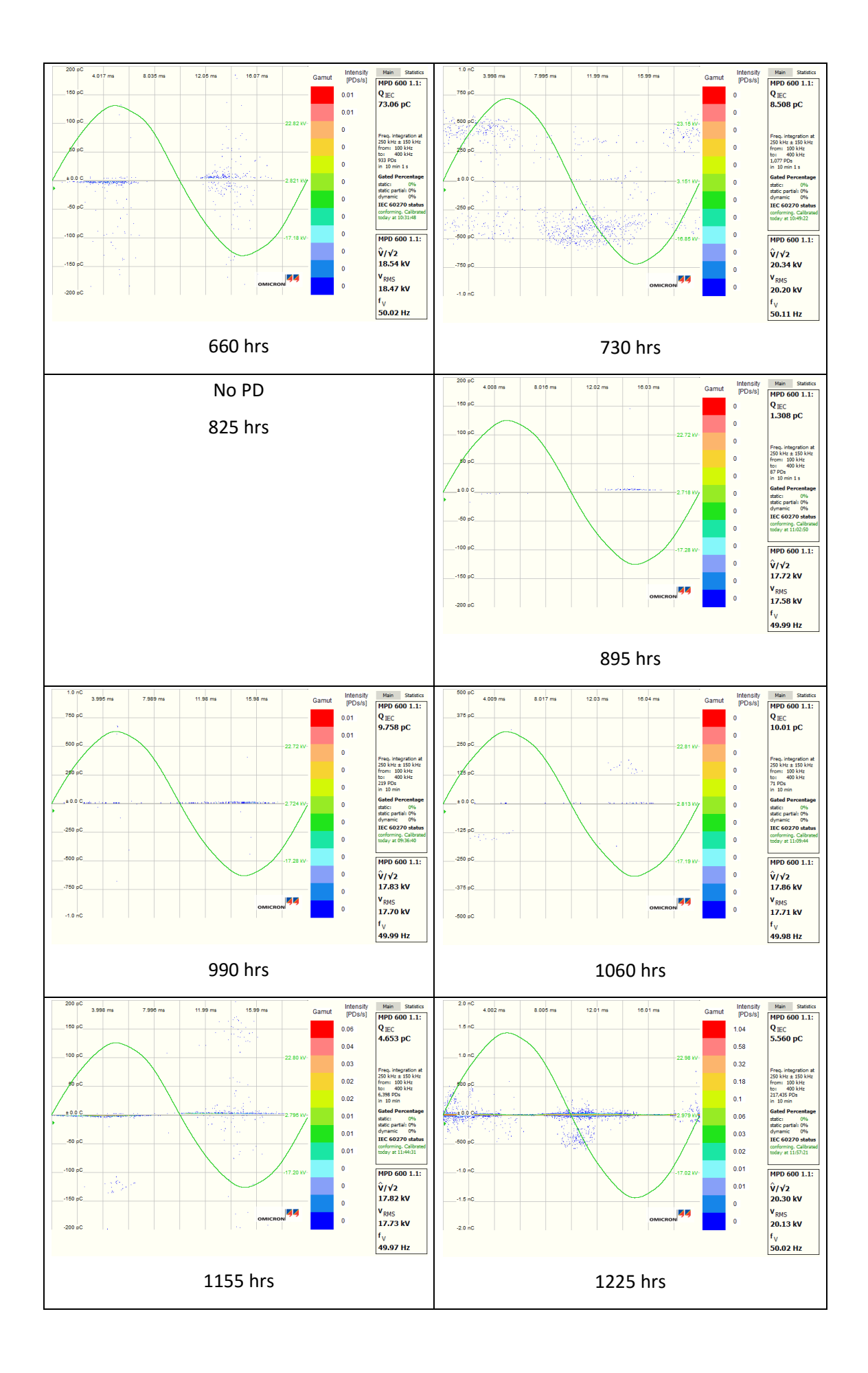
Sample C12

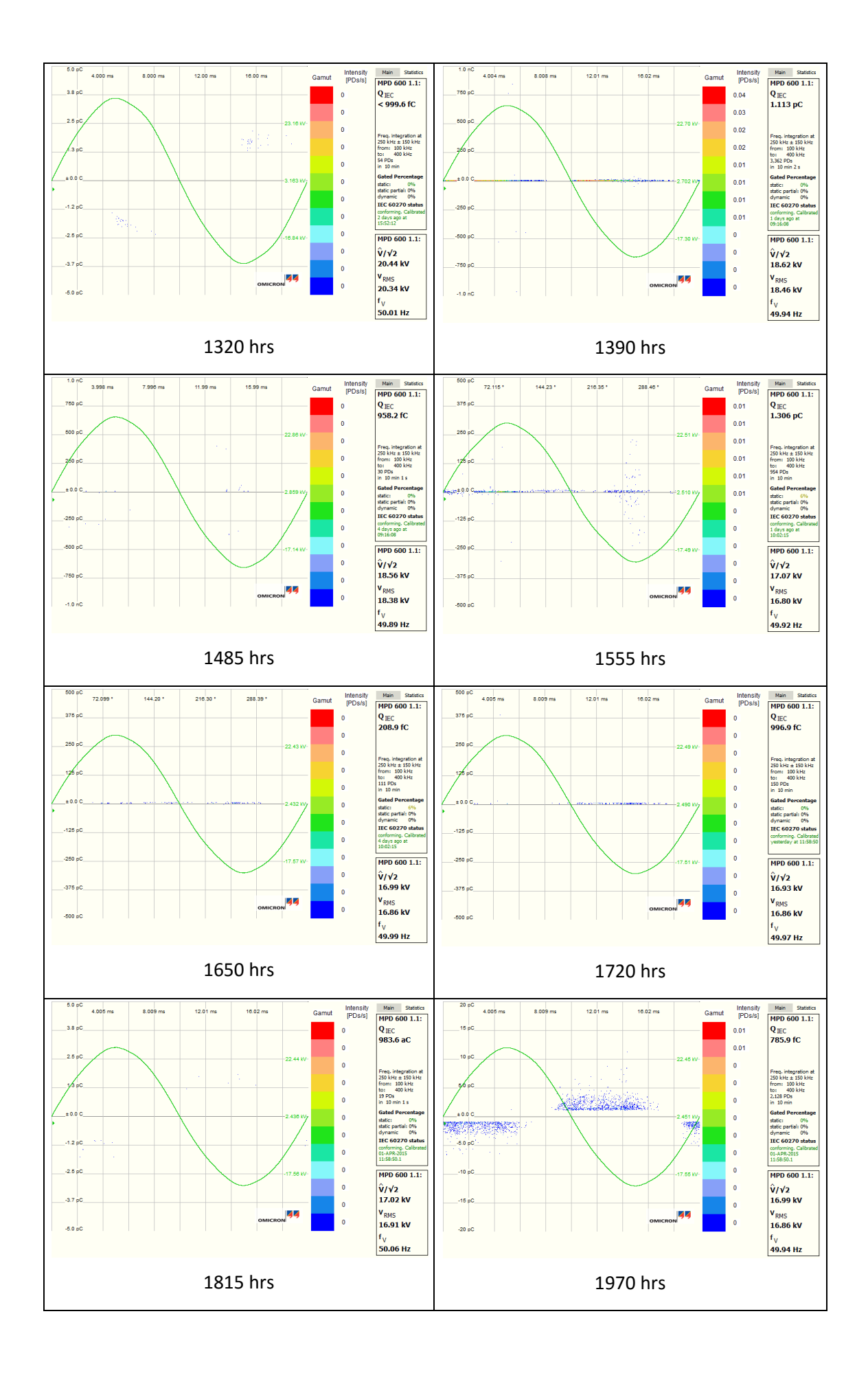




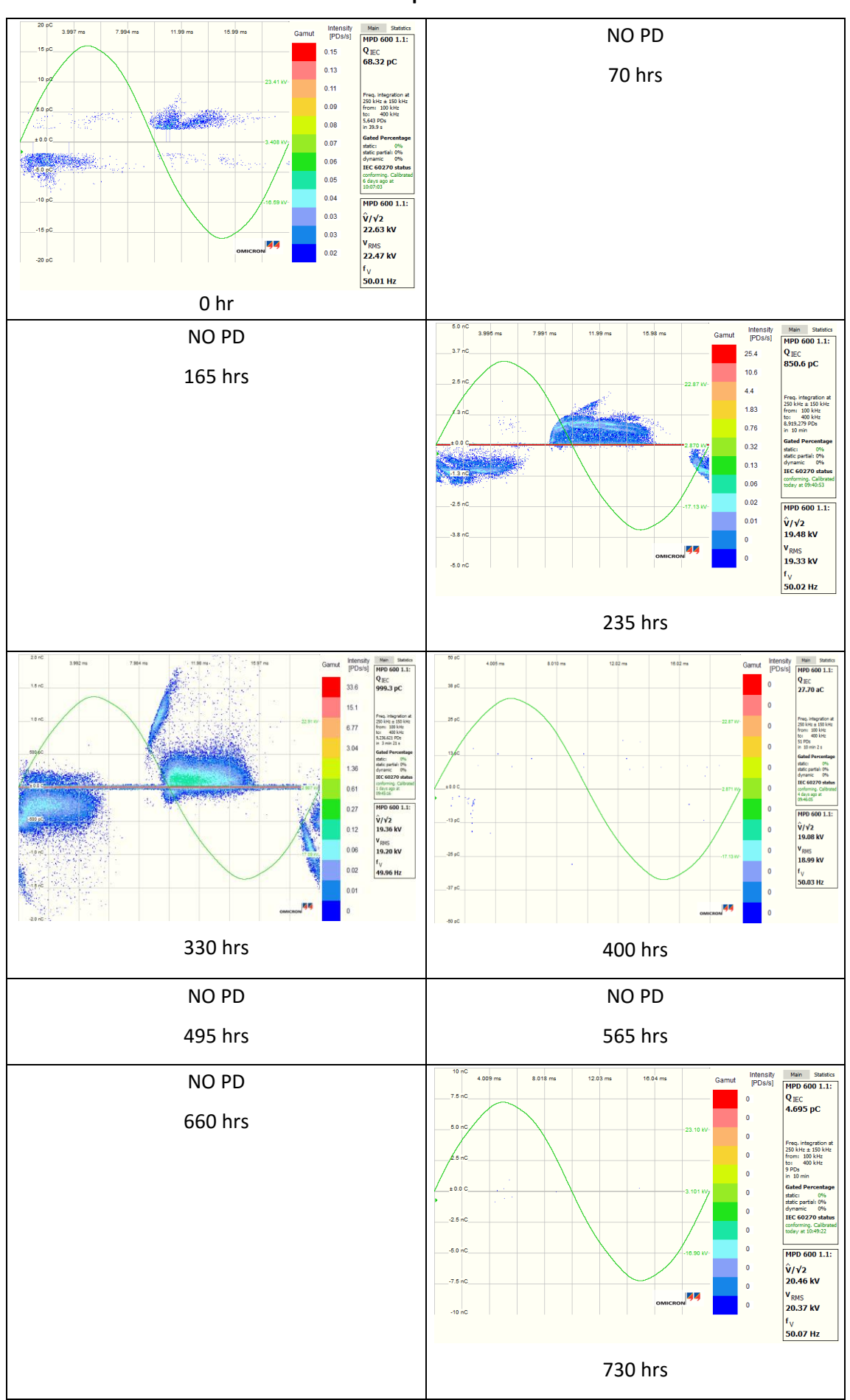
Sample C13

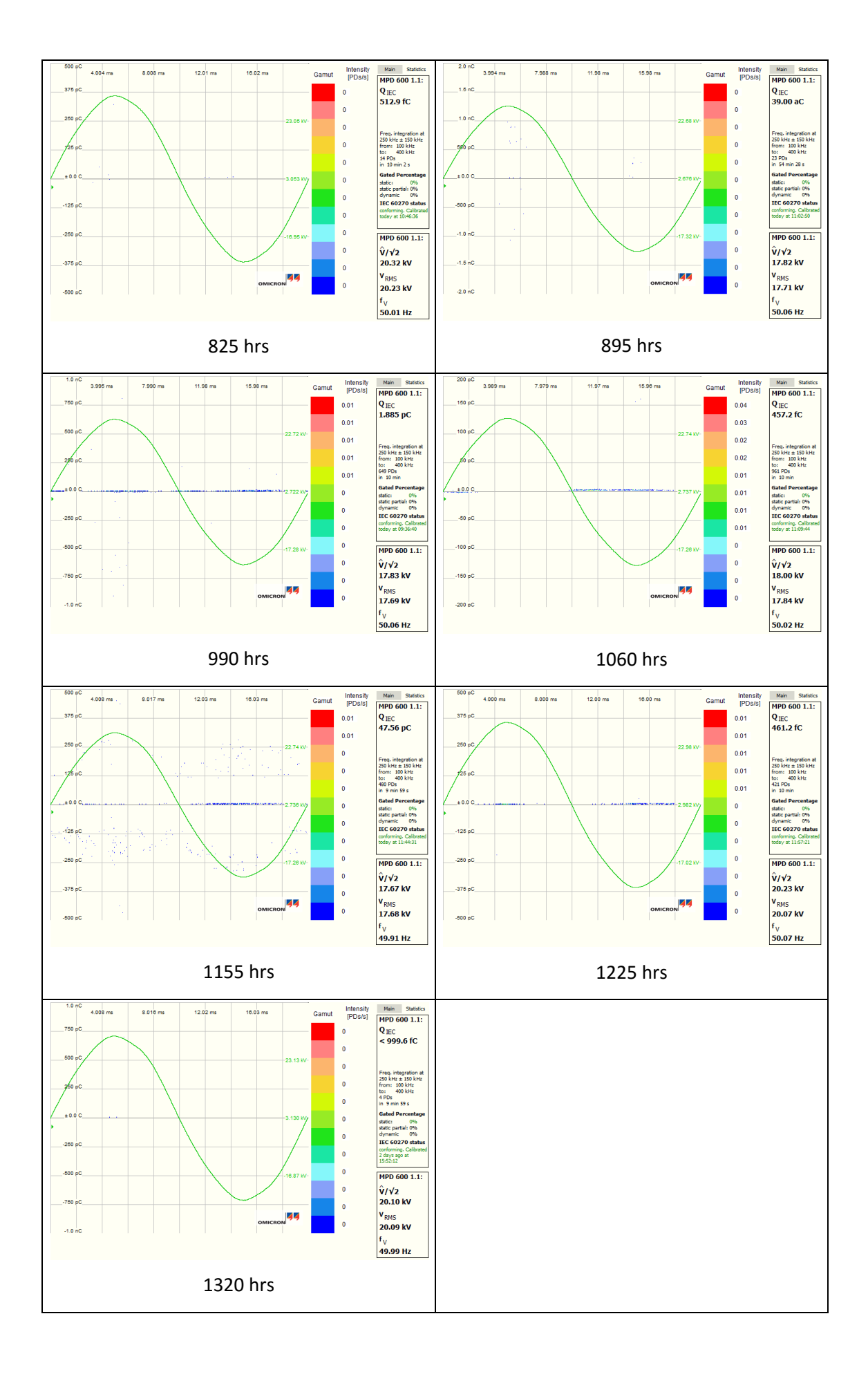




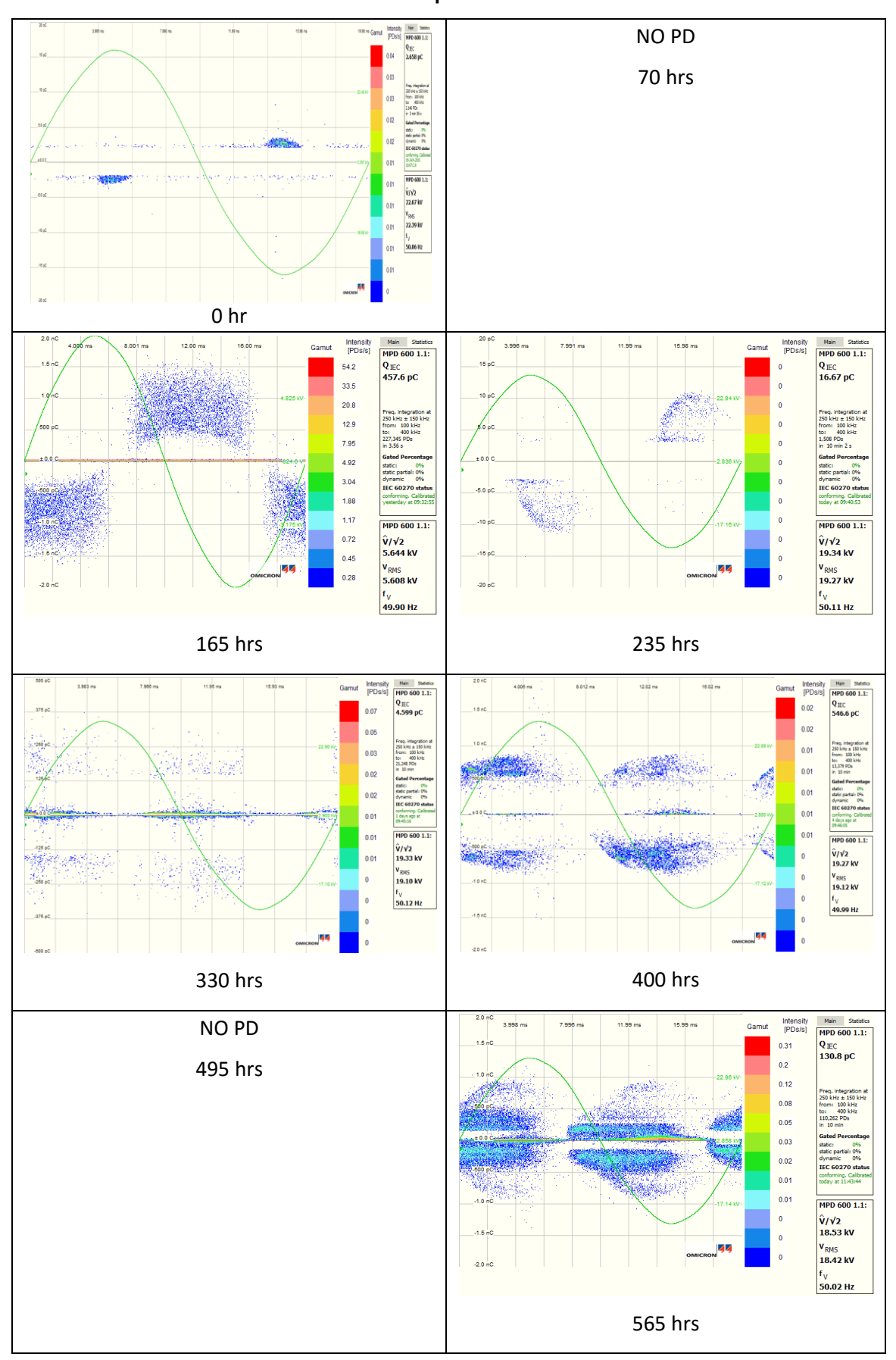


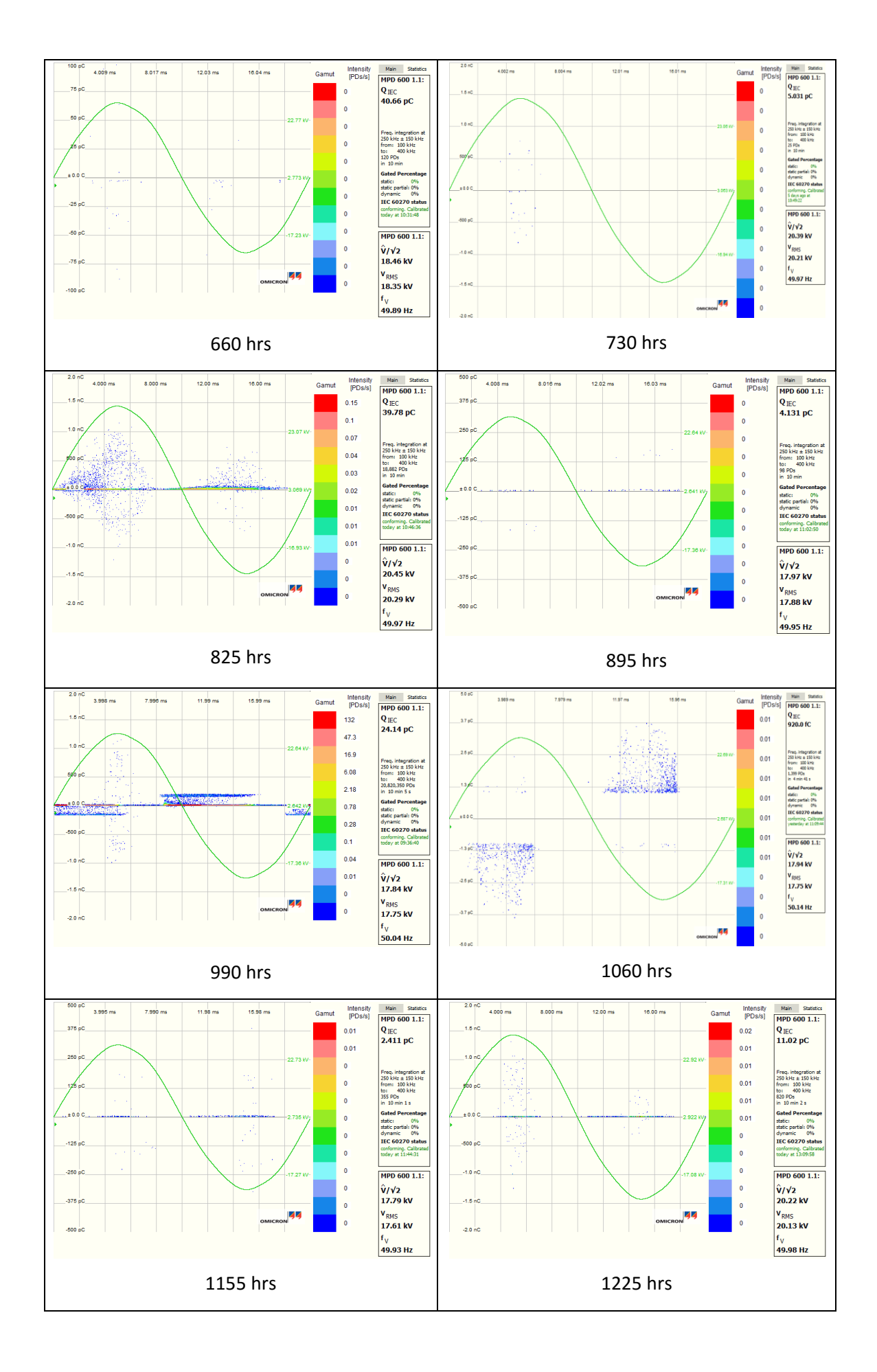
Sample C14

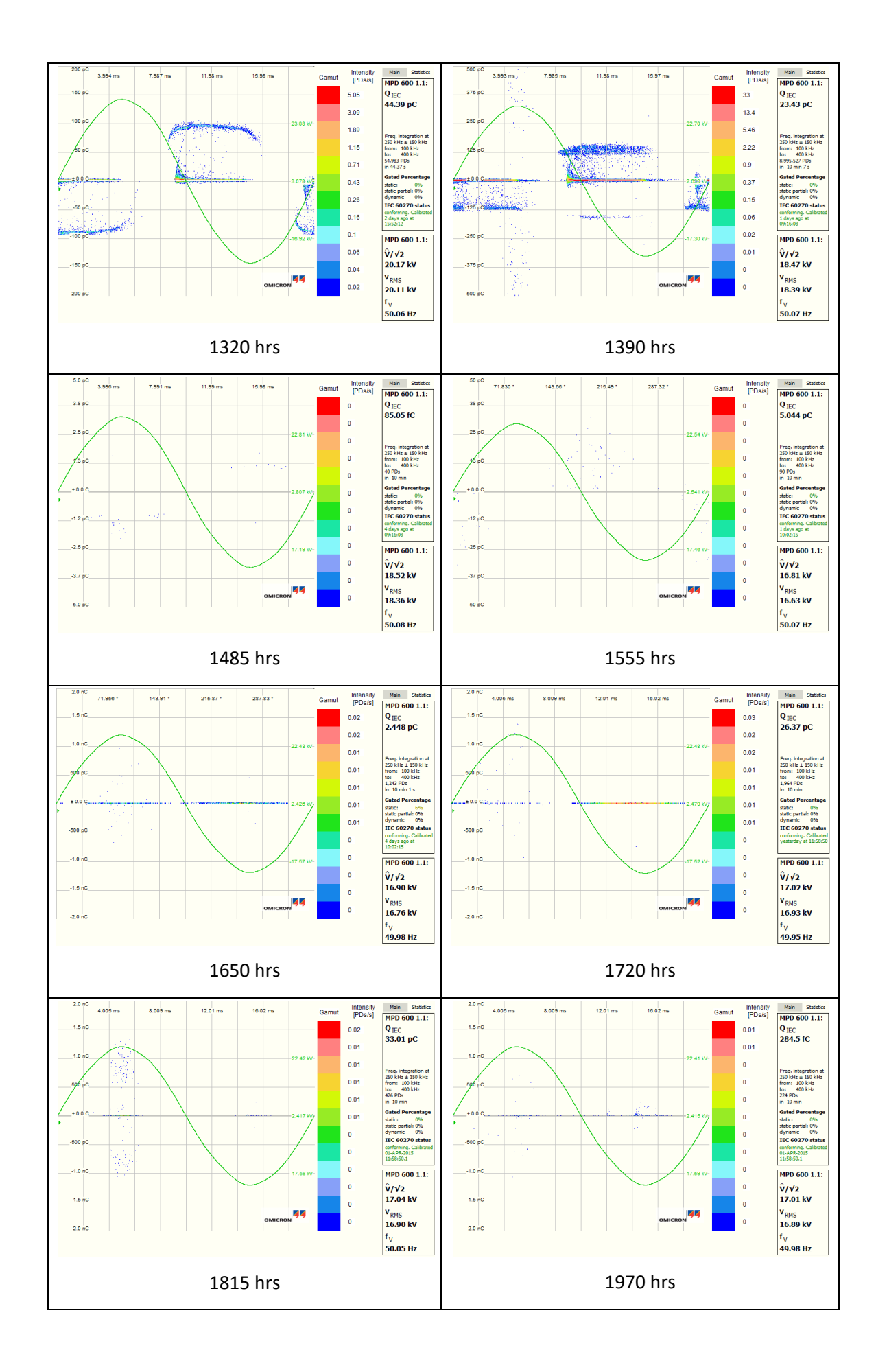




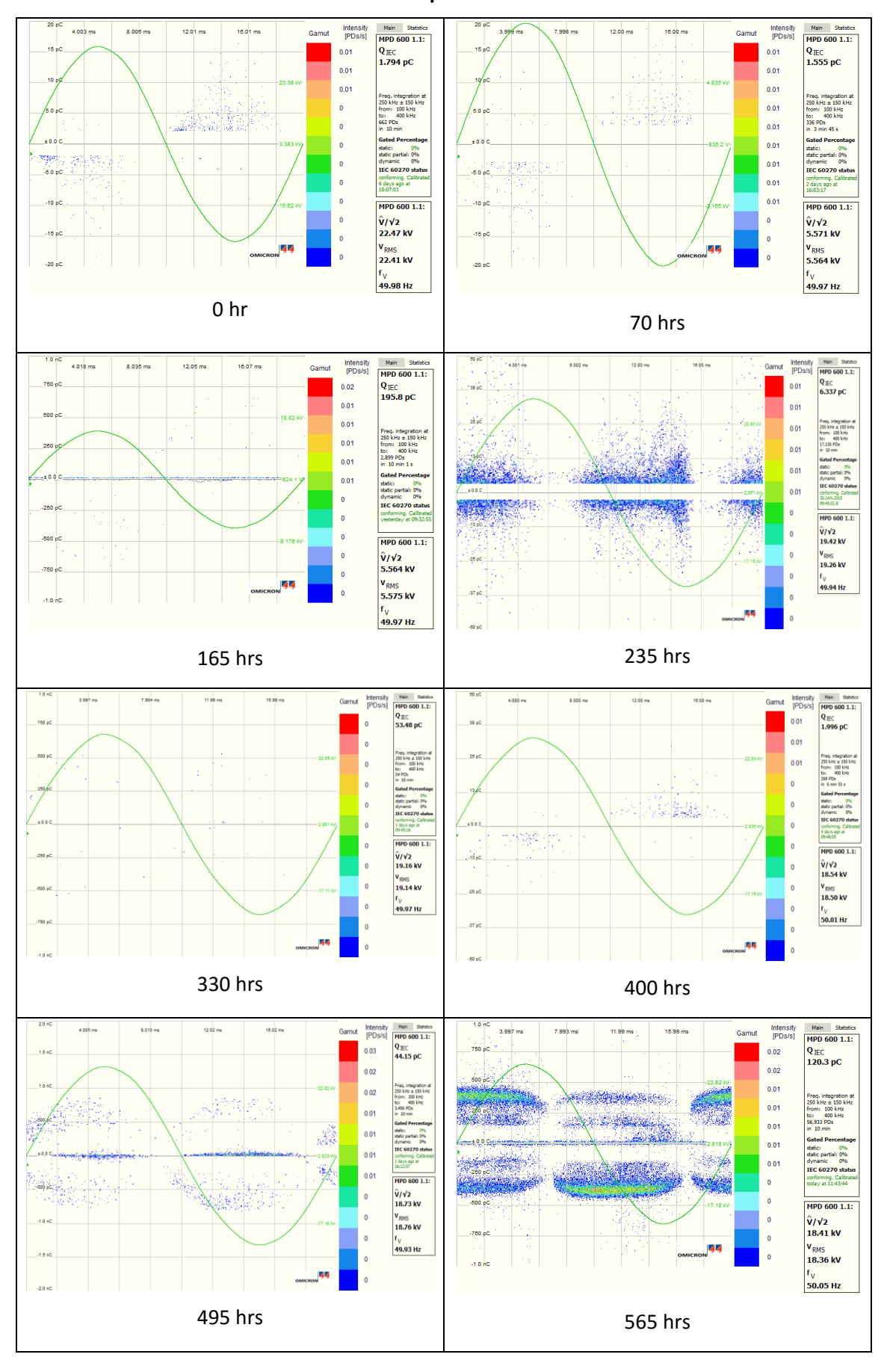
Sample C15

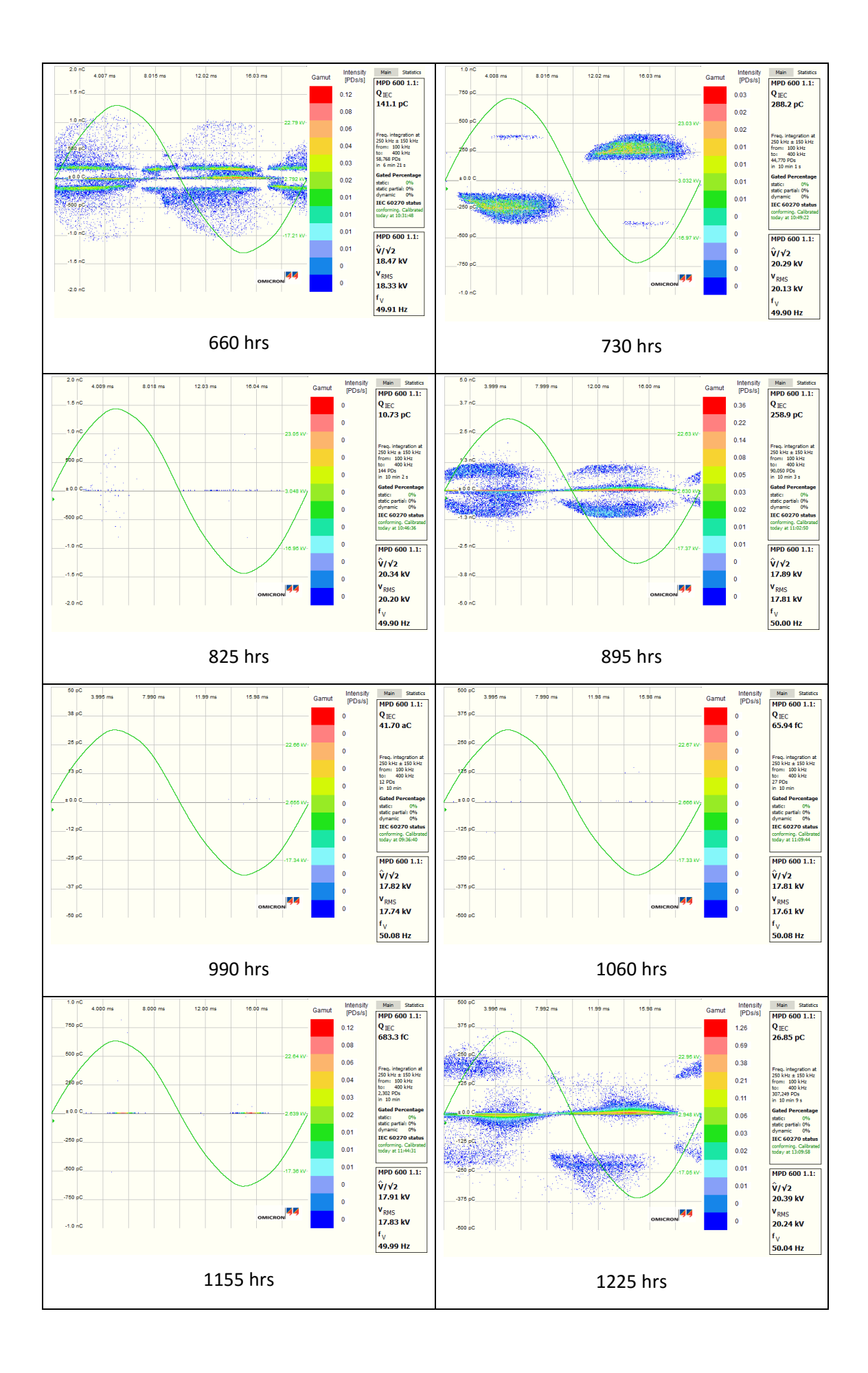


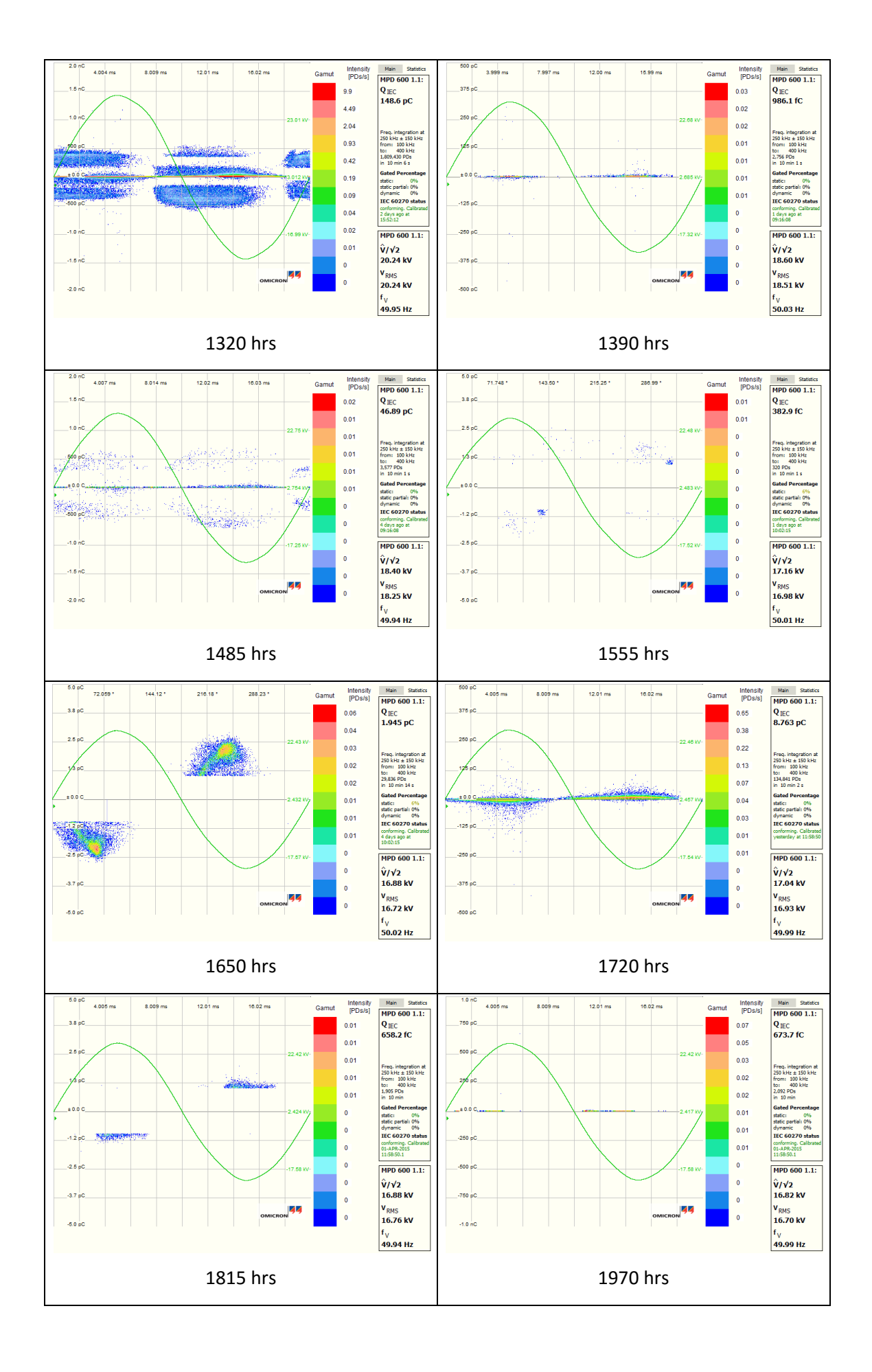




Sample C16

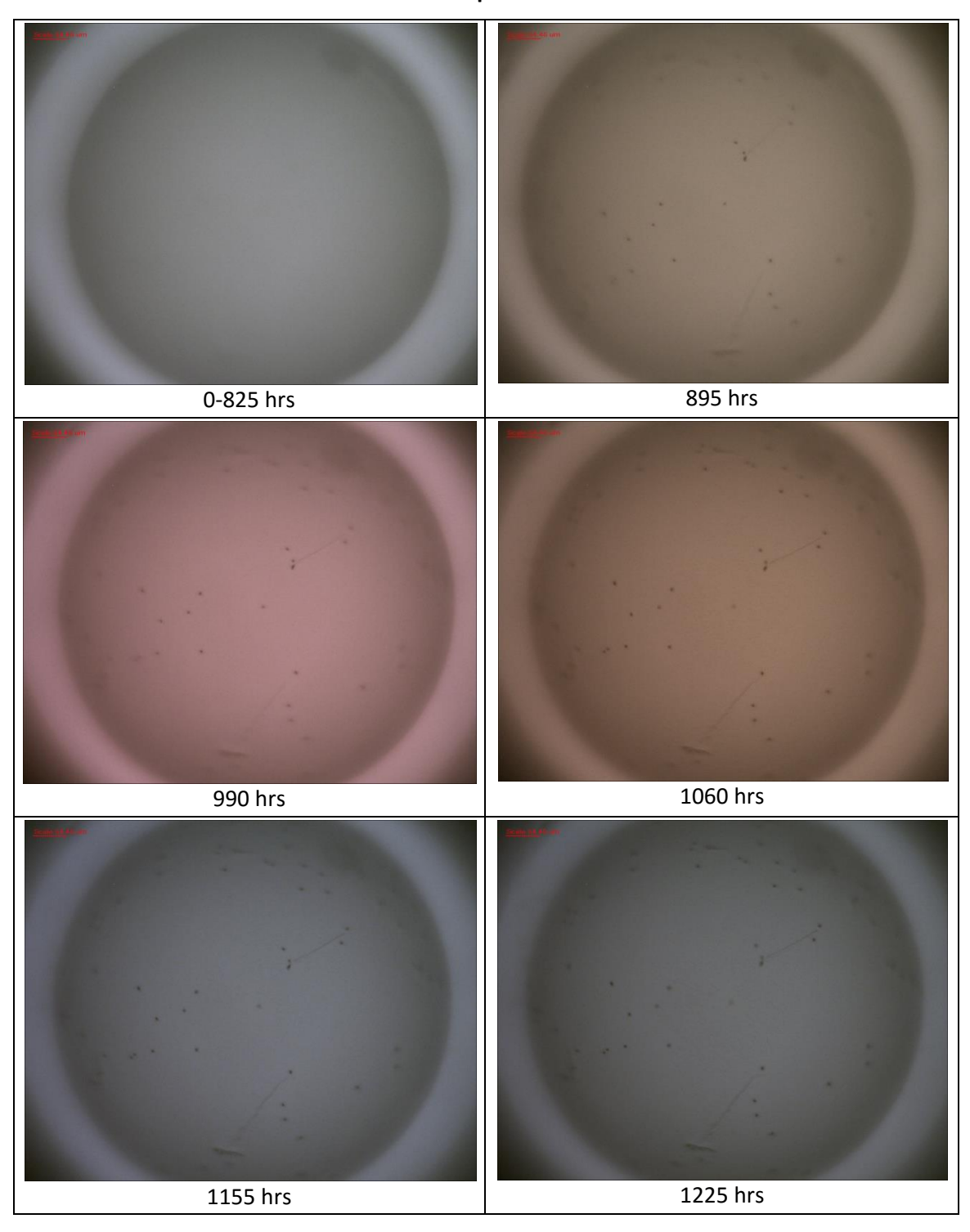


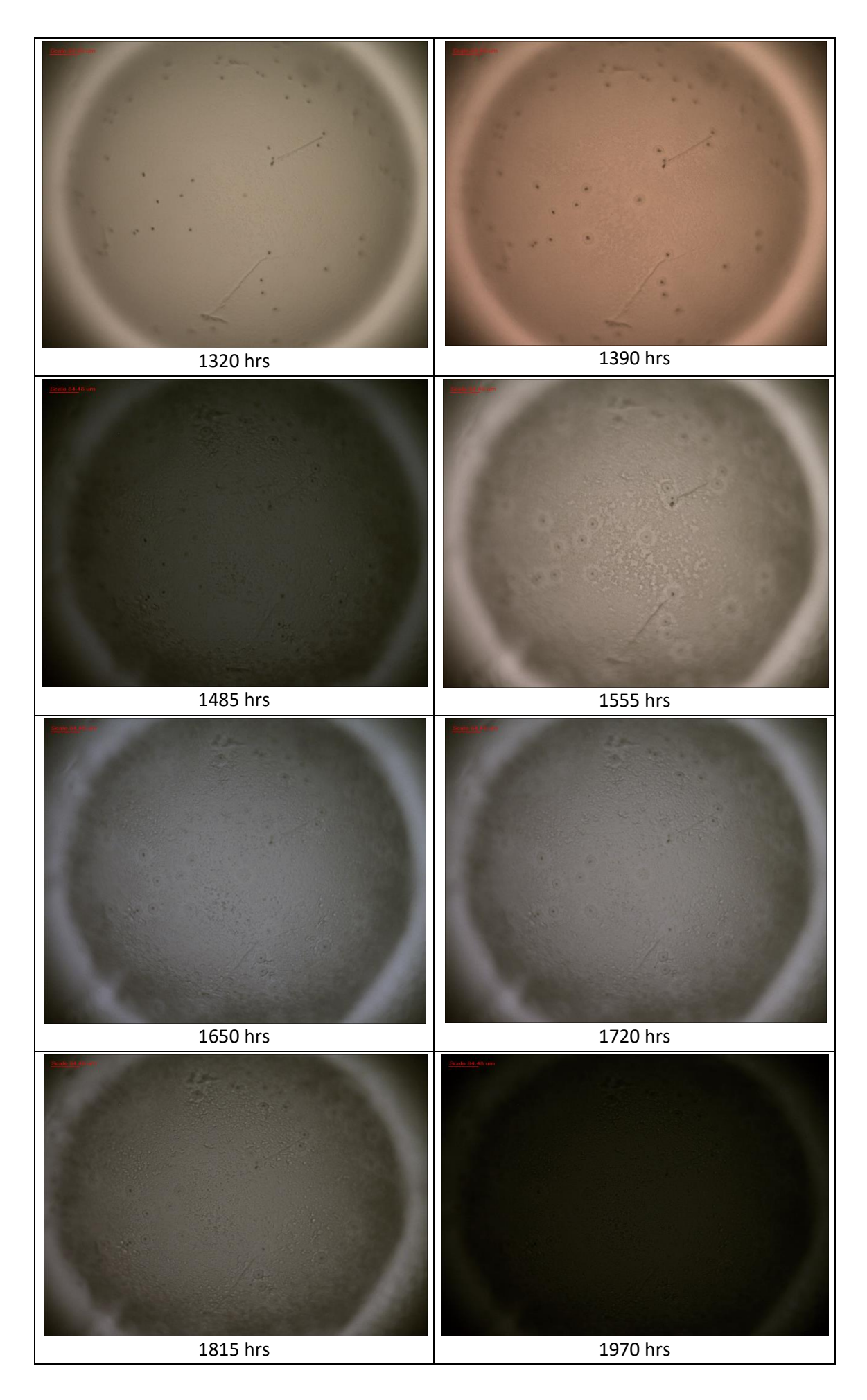




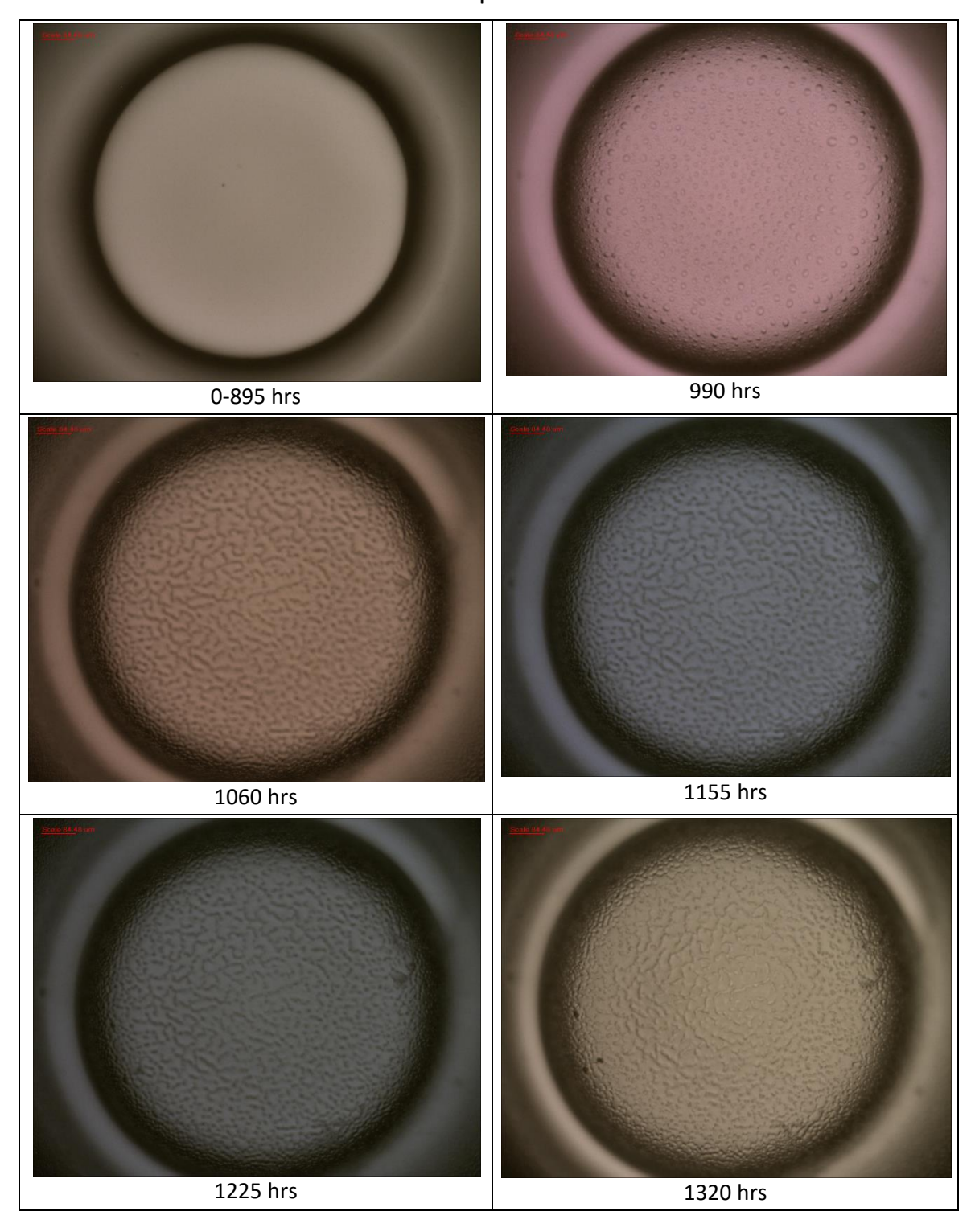
Appendix C Microscopic images of sample group C.

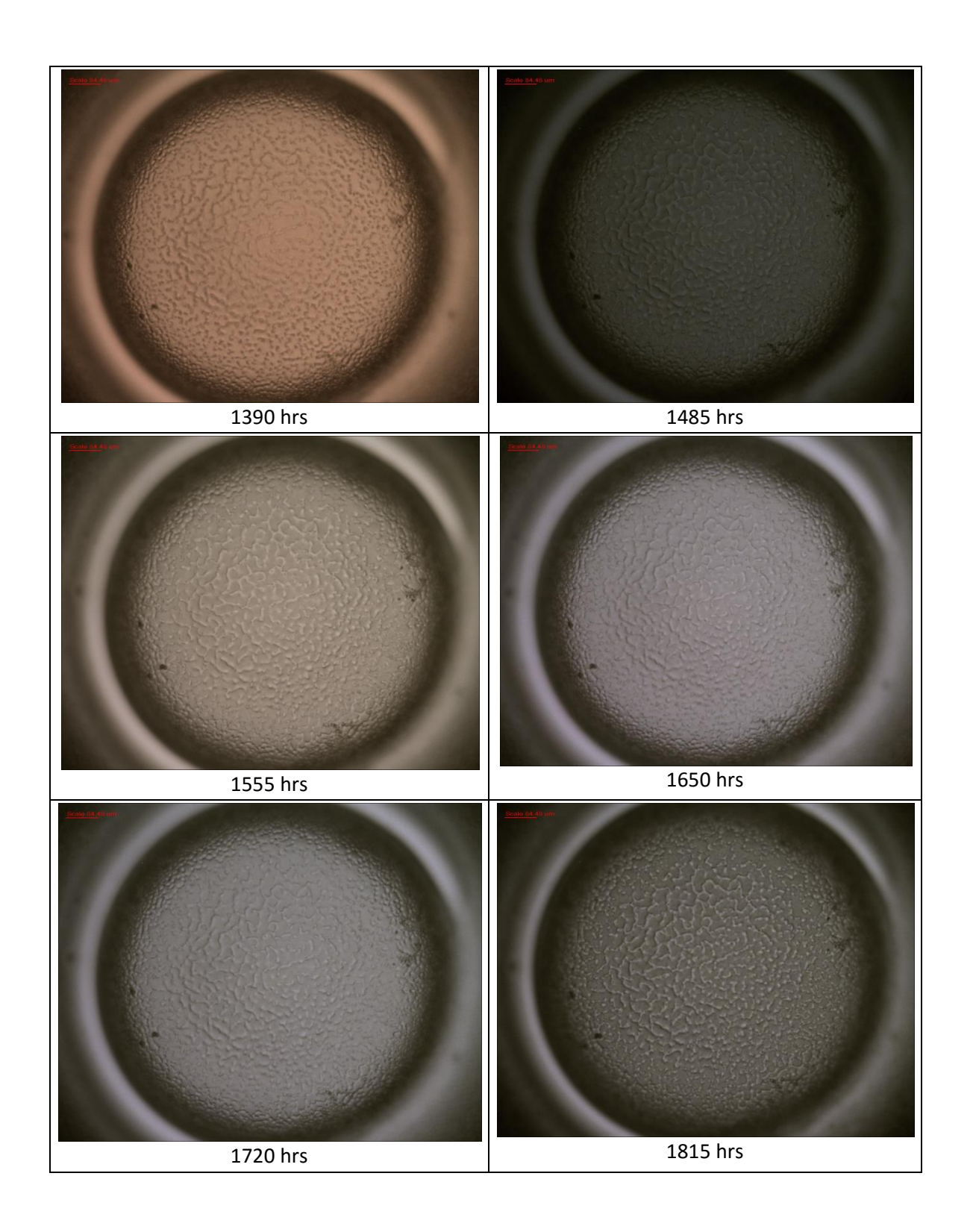
Sample C1

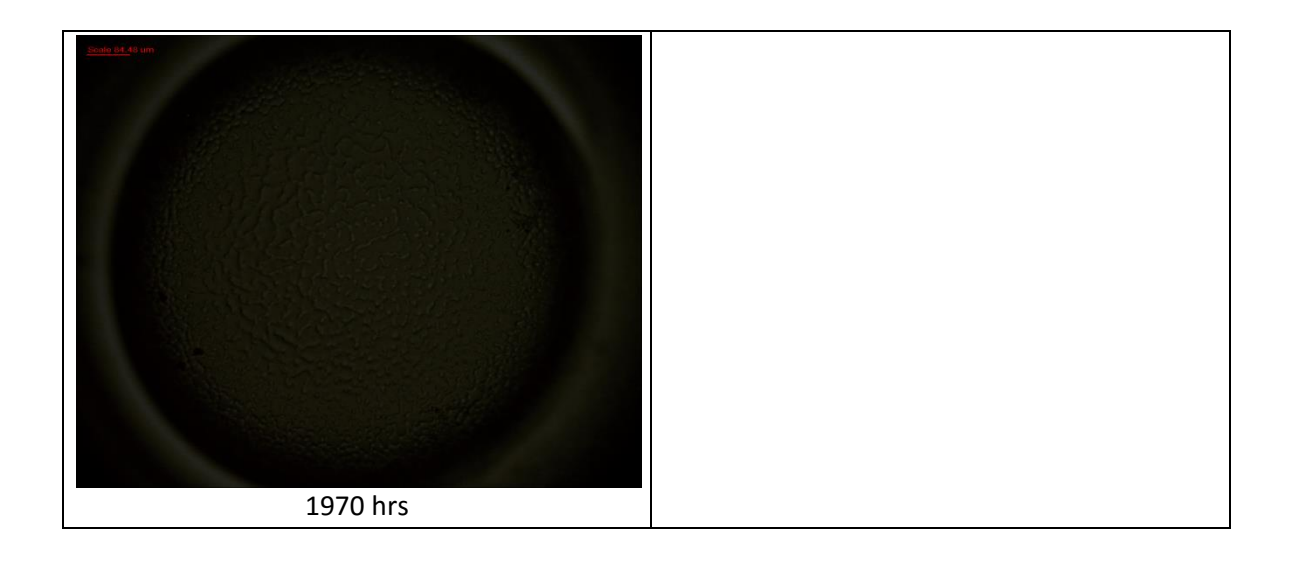




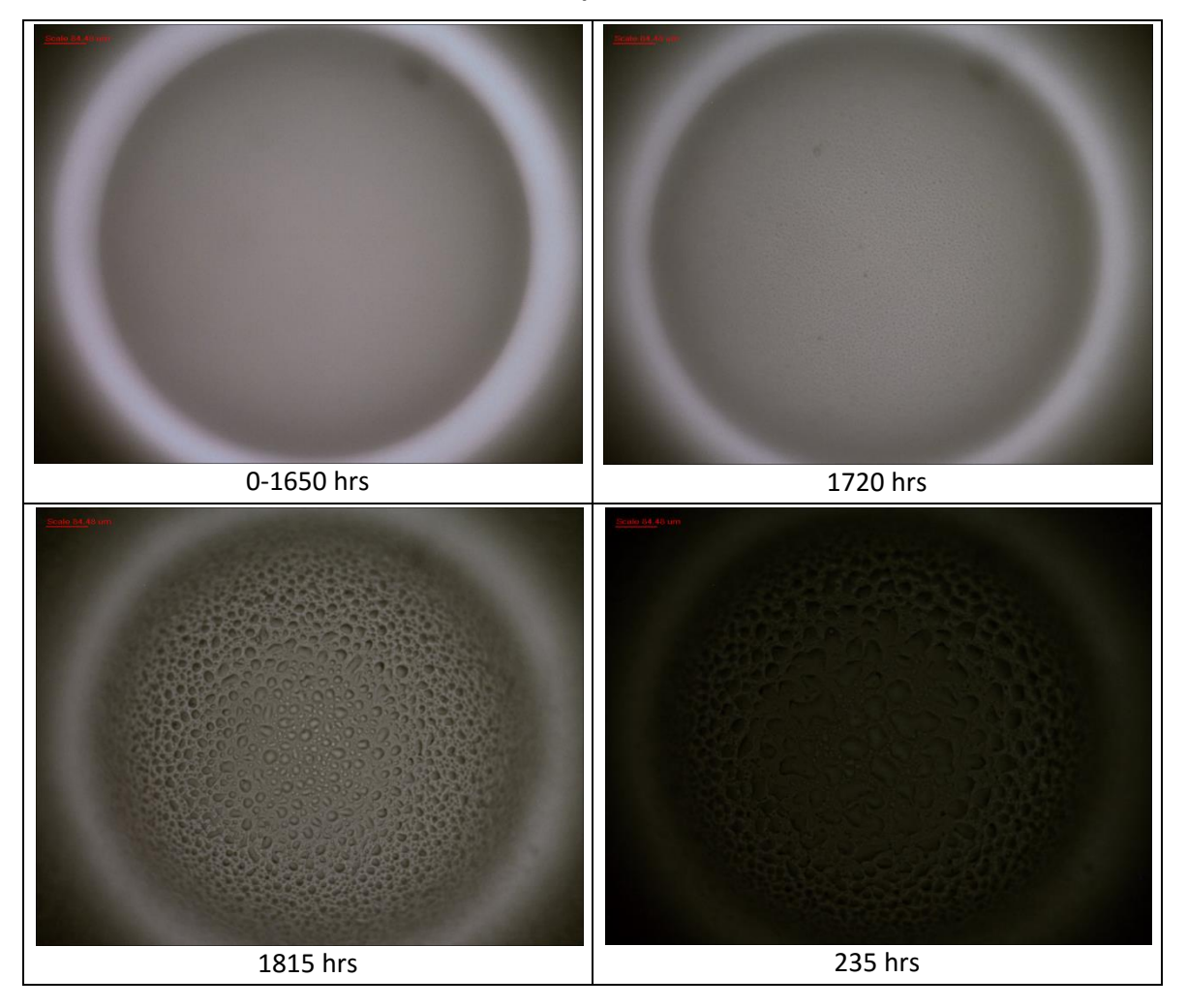
Sample C2



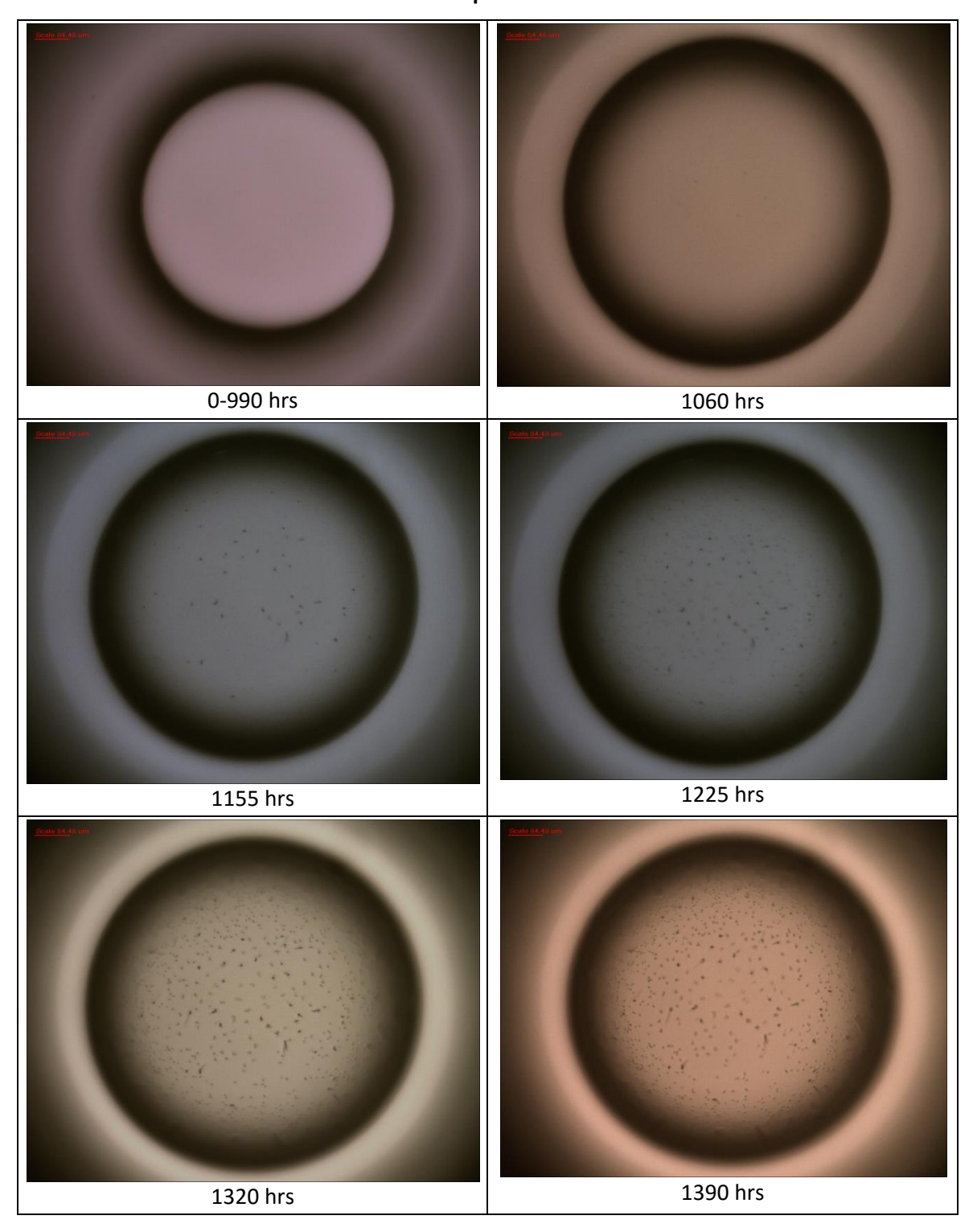


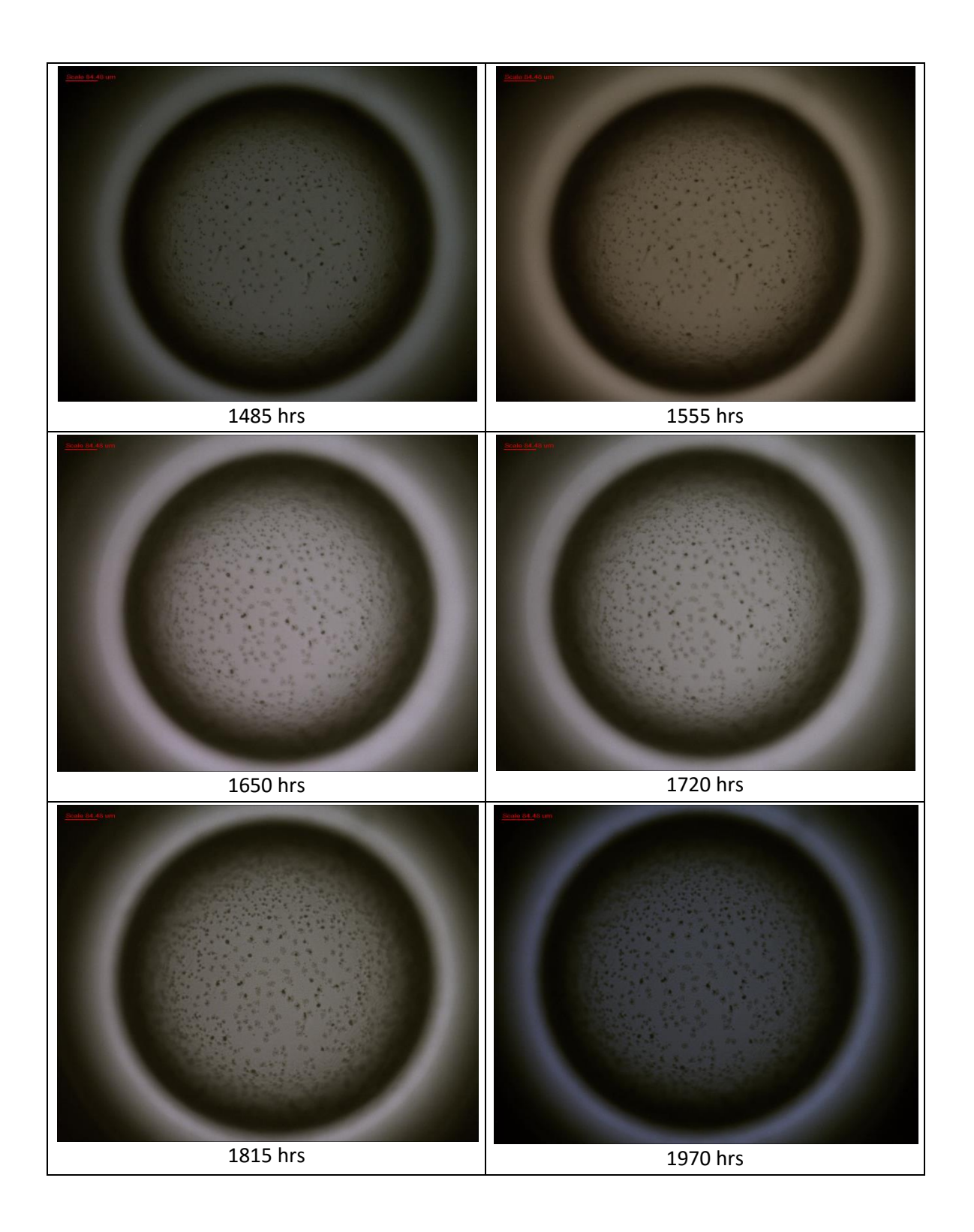


Sample C4

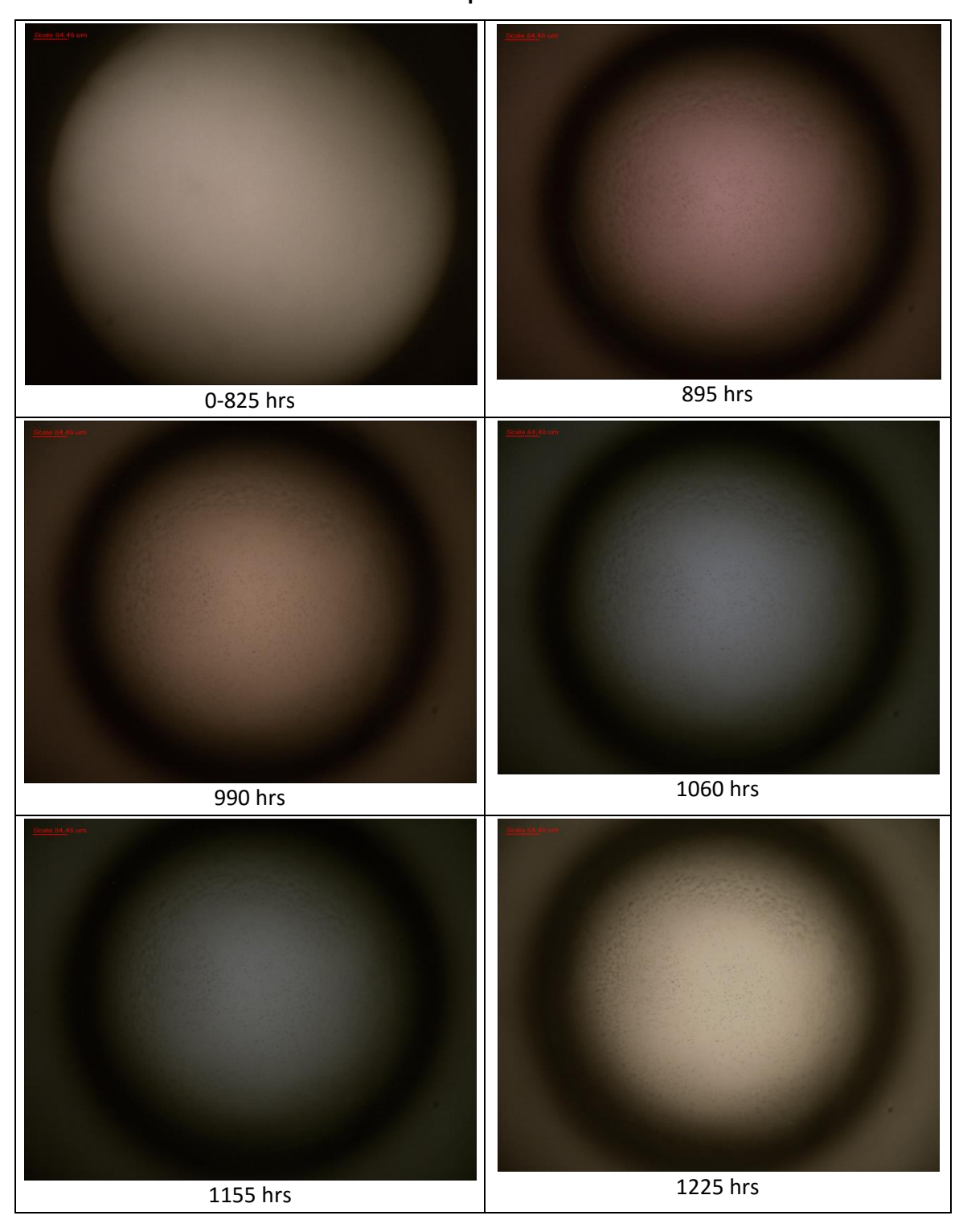


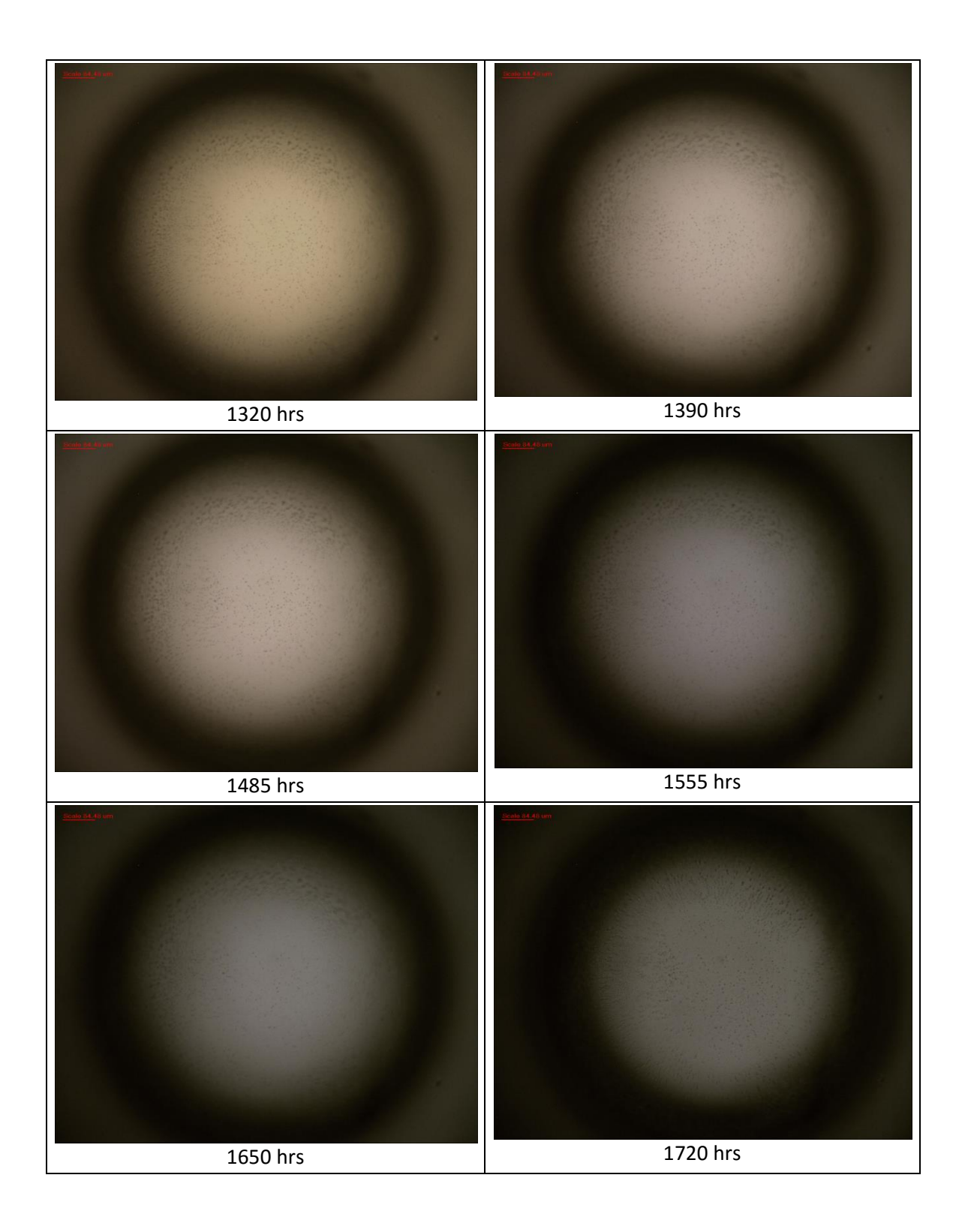
Sample C10

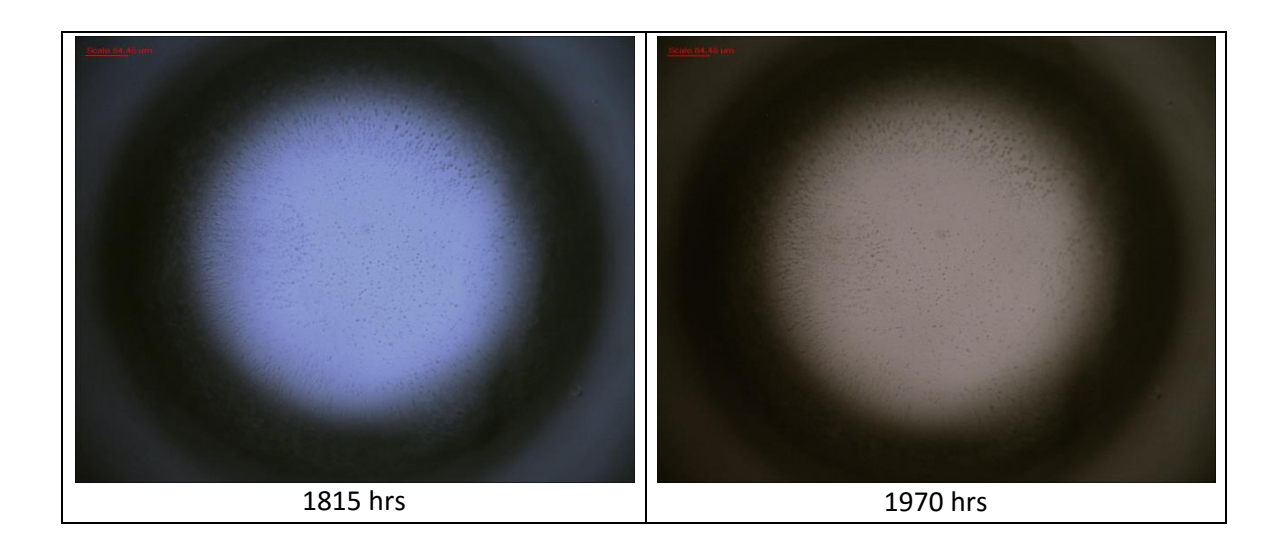




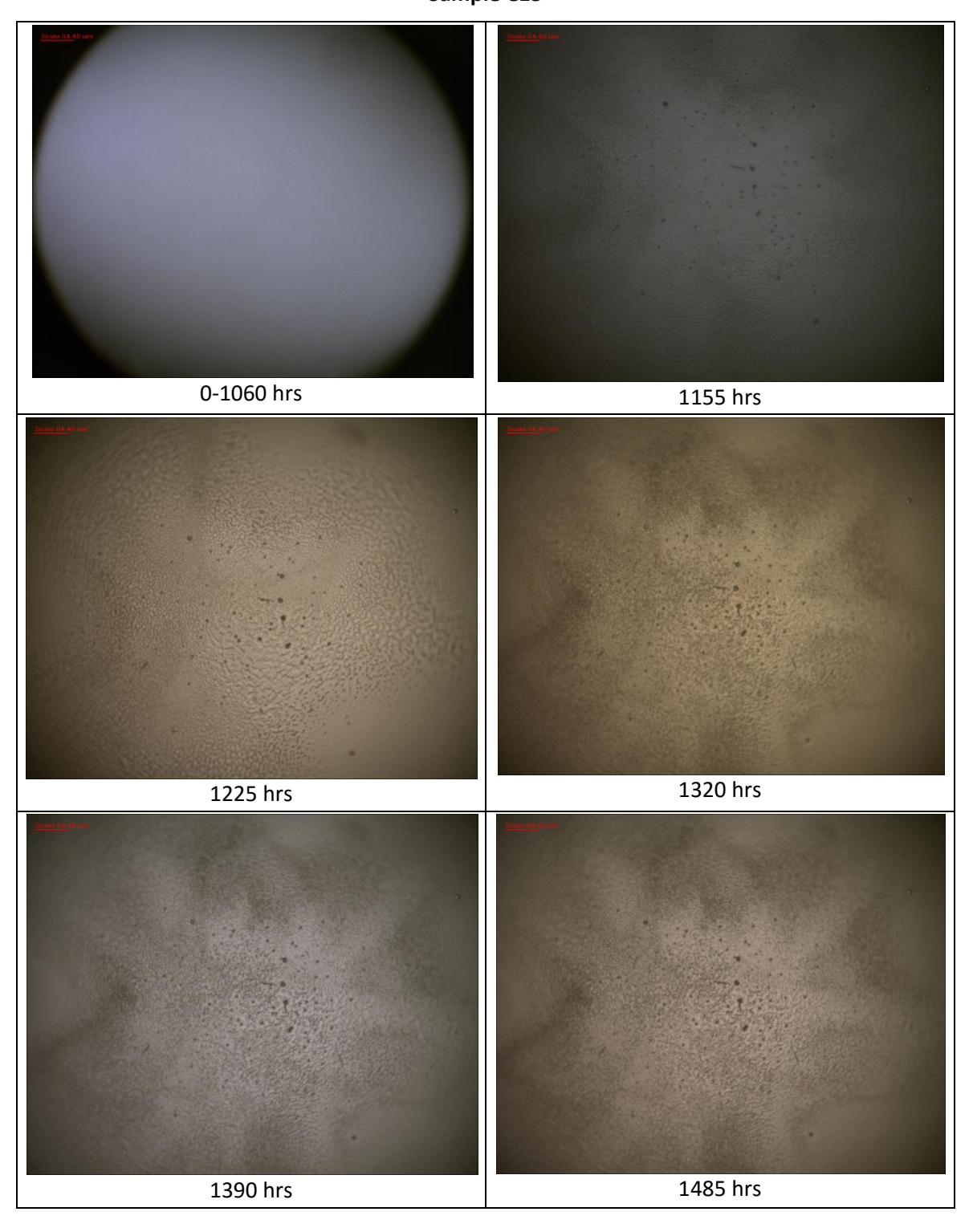
Sample C11





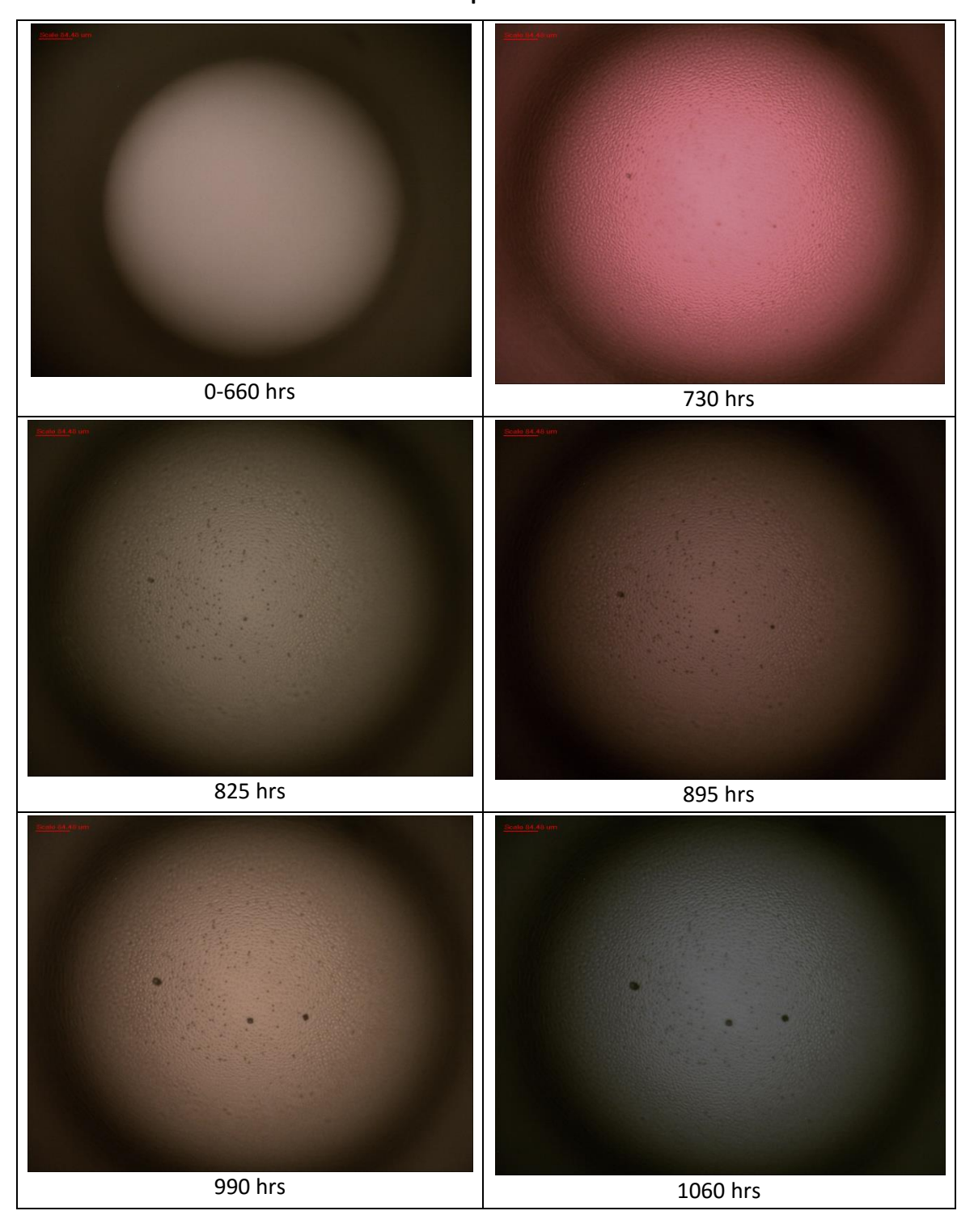


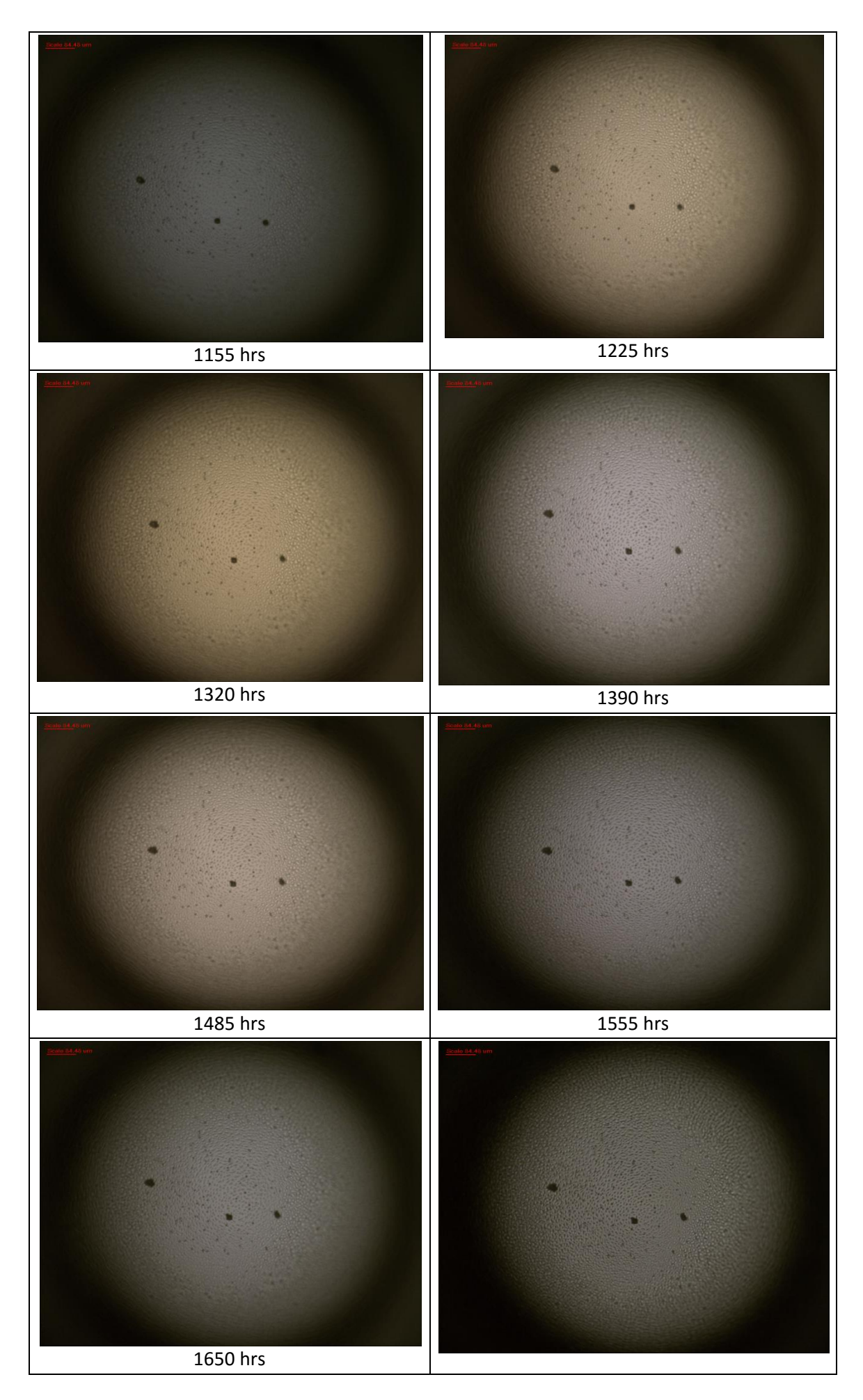
Sample C13

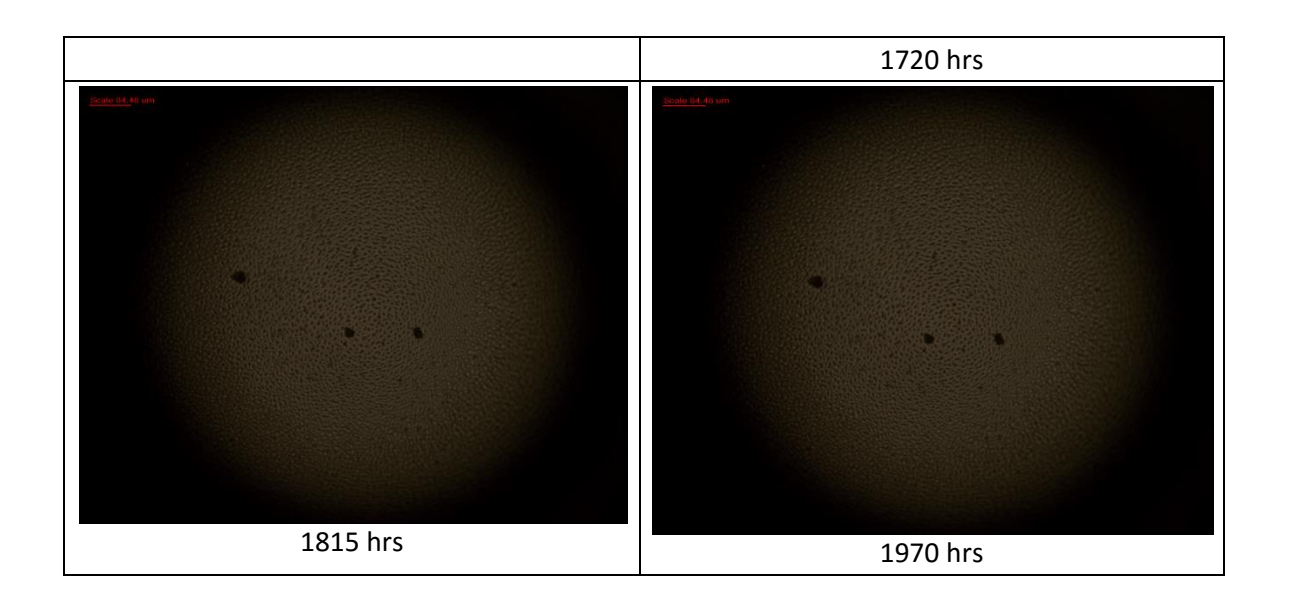




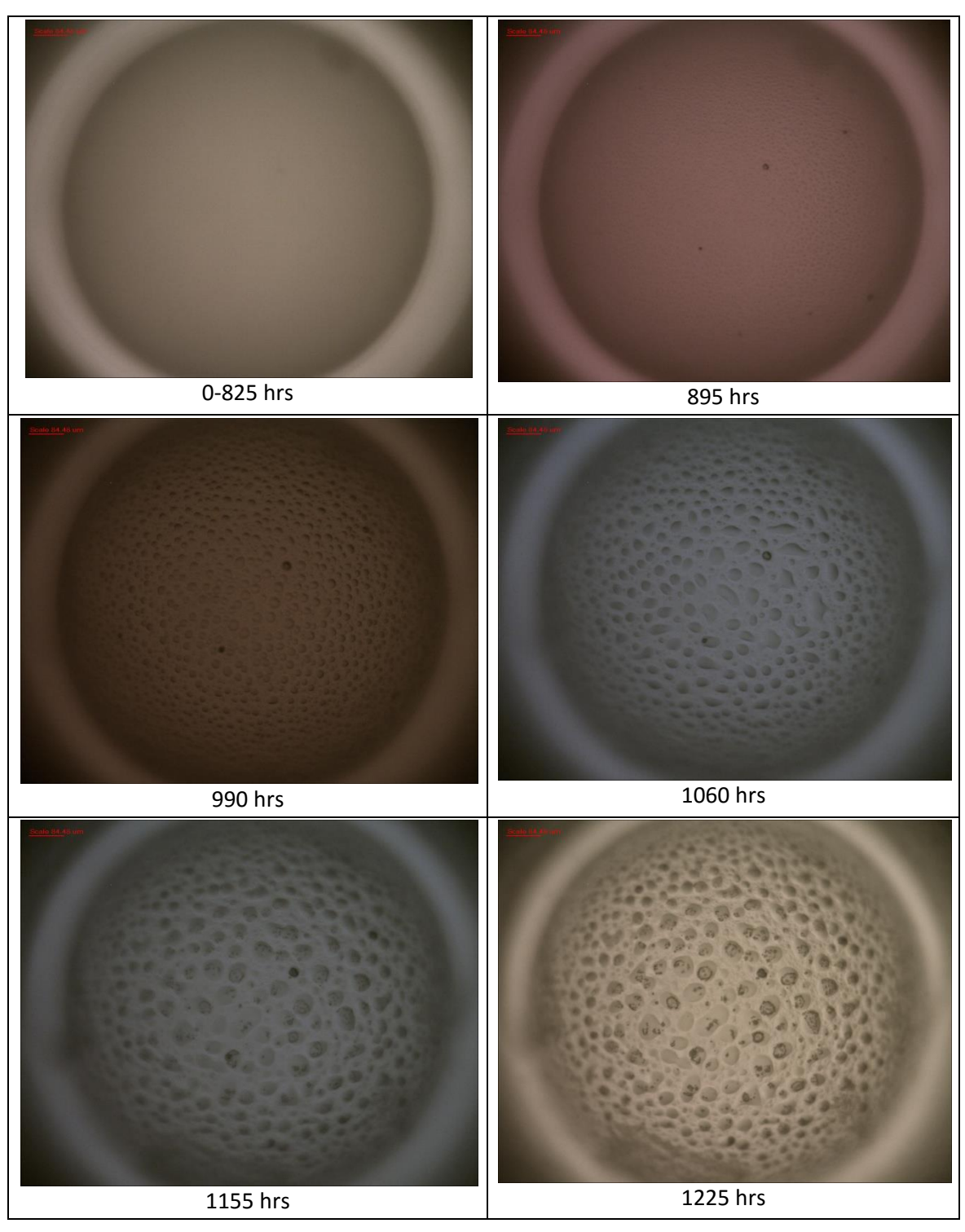
Sample C15

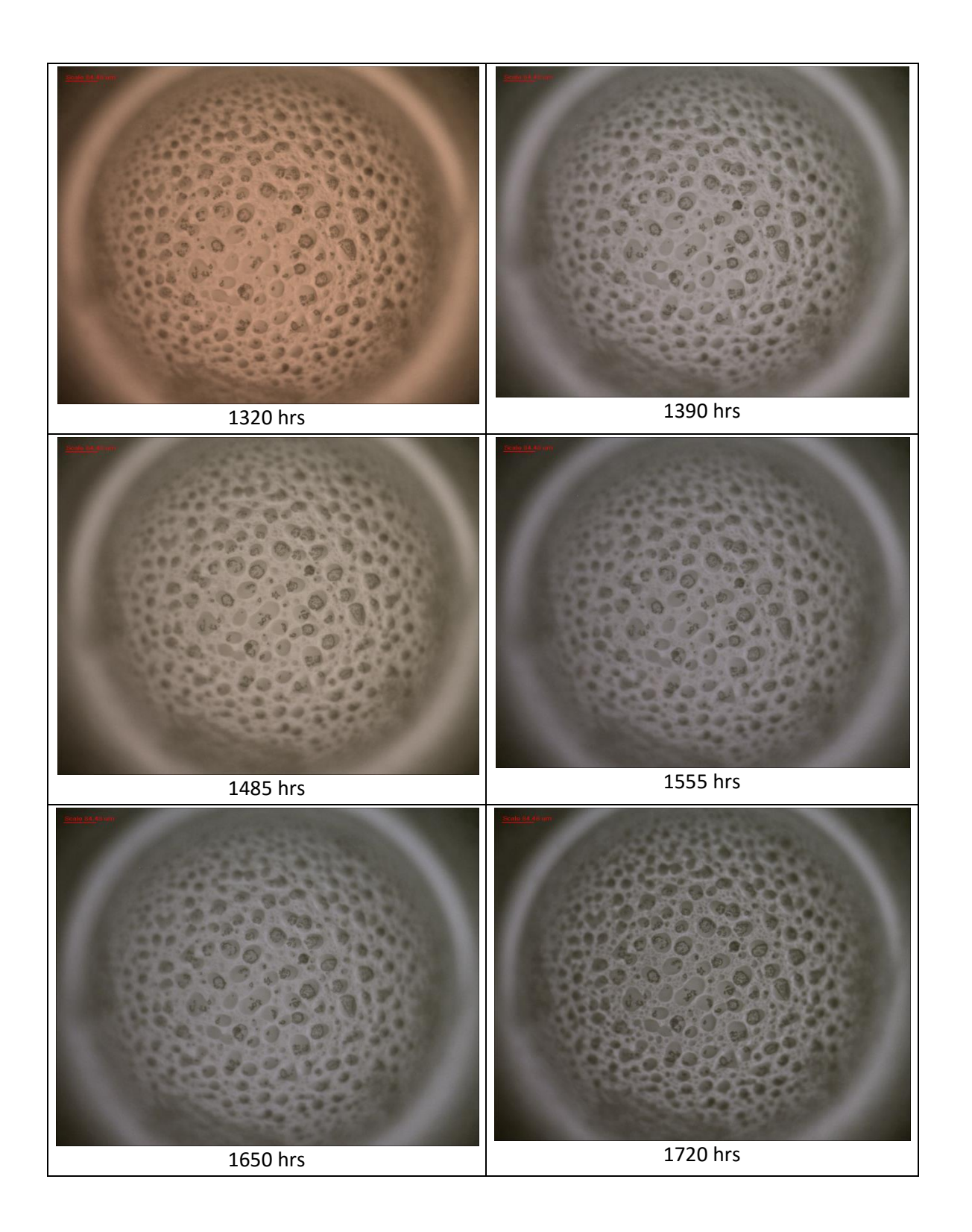


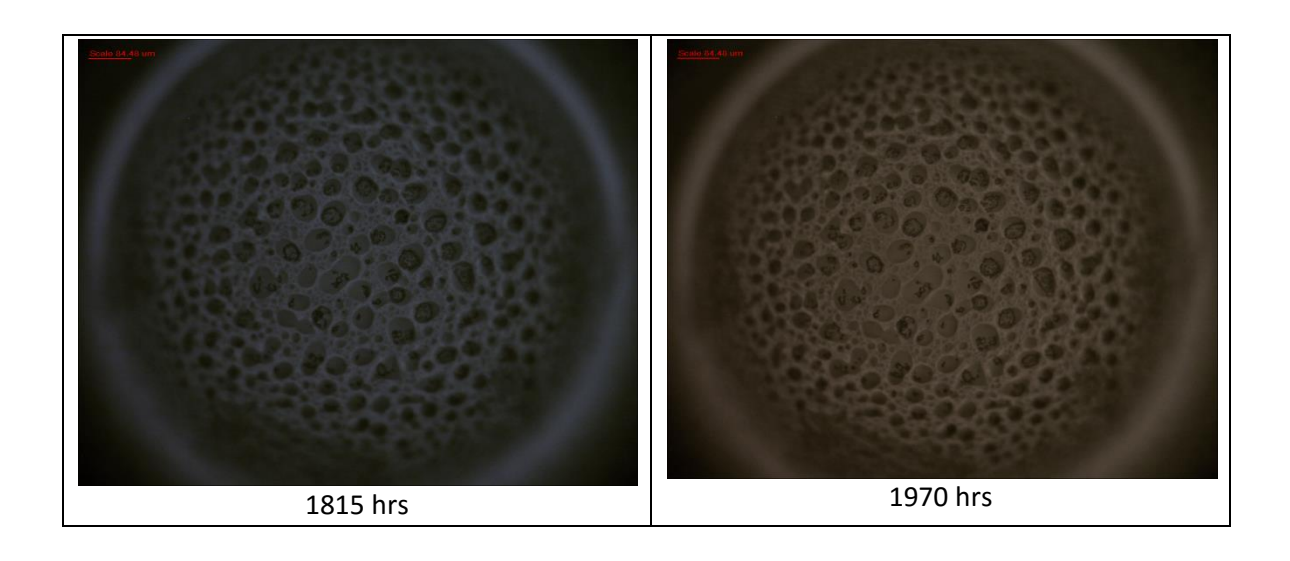




Sample C16







Appendix D Simulation code based on Niemeyer's algorithm.

```
% ***** UPDATED NIEMEYER'S MODEL*****
clear all; close all; clc; tic;
freq = 50; Time_p = 1/freq; Phase = 'A';
t step = 10e-6; %Chosen arbitarily
max_t_input = input('Please input simulation time: ','s');
max_t = str2num(max_t_input);
Ks input = input('Please input surface conductivity: ','s');
K s = str2num(Ks input);
work_function_input = input('Input the Work function: ','s');
work_function= str2num(work_function_input);
Pressure_input = input('Input the Pressure in Pa : ','s');
pre = str2num(Pressure_input);
epsilon_p_n = 1;
tau_input = input('Input the Decay time in Sec : ','s');
t = str2num(tau input);
time = 0:t step:max t; omega = 2*pi*freq; cycle = max t/Time p;
con = Time p/360;
Epcr = 25.2; B = 8.6; R = 0.0025; b = R/2; a = b; n = 1/2; K = 3;
Er = 3.7; E0 = 5500000; Estr = Epcr*pre*(1+(B/((2*pre*a)^n)));
ff = (K*Er) / (1 + ((K-1)*Er)); Ei = (ff*E0)*sin(omega*time);
gamma 1=0.35; e0 = 8.854*10^{-12}; D = 0.0025; x = Ei;
U0 = E0*D; U str = (Estr/ff)*D; epsilon p = 1; e charge = 1.6*1e-19;
epsilon n = epsilon p/epsilon p n; epsilon = 0;k = 8.617*1e-5;
Temp = 300; v0 = (1e13 + 1e14)/2;
C rad O rad = 2e6; p p0 = 10^-5; vir v = 1; % 1 = Virgin Void,0 is not
v = U0/U str; actual size PD = round(v*2*cycle);
%***** DEFINING PARAMETERS FOR SIMULATION ****
E q = zeros(1,1); del E = zeros(1,1); t interval = zeros(1,1);
q = zeros(1,1); Q s = zeros(1,1); t lag static = zeros(1,1);
t PD = zeros(1,1); Ndt1 = zeros(1,1); Ndt2 = zeros(1,1);
Prob = zeros(1,1); angle = zeros(1,1); Ndt3 = zeros(1,1);
App charge = zeros(1,1); time inc = zeros(1,1); PD = zeros(1,1);
Charge s = 0 * time; Eq surface = 0 * time; Pre drop = 0; Sub to PD = 0;
j = 1; Num PD = 1; Charge_change = zeros(1,1); Pot_drop =
0; Ref wave=zeros(1,1);
Prob coll=zeros(1,1);Est c=zeros(1,1);first void=1;random=zeros(1,1);
E ch=0;Y collect(Num PD) = zeros(1,1); change in prob=0;
forced to virgin=0;PD check=0;Changed=0;
% **** CALCULATION OF CONSTANT VALUES *****
con_q = e0*pi*(b^2)*(1+(Er*(K - 1))); constant_Eq = con_q; % Con = con_q = c
Constant
con_app_charge = (-4/3)*pi*a*(b^2)*e0*Er*K*(1/D);
con N dt 1= e charge / (4*pi*e0); con N dt 2 = k*Temp;
%**** CALCULATION OF VOLUME GENERATION RATE *****
Ni rad = C rad O rad*p p0; Veff = (4/3)*pi*(b^3)*(1-(v^(-1/n)));
N v = C rad O rad * p pO * pre * Veff * t step;
t inc = ((4/3) *C rad O rad*p p0*pre*((pi*a*(b^2)))*(1-(v^(-1/n))))^-1;
%***** START OF THE SIMULATION
while (j<= length(time))</pre>
       if(vir v ==1)
       Ei(j) = Ei(j)-Pre drop;
       end
       if(vir v == 0)
       Charge_s(j) = Q_s(Num_PD-1);
       Ei(j) = Ei(j) - Pre drop;
       dt = time(j) - time(j-1);
```

```
Pot drop = abs(Ei(j));
    Charge change = (pi/2) *K s*Pot drop*2*a*dt;
    if(((Charge s(j)/Ei(j)<0) \&\& (abs(Charge s(j))> abs(Ei(j))))...
        \mid \mid (Charge s(j)/Ei(j)>0))
        if(Charge s(j) > 0)
            Charge change = abs(Charge change);
        if (Charge s(j) < 0 && Charge change > 0)
            Charge change = -Charge change;
        Charge s(j) = Charge s(j) - Charge change;
        if(Q s(Num PD-1)/(Charge s(j)-Charge change) < 0)</pre>
            Charge s(j) = 0;
        end
        Q s(Num PD-1) = Charge s(j);
        E q(Num PD-1) = Q s(Num PD-1)/constant Eq;
        Ei(j) = Ei(j) + Pre drop;
        Pre drop = E q(Num PD-1); Ei(j) = Ei(j) - Pre drop;
    end
end
% if (changed==1 && i>0)
% if(y(i)/y(i-1)<0)
% virgin void = 1;first void=1;subject to PD = 0;
% forced to virgin= forced to virgin + 1;
% end
% end
if(Ei(j)> Estr || Ei(j)< -Estr)</pre>
    if(Ei(j) > 0)
        E ch = gamma 1*Epcr*pre;
        E ch = abs(E ch);
    end
    if(Ei(j) < 0 \&\& E ch > 0)
        E ch = gamma 1*Epcr*pre;
        E ch = -E ch;
    if(vir v == 0 \&\& Sub to PD == 1)
        time inc(Num PD) = time(j);
    if (\text{vir } v == 0 \&\& PD(\text{Num } PD-1)/\text{Ei}(j) >= 0)
        eps = epsilon p;
    else
        eps = epsilon n;
    end
if(vir v == 0)
    t interval(Num PD) = time(j) - t PD(Num PD-1);
    Ndt3(Num_PD) = eps * (abs(q(Num_PD-1))/e_charge);
    Ndt1(Num_PD) = Ndt3(Num_PD) * exp (-t_interval(Num_PD)/t);
    Ndt2(Num_PD) = Ndt1(Num_PD) * v0 * exp(-((work_function - ...
                     (sqrt(con N dt 1*abs(Ei(j)))))/con N dt 2));
    Prob (Num_PD) = (Ndt2(Num_PD)*t_step) + N_v;
    if(Prob (Num PD) == N v)
        vir v = 1; Sub to PD = 0;
        disp('probability has reached zero'); time(j);
    else
    Prob (Num PD) = 1-(\exp(-Prob(Num PD)));
    if (Prob (Num PD) > rand(1))
        del E(Num PD) = Ei(j) - E ch;
        q(Num PD) = con q * del E(Num PD);
        t lag static(Num PD) = time(j) - time_inc(Num_PD-1);
        Sub to PD = 1; PD(Num PD) = Ei(j); t PD(Num PD) = time(j);
PD check=Ei(j);
        angle (Num PD) = (t PD(Num PD) -
(floor(t PD(Num PD)/Time p)*Time p))/con;
        random (Num PD) = rand;
```

```
Q s(Num PD) = q(Num PD) + Q s(Num PD-1);
        E q(Num PD) = Q s(Num PD)/constant Eq; Pre drop = E q(Num PD);
        App charge(Num PD) = del_E(Num_PD) *con_app_charge;
        Y collect(Num PD) = Ei(j);
        Prob coll(Num PD) = Prob(Num PD);
        Est c(Num PD) = Estr;
        if((del E(Num PD) / App charge(Num PD) < 0) || (PD(Num PD) /</pre>
App charge (Num PD) < 0 ))
        App charge (Num PD) = App charge (Num PD) *-1;
        Num PD = Num PD + 1; Changed=1;
    end
    end
end
if (vir_v == 1 && first_void==1)
    if(Sub to PD == 0)
        t_{inc} = (C_{rad_0_rad*p_p0*pre*((pi*a*(b^2)))*(1-(v^(-1/n))))^-1;
        time inc(Num PD) = time(j);
        Prob(Num PD) = t step/t inc;
        first void=100; Prob(Num PD) = 1; change in prob=
change in prob+1;
        random(Num PD) = rand;
        del E(Num PD) = Ei(j) - E ch;
        q(Num PD) = con q * del E(Num PD);
        Q s(Num PD) = q(Num PD);
        E q(Num PD) = Q s(Num PD)/constant Eq; Pre drop = E q(Num PD);
        t interval(Num PD) = time(j);
          _{\rm lag\_static(Num\_PD)} = time(j)-time inc(Num PD);
        \overline{\text{vir}} \, \, \text{v} = 0; Sub to PD = 1;
        PD(Num PD) = Ei(j); t PD(Num PD) = time(j);
        angle(Num_PD) = (t_PD(Num_PD) -
(floor(t PD(Num_PD)/Time_p)*Time_p))/con;
        App charge(Num_PD) = del_E(Num_PD)*con_app_charge;
        Y collect(Num PD) = Ei(j);
        Prob coll(Num_PD) = Prob(Num_PD); Est_c(Num_PD) = Estr;
        if((del_E(Num_PD)/App_charge(Num_PD) < 0) || (PD(Num_PD) /</pre>
App charge (Num PD) < 0))
        App charge (Num PD) = App charge (Num PD) *-1;
        Num PD = Num PD + 1;
    end
end
if(vir v == 1)
    if (Sub to PD == 0 && (j>0) && (Ei(j)/Ei(j-1)<0))
        t_{inc} = (C_{rad_0_rad*p_p0*pre*((pi*a*(b^2)))*(1-(v^(-1/n))))^-1;
        time_inc(Num_PD) = time(j);
        Prob(Num_PD) = t_step/t_inc;
        first_void=100; Prob(Num_PD) = 1; change in prob=
change_in_prob+1;
        random(Num PD) = rand;
        del E(Num PD) = Ei(j) - E ch;
        q(Num PD) = con q * del E(Num PD);
        Q s(Num PD) = q(Num PD);
        E q(Num PD) = Q s(Num PD)/constant Eq; Pre drop = E q(Num PD);
        t interval(Num_PD) = time(j);
        t lag static (Num PD) = time(j)-time inc(Num PD);
        vir v = 0; Sub to PD = 1;
        PD(Num PD) = Ei(j); t PD(Num PD) = time(j);
        angle(Num PD) = (t PD(Num PD) -
(floor(t PD(Num PD)/Time p)*Time p))/con;
        App charge (Num PD) = del E (Num PD) *con app charge;
        Y collect(Num PD) = Ei(j);
        Prob coll(Num PD) = Prob(Num PD); Est c(Num PD) = Estr;
```

```
if((del E(Num PD)/App charge(Num PD) < 0) || (PD(Num PD) /</pre>
App charge (Num PD) < 0))
        App charge (Num PD) = App charge (Num PD) *-1;
        end
        Num PD = Num PD + 1;
    end
end
end
j = j + 1;
end
%**** END OF SIMULATION****
Num PD = Num PD - 1;
if (length(q) ~= length(angle))
    q = q(1:length(angle));
q = q/1e-12; App charge = App charge/1e-12;
Eq surface = Charge_s / constant_Eq; Charge_s = Charge_s/1e-12;
% ***** VARIABLE FOR PLOTS ****
Nhw = (Num PD/cycle)/2; %Number of PD pulses per half cycle
q minimum = (-2/3)*e0*Er*K*pi*b^2*Epcr*pre*
    (1-gamma 1+(B/((2*a*pre)^n)))*2*a*(1/D) / 1e-12; %minimum charge
q \text{ maximum} = (-4/3) *pi*a* (b^2) *e0*Er*K* ...
    ((2*ff*E0)-E ch)*(1/D)/1e-12; %maximum charge
t 1 period = 0:t step: Time p; % Define the time for a single period
  1 \text{ per deg} = \text{t } 1 \text{ period/con};
t_1_per_deg(length(t_1_per_deg)) = ...
    round (t 1 per deg (length (t 1 per deg)));
q \max = \max(q) + \max(abs(q));
reference waveform = abs(q max)*sin(omega*t 1 period); E ch = E ch/1e6;
Ei = Ei/le6; x = x/le6; Eq surface = Eq surface/le6; Estr = Estr/le6;
% *** ELECTRIC FIELD AND FIELD DENSITY
figure(1);
subplot(2,1,1); plot(time,Ei, 'Color', 'blue'); hold on;
xL= get (gca, 'XLim'); line(xL, [Estr Estr], 'Color', 'black');
line(xL, [-Estr -Estr], 'Color', 'black');
plot(time,x,'Color', 'r'); line(xL, [E ch E ch],'Color','black');
line(xL, [-E ch -E ch], 'Color', 'black'); plot (time, Eq surface, 'Color',
'g');
if (Time p*20 \le max t)
    xlim ([0, Time p*20]);
else
    xlim ([0, max_t]);
end
xlabel('Time (seconds)', 'Fontsize', 12);
ylabel('Amplitude (kV/m)','Fontsize' ,12);
title(sprintf('Electric field (Phase %s) ',Phase), 'Fontsize',14);
subplot(2,1,2); stem(t_PD,q,'.');
if (Time_p*20 \le max t)
    xlim ([0, Time p*20]);
else
    xlim ([0, max t]);
end
xlabel('Time (seconds)','Fontsize',12);
ylabel('Amplitude (pC)', 'Fontsize', 12);
title(sprintf('PD charge (Phase %s)', Phase), 'Fontsize', 14);
%**** APPARENT CHARGE AND REAL CHARGE ****
figure(2); hold on; plot(angle, App charge, '.'); grid on;
plot(t 1 per deg, reference waveform, 'Color', 'r');
xlim ([0,360]); set(gca,'XTick',0:20:360);
set (gca, 'XTickLabel', {'O', '20', '40', '60', '80', '100', '120', '140',
'160'
 '180','200','220','240','260','280','300','320','340',
'360' });
xlabel('Phase(degree)', 'Fontsize', 12);
```

```
ylabel('Amplitude (pC)','Fontsize',12);
title(sprintf('Apparent charge (Phase %s)', Phase), 'Fontsize', 14);
figure(8); hold on; scatter(time, Ei, 3, 'fill'); grid on;
xlabel('Phase(degree)','Fontsize', 12);ylabel('Amplitude
(pC)','Fontsize',12);
title(sprintf('Apparent charge (Phase %s)', Phase), 'Fontsize', 14);
% ***** PROBABILITY PLOT W.R.T ANGLE ***
figure(3); hold on; grid on; scatter(angle, Prob coll, 3, 'fill');
Ref_wave=sin(omega*t_1_period);plot(t_1_per_deg,Ref_wave,'Color','r');
xlim([0,360]); ylim([-1.1,1.1]);
figure(4);hold on;grid on;scatter(angle,Est c,3,'fill');
Ref_wave=sin(omega*t_1_period);plot(t_1_per_deg,Ref_wave,'Color','r');
figure(5);hold on;grid on;scatter(angle,random,3,'fill');
Ref_wave=sin(omega*t_1_period);plot(t_1_per_deg,Ref_wave,'Color','r');
% ***** 2D PRPD PLOT ******
Uni = unique(angle); Density = ones(1,length(angle));
for k = 1:length(Uni)
    Uni2 = find(Uni(k) == angle);
    for j = 1:length(Uni2);Density(Uni2(j)) = length(Uni2);
end
Uni = unique(q); Density2 = ones(1,length(q));
for k = 1:length(Uni)
    Uni2 = find(Uni(k) == q);
    for j = 1:length(Uni2); Density2(Uni2(j)) = length(Uni2);
    end
end
figure(6); subplot(3,1,1); hold on;
stem(angle,q,'.','Color','b'); xlim ([0, 360]); set(gca,'XTick',0:90:360);
set(gca, 'XTickLabel', {'0', '90', '180', '270', '360'});
xlabel('Phase(degree)','Fontsize',12);ylabel('Amplitude
(pC)','Fontsize',12);
title(sprintf('Apparent charge (Phase %s) ', Phase), 'Fontsize', 12);
subplot(3,1,2); hold on; stem(angle, Density, '.', 'Color', 'b');
xlim ([0, 360]); set(gca, 'XTick', 0:90:360);
set(gca, 'XTickLabel', {'0', '90', '180', '270', '360'});
xlabel('Phase(degree)','Fontsize',12);ylabel('Number','Fontsize',12);
title(sprintf( ...
'Number of PD occurrence at same phase(Phase %s) ', Phase), 'Fontsize', 12);
subplot(3,1,3); hold on; stem(angle,q/Num\_PD,'.','Color','b');
xlim ([0,360]); set(gca,'XTick',0:90:360);
set (gca,'XTickLabel',{'0', '90' , '180'
                                         ,'270' ,'360' });
xlabel ('Phase (degree)', 'Fontsize', 12);
ylabel('Average amplitude (pC)', 'Fontsize',12);
title(sprintf('Average apparent charge(Phase %s) ', Phase), 'Fontsize', 12);
% ******** 3D PRPD PLOT ******
Abs_mag = abs(q); amp = max(Abs_mag);
Abs_mag_x_axis=linspace(0,amp,201); pstep=360/200;
s step=max(Abs mag)/200; ang y axis=linspace(0,360,201);
[grid angle, abs magnitude grid] = meshgrid(ang y axis, Abs mag x axis);
Grid density=zeros(size(grid angle));
for j=1:Num PD
    pos1=round(Abs mag(j)/s step)+1; pos2=round(angle(j)/pstep)+1;
%Find respective signal gauge which is the relative index of each signal
    if Abs mag(j) \sim = 0;
        Grid density(pos1,pos2) = Grid density(pos1,pos2) + 1;
    end
%Increase the number of specific signal gauge
abs magnitude grid = abs magnitude grid * -1;
figure (7); contour 3 (grid angle, abs magnitude grid, Grid density, 400);
grid on; colormap(jet); shading interp; set(gca, 'XTick',0:45:360)
xlabel('Phase (Degree)'); ylabel('Amplitude (pC)'); zlabel('Number');
```

```
xlim([0 360]); ylim([-q_max 0]);title(sprintf('Phi-q-n
(Phase %s)',Phase),'Fontsize',14);toc;
```

References

- [1] T. Seghir, D. Mahi, T. Lebey, and D. Malec, "Analysis of the electric field and the potential distribution in cavities inside solid insulating electrical materials," in *Proceedings of the COMSOL User Conference*, 2006.
- [2] N. Ahmed, and N. Srinivas, "PD types and their detection possibilities by PD test methods," in *Electrical Insulation and Dielectric Phenomena*, 2001 Annual Report, pp. 307-310, 2001.
- [3] H. Edin, "Partial discharges studied with variable frequency of the applied voltage," PhD Thesis, Royal Institute of Technology (KTH), Stockholm, Sweden, 2001.
- [4] R. Bodega, P. H. F. Morshuis, M. Lazzaroni, and F. J. Wester, "PD recurrence in cavities at different energizing methods," in *IEEE Transactions on Instrumentation and Measurement,* vol. 53, no. 2, pp. 251-258, 2004.
- [5] H. Edin, and C. Forssen, "Variable frequency partial discharge analysis of in-service aged machine insulation," in *Proceedings Nordic Insulation Symposium*, pp. 29-35, 2003.
- [6] R. Bodega, A. Cavallini, P. H. F. Morshuis, and F. J.Wester, "The effect of voltage frequency on partial discharge activity," in *Conference on Electrical Insulation and Dielectric Phenomena*, pp. 685-689, 2002.
- [7] W. Hauschild, A. Cavallini, and G. C. Montanari, "Effect of supply voltage frequency on testing of insulation system," in *IEEE Transactions on Dielectrics and Electrical Insulation*, vol. 13, no. 5, pp. 1189-1191, 2006.
- [8] E. Lindell, T. Bengtsson, J. Blennow, and S. M. Gubanski, "Measurement of partial discharges at rapidly changing voltages," in *IEEE Transactions on Dielectrics and Electrical Insulation,* vol. 15, no. 3, pp. 823-831, 2008.
- [9] M. Hoof and R. Patsch, "A physical model, describing the nature of partial discharge pulse sequences," in *International Conference on Properties and Applications of Dielectric Materials*, vol. 1, pp. 283-286, 1997.
- [10] H. A. Illias, G. Chen, and P. L. Lewin, "Modelling of temporal temperature and pressure

- change due to partial discharge events within a spherical cavity in a solid dielectric material using finite element analysis," in *International Conference on High Voltage Engineering and Application*, pp. 501-504, 2010.
- [11] L.A. Dissado and J.C. Fothergill, "Electrical degradation and breakdown in polymers," in Peter Peregrinus Ltd., 1992.
- [12] L. Niemeyer, "A generalized approach to partial discharge modeling," in *IEEE Transactions* on *Dielectrics and Electrical Insulation, vol. 2, no. 4, pp. 510-528*, 1995.
- [13] T. Okamoto, T. Kato, Y. Yokomizu, Y. Suzuoki, and T. Tanaka, "PD characteristics as a stochastic process and its integral equation under sinusoidal voltage," in *IEEE Transactions* on *Dielectrics and Electrical Insulation*, vol. 8, no. 1, pp. 82-90, 2001.
- [14] N. Hozumi, H. Nagae, Y. Muramoto, M. Nagao, and X. HengKyun, "Time-lag measurement of void discharges and numerical simulation for clarification of the factor for partial discharge pattern," in *Proceedings of International Symposium on Electrical Insulating Materials, pp.* 29-32, 2001.
- [15] U. Garfert, H. Edin, and C. Forssen, "Modelling of partial discharge spectra measured with variable applied frequency," in *Proceedings Conference on Properties and Applications of Dielectric Materials*, pp. 839-842, 2003.
- [16] H. A. Illias, "Measurement and simulation of partial discharges within a spherical cavity in a solid dielectric material," in *PhD Thesis*, *University of Southampton*, *Southampton*, *U.K*, 2011.
- [17] A. Pedersen, G. C. Crichton, and I. W. McAllister, "The functional relation between partial discharges and induced charge," in *IEEE Transactions on Dielectrics and Electrical Insulation*, vol. 2, no. 4, pp. 535-543, 1995.
- [18] A. Pedersen, G. C. Crichton, and I. W. McAllister, "The theory and measurement of partial discharge transients," in *IEEE Transactions on Electrical Insulation, vol. 26, no. 3, pp. 487-497*, 1991.
- [19] M. G. Danikas, I. W. McAllister, G. C. Crichton, and A. Pedersen, "Discussion: partial discharges in ellipsoidal and spheroidal voids," in *IEEE Transactions on Electrical Insulation*, vol. 26, no. 3, pp. 537-539, 1991.

- [20] A. Pedersen, "On the electrodynamics of partial discharges in voids in solid dielectrics," in *Conference on Conduction and Breakdown in Solid Dielectrics, pp. 107-116*, 1989.
- [21] A. Pedersen, G. C. Crichton, and I. W. McAllister, "PD-related stresses in the bulk dielectric for ellipsoidal voids," in *Conference on Electrical Insulation and Dielectric Phenomena*, pp. 79-84, 1994.
- [22] G. C. Crichton, P. W. Karlsson, and A. Pedersen, "Partial discharges in ellipsoidal and spheroidal voids," in *EEE Transactions on Electrical Insulation*, vol. 24, no. 2, pp. 335-342, 1989.
- [23] L. Niemeyer, B. Fruth, and F. Gutfleisch, "Simulation of partial discharges in insulation systems," in 7th ISH, Proceeding 05, Paper 71, 1991.
- [24] N. Wiegart, L. Niemeyer, F. Pinnekamp, W. Boeck, J. Kindersberger, R. Morrow, W. Zaengl, M. Zwicky, I. Gallimberti, and S. A. Boggs, "Inhomogeneous field breakdown in SFs," in *EEE Transactions on Power Delivery, vol. 3, pp 923-946*, 1988.
- [25] G. Chen, and F. Baharudin, "Partial discharge modelling based on a cylindrical model in solid dielectrics," in *International Conference on Condition Monitoring and Diagnosis*, pp 74-78, 2008.
- [26] H. A. Illias, G. Chen, and P. L. Lewin, "The influence of spherical cavity surface charge distribution on the sequence of partial discharge events," in *Journal of Physics D: Applied Physics*, vol. 44, no. 24, 2011.
- [27] H. A. Illias, G. Chen, and P. L. Lewin, "Effect of surface charge distribution on the electric field in a void due to partial discharges," in *Conference Proceedings of ISEIM*, 2011.
- [28] H. A. Illias, G. Chen, and P. L. Lewin, "Modelling of surface charge decay in a spherical cavity within a solid dielectric material using finite element analysis," in *Proceedings of the 16th International Symposium on High Voltage Engineering*, 2009.
- [29] H. A. Illias, G. Chen, and P. L. Lewin, "Comparison of partial discharge measurement and simulation results for spherical cavities within solid dielectric materials as a function of frequency using Finite Element Analysis method," in *IEEE Transactions on Electrical Insulation*, pp. 1-5, 2010.
- [30] H. A. Illias, G. Chen, and P. L. Lewin, "Partial discharge behavior within a spherical cavity in a

- solid dielectric material as a function of frequency and amplitude of the applied voltage," in *IEEE Transactions on Dielectrics and Electrical Insulation, vol. 18, no. 2, pp. 432-443*, 2011.
- [31] H. A. Illias, G. Chen, and P. L. Lewin, "Partial discharge measurements for spherical cavities within solid dielectric materials under different stress and cavity conditions," in *IEEE Conference on Electrical Insulation and Dielectric Phenomena*, pp. 388-391, 2009.
- [32] H. A. Illias, G. Chen, and P. L. Lewin, "Modelling of partial discharge behaviour in a spherical cavity within a solid dielectric material as a function of temperature," in 2010 Annual Report Conference on Electrical Insulation and Dielectric Phenomena, pp. 1-4, 2010.
- [33] IEC 505, "Evaluation and identification of electrical insulation systems. Part 1: general Principles and Guide to Application," 1975.
- [34] P. K. David, "Correlation of Arrhenius parameters: the electrotechnical aging compensation effect," in *IEEE Transactions on Electrical Insulation*, vol. 22, pp. 229-236, 1987.
- [35] P. K. David, and G. C. Montanari, "Compensation effect in thermal aging investigated according to Eyring and Arrhenius models," in *ETEP*, vol. 2, no. 3, pp. 187-194, 1992.
- [36] G. C. Montanari, and F. J. Lebok, "The thermal degradation of electrical insulating materials and the thermokinetical background. Theoretical basis. Experimental data," in *IEEE Transaction on Electrical Insulation*, vol. 25, pp. 1029-1045, 1990.
- [37] J. P. Crine, J. L. Parpal, and G. Lessard, "A model of aging of dielectric extruded cables," in Proceedings of the 3rd International Conference on Conduction and Breakdown in Solid Dielectrics, pp. 347-351, 1989.
- [38] S. N. Zhurkov, "Kinetic concept of the strength of solids," in *International Journal of Fracture Mechanics*, vol. 1, pp. 311-323, 1965.
- [39] W. T. Starr, and H. S. Endicott, "Progressive stress: a new accelerated approach to voltage endurance," in *IEEE Transaction on Power Apparatus Systems, pp. 515-522*, 1961.
- [40] A. Many, and G. Rakavy, "Theory of transient space-charge-limited current in solids in the presence of trapping," in *Physical Review*, vol. 126, pp. 1980-1988, 1962.
- [41] J. J. O'Dwyer, "The theory of electrical conduction and breakdown in solid dielectrics," in *Clarendon Press, Oxford, U.K*, 1973.

- [42] A. See, L.A. Dissado, and J.C. Fothergill, "Electric field criteria for charge packet formation and movement in XLPE," in *IEEE Transaction on Dielectrics and Electrical Insulation, vol. 8, pp. 859-866*, 2001.
- [43] K. Kaneko, T. Mizutani, and Y. Suzuoki, "Computer simulation on formation of space charge packets in XLPE films," in *IEEE Transaction on Dielectrics and Electrical Insulation, vol. 6, pp.* 152-158, 1999.
- [44] N. F. Mott and R. W. Gurney, "Electronic processes in ionic crystals," in *OUP, New York*, 1940.
- [45] Z. Zheng, and S. Boggs, "Defect tolarance of solid dielectrics transmission class cable," in IEEE Electrical Insulation Magazine, 2005.
- [46] G. Jiang, J. Kuang, and S. Boggs, "Critical parameters for electrical tree formation in XLPE," in *IEEE Transaction on Power Delivery, vol. 13, pp. 292-296*, 1998.
- [47] S. A. Boggs, "Theory of defect-tolerant dielectric systems," in *IEEE Transaction on Ielectrical Insulation*, vol. 28, pp. 365-371, 1993.
- [48] L. A. Dissado, G. Mazzanti, and G. C Montanari, "The incorporation of space charge degradation in the life model for electrical insulating materials," in *IEEE Transaction on Dielectrics and Electrical Insulation, Vol. 2, pp. 1147-1158*, 1995.
- [49] G. Mazzanti, G. C. Montanari, and L.A. Dissado, "A space-charge life model for AC electrical aging of polymers," in *IEEE Transaction on Dielectrics and Electrical Insulation, vol. 6, pp.* 864-875, 1999.
- [50] G. Mazzanti, G. C. Montanari, and L.A. Dissado, "Life modeling of AC cable insulation based on space-charge inference," in *Proceedings of the 5th International Conference on Insulated Power Cables, pp. 707-712*, Versailles, France, 1999.
- [51] L. A. Dissado, G. Mazzanti, and G. C. Montanari, "Elemental strain and trapped space charge in thermoelectrical aging of insulating materials. Part 1: elemental strain under thermoelectrical-mechanical stress," in *IEEE Transaction on Dielectrics and Electrical Insulation*, vol. 8, pp. 959-965, 2001.
- [52] T. J. Lewis, "Ageing- a perspective," in *IEEE Electrical Insulation Magazine, vol. 17, no. 4, pp. 6-16*, 2001.

- [53] T. J. Lewis, "Polyethylene under electric stress," in *IEEE Transaction on Dielectrics and Electrical Insulation*, vol. 9, pp. 717-729, 2002.
- [54] C. Hudon, R. Bartnikas, and M. R. Wertheimer, "Effect of physico-chemical degradation of epoxy resin on partial discharge behavior," in *IEEE Transaction on Dielectrics and Electrical Insulation*, vol. 2, no. 6, pp. 1083-1094, 1995.
- [55] J. T. Holboll, and M. Henriksen, "Partial discharge patterns related to surface deterioration in voids in epoxy," in Conference Record of IEEE International Symposium on Electrical Insulation, pp. 115-119, Toronto, Canada, 1990.
- [56] L. Sanche, "Nanoscopic aspects of electronic ageing in dielectrics," in *IEEE Transaction on Dielectrics and Electrical Insulation*, vol. 4, no. 5, pp. 507-543, 1997.
- [57] S. Serra, G. C. Montanari, and G. Mazzanti, "Theory of inception mechanism and growth of defect-induced damage in polyethylene cable insulation," in *Journal of Applied Physics, vol.* 98, issue 3, pp. 034102 034102-15, 2005.
- [58] L. Testa, S. Serra, and G. C. Montanari, "Advanced modeling of electron avalanche process in polymeric dielectric voids: Simulations and experimental validation," in *Journal of Applied Physics*, vol. 108, issue 3, pp. 034110 034110-10, 2010.
- [59] L. A. Dissado, and P.I. Williams, "Physical origin for differences in electrical tree structures," in *IEEE Annual Report Conference on Electrical Insulation and Dielectric Phenomena*, 1994.
- [60] C. Y. Kim, J. Evans, and D. A. I. Goring, "Corona-induced authoesion of polyethelene," *Journal of Applied Polymer Science*, vol. 15, no. 6, p. 1365, 1971.
- [61] L. A. Dissado, and P. J. J. Sweeney, "Physical model for breakdown structures in solid dielectrics," *Physical Review B*, vol. 48, no. 22, pp. 16261-16268, 1993.
- [62] J. H. Mason, "The deterioration and breakdown of dielectrics resulting from internal discharge," in *Proceedings of the IEE Part I: General, vol. 98, pp. 44-59,* 1951.
- [63] P.H.F. Morshuis, "Assessment of dielectric degradation by ultrawide-band PD detection," in *IEEE Transactions on Dielectrics and Electrical Insulation, vol. 2, issue 5, pp. 744-760*, 1995.
- [64] K. D. Wolter, J. Tanaka, J. F. Johnson, "A study of the gaseous degradation products of corona-exposed polyethylene," in *IEEE Transactions on Electrical Insulation, vol. El-17, issue*

- *3, pp.248-252*, 1982.
- [65] P.H.F. Morshuis, "Partial discharge mechanisms," in *PhD Thesis, Delft University of Technology*, 1993.
- [66] M. Goldman, A. Goldman, and J. Gatellet, "Physical and chemical aspects of partial discharges and their effects on materials," in *IEE Proceedings Science, Measurement and Technology, Volume: 142, Issue: 1, pp. 11-16,* 1995.
- [67] R.S. Sigmond, T. Sigmond, A. Goldman, and M. Goldman, "In situ mass spectrometric analysis of the deterioration of polymer surfaces by low pressure AC discharges," in *Proceedings of the 3rd International Conference on Conduction and Breakdown in Solid Dielectrics, pp.451-455*, 1989.
- [68] P.H.F. Morshuis, "Degradation of solid dielectrics due to internal partial discharge: some thoughts on progress made and where to go now," in *IEEE Transactions on Dielectrics and Electrical Insulation*, vol.12, issue 5, pp.905-913, 2005.
- [69] T. Tanaka, "Internal partial discharge and material degradation," in *IEEE Transactions on Electrical Insulation*, vol. El-21, issue 6, pp. 899-905, 1986.
- [70] T. Ishida, Y. Mizuno, M. Nagao, and M. Kosaki, "Development and application of partial discharge analyzing system for swarming pulsive microdischarges," in *Proceedings of the 3rd International Conference on Properties and Applications of Dielectric Materials, vol. 2, pp.* 676-679, 1991.
- [71] Y. Sekii, and T. Sugai, "A study on the deterioration of LDPE and epoxy insulation by partial discharge," in *Conference on Electrical Insulation and Dielectric Phenomena, vol.2, pp. 516-520*, 1997.
- [72] Y. Sekii, T. Fukuyama, and K. Kikuchi, "Deterioration by partial discharges of polyethylene in oxygen containing gas atmosphere," in *Proceedings of the 6th International Conference on Properties and Applications of Dielectric Materials, vol.1, pp. 479-482*, 2000.
- [73] Y. Sekii, "Degradation of low-density polyethylene and cross-linked polyethylene by partial discharge," in *IEEE Transaction on Dielectrics and Electrical Insulation, Vol. 17, pp. 116-124*, 2010.
- [74] Y. Sekii, M. Ohno, and H. Oguma, "Effect of antioxidants, on deterioration by partial

- discharge in LDPE and XLPE," in Annual Report Conference on Electrical Insulation and Dielectric Phenomena, pp. 547-550, 2004.
- [75] Y. Sekii, H. Oguma, H. Takeo, and K. Yamauchi, "GC-MS and FTIR analysis of LDPE and XLPE deteriorated by partial discharge," in *Annual Report Conference on Electrical Insulation and Dielectric Phenomena*, pp. 237-240, 2005.
- [76] C.S. Kim, T. Kondo, and T. Mizutani, "Change in PD pattern with aging," in *IEEE Transactions* on *Dielectrics and Electrical Insulation*, vol. 11, issue 1, pp. 13-18, 2004.
- [77] T. Ito, "Analysis of internal discharge degradation of polyethylene by simultaneous chemical and electrical measurement," in *Transactions of the institute of Electrical Engineers of Japan, Vol. 109, pp. 457-463,* 1989.
- [78] K. Nakao, Y. Suzuoki, and T. Mizutani, "PD patterns and PD current shapes of LDPE specimen with a void," in *IEEE Conference on Conduction and Breakdown in Solid Dielectrics, pp. 157-160*, 1998.
- [79] T. Mizutani, C.S. Kim, K. Ichikawa, and Y. Tani, "Changes in PD pattern and PD current shape for a void in LDPE," in *Annual Report Conference on Electrical Insulation and Dielectric Phenomena*, vol.2, pp670-673, 2000.
- [80] T. Mizutani, T. Kondo, and K. Nakao, "Change in partial discharge properties of a void in LDPE," in *Annual Report Conference on Electrical Insulation and Dielectric Phenomena*, vol.1 pp. 257-260, 1999.
- [81] P.H.F. Morshuis; F.H. Kreuger, "A relation between time-resolved discharge parameters and ageing," in *Sixth International Conference on Dielectric Materials, Measurements and Applications, pp. 37-40*, 1992.
- [82] P.H.F. Morshuis, and F.H. Kreuger, "Transition from Streamer to Townsend Mechanisms in Dielectric Voids," in *J. Phys. D: Appl. Phys. 23 (1990) 1562-1568*, 1990.
- [83] P.H.F. Morshuis, "Partial discharge mechanisms in voids related to dielectric degradation," in *IEE Proceedings Science, Measurement and Technology, vol.142, issue 1, pp. 62-68*, 1995.
- [84] P. H. F. Morshuis, "Ageing of polymers studied by spectral analysis of UWB partial discharge signals," IEEE Conference on Electrical Insulation and Dielectric Phenomena, pp. 226-229,

1995.

- [85] C. Hudon, R. Bartnikas, and M.R. Wertheimer, "Surface conductivity of epoxy specimens subjected to partial discharges," in *IEEE International Symposium on Electrical Insulation, pp.* 153-155, 1990.
- [86] B. Luczynski, "Partial discharges in artificial gas filed cavities in solid high voltage insulators," in *PhD Thesis, Technical University of Denmark*, 1979.
- [87] C. Hudon, and R. Bartnikas, "Surface and gas phase reactions arising with epoxy exposed to partial discharges," in *Conference on Electrical Insulation and Dielectric Phenomena, pp. 725-734*, 1992.
- [88] C. Hudon, R. Bartnikas, and M.R. Wertheimer, "Spark-to-glow discharge transition due to increased surface conductivity on epoxy resin specimens," in *IEEE Transactions on Electrical Insulation*, vol. 28, issue 1, pp. 1-8, 1993.
- [89] C. Hudon, R. Bartnikas, and M.R. Wertheimer, "Chemical and physical degradation effects on epoxy surfaces exposed to partial discharges," in *Proceedings of the 4th International Conference on Properties and Applications of Dielectric Materials, vol.2, pp. 811-814*, 1994.
- [90] D.M. Hepburn, I.J. Kemp, A.J. Shields, and R.T. Richardson, "The degradation of epoxy resin by partial discharge stressing," in *Proceedings of the 4th International Conference on Properties and Applications of Dielectric Materials, vol. 1, pp. 31-34*, 1994.
- [91] D.M. Hepburn, I.J. Kemp, A.J. Shields, and J. Cooper, "Degradation of epoxy resin by partial discharges," in *IEE Proceedings Science, Measurement and Technology, vol. 147, issue 3, pp. 97-104*, 2000.
- [92] D. Adhikari, D.M. Hepburn, and B.G. Stewart, "Comparison of partial discharge characteristics and degradation in several polymeric insulators," in *Science, Measurement & Technology, IET*, vol. 6, issue 6, pp. 474-484, 2012.
- [93] G.C. Montanari, A. Cavallini, L. Testa, S. Serra, and L.A. Dissado, "Model of ageing inception and growth from microvoids in polyethylene-based materials under AC voltage," in *Annual Report Conference on Electrical Insulation and Dielectric Phenomena*, pp. 29-32, 2008.
- [94] L. Wang, L. Testa, A. Cavallini, and G.C. Montanari, "Relation between the trend of partial discharges and aging models under AC voltage," in *IEEE 9th International Conference on the*

- Properties and Applications of Dielectric Materials, pp. 268-271, 2009.
- [95] L. Wang, A. Cavallini, G.C. Montanari, and L. Testa, "Patterns of partial discharge activity in XLPE: From inception to breakdown," in 10th IEEE International Conference on Solid Dielectrics (ICSD), pp. 1-4, 2010.
- [96] L. Wang, A. Cavallini, G.C. Montanari, "Time behavior of gas pressure and PD activity in insulation cavities under AC voltage," in *Annual Report Conference on Electrical Insulation and Dielectric Phenomena (CEIDP)*, pp.1-4, 2010.
- [97] L. Wang, A. Cavallini, G.C. Montanari, and L. Testa, "Evolution of pd patterns in polyethylene insulation cavities under AC voltage," in *IEEE Transactions on Dielectrics and Electrical Insulation*, pp. 533-542, 2012.
- [98] N. Freebody, "The Use of Raman Microprobe Spectroscopy in the Analysis of Electrically Aged Polymeric Insulators," Phd Thesis, University of Southampton, 2012.
- [99] T. Bai, "Degradation process of voids in solid dielectrics under AC applied fields," MPhil Thesis, University of Southampton, 2013.
- [100] K. Wu, Y. Suzuoki, T. Mizutani, and H. Xie, "Model for partial discharges associated with treeing breakdown: III. PD extinction and re-growth of tree," in *Journal of Physics D: Applied Physics*, vol. 33, pp 1209-1218, 2000.
- [101] S. Dodd, N. Chalashkanov, and J. Fothergill, "Partial discharge patterns in conducting and non-conducting electrical trees," in *IEEE International Conference on Solid Dielectrics*, pp. 1-4, 2010.
- [102] A. Cavallini, R. Ciani, M. Conti, P.H.F. Morshuis, and G.C. Montanari, "Modeling memory phenomena for partial discharge processes in insulation cavities," in *Annual Report*.

 Conference on Electrical Insulation and Dielectric Phenomena, pp.723-727, 2003.
- [103] J.T. Holboll, M. Henriksen, "Partial discharge patterns and surface deterioration in voids in filled and unfilled epoxy," in *IEEE International Symposium on Electrical Insulation, pp. 354-358*, 1992.
- [104] L. Centurioni, F. Guastavino, and E. Torello, "An investigation about the PD degradation of thin polymer films and its correlation with surface charge decay measurements," in *IEEE International Symposium on Electrical Insulation*, pp. 371-374, 2002.

- [105] M. Hikita, K. Yamada, A. Nakamura, T. Mizutani, A. Oohasi, and M. Ieda, "Measurements of partial discharges by computer and analysis of partial discharge distribution by the Monte Carlo method," in *IEEE Transactions on Electrical Insulation*, vol. 25, issue. 3, pp. 453-468, 1990.
- [106] Suwarno; Mizutani, T., "Diagnosis of insulation conditions: Interpretation of partial discharges from φ-q-n pattern, pulse-sequence and pulse waveform," in *International Conference on Condition Monitoring and Diagnosis*, pp. 60-63, 2008.
- [107] K. Wu, and Y. Suzuoki, "Effects of discharge area on PD patterns in voids," in *Annual Report Conference on Electrical Insulation and Dielectric Phenomena*, vol. 1, pp. 227-230, 1999.
- [108] K. Wu, T. Okamoto, and Y. Suzuoki, "Effects of discharge area and surface conductivity on partial discharge behavior in voids under square voltages," in *IEEE Transactions on Dielectrics and Electrical Insulation*, vol. 14, issue 2, pp. 461-470, 2007.
- [109] K. Wu, T. Ijichi, T. Kato, Y. Suzuoki, F. Komori, and T. Okamoto, "Contribution of surface conductivity to the current forms of partial discharges in voids," in *IEEE Transactions on Dielectrics and Electrical Insulation, vol. 12, issue 6, pp. 1116-1124*, 2005.
- [110] Y. Suzuoki, Y. Kodani, F. Komori, and T. Kato, "Relation between Concentration of Partial Discharge and Surface Degradation and Breakdown," in *Annual Report Conference on Electrical Insulation and Dielectric Phenomena*, pp. 404-407, 2008.
- [111] M. Hoof and R. Patsch., "Pulse-sequence analysis: a new method for investigating the physics of pd-induced ageing," in *Science, Measurement and Technology, IEE Proceedings,* 142(1):95-101, 1995.
- [112] M. Hoof and R. Patsch., "Analyzing partial discharge pulse sequences-a new approach to investigate degradation phenomena," in *IEEE International Symposium on Electrical Insulation*, pp. 327-331, 1994.
- [113] P. H. F. Morshuis, and E. Gulski, "Diagnostic tools for condition monitoring of insulating materials," IEEE Conference on Electrical Insulation and Dielectric Phenomena, pp. 327-330, 1995.
- [114] P. H. F. Morshuis, and F. H. Kreuger, "The evolution of the discharge mechanism in a dielectric bounded cavity due to surface effects," IEEE Conference on Properties and

- Applications of Dielectric Materials, Vol. 2, pp. 672-675, 1991.
- [115] P. H. F. Morshuis, and F. H. Kreuger, "The spatial distribution and electrical parameters of partial discharge in polyethylene insulation during ageing," IEEE Conference on Conduction and Breakdown in Solid Dielectrics, pp. 209-214, 1992.
- [116] P. H. F. Morshuis, and L. Niemeyer, "Measurement and simulation of discharge induced ageing processes in voids," IEEE Annual Report of the Conference on Electrical Insulation and Dielectric Phenomena, Vol. 2, pp. 520-524, 1996.
- [117] D. L. Donoho, and I. M. Johnstone, "Ideal spatial adaptation by wavelet shrinkage," Biometrika, Vol. 81, pp. 425-455, 1994.
- [118] D. L. Donoho, and I. M. Johnstone, "Adapting to unknown smoothness via wavelet shrinkage," Department of Statistics, Stanford University., 1995.
- [119] D. Evagorou, A. Kyprianou, P. L. Lewin, and A. Stavrou, "Feature extraction of partial discharge signals using the wavelet packet transform and classification with a probabilistic neural network," Science, Measurement & Technology, Vol. 4, pp. 177-192, 2010.
- [120] A. Contin, A. Cavallini, G. C. Montanari, G. Pasini, and F. Puletti, "Digital detection and fuzzy classification of partial discharge signals," IEEE Transactions on Dielectrics and Electrical Insulation, Vol. 9, pp. 335-348, 2002.
- [121] A. Cavallini, G. C. Montanari, A. Contin, and F. Pulletti, "A new approach to the diagnosis of solid insulation systems based on PD signal inference," IEEE Electrical Insulation Magazine, Vol. 19, pp. 23-30, 2003.
- [122] A. Cavallini, A. Contin, G. C. Montanari, and F. Puletti, "Advanced PD inference in on-field measurements. I. noise rejection," IEEE Transactions on Dielectrics and Electrical Insulation, Vol. 10, pp. 216-224, 2003.
- [123] T. Mizutani, Y. Suzuoki, H. Kaneiwa, and K. Shizu, "Partial Discharge and Light Emission from Tree Chaninels in LDPE," in *Electrical Insulation and Dielectric Phenomina, Annual Report,* vol. 1, pp 31-34, 1998.
- [124] Suwarno, H. Ichikawa, Y. Suzuoki, and T. Mizutani, "Partial discharge patterns of electrical treeing in polyethylene," in *Properties and Applications of Dielectric Materials, Proceedings of the 4th International Conference. vol. 1, pp. 379-382.*, 1994.

- [125] P. Dejean, G. Berg, M. Goldman, and H. Dejean, "Chemical aspects of the aging of solid insulating materials submitted to partial discharges," in 4th Int. Conf. On Conduction and Breakdown in Solid Dielectrics, pp. 181-185, 1992.
- [126] J.L. Goldstein, Scanning electron microscopy and X-ray microanalysis, 3rd ed. New York Springer., 2003.
- [127] L. Dolgov, O. Yaroshchuk, and L. Qiu, "SEM investigations of polymer morphology in the liquid crystal-polymer composites with different polymer contents," in *Molecular crystals and liquid crystals*, pp. 687-696, 2007.
- [128] C. Hudon, R. Bartnikas, and M.R. Wertheimer, "Analysis of degradation products on epoxy surfaces subjected to pulse and glow type discharges," in *IEEE Electr. Insul. Dielectr. Phenom. (CEIDP)*, pp. 237-243, 1991.
- [129] Mayoux, C. J., "Partial-discharge phenomena and the effect of their constituents on polyethylene," in *IEEE Transactions on Electrical Insulation, Vol. El-11, pp. 139-149*, 1976.
- [130] N. Hattori, Y. Ehara, H. Kishida, and T. Ito, "Pit observation and partial discharge measurement before tree initiation," in *Electrical Insulation and Dielectric Phenomena*, 2002 Annual Report Conference on, 2002.
- [131] V. Thatte, "Aging and degradation in the epoxy resin using partial discharge technique," University of Southampton, 2013.
- [132] L. Niemeyer, and F. Gutfleisch, "Measurement and simulation of PD in epoxy voids," in *Dielectrics and Electrical Insulation, IEEE Transaction on, vol. 2, pp 729-743*, 1995.
- [133] R. Schifani, "On PD mechanisms at high temperature in voids included in an epoxy resin," in *Dielectrics and Electrical Insulation, IEEE Transaction on, vol. 8, pp. 589-597*, 2001.
- [134] T. Mizutani, and T. Kondo, "PD patterns and PD current shapes of a void in LDPE," in Proceedings of the 6th International Conference on Properties and Applications of Dielectric Materials, vol. 1, pp. 276-279, 2000.
- [135] P.H.F. Morshuis, A. Cavallini, G.C. Montanari, F. Puletti, and A. Contin, "The behavior of physical and stochastic parameters from partial discharges in spherical voids," in Proceedings of the 6th International Conference on Properties and Applications of Dielectric Materials, vol. 1, pp. 304-309, 2000.

- [136] Paithankar, A.A.; Mokashi, A.D., "Recognition of PD faults using chaos mathematics," in *IEEE 6th International Conference on Conduction and Breakdown in Solid Dielectrics, pp.* 177-180, 1998.
- [137] Chelai Yin; Lixing Zhou; Yini Luo, "Applications of chaos theory on Partial Discharge detection and character analysis," in *IEEE International Conference on Industrial Technology,* pp.1-4, 2008.
- [138] Dissado, L.A., "Deterministic chaos in breakdown. Does it occur and what can it tell us?," in *IEEE Transactions on Dielectrics and Electrical Insulation, vol. 9, issue 5, pp.752-762*, 2002.
- [139] Paithankar, A.A.; Mokashi, A.D., "Can PD phenomenon be analysed by deterministic chaos?," in *Proceedings Electrical Insulation Conference, pp. 283-289*, 1997.
- [140] W.H. Steed, The Nonlinear Workbook, World Scientific Publishing Co. Pte. Ltd, 1999.
- [141] Petrov, L.A.; Lewin, P.L.; Czaszejko, T., "On the applicability of nonlinear time series methods for partial discharge analysis," in *IEEE Transactions on Dielectrics and Electrical Insulation*, vol. 21, issue 1, pp. 284-293, 2014.